Exon skipping as a therapeutic strategy in dysferlinopathy

Inaugural-Dissertation
to obtain the academic degree
Doctor rerum naturalium (Dr. rer. nat.)

submitted to

Department of Biology, Chemistry and Pharmacy
of Freie Universität Berlin

and
in cotutelle to

Ecole doctorale: 569
Innovation thérapeutique: du fondamental à l'appliqué (ITFA)
of Université Paris-Saclay

by

Jakub Malcher
from Poznań, Poland

2017

PREFACE

The preparation of the molecular and therapeutic tools for exon skipping, cloning of dysferlin constructs and production of AAVs and lentiviruses was conducted between 01.01.2013 and 30.06.2016 in collaboration with the laboratory of Dr. Luis Garcia at the UFR des sciences de la santé Simone Veil, Université de Versailles Saint-Quentin-en-Yvelines, 2 Avenue de la Source de la Bièvre, 78180 Montigny-le-Bretonneux, France and with mentoring from Dr. Aurelie Goyenvalle and Dr. Rachid Benchaouir. The validation of the therapy in the MMex38 mouse model, in vitro experiments on MMex38 satellite cells and laser wounding assay using human primary myoblasts were performed between 1.07.2016 and 30.09.2017 with the support from Dr. Andreas Marg and Dr. Helena Escobar Fernandez and under supervision of Prof. Dr. med. Simone Spuler at the Experimental and Clinical Research Center- a collaboration between the Max Delbrück Center for Molecular Medicine and the Charité, Lindenberger Weg 80, 13125 Berlin, Germany.

Members of Jury

Thesis director from Freie Universität Berlin:	**Prof. Dr. med. Simone Spuler**
Thesis co-director from Université de Versailles Saint-Quentin-en-Yvelines:	**Dr. Luis Garcia, Directeur d'Unite INSERM U1179**
Reviewer and Examiner from Freie Universität Berlin:	**Prof. Dr. rer. nat. Florian Heyd**
Examiner from Université Paris- Saclay:	**Prof. Dr. med. Helge Amthor**
External Reviewer and Examiner from Royal Holloway- University of London:	**Prof. Dr. George Dickson**
External Reviewer and Examiner from University of Reading:	**Prof. Dr. Ketan Patel**
Postdoctoral research fellow from Freie Universität Berlin:	**Dr. Marco Preußner**

Date of defense: 26.03.2018
Place of defense: Berlin

ACKNOWLEDGEMENTS

I would like to express my special thanks to Prof. Simone Spuler for supervising my work and giving me opportunity to do my PhD in her laboratory at the Experimental and Clinical Research Center. I would also like to thank Dr. Luis Garcia for inviting me for a cooperation to his laboratory at the Université de Versailles Saint-Quentin-en-Yvelines and for his mentoring during my stay.

I want to thank Susanne Wissler for helping me with all the organizational and bureaucratic aspects of the MyoGrad program. I also thank Susanne Wissler and Helge Amthor for putting a lot of effort in finalizing my cotutelle agreement. I want to thank DFG and Association Monégasque contre les Myopathies (AMM) for the financing my PhD.

I want to thank to Dr. Aurelie Goyenvalle for her mentoring in the field of gene therapy, exon skipping and for her help with the animal experiments. I also want to thank her for a very warm welcome and for helping me finding my way in Montigny-le-Bretonneux during first months of my stay.

I want to thank Dr. Rachid Benchaouir for introducing me to the topic of viral vectors and for supervising my work with adeno-associated and lenti viruses in the biosafety level 3 laboratory.

I want to thank Dr. Verena Schöwel for introducing me to the lab in Berlin, for her help with the animal experiments application and for setting up the animal breeding for my experiments in Berlin.

I want to thank Dr. Andreas Marg for thorough mentoring during my work with the confocal and fluorescent microscope and during the microinjections. I am also very grateful for all his hints for the tricky human primary cell culture.

I want to thank Dr. Helena Escobar for her involvement in the FACS experiments, for the help with the satellite cell isolations, their culture and for our continuous exchange of ideas during planning of experiments.

I want to thank Dr. Aurelie Avril for the introduction into exon skipping in dysferlin and for numerous ideas for the design of skipping strategies.

I want to thank Benoit Maury for introducing me to the flow cytometry and FACS platform at UVSQ.

ACKNOWLEDGEMENTS

I want to thank Prof. Carmen Bichmeier and Dr. Ines Lehman for sharing the know-how about satellite cell isolation and providing the necessary reagents to start the experiments.

I want to thank Prof. Oliver Daumke for a brief introduction into the homology modeling of dysferlin protein.

I want to thank Cyriaque for answering my numerous questions about cloning and for being a very supportive labmate during long evenings and weekends spent in the lab, especially when yet another experiment failed.

I want to thank Graziella Griffith, Dr. Valérie Robin, Pierre-Olivier Buclez for a very warm welcome in the lab, for teaching me the new lab techniques and for hundreds of happy moments during my stay in Montigny-le-Bretonneux.

I want to thank Dr. Sonia Relizani, Dr. Amalia Stantzou, Gabriella Diaz, Marine Imbert, Fauzie Zarrouki and Julien Dattola for the day-to-day support in the lab in Montigny-le-Bretonneux and for the fantastic atmosphere in the office.

I want to thank Steffi Haafke for her involvement in the cloning work and the protein analysis, Stefanie Meyer-Lisner for the involvement in the primary cell culture of human myoblasts and in animal work and Adrienne Rothe for her involvement in the mice injections.

I want to thank Eric Metzler, Henning Lange, Vinko Palada and Silvia di Francescantonio for the great lab atmosphere, inspiring lunch breaks and nice time spent outside the office. I also want to thank Kornelia Gräning for very supportive talks that we had over a lab bench.

Finally, I want to express special thanks to my wife for her immense engagement in our family life and for the continuous support, motivation and encouragement during my PhD work in France and Germany. I also want to thank my parents and my parents in law for their help and for enabling things that at the first glance looked sometimes impossible.

TABLE OF CONTENTS

LIST OF FIGURES

LIST OF FIGURES

LIST OF FIGURES

LIST OF FIGURES

LIST OF TABLES

LIST OF ABBREVIATIONS

2’OMe	2'O-Methyl
3’ss	3’ splice site
5’ss	5’ splice site
A	adenine nucleotide
AAV	adeno-associated virus
AAVS1	region o long arm of chromosome 19 (19q13-qter) were AAV integrates
AB320	dysferlin deficient immortalized human myoblast (see Table **6** for details)
Ad	adeno virus
APP	assembly-activating protein
AS	acceptor site
BCA	bicinchoninic acid assay
bc-DNA	bicyclo-DNA
BL10	black 10 mouse model
BP	branchpoint
bp	base pair
C	cytosine nucleotide
c25	healthy immortalized human myoblasts
C2C12	WT immortalized mouse myoblast cell line
CDS	coding sequence
CTD	carboxy-terminal domain of RNA polymerase II
CK	creatine kinase
cPPT	central polypurine tract

DGC	dystrophin-associated glycoprotein complex
dKO	dystrophin/utrophin double-knockout mice
DMAT	distal myopathy with anterior tibial compartment onset
DNA	deoxyribonucleic acid
DS	donor site
dsDNA	double stranded DNA
DYSF	canonical dysferlin transcript
DYSF_v1	dysferlin transcript with an alternative promotor and exon 1
EGFP	enhanced green fluorescent protein
EGFR	epidermal growth factor receptor
EHD2	Eps15 homology EH-domain-containing protein 2
env	envelope protein
ER	endoplasmic reticulum
ESE	exonic splice enhancer
ESS	exonic splice silencer
FACS	fluorescence activated cell sorting
FER1L1	dysferlin
FER1L2	otoferlin
FER1L3	myoferlin
FIV	feline immunodeficiency virus
G	guanine nucleotide
gag	group specific antigen
GRP78	78-kDa glucose-regulated protein
hDYSF	human dysferlin gene
HIV	human immunodeficiency virus

HMZ	homozygote
hnRNPA1/A2	heterogeneous nuclear ribonucleoprotein A1/A2
HTZ	heterozygote
HSF	human splice finder
HSV	herpes simplex virus
i379	dysferlin deficient immortalized human myoblast (see Table **6** for details)
i814	dysferlin deficient immortalized human myoblast (see Table **6** for details)
i.m.	intramuscular injection
ITR	inverted terminal repeat
ISE	intronic splice enhancer
i.v.	intravenous injection
LGMD2B	Limb-girdle muscular dystrophy, type 2B
LIF	leukemia inhibitory factor
LNA	locked nucleic acid
LOVD	Leiden Open Variation Database
LTR	long terminal repeat
MCS	multiple cloning site
MOI	multiplicity of infection
MM	Miyoshi myopathy
MMex38	dysferlinopathy mouse model with the mutation Dysf p.L1360P in exon38 of the dysferlin gene
MG53	Mitsugumin 53 protein
mRNA	messenger RNA

n.s.	not significant
nt	nucleotide
ORF	open reading frame
PBS	primer binding site
PCR	polymerase chain reaction
PDGFR-α	platelet-derived growth factor receptor
PenStrep	penicillin and streptomycin
PGK	phosphoglycerate kinase
PMO	phosphorodiamidate morpholino oligomer
PNA	peptide nucleic acid
pol	reverse transcriptase and integrase
pre-mRNA	precursor mRNA
Psi (Ψ)	packaging signal
rAAV	recombinant adeno associated virus
rev	regulator of expression of virion proteins
RBPs	RNA binding proteins
RCL	replication competent lentivirus
RNA	ribonucleic acid
RRE	rev regulatory element
RSV	Rous sarcoma virus promoter
RT-PCR	reverse transcription polymerase chain reaction
RyR1	ryanodin-receptor
SEM	standard error of mean
SIV	simian immunodeficiency virus
SLE	systemic lupus erythematosus

snRNA	small nuclear ribonucleic acid
snRNP	small nuclear ribonucleoprotein
ssDNA	single stranded DNA
ssRNA	single stranded RNA
SR	serine rich protein
tcDNA	tricycloDNA
qPCR	quantitative PCR
T	thymine nucleotide
TA	tibialis anterior
tar	tat-activation region
U	uracil nucleotide
UMD-DYSF	Universal Mutation Database for Dysferlin
UTR	untranslated region
UV	ultraviolet light
VSV-G	vesicular stomatitis virus G glycoprotein
WPRE	Woodchuck hepatitis virus posttranscriptional regulatory element
WT	wild type

SI units were used according to the International System of Units.

SUMMARY

Titel: Exon skipping as a therapeutic strategy in dysferlinopathy.

Keywords: dysferlinopathy, LGMD2B, dysferlin, exon skipping, U7 snRNA, rAVV

Dysferlinopathy is a muscular dystrophy that manifests as two major phenotypes: limb-girdle muscular dystrophy type 2B (LGMD2B) or Miyoshi myopathy (MM). It is caused by mutations in the dysferlin gene. Dysferlin is a membrane protein expressed in skeletal muscle. It is responsible for the repair of sarcolemma microlesions produced by muscle contractions. A compromised membrane repair leads to slowly progressing muscle wasting.

This thesis explores the therapeutic potential of an antisense mediated splice switching strategy in LGMD2B caused by the missense mutation c4022T>C in the exon 38 of the dysferlin gene. Antisense oligonucleotides and U7 snRNAs delivered by an adeno-associated viral vector were used as tools to trigger exon skipping in vitro and in vivo. The thesis investigates also if the truncated dysferlin maintains a proper membrane localization and its membrane repair ability.

The splice switching strategy was developed after a bioinformatic analysis of targeted dysferlin pre-mRNA. The in silico analysis provided numerous exonic splice enhancers (ESEs) as possible targets and showed that exon 37 and 38 are in close proximity suggesting that they could be removed simultaneously. Thirteen AONs masking exon 37, 38 and intron 37-38 of human dysferlin pre-mRNA were designed. The AON-based splice switching strategy was screened in vitro. Out of thirteen AONs only five demonstrated low level of skipping exon 38. The activity of these oligonucleotides was verified in vivo by intramuscular injections in WT mice. None of these AONs was able to evoke detectable skipping of exon 38 or both exon 37 and 38 at the RNA level.

As an alternative splice switching strategy U7 snRNA approach was used. Twelve antisense sequences targeting exon 38 were cloned into the U7 snRNA backbone. For screening, the constructs were delivered intramuscularly into MDX mice using AAV2/9 vector. Three out of twelve U7 snRNAs were able to skip exon 37 and 38 simultaneously. The exon skipping activity of these three constructs was also verified in MMex38 dysferlin deficient mice. Two constructs evoked minor exon skipping detectable only at the RNA level. The activity of the three U7 constructs delivered in AAV2/9 was also tested in vitro in C2C12 cells and in MMex38 primary mouse myoblasts. Exon skipping was detected at the RNA level only in C2C12 cells.

The thesis investigates also if dysferlin without exons 37 or 38 maintains a proper membrane localization and its membrane repair ability. The truncated dysferlin constructs: Δexon37, Δexon38, Δexon37&38 and the full dysferlin were delivered to dysferlin deficient human primary myoblasts using a lentivirus. The dysferlin functionality was investigated using a membrane wounding assay. The dysferlin without exon37 or without exon37&38 demonstrated the same membrane resealing property as the full dysferlin. Dysferlin without exon 38 performed worse than the full dysferlin, however, still significantly better than the non-transduced dysferlin deficient myotubes.

For a localization study of the truncated dysferlin in vitro, immunostainings of transduced dysferlin-deficient myoblasts and myotubes were performed. The full dysferlin was detected as expected at the membrane of the myotubes. The truncated dysferlin constructs did not demonstrate the membrane localization. Furthermore, the truncated dysferlin is expressed less than the full protein and it localizes in the cytoplasm near nuclei.

ZUSAMMENFASSUNG

Titel: Exon Skipping als therapeutische Strategie in Dysferlinopathie.

Keywords: Dysferlinopathie, LGMD2B, Dysferlin, Exon Skipping, U7 snRNA, rAVV

Dysferlinopathie ist eine Muskeldystrophie, die sich in zwei Hauptphänotypen manifestiert: Gliedergürtelmuskeldystrophie Typ 2B type 2B (LGMD2B) oder Miyoshi Myopathie (MM). Sie wird durch Mutationen im Dysferlin-Gen verursacht. Dysferlin ist ein Membranprotein, das im Skeletmuskel exprimiert wird. Es ist verantwortlich für die Reparatur von Mikroläsionen am Sarkolemm. Nichtfunktionierende Membranreparatur führt zu progressiver Muskelschwäche.

Diese Dissertation untersucht die therapeutischen Möglichkeiten einer Antisense-Splice-Switching-Strategie bei LGMD2B, die durch die Missense-Mutation c4022T>C im Exon 38 des Dysferlin-Gens verursacht wird. Antisense-Oligonukleotide und U7 snRNAs, die durch einen adeno-assoziierten viralen Vektor geliefert wurden, sind Werkzeuge, die für das Exon Skipping in vitro und in vivo eingesetzt wurden.

Die Splice-Switching-Strategie wurde nach einer bioinformatischen Analyse der Dysferlin Prä-mRNA entwickelt. Die in silico Analyse hat viele ESEs als mögliche Ziele identifiziert und auch gezeigt, dass Exon 37 und 38 nicht weit auseinanderliegen und eventuell gleichzeitig entfernt werden könnten. Dreizehn AONs, die Exons 37, 38 und Intron 37-38 der humanen Dysferlin Prä-mRNA maskierten, wurden entworfen. Die AON-basierte Splice-Switching-Strategie wurde in vitro getestet. Von den dreizehn AONs erreichten nur fünf ein niedriges Skippingniveau des Exons 38. Die Exon Skippingaktivität dieser vier Oligonukleotide wurde in vivo in WT Mäusen durch intramuskuläre Injektion verifiziert. Keine der AONs war in der Lage, ein detektierbares Skipping des Exons 38 oder der beiden Exons 37 und 38 auf der RNA Ebene zu erreichen.

Als alternative Splice-Switching-Strategie wurde U7 snRNA ausgewählt. Dafür wurden zwölf Antisense-Sequenzen, die das Exon 38 gezielt haben, in das U7 snRNA Rückgrat einkloniert. Die Konstrukte wurden mittels AAV2/9 intramuskulär in die MDX Maus injiziert und für das Skippingergebnis untersucht. Drei der zwölf U7 snRNA waren in der Lage, die Exons 37 und 38 gleichzeitig zu entfernen. Bei diesen drei Konstrukten wurde die Exon Skipping Aktivität in vivo bei Dysferlin-defizienten Mäusen (MMex38) getestet. Zwei Konstrukte verursachten ein minimales Exon Skipping, das nur auf RNA-Ebene detektiert wurde. Die Aktivität der U7 snRNAs, die mittels AAV2/9 geliefert wurden, wurde auch in vitro in C2C12 Zellen und in den primären Myoblasten aus der Dysferlin-defizienten Maus (MMex38) getestet. Das Exon-Skipping wurde auf RNA Ebene nur in den C2C12 Myotuben detektiert.

Die Dissertation untersucht auch, ob Dysferlin ohne Exons 37 oder 38 am Sarkolemm lokalisiert und ob es noch die Membranreparaturfähigkeit besitzt. Zu diesem Zweck wurden drei Dysferlin- Konstrukte: ΔExon37, ΔExon38, ΔExone37&38 und das native Dysferlin und mittels Lentiviren in die Dysferlin-defizienten humanen primären Myoblasten eingebracht. Die Dysferlin-Funktionalität wurde mit Laser Wounding Assays untersucht. Das Dysferlin ohne Exon 37 und ohne die beiden Exons 37 und 38 verfügt über die gleiche Membranreparaturfähigkeit wie das vollständige Dysferlin. Das Dysferlin ohne Exon 38 schnitt im Laser Wounding Assay zwar schlechter als das vollständige Dysferlin ab, jedoch immer noch besser als die nicht transduzierten Dysferlin-defizienten Myoblasten.

Für die Lokalisationsstudie des verkürzten Dysferlins wurden in vitro Immunfärbungen der transduzierten Dysferlin-defizienten humanen primären Myoblasten und Myotuben angefertigt. Das vollständige Dysferlin wurde, wie erwartet, an der Membran der Myotuben entdeckt. Die Immunfärbungen der Myotuben mit den verkürzten Dysferlin-Konstrukten zeigten keine Lokalisierung am Sarkolemm. Es ließ sich ebenfalls beobachten, dass das verkürzte Dysferlin schlechter als das native Dysferlin exprimiert wurde und sich im Zytoplasma in der Nähe der Nuclei akkumulierte.

RÉSUMÉ

Titre: Le saut d'exon thérapeutique pour le traitement des dysferlinopathies.

Mots clés: dysferlinopathies, LGMD2B, dysferline, saut d'exon, U7 snRNA, vecteurs rAAV

Les dysferlinopathies sont des dystrophies musculaires qui se manifestent par la dystrophie musculaire des ceintures de type 2B (LGMD2B) ou la myopathie de Miyoshi (MM). Elles sont causées par des mutations dans le gène dysferline. La dysferline est une protéine membranaire exprimée dans le muscle squelettique, responsable de la réparation des microlésions du sarcolemme. L'absence d'une telle réparation de la membrane entraîne une atrophie musculaire progressive. Ce travail de thèse explore le potentiel thérapeutique d'une stratégie de modulation d'épissage pour le traitement de la LGMD2B causée par la mutation faux-sens c4022T>C dans l'exon 38 du gène dysferline. Des oligonucléotides antisens et des petits ARN U7 délivrés par un vecteur viral de type adéno-associé ont été utilisés comme outils pour induire un saut d'exon in vitro et in vivo. Ce projet de thèse étudie également la capacité de la dysferline tronquée à se localiser de façon appropriée à la membrane et ainsi la réparer.

Cette stratégie de modulation d'épissage a été développée après une analyse bioinformatique du pré-ARNm de la dysferline ciblée. L'analyse in silico a identifié de nombreuses sequences activatrices d'epissage (ESE) comme cibles potentielles et a montré que les exons 37 et 38 sont très proches, ce qui suggère qu'ils pourraient être éliminés simultanément. Treize AON masquant les exons 37, 38 et l'intron 37-38 du pré-ARNm de la dysferline humaine ont été conçus. Sur treize AON seulement cinq ont démontré un faible niveau de saut d'exon 38 in vitro. L'activité de ces oligonucléotides a ensuite été vérifiée in vivo par des injections intramusculaires chez des souris WT et aucun de ces AON n'a été capable d'induire un saut détectable de l'exon 38 ou des deux exons 37 et 38.

Afin d'évaluer une stratégie alternative de modulation d'epissage, l'approche vectorisée U7snRNA a été utilisée. Douze séquences antisens ciblant l'exon 38 ont été clonées dans la cassette U7snRNA puis introduites dans des vecteurs viraux recombinants AAV de type 2/9 et injectés par voie intramusculaire à des souris MDX. Trois U7snRNA modifiés sur 12 ont permis un saut des exons 37 et 38 simultanément. L'activité de ces trois constructions a également été vérifiée chez des souris déficientes en dysferline (MMex38). Deux constructions ont induit un saut d'exon mineur détectable seulement au niveau de l'ARN. L'activité de ces trois constructions U7 délivrées par des vecteurs AAV2/9 a également été

testée in vitro dans des cellules C2C12 et dans des myoblastes primaires de souris MMex38. Un saut d'exon a été détecté uniquement au niveau de l'ARN des cellules C2C12.

Ce travail de thèse s'est également intéressé à la fonction de la dysferline dépourvue des exons 37 ou 38 en étudiant notamment sa capacité de localisation et de réparation membranaire. Les constructions de dysferline tronquée: Aexon37, Aexon38, Aexon37 & 38 ainsi que la dysferline complète ont été administrées à des myoblastes primaires humains déficients en dysferline en utilisant un vecteur lentiviral. La fonctionnalité de la dysferline a été étudiée en utilisant un test de blessure membranaire. La dysferline dépourvue de l'exon 37 ou des exons 37 et 38 a démontré la même propriété de réparation membranaire que la dysferline complète. La dysferline dépourvue de l'exon 38 est apparue moins performante que la dysferline complète, mais capable d'améliorer significativement le phénotype des myotubes déficients en dysferline.

Afin d'étudier plus précisément la localisation de la dysferline tronquée in vitro, des immunomarquages ont été réalisés sur myoblastes et myotubes déficients en dysferline. La dysferline complète a été détectée à la membrane des myotubes comme attendu, alors que les constructions de dysferline tronquées n'ont pas démontré de localisation à la membrane. De plus, ces résultats ont démontré que la dysferline tronquée est moins exprimée que la protéine entière et se localise dans le cytoplasme près des noyaux.

1. INTRODUCTION

1.1. Dysferlinopathy

Dysferlinopathy is a term that describes a group of autosomal recessive muscular dystrophies caused by mutations in the dysferlin gene. (Liu et al., 1998b) It is characterized by progressive muscle wasting with late onset. Although the first clinical symptoms manifest in early adolescence (on average at the age of 20-25 year) (Ueyama et al., 2002), there are also reported cases of very late onset at the age of over 40. (Nakagawa et al., 2001; Suzuki et al., 2004). The disease affects skeletal muscle of limbs and limb girdle that includes shoulders and pelvis. It progresses slowly and the patients experience first walking difficulties in 10-30 years after a diagnosis. Initially, patients exhibit highly elevated (20-100 times) creatine kinase (CK) levels that decrease over time. (Harris et al., 2016) A histologic picture is typical for a dystrophic change and was well characterized by Miyoshi. A muscle cross-section from an affected patient presents signs of necrosis and accumulation of fatty and connective tissue. Fibers decrease in number, vary in size and have rounded shape. Frequent fiber splitting in hypertrophic fibers is observed. Furthermore, a central location of myonuclei is an indication of regeneration. (Miyoshi et al., 1986) An ongoing inflammatory process can be observed by perivascular infiltrates consisting of macrophages and T-helper cells. (Gallardo et al., 2001)

1.1.1. Clinical manifestation

Dysferlinopathy is described by three major clinical subphenotypes: limb-girdle muscular dystrophy type 2B (LGMD2B) (Bashir et al., 1994), Miyoshi myopathy (MM) (Miyoshi et al., 1986) and distal myopathy with anterior tibial compartment onset (DMAT) (Illa et al., 2001). A differential diagnosis can be made based on muscle groups affected in the initial stage of the disease. LGMD2B is characterized by weakness in the proximal muscle that is in upper arms and thighs (Bashir et al., 1994) whereas MM manifests in the distal muscle that includes lower arms and calves (Miyoshi et al., 1986). The phenotypic differences can be distinguished in the early stage of the disease, however, it has been also reported that an identical dysferlin mutation can cause symptoms typical for both LGMD2B and MM, suggesting that additional genetic or nongenetic factors influence the phenotypic outcome of the mutation. (Harris et al., 2016; Illarioshkin et al., 2000; Weiler et al., 1996, 1999)

1.1.2. Prevalence

Dysferlinopathy belongs to the group of rare diseases. The prevalence in terms of a larger population was described in the study by Norwood et al. who estimated frequency of various genetic muscle diseases taking into account data of 1.100 dystrophic patients since 1954 from the region of Northern England inhabited by a population of 3 million people. For the LGMD2B the prevalence of only 0,13 to 100.000 was estimated. (Norwood et al., 2009). High dysferlinopathy prevalence and founder effect mutations were described in couple of ethnic clusters. One group is the Libyan Jews community in which the prevalence was estimated for at least 1 to 1.300 and the carrier rate for the specific 1624delG mutation was calculated at about 10%. (Argov et al., 2000) Another ethnic cluster are Jews originating from Caucasus were the carrier rate of the mutation 2779delG was estimated at 4%. (Leshinsky-Silver et al., 2007) In both communities pedigrees with consanguineous marriages were observed. The high carrier rate was also an indicator for the founder effect mutations.

1.2. Dysferlin Gene

1.2.1. Genomic organization

Dysferlin gene is located on chromosome 2p13 and spans the genomic region of 233,6Kb. (Bashir et al., 1994, 1996; Bejaoui et al., 1995) The coding sequence has 6.243 bp and consists of 55 exons. The splice donor and acceptor sites that define exon-intron boundaries are conserved in all exons and correspond to GT and AG sequences. (Aoki et al., 2001)

1.2.2. Transcript variants and expression patterns

There are two main splice variants of the human dysferlin gene that differ in the location of exon 1 and use of an alternative promotor. The cannonical one (DYSF) is available under the GenBank accession number AF075575 and the variant 1 (DYSF_v1) with the alternative promotor and exon 1 situated inside intron 1 is categorized under DQ267935 (Figure 1).

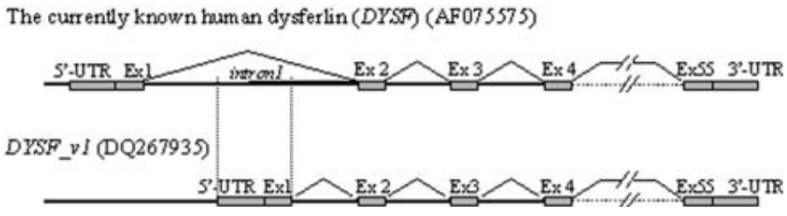

Figure 1 Two main dysferlin transcript variants originating from the use of the alternative promotor.

The graphic was reproduced from (Pramono et al., 2006).

These two main splice variants are also available in the mouse genome: the canonical form (Dysf v2) and the alternative promotor version (Dysf v1).

Dysferlin exons 5a, 17 and 40a are also alternative spliced exons. They can form 7 possible versions of dysferlin transcripts. Because each of these variants can have the alternative promotor and exon 1 there are 14 possible transcripts that were depicted on Figure 2.

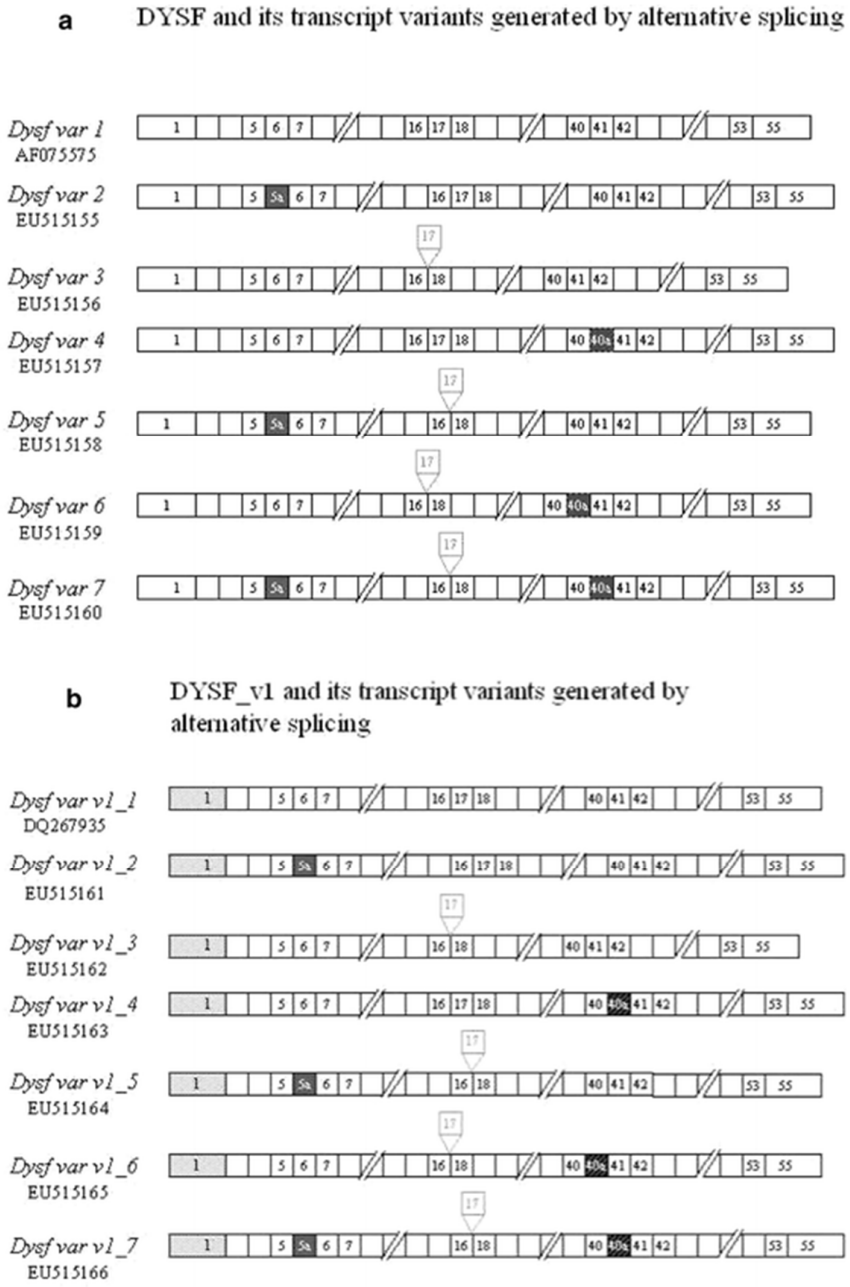

Figure 2 Alternatively spliced dysferlin transcripts.

Part a) contains mRNA variants of alternatively spliced canonical DYSF transcript. Part b) contains the mRNA variants of alternatively spliced DYSF_v1 transcript. The graphics was reproduced from (Pramono et al., 2009).

Dysferlin is essential for the limb formation and it is expressed already at the embryonic age from 5 to 6 weeks when limbs exhibit regional differentiation. (Anderson et al., 1999) The canonical variant of dysferlin is expressed in various human tissue: brain, heart muscle, skeletal muscle, spleen, kidney, liver, small intestine, placenta, lung, and peripheral blood leucocytes. (Ho et al., 2002; Pramono et al., 2006) It exhibits the highest levels in skeletal muscle, heart and kidney. (Anderson et al., 1999)

As far as the skeletal muscle is concerned, 81,3% of total dysferlin available in this tissue IS represented by the canonical form and only 18,7% by the alternative promotor transcripts (Table 1). The most abundant transcripts in the muscle tissue exclude exon 5a and 40a and includes all other exons the represent 73% of the canonical dysferlin transcripts (DYSF var1) and 13% of transcripts with the alternative promotor (DYSF var v1_1). In the blood 88,8% and 11,2% of total dysferlin transcripts are represented by the canonical and the alternative exon 1 mRNAs respectively. Interestingly, the most abundant transcript variant in skeletal muscle (DYSF var1) is not available in the blood. The blood contains mainly DYSF var5 (exon 5a inclusion and exon 17 exclusion) and var7 (exon 5a and 40a inclusion and exon 17 exclusion). They account for 62% of the total canonical dysferlin (Table 1). (Pramono et al., 2009)

Skeletal muscle				Blood			
DYSF		*DYSF_v1*		*DYSF*		*DYSF_v1*	
		23% of *DYSF*[a]				12.6% of *DYSF*[a]	
81.3% of total dysferlin		18.7% of total dysferlin		88.8% of total dysferlin		11.2% of total dysferlin	
dysf var 1	73.17%	*dysf var v1_1*	13.09%	*dysf var 1*	0	*dysf var v1_1*	1.68%
dysf var 2	4.065%	*dysf var v1_2*	1.87%	*dysf var 2*	8.88%	*dysf var v1_2*	0.56%
dysf var 3	0	*dysf var v1_3*	1.87%	*dysf var 3*	8.88%	*dysf var v1_3*	4.48%
dysf var 4	4.065%	*dysf var v1_4*	0	*dysf var 4*	0	*dysf var v1_4*	0.56%
dysf var 5	0	*dysf var v1_5*	0.935%	*dysf var 5*	44.4%	*dysf var v1_5*	1.12%
dysf var 6	0	*dysf var v1_6*	0.935%	*dysf var 6*	8.88%	*dysf var v1_6*	2.24%
dysf var 7	0	*dysf var v1_7*	0	*dysf var 7*	17.76%	*dysf var v1_7*	0.56%
Total: 100%				Total: 100%			

Table 1 Percentage distribution of dysferlin transcript variants in skeletal muscle and blood.

The table was reproduced from (Pramono et al., 2009).

1.2.3. Dysferlin mutations

There are two public databases available that track the new mutations in the dysferlin gene: Leiden Open Variation Database (LOVD, www.dmd.nl) and Universal Mutation Database for Dysferlin (UMD-DYSF, www.umd.be/DYSF/) (Blandin et al., 2012). LOVD stores information on both disease-causing and polymorphic dysferlin variations, UMD-DYSF collects deleterious dysferlin mutations that have been published so far and can be assigned to a dystrophic

phenotype of a patient. LOVD reported 1.656 cases of dysferlin variants which can be grouped into 511 unique mutations. 140 of these unique mutations have no noticeable phenotypic effect (last update: March 31, 2017). UMD-DYSF stores 1.174 cases of dysferlin variants and they are grouped into 418 unique disease causing-mutations (last update June 16, 2015) The unique mutations are distributed evenly across the dysferlin gene. They don't show any clustering around particular exon or intron, hence, there are no mutational hotspots in the dysferlin gene. (Krahn et al., 2009) Almost half of the missense mutations fall into C2 or Dysf domains. (Therrien et al., 2006) The current statistics and distribution of dysferlin mutations was presented in the Figure 3.

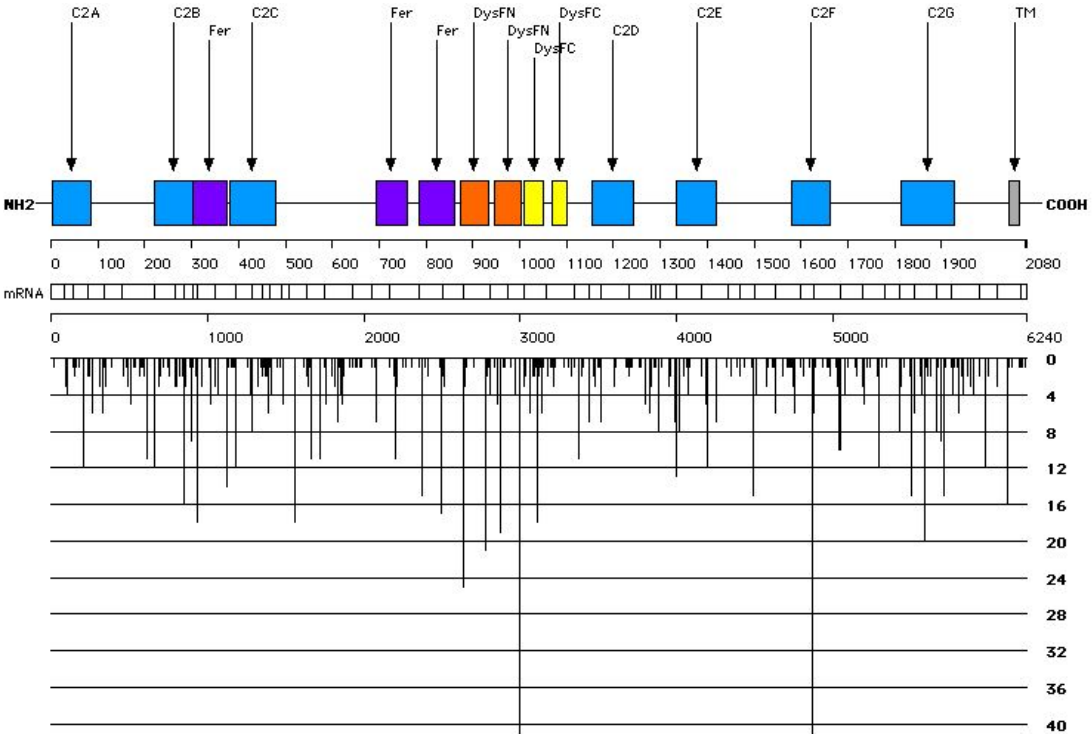

Figure 3 Distribution and frequency of unique mutations in the dysferlin coding sequence.

The top of the graphics represents the schematic distribution of the dysferlin domains and their names. Below there is a horizontal axis with numbers corresponding to the location of 2080 amino acids. Next, there is a schema of exons in mRNA and below the numbers corresponding to the nucleotide position. The bar chart at the bottom presents the position of each mutation in the coding sequence and its occurrence frequency in the UMD_DYSF database. (UMD-DYSF, www.umd.be/DYSF/) (Last update June 16, 2015)

1.2.4. Dysferlin c.4022T>C mutation

The homozygous mutation c.4022T>C in the dysferlin gene, which was investigated in this thesis, was discovered in a family that originates from Arabic Middle East. (Wenzel et al., 2006) The patient was a 52 year old man with advanced muscle wasting resulting in walking disability. His family pedigree was illustrated in the Figure 4. His mother and uncle were

affected by muscle weakness with late onset. His cousins have been also suffering from muscle wasting already as teenagers. The patient's muscle biopsy confirmed the dystrophic phenotype. On the muscle cross sections one could observe fiber size variation and an increased amount of connective tissue. Dysferlin was not localized at the membrane but was accumulating in the cytoplasm (Figure 4). (Wenzel et al., 2006) The c.4022T>C mutation leads to an exchange of leucine to proline (p.L1341P) in the dysferlin C2E domain. Leucine is a hydrophobic amino acid that is highly conserved in synaptotagmin I C2 domain, so it seems to be crucial for the proper folding of the C2E domain. Its replacement with proline can have a deteriorating effect on a domain structure that can eventually lead to misfolding and aggregation of the mutated dysferlin. (Wenzel et al., 2006) It is noteworthy that the aggregation of mutated dysferlin in cytoplasm of skeletal muscle was observed also for other dysferlin mutations (Spuler et al., 2008).

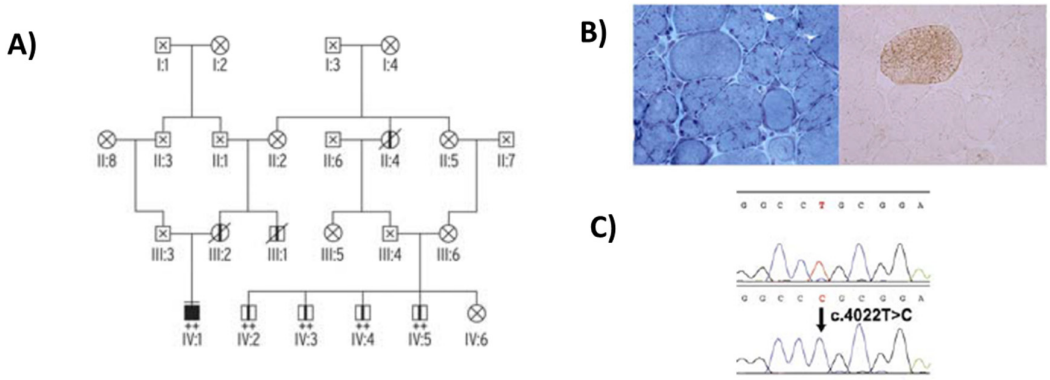

Figure 4 Profile of the patient carrying the c.4022T>C (p.L1341P) dysferlin mutation.

Panel A) Pedigree of the family carrying the c.4022T>C (p.L1341P) dysferlin mutation. Squares are males, circles are females, symbols with a solid bar are affected members by hearsay, solid symbols are affected members, a horizontal bar above a symbol is a patient clinically investigated, a diagonal bar is a deceased person, + is an allele with the mutation, - is an allele without the mutation, x- is a member not investigated. Panel B) Gomori-trichrome staining and dysferlin immunostaining of muscle cross section from the patient IV:1. Panel C) Sequencing result showing the c.4022T>C mutation discovered in the patient IV:1. The picture was adapted from (Wenzel et al., 2006).

1.3. Dysferlin Protein

1.3.1. Family of ferlins

Dysferlin is a membrane protein that belongs to the family of human ferlins, which include dysferlin (FER1L1), otoferlin (FER1L2), myoferlin (FER1L3), FER1L4, FER1L5 and FER1L6. (Lek et al., 2012) It shows 28% identity with the C.elegans fer-1 protein that is involved in the spermatogenesis and which mutations hinder fusion of submembraneous vesicles in spermatozoa (Argon and Ward, 1980; Bashir et al., 1998; Britton et al., 2000). Furthermore, it exhibits a 64% and 68% similarity with otoferline and myoferlin protein respectively. (Britton et al., 2000) Otoferlin is expressed in the sensory hair cells and its mutations lead to the autosomal recessive, nonsyndromic prelingual deafness. (Yasunaga et al., 1999, 2000) Myoferlin is mainly expressed in the heart muscle and in the skeletal muscle and is important for the fusion of myoblasts and maturation of myotubes. (Davis et al., 2000; Doherty et al., 2005) High levels of myoferlin are observed during differentiation of myoblasts hence the myoferlin deficient myoblasts fuse to smaller myotubes. The myoferlin knock-out mice have reduced muscle size, smaller fiber diameter and show impaired muscle regeneration. (Doherty et al., 2005) Nevertheless, no human muscular dystrophy have been reported as a result of myoferlin mutation.

1.3.2. Structure and localisation

Dysferlin protein consists of 2.080 amino acids and its size is estimated at 230 kDa. (Liu et al., 1998b) Just like fer-1, it has a modular structure (Figure 5 panel A) that is characterized by calcium binding motifs homologus to the C2-domain of synaptogamin.

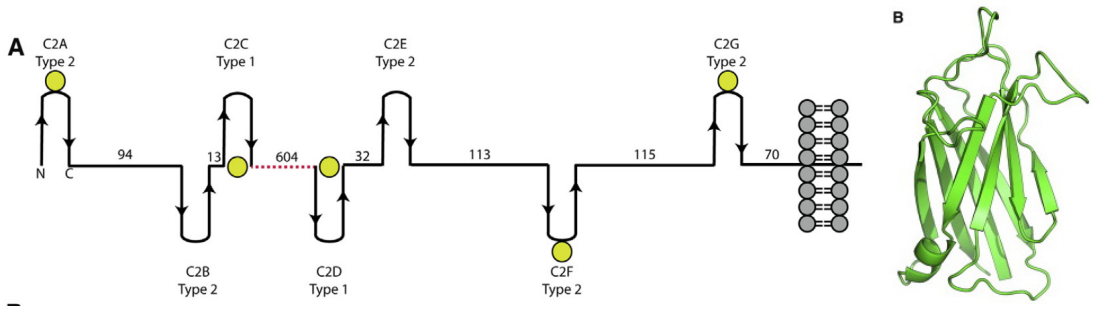

Figure 5 Schematic structure of dysferlin and its domains.

Panel A) Modular structure of dysferlin. Yellow circles represent Ca^{2+} ions, the dotted red line corresponds to the DysfF domains. Sarcolemma was shown as gray circles with black sticks. Panel B) A model of C2A domain consisting of eight β strands. The picture was adapted from (Fuson et al., 2014).

Dysferlin possesses seven C2 domains that are named as follows: C2A, C2B, C2C, C2D, C2E, C2F, C2G. Five out of seven C2 domains were predicted to coordinate Ca2+ ions. (Therrien et al., 2006) Type 1 C2 domain has high similarity to the mouse synaptotagmin III C2 domain and contains a single high affinity binding site that coordinates Ca^{2+} ions with five Glu/Asp residues. Type II C2 domain is homologues to human protein kinase Cδ domain and lacks one or more Glu/Asp residues in comparison to the type I domain. It possesses couple of low affinity Ca^{2+} binding sites. (Therrien et al., 2006) Furthermore, one can find dysferlin domains (DysfF) of unknown function. At the C-terminus there is a transmembrane domain which anchors dysferlin in the membrane. The X-ray structure of the canonical C2A domain was resolved at 2.0 Å resolution. The domain is a β sandwich fold of eight β strands (Figure 5 panel B). (Fuson et al., 2014)

It was also demonstrated that dysferlin is able to bind to variety of proteins available in cytosol and in membrane: AHNAK, caveolin-3, MG53 and annexins A1 and A2. (Cai et al., 2009a; Huang et al., 2007; Lennon et al., 2003; Matsuda et al., 2001)

Dysferlin is localized at sarcolemma, thus mutated dysferlin fails to integrate into the membrane. The immunofluorescent stainings of muscle cross sections coming from the patients affected by LGMD2B or MM do not detect dysferlin at sarcolemma (Figure 6). (Matsuda et al., 1999)

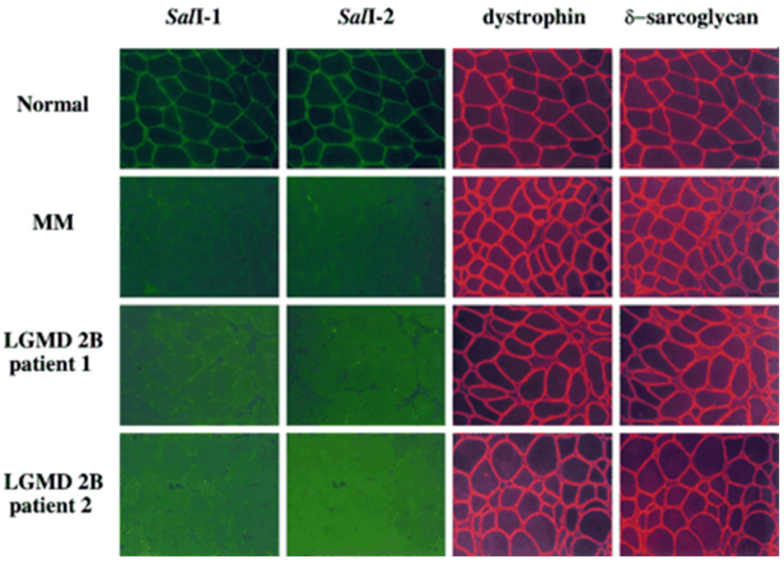

Figure 6 Immunofluorescent staining of dysferlinopathy affected muscle.

Dysferlin immunostaining was performed with affinity-purified *Sal*I-1 and *Sal*I-2 anti-dysferlin antibodies. The picture was reproduced from (Matsuda et al., 1999).

The immunostainings for dystrophin, and d-sarcoglycan demonstrate that the dystrophin-associated glycoprotein complex (DGC) is not affected by the absence of dysferlin. Furthermore, DGC purification and fractioning showed that dysferlin is not a part of DGC, thus it does not trigger the dystrophic process through destabilization of the linkage between cytoskeleton and extracellular matrix. (Piccolo et al., 2000)

1.3.3. Function in muscle

Mechanical stress like physical exercise causes damage to the sarcolemma of skeletal muscle. (Fridén et al., 1983; Macpherson et al., 1996; McNeil and Khakee, 1992) In rodents skeletal and heart muscle are tissues with the highest percentage (20-30%) of membrane disruptions. (McNeil, 1993) In order to rescue the damaged tissue not overwhelming its renewal capacity the eukaryotic cells developed a membrane resealing response. (McNeil and Terasaki, 2001) These micro-lesions are repaired in healthy cells by a Ca^{2+} dependent cell resealing mechanism known as the reparative patch model. It involves submembranous vesicles which are recruited to the damaged site and fuse with the destroyed membrane to seal the lesion. (Bi et al., 1995; McNeil et al., 2000; Terasaki et al., 1997)

In dysferlinopathy patients the membrane repair mechanism is impaired. This deficit manifests via sarcolemma discontinuities observable in the smooth muscle fibers affected by dysferlin mutations. (Selcen et al., 2001) The lesions lead finally to cell necrosis and a dystrophic phenotype. It was speculated that dysferlin can be engaged in the resealing mechanism because of the membrane localization, its association with the dystrophic phenotype and the discovery that its C2A domain binds lipid vesicles containing 50% phosphatidylinositol and 50% phosphatidylethanolamine in a calcium-sensitive fashion (Davis et al., 2002). By means of a laser wounding assay, Bansal et al. demonstrated eventually that disruption of the sarcolemma repair process is an underlying mechanism of muscle wasting in dysferlinopathy and that dysferlin is crucial for the successful calcium-dependent membrane resealing (Figure 7). (Bansal and Campbell, 2004; Bansal et al., 2003)

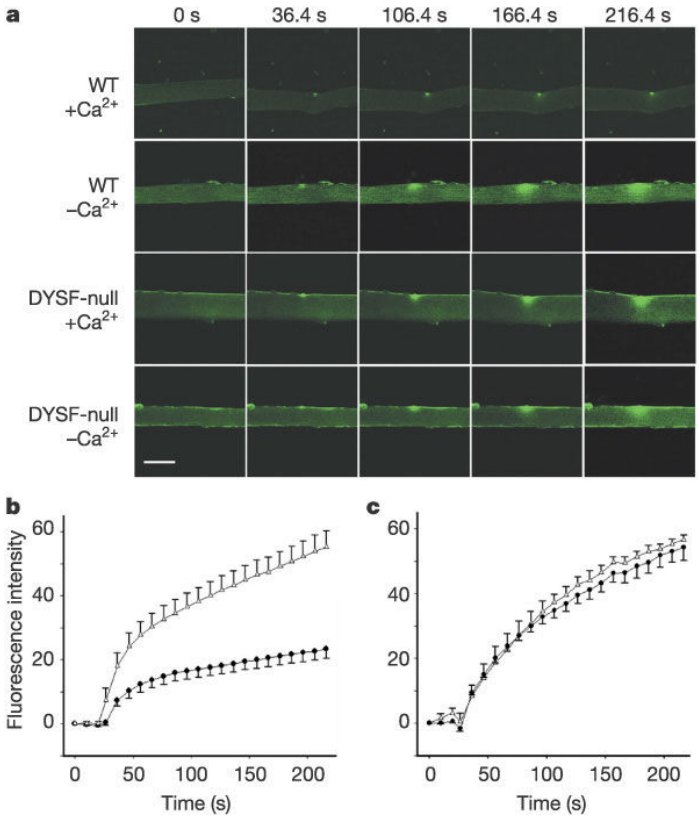

Figure 7 Ca^{2+} dependent membrane repair of single muscle fibers.

Results of a membrane wounding assay. Panel A) Time course of a fluorescent dye influx in the presence or absence of Ca^{2+} into a wounded singe muscle fiber from a WT and dysferlin deficient mice. Panel B) Quantification of the fluorescent dye influx into WT fibers (solid circles) and Dysf (-/-) fibers (empty circles) in the presence of Ca^{2+}. Panel C) Quantification of the fluorescent dye influx into WT fibers (solid circles) and Dysf (-/-) fibers (empty circles) in the absence of Ca^{2+}. The image and graphs were reproduced from (Bansal et al., 2003).

Furthermore, the assay showed that the resealing is accompanied by an accumulation of submembranous vesicles and enrichment of dysferlin at the site of wounding. The process corresponds to the reparative patch model.

By genetic transfer of dysferlin using dual adeno-associated vector into the dysferlin knock-out mice B6.A/J-*Dysf*^{prmd}, Lostal et al. reinforced the hypothesis that dysferlin is necessary for the rescue of the membrane repair process. (Lostal et al., 2010) Also use of mini-dysferlin gene construct consisting of only C2F, C2G and the transmembrane domains proved to restore membrane resealing process in the B6.A/J-*Dysf*^{prmd} mice. (Krahn et al., 2010)

Further research in the field of dysferlin-mediated membrane repair revealed new interaction partners of dysferlin necessary for a successful resealing. For instance, Ca^{2+} activated annexin 1 is recruited from cytoplasm of wounded myotubes and helps to aggregate and fuse vesicles available at the site of injury. (Lennon et al., 2003; McNeil et al., 2006) Annexin 2 is

responsible for fusion of endosomes which can be also used to patch membrane discontinuity. (Mayorga et al., 1994) Annexin 6 was shown to accumulate simultaneously to dysferlin at the place of injury and it was suggested that it is essential for the recruitment of annexin 1 and 2 in a later stage of patch formation. (Roostalu and Strähle, 2012) Also Mitsugumin 53 (MG53) protein is involved in the resealing process. It is tethered to sarcolemma and submembranous vesicles by phosphatidylserine interaction and mediates recruitment of vesicles via oxidation-dependent oligomerization to an injured area. (Cai et al., 2009b) EHD2 (Eps15 homology EH-domain-containing protein 2) was shown to accumulate during the resealing process at a membrane disruption site and may play role in membrane remodeling after a patch formation. (Marg et al., 2012a)

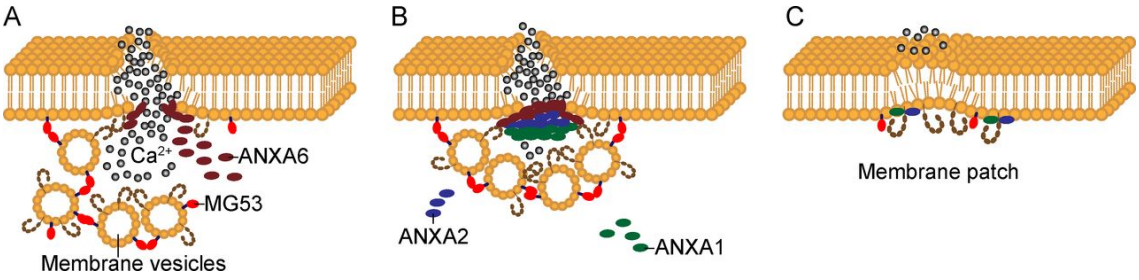

Figure 8 Dysferlin-mediated sarcolemma repair mechanism.

Extracellular components are shown as gray circles, dysferlin as brown rods. The graphic was reproduced from (Rahimov and Kunkel, 2013).

Apart from sarcolemma repair process, dysferlin was also shown to regulate transverse tubule formation and maintenance. It was shown that during the process of myotube formation and maturation dysferlin is localized mainly in T-tubule system and at the boarder of myoblast fusion. (Klinge et al., 2007) The dysferlin and myoferlin deficient mice suffer from dilatation of the sarcoplasmic reticulum and misalignment of transverse tubules in the skeletal muscle. (Demonbreun et al., 2014) Furthermore, it was demonstrated that dysferlin localizes in T-tubules in the early stage of muscle regeneration, hence dysferlin is important for the proper development of the T-tubule system. (Klinge et al., 2010) Interestingly, dysferlin, MG53, and annexin A1 are also enriched in transverse and longitudinal tubules of a stretched muscle indicating their function in the maintenance and protection of T-tubule system from the damage caused by stretching. (Waddell et al., 2011)

1.4. Understanding pre-mRNA splicing

1.4.1. Transcription of genetic information

Human genome contains genetic information saved in 2,9 billion base pairs of deoxyribonucleic acid (DNA) and arranged in 23 pairs of chromosomes. Only a very minor part of the genome (about 1,1%) is occupied by the protein coding sequences. (Lander et al., 2001; Venter et al., 2001) The gene coding sequences are clustered in exons that are separated by non-coding sequences of various length called introns.

Before the genetic information is translated into protein, the DNA code of a gene has to be converted into a precursor messenger RNA (pre-mRNA) and subsequently to a messenger RNA (mRNA). The conversion of DNA into pre-mRNA is done during a transcription process performed by a RNA polymerase II. The enzyme reads a DNA noncoding strand from a 3' to 5' direction and creates pre-mRNA in a 5' to 3' direction. The transcribed pre-mRNA is immediately processed. First it receives the 7-methylguanosine residue, a cap, at the 5' end to protect the transcript from RNAse degradation and to mark it as a ribosomal entry site. Next, it undergoes splicing which removes the intronic sequences from the transcript leaving only the information encoded in exons. Finally, the transcript is cleaved at the 3' end behind the polyadenylation signal and is elongated with a chain of about 250 adenosine monophosphates, known as a poly-A tail. This tail protects mRNA from degradation and marks it for transport to cytoplasm. The fully processed transcript, the messenger RNA (mRNA), consists of the cap, 5' untranslated region (UTR), coding sequence (CDS), 3' untranslated region (UTR) and the poly-A tail. From now on it can be directed to cytoplasm for translation to a protein sequence. The 5'UTR contains a Kozak sequence (Kozak, 1987) necessary for the ribosome to initiate translation from the AUG codon. The 3'UTR region is responsible for post-transcriptional modification of mRNA and post-transcriptional gene expression. It contains the signal for polyadenylation and can be a target for miRNA or repressor proteins blocking translation to reduce transcript expression.

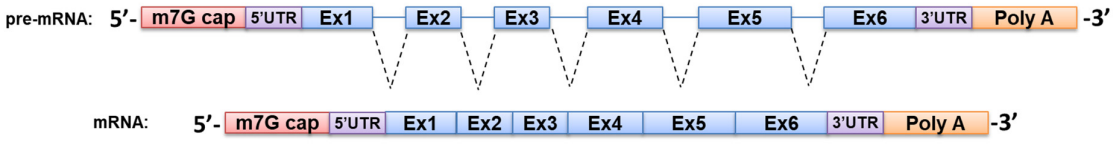

Figure 9 Schematic representation of pre-mRNA and mRNA structure after splicing.

Exons were depicted as solid blue rectangles, introns as the blue horizontal lines. 7-methylguanosine residue cap as a red rectangle and poly-A tail as a yellow rectangle. The UTRs were shown ash violet rectangles. The splicing process was represented by a black dashed line.

1.4.2. Mechanism of pre-mRNA splicing

The pre-mRNA splicing removes non-coding sequences from transcripts, hence is crucial for compacting and maintaining coherency of a coding sequence in mRNA. This is a complicated process that is directed by a complex of proteins called a spliceosome. The spliceosome consists of snRNPs and its assembly is facilitated by a number of non-snRNP that include auxiliary factors and splicing factors. It is also a dynamic complex because it changes its components at different stages of the splicing process. One can distinguish two types of spliceosome: major/U2-dependent and minor/U12-dependent spliceosome. (Patel and Steitz, 2003) The major spliceosome consists of five snRNPs: U1, U2, U4, U5, U6. (Grabowski and Sharp, 1986; Tatei et al., 1984) The minor spliceosome contains five snRNPs: U5, U11, U12, U4atac, and U6atac. (Hall and Padgett, 1996; Tarn and Steitz, 1996) For the scope of this thesis only the major spliceosome process will be discussed.

The key aspect of the pre-mRNA splicing is the recognition of the exon-intron boundaries by snRNPs. (Green, 1991) In the case of introns spliced with the U2-dependent mechanism, the splice sites are defined by conserved sequences: splicing donor site (DS)/5' splice site (5'ss) containing GU nucleotides at the 5'end of an intron, splicing acceptor site (AS)/3'splice site (3'ss) containing the AG nucleotides at the 3'end of the intron, polypyrimidine tract made of C and U nucleotides upstream of the AS and a branchpoint (BP) defined by an A nucleotide and localized 20-40 bp upstream of the AS (Figure 10). (Berg et al., 2002; Breathnach et al., 1978)

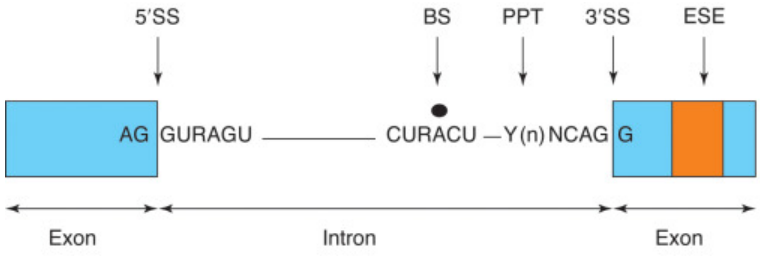

Figure 10 Consensus splice site sequences in a mammalian pre-mRNA.

5'ss- 5' splice site, 3'ss- 3' splice site, BS- branch site, PPT- polypyrimidine tract, ESE- exonic splice enhancer, R- purine, Y- pyrimidine. The graphics was reproduced from (Blencowe, 2000).

The spliceosome assembly takes place immediately after the first exons and introns are synthesized by the polymerase II (Figure 11). Thus the splicing process is performed co-transcriptionally and involves the carboxy-terminal domain of RNA polymerase II (CTD) in the attachment of spliceosome. (Beyer and Osheim, 1988; Khodor et al., 2011)

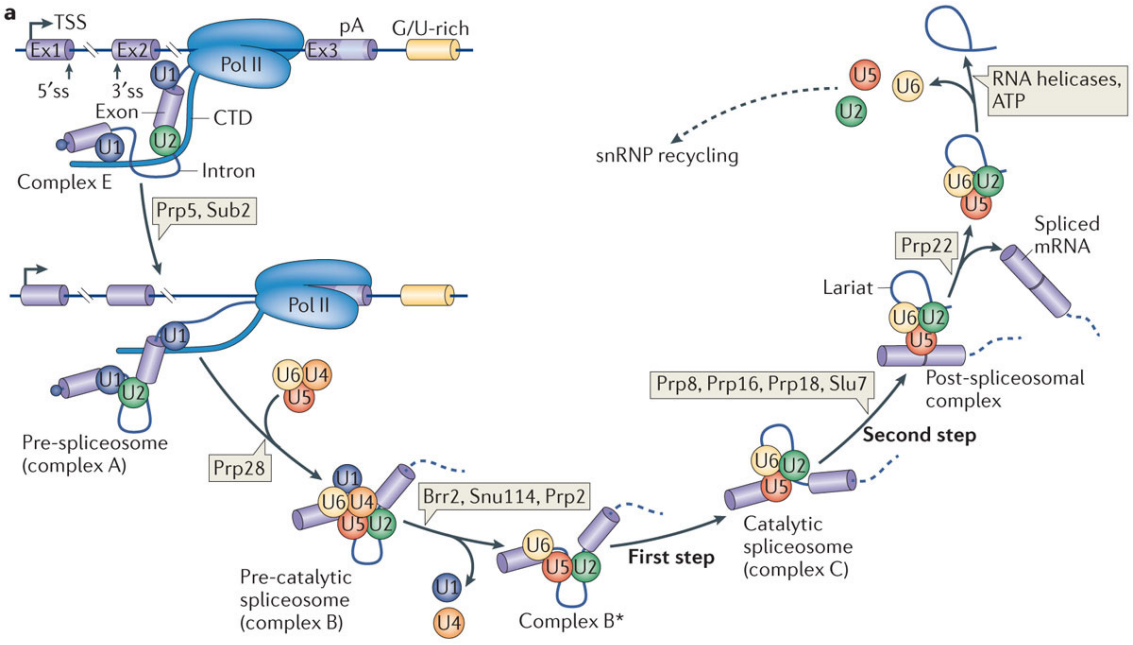

Figure 11 Stages of spliceosome assembly and splicing reaction.

Prp, Brr, Snu, Slu are helicases that support rearrangements and conformational changes of the spliceosome at various stages of splicing. CTD- carboxy-terminal domain of RNA polymerase II. The image was reproduced from (Matera and Wang, 2014).

The U1 snRNP, SF1/BBP, U2AF65 and U2AF35 auxiliary factors recognize and dock on the DS and BP, polypyrimidine tract and AS of newly synthesized RNA respectively (complex E). (Black et al., 1985; Tatei et al., 1984) Afterwards, the SF1/BBP factor is released and replaced by U2 snRNP binding to BP (complex A). The snRNPs interact in order to bring the DS and the BP in proximity forming a pre-spliceosome. Next the U4, U5 and U6 snRNPs are recruited to the spliceosome to form complex B. (Sontheimer and Steitz, 1993; Wassarman and Steitz, 1992) Afterwards the U1 and U4 snRNPs are released and the spliceosome is remodeled to an activated complex B, a catalytic core of spliceosome. (Yean and Lin, 1991) This stage triggers the first transesterification reaction in which the 2'OH group of the adenosine from the BP performs a nucleophilic attack on the phosphate group at the DS (Figure 12). (Padgett et al., 1984) As a result the upstream exon at its 5' site is released and a lariat intermediate is created. (Ruskin et al., 1984) Next, a new rearrangement of the catalytic core of the spliceosome lead to a complex C formation. Subsequently the second transesterification reaction starts in which 3'OH of the upstream exon performs a nucleophilic attack on the phosphate group at the AS (Figure 12). (Padgett et al., 1984) It leads to a scarless joining of spliced exons, removal of the intron for degradation and release of the U2, U5 and U6 snRNPs for another splicing reaction.

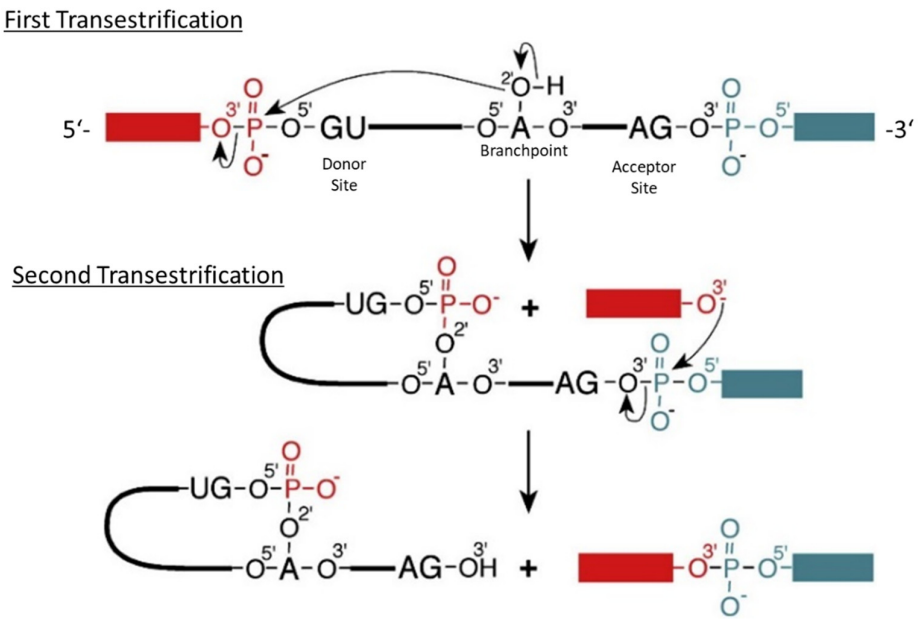

Figure 12 Mechanistic view on RNA splicing and stages of spliceosome assembly.

The left panel represents two transesterification reactions of splicing. The upstream exon is represented in red and the downstream region is represented in blue. The short arrows show the shift of electrons and the large arrows the direction of the nucleophilic substitutions. The figure was adapted from (Sperling et al., 2008) and modified with the labels.

1.4.3. Regulatory elements and proteins of alternative splicing

It was previously described that the splicing process is orchestrated by time-depended interaction of snRNAs, auxiliary factors, splicing factors and helicases. This mechanism, however, is additionally modulated by cis-acting regulatory elements and trans-acting proteins that play a repressing or activating function in splicing. The interaction between these splicing regulatory elements in response to the cell internal and external signals defines the outcome of the pre-mRNA splicing. Thus, the same pre-mRNA molecule can be spliced in various ways in a process known as alternative splicing (Figure 13). The mechanism of alternative splicing allows to produce multiple transcript and finally protein variants from a single gene. It was estimated that 95% of human multi-exonic genes undergo alternative splicing. (Pan et al., 2008), so understanding the principles governing this mechanism is essential for therapeutic approaches targeting pre-mRNA.

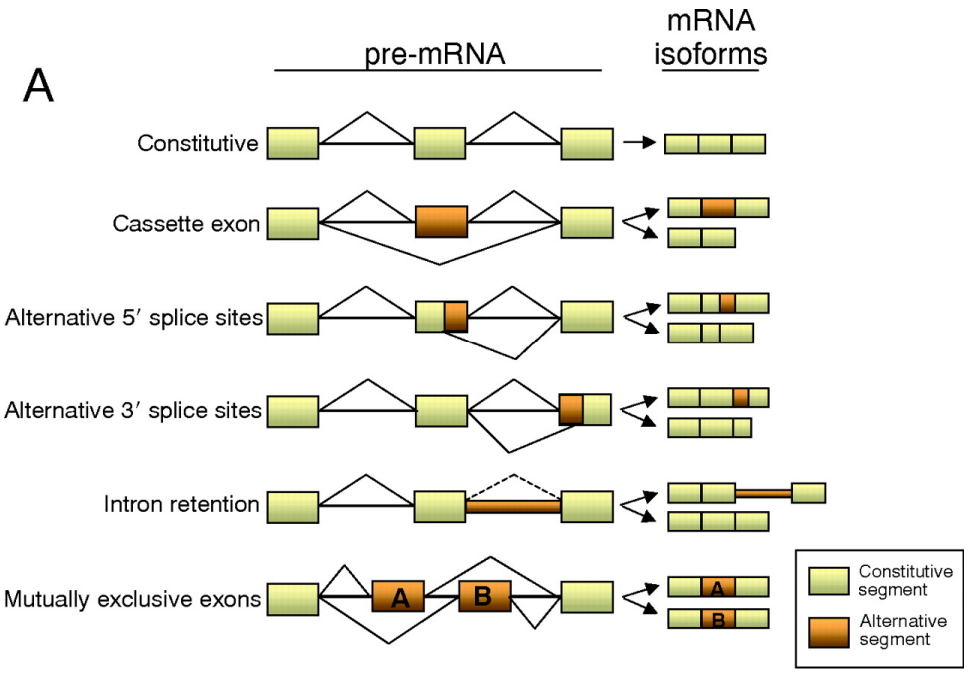

Figure 13 Types of alternative splicing.

Exons are represented as green and brown rectangles and introns are drawn as horizontal black or brown lines. The diagonal lines illustrate the splicing alternatives. The cassette exon refers to exon skipping. The graphics was reproduced from (Srebrow and Kornblihtt, 2006).

The constitutive splicing relays on exon definition by means of conserved sequences of DS, AS, BPS and the association of U1 and U2 snRNPs to these sites during commitment of pre-mRNA to the splicing process. (Robberson et al., 1990) In the alternative splicing the outcome is determined by strength of splice site sequences and fine balance between cis- and trans-acting factors that are location, context and time dependent.

The cis-acting elements are sequences that can play either enhancer or silencer role. Depending if they are found in exon or intron and whether they promote or inhibit exon splicing, they are called exonic splice enhancers (ESEs), exonic splice silencers (ESSs), intronic splice enhancers (ISEs) and intronic splice silencers (ISSs). These sequences are recognized by numerous trans-acting factors that include serine and arginine-rich proteins (SR) or heterogeneous nuclear ribonucleoproteins (hnRNPs). Binding of appropriate factors to an enhancer or silencer sequence forms an intricate splicing code that increases or decreases probability of using a particular splice site by the spliceosome (Figure 14). Consequently, the interaction of cis and trans-factors can activate or repress retention or skipping of an exon or an intron in the final mRNA transcript.

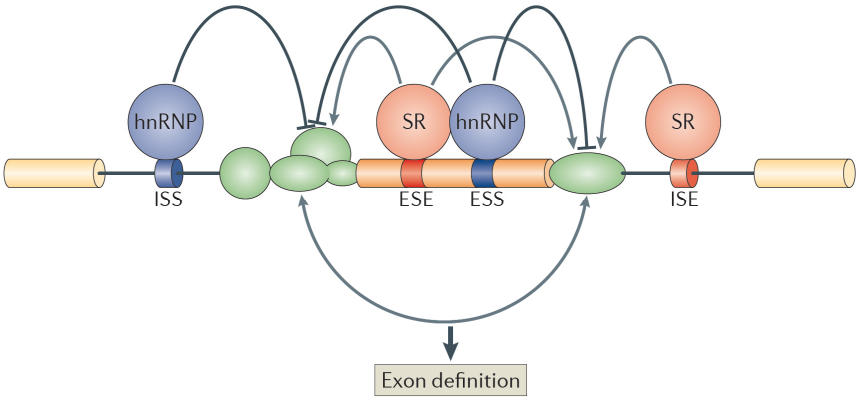

Figure 14 Schematic view on regulatory sequences and factors involved in alternative splicing.

The snRNPs (U1, U2) and splicing factors (U2AF, SF1/BBP) defining the exon are depicted in green. The Ser/Arg-rich proteins are represented in red and hnRNPs in blue. Solid cylinders are exons and introns are black lines. The repressing activity is illustrated by an arrow with a dash and the activator role by an arrow. The image was reproduced from (Kornblihtt et al., 2013).

Serine and arginine rich proteins (SR) are RNA binding proteins (RBPs) that can modulate splicing events in trans. They share a common structure characterized by the arginine and serine rich C-terminal domain (RS) that is responsible for protein-protein and protein-RNA interactions and the N-terminal domain with an RNA recognition motif (RRM) (Figure 15).

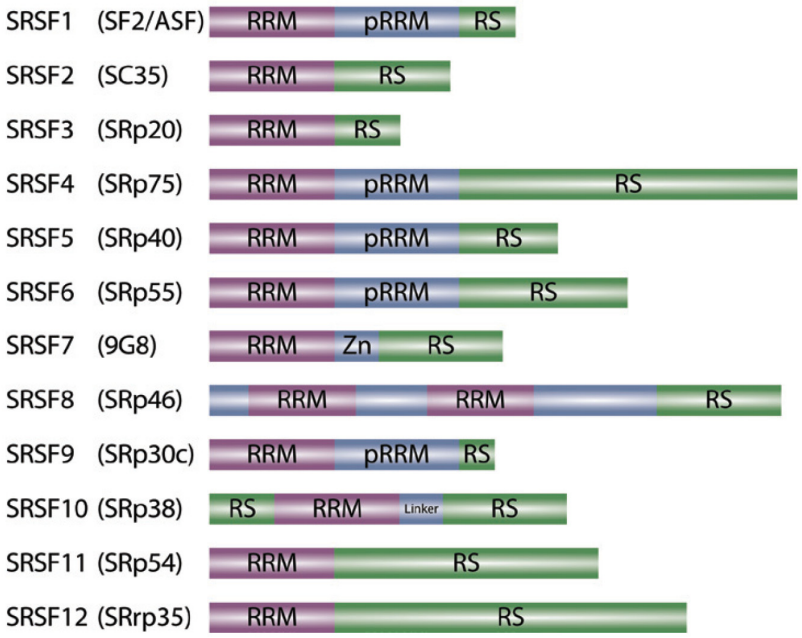

Figure 15 Serine-arginine-rich (SR) proteins and their domain structure.

The first column represents the current nomenclature and the second column the old names. The graphics demonstrates the location of domains in SR-protein: RNA recognition motif (RRM), pseudo RRM domains (pRRM), RS arginine-serine rich domain, Zn- zinc finger domain. The graphics was reproduced from (Mueller and Hertel, 2011).

SR-proteins are recruited co-transcriptionally to pre-mRNA and bind ESEs or ISEs to promote mostly inclusion of an exon in mRNA. They exhibit both specific and degenerate binding profiles. (Listerman et al., 2006) For instance, it was shown that ESEs targeted by SFSR5(SRp40) can be also used by SRSR6(SRp55) but not by SFSR1(SF2/ASF). (Liu et al., 1998a) In the first stage of splicing SR-proteins help recruiting U1 snRNP and U2AF35/65 auxiliary factors to 5'ss and 3'ss respectively (reviewed in (Reed, 1996)). Thus, they contribute to the definition of an exon especially if the constitutive exon definition based on the AS, DS and BP is weak, meaning these sites do not exhibit the conserved sequences. After binding the SR-proteins interact with splicing factors and components of the spliceosome to strengthen the exon definition and facilitate spliceosome assembly (Figure 16). (reviewed in (Mueller and Hertel, 2011))

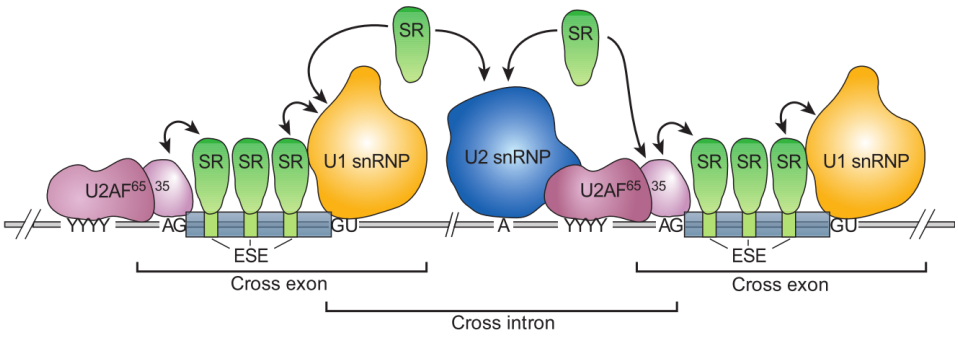

Figure 16 Exon definition.

The SR-proteins attach to ESEs and recruit U2AF and U1 snRNP to the splicing sites to define exons (cross exon definition). Next U2AF65 recruits U2snRNP. The SR-proteins interact with U1, U2 snRNPs and U2AF to define intron (cross intron definition). The graphics was reproduced from (Maniatis and Tasic, 2002).

Although it has been generally considered that the SR-proteins favor exon inclusion, it was also shown that the SR-protein SRSF1(SF2/ASF) can act as both an enhancer or repressor of splicing. Its activity depends if the binding sequence is located in the intronic or exonic region. (Kanopka et al., 1996) Hence, the regulating activity of the trans-acting factor is location dependent.

It was also demonstrated that the activity of SR-proteins can be modified by antagonizing heterogeneous nuclear ribonucleoproteins (hnRNPs) and depends on relative concentration of these factors in specific tissue. The SRSF2(SC35) protein, for instance, is highly dependent on the neighboring trans-acting factors like hnRNP, which is known to promote splicing repression. A ratio between the two factors is essential for the selection of the alternative 5' splice site. In the case of hnRNP excess, a distal 5' splice site is selected and in the case of SRSF2(SC35) excess, the proximal site is favored (Mayeda and Krainer, 1992) Another

example demonstrates that the ratio between SRSF1(SF2/ASF) and hnRNP A1 is responsible for the selection of proximal or distal splice sites in the splicing of exon 3 of human adenylyl cyclase stimulatory G-protein. Interestingly, the splicing outcome was different in HeLa and human myometrial smooth muscle cells This result might be attributed to different ratios of SRSF1(SF2/ASF) and hnRNP A1 in these cells. (Pollard et al., 2002) Yan et al. showed that alternative splicing of human glucocorticoid receptor (GR) exon 9 depends on SRSF5(SRp40) and shifts the balance towards alternatively spliced version that includes exon 9β. Furthermore, they noticed that this effect is cell dependent because it was observable in HeLa but not in 293T cells. (Yan et al., 2010) The tissue dependent effect of SRSF1(SF2/ASF) concentration on splicing of different isoforms of rat 3-tropomyosin pre-mRNA was demonstrated by Caceres et al. in smooth muscle and skeletal muscle tissue. (Caceres et al., 1994) Using a rat model, Hanamura et al. showed that the concentration of antagonistic SRSF1(SF2/ASF) and hnRNP A1 is tissue specific. (Hanamura et al., 1998) Taken together the time- and tissue-dependent concentration of the SR-proteins and hnRNPs is crucial for the outcome of splicing.

hnRNPs are RNA binding proteins and were shown to promote an exon exclusion, which is an antagonistic activity to the SR-proteins like SF2/ASF or SC35. The best described hnRNPs belong the A/B family (e.g. hnRNP A1, hnRNP A2, hnRNP B1). They differ between one another in the RNA binding affinity and their repressing strength on splicing. (Mayeda et al., 1994) The hnRNP A/B have three domains (Figure 17): RNA recognition motif (RRM) for binding to RNA, Arg-Gly-Gly rich domain (RGG box) responsible for RNA binding and glycine rich domain that is an auxiliary domain used for an interaction with other hnRNPs (Geuens et al., 2016)

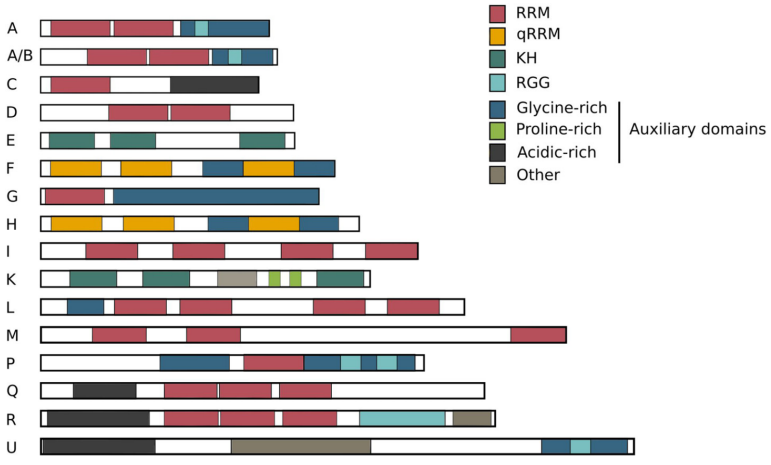

Figure 17 Family of hnRNPs and schematic structure of their domains.

Four RNA binding domains are present in the family of hnRNPs: RNA recognition motif (RRM), quasi-RRM, a glycine- rich domain, Arg-Gly-Gly domain (RGG box) and a KH domain (Geuens et al., 2016)

One model of hnRNP A1 driven exon skipping proposed by Zu et al. is a cooperative propagation along an exon. First, hnRNP A1 attaches to an appropriate ESS and recruits other hnRNPs A1 to the exon displacing the SR-proteins form an ESE (Figure 18). Interestingly, Zu et al. showed that the cooperative propagation of hnRNP A1 can be disrupted by SRSF1(SF2/ASF) but not by SRSF2(SC35). (Zhu et al., 2001)

Figure 18 hnRNP A1 cooperative propagation.

The oval with A1 represents the hnRNP A1 protein. The figure was adapted from (Zhu et al., 2001).

Both SR-proteins and hnRNPs have different modes of interaction among each other. The interaction is context dependent. For instance, two different SR-proteins or hnRNPs can bind neighboring ESE or ESS in a cooperative way, thus enforcing their effect on splicing (Figure 19a). However, binding can be also less specific and in this situation the proteins may compete for the same cis-acting element (Figure 19b). (reviewed in (Fu and Ares Jr., 2014)). The competition between SC35 and ASF/SF2 or between SRp40/SC35 and SRp55 for the same ESE was shown to determine the splicing pattern of both a human growth hormone and a tissue factor. (Chandradas et al., 2010; Solis et al., 2008) A more recent genome wide study of interaction between SRSF1 and SRSF2 proteins showed both competitive and collaborative activity. In the case of a depletion of one of the proteins, a compensatory function of the counterpart was observed. (Pandit et al., 2013) Interestingly, the outcome of the competitive binding depends on the time and concentration of the factors. It is also possible that the speed of transcription may influence which trans-acting factors are going to bind pre-mRNA creating a window of opportunity for their activity (Figure 19c). (reviewed in (Fu and Ares Jr., 2014)).

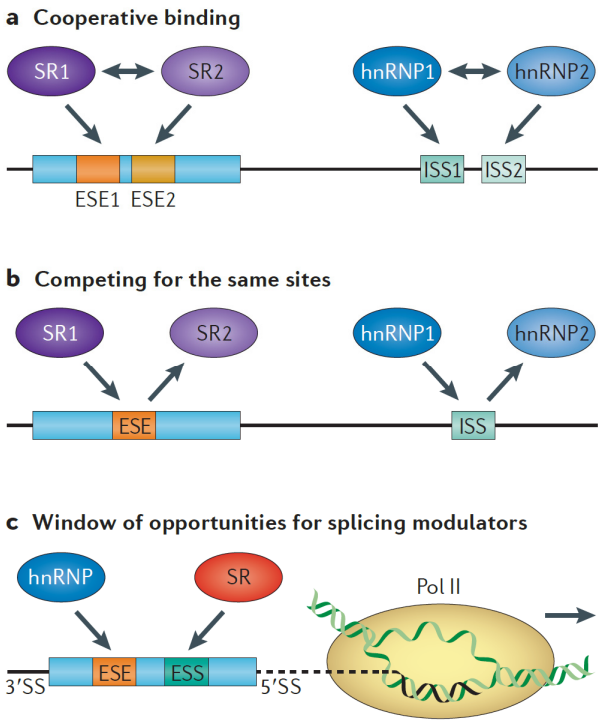

Figure 19 Cooperation and competition of cis-acting factors.

The graphics was reproduced from (Fu and Ares Jr., 2014).

Apart from the regulatory sequences and proteins, the splicing pattern can be also influenced by RNA secondary structure. The mechanism behind this interaction involves either reduction of the distance between cis-acting elements or modification of accessibility to these sequences (Figure 20). (reviewed in (Buratti and Baralle, 2004; Warf and Berglund, 2010))

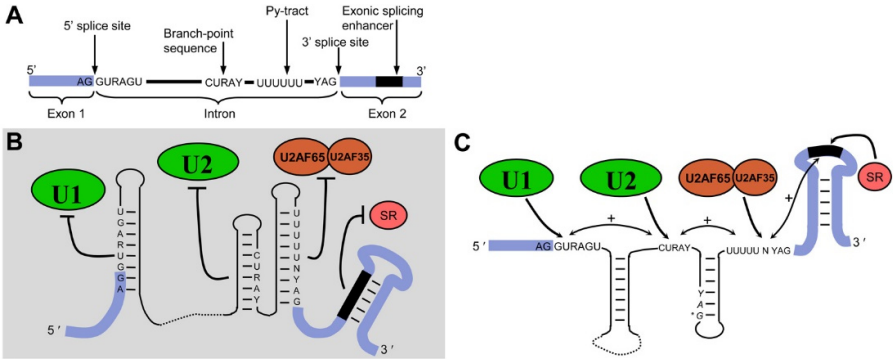

Figure 20 Positive and negative impact of RNA secondary structure on cis- and trans-acting elements.

Panel A depicts the constitutive splicing signals in pre-mRNA. Panel B presents a negative effect of RNA hairpins on accessibility of splice sites, branch point, and polypyrimidine tract for snRNPs and SR-proteins. Panel C shows a positive effect of RNA hairpins that bring the splicing signals closer together, hide cryptic splice site and expose regulatory sequences for trans-acting factors. The graphics was adapted from (Warf and Berglund, 2010)

Also in the case of RNA secondary structure one can speak about competitive activities. The competition takes place between hybridization of complementary sequences inside of RNA and pairing of RNA with snRNPs. Hence, it seems plausible to assume that only the most stable RNA secondary structures will have a modifying effect on the splicing outcome. Three interesting examples provide a good understanding how RNA hairpins can influence alternative splicing. (reviewed in (Buratti and Baralle, 2004)) The actin pre-mRNA of yeast forms a secondary structure in the intron 1-2 in order to hide a cryptic splice site and to bring a BPS closer to a constitutive 3'ss (Figure 21).

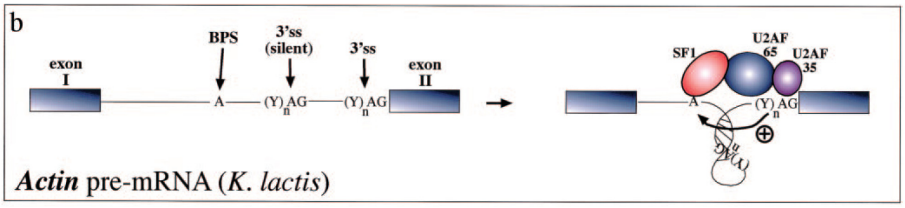

Figure 21 Stem-loop structure in yeast actin pre-mRNA.

The interaction between BPS and 3'ss was shown by an arrow and a plus sign. The graphics was reproduced from (Buratti and Baralle, 2004).

In the case of mouse fibronectin, the EDA exon forms a hairpin in order to expose an ESE on a loop to the SF2/ASF protein, which promotes exon inclusion. A deletion in the region of the secondary structure results in a shift of the ESE into the stem structure making it unavailable for SF2/ASF (Figure 22).

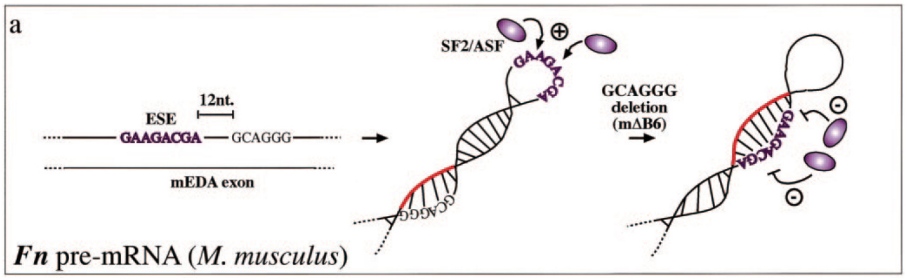

Figure 22 Stem-loop structure in mouse fibronectin pre-mRNA.

The positive interaction was shown by an arrow and a plus sign, negative one by an arrow with a dash and a minus sign. The graphics was reproduced from (Buratti and Baralle, 2004).

In the pre-mRNA of the Tau protein a stem-loop structure at the 5'ss of exon 10 and intron 10-11 decreases the availability of the splice site to the U1 snRNP. (Figure 23) Consequently, the exon 10 is skipped. The mutations that decrease the stability of the hairpin expose 5'ss to U1 snRNP and increase the level of exon inclusion in the transcript which is associated with Parkinson and dementia.

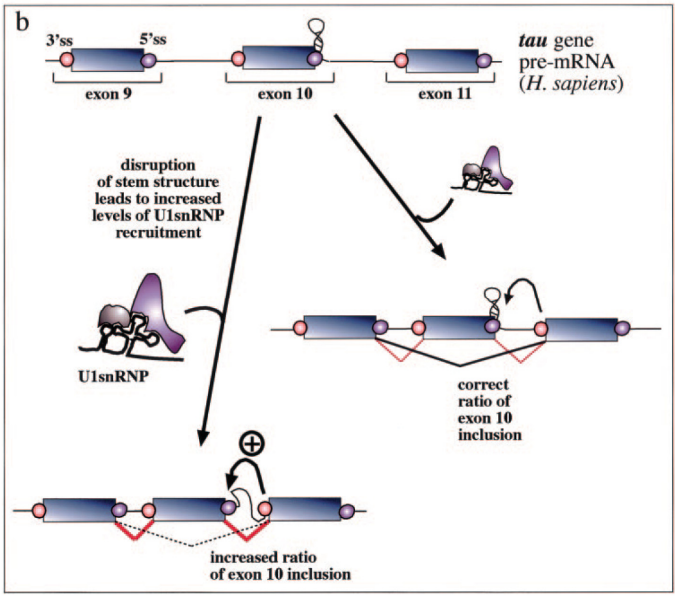

Figure 23 Stem-loop structure in human tau pre-mRNA.

The positive interaction was shown by an arrow and a plus sign and negative one by arrow with a dash and a minus sign. The graphics was reproduced from (Buratti and Baralle, 2004).

1.5. Exon skipping as RNA repair strategy

1.5.1. AON-based exon skipping in pre-mRNA

Antisense-mediated modulation of splicing is a technique that uses short single stranded nucleic acid analogs to change a splicing pattern of pre-mRNA. This splice switching strategy can cause skipping or retention of an exon, use of cryptic splice sites or inclusion of an intron. The technique can be used as a molecular therapy in monogenic diseases to remove mutation carrying exons from pre-mRNA transcripts. Excision of exons leads to production of truncated version of a protein that may exhibit full or partial functionality of the native protein that can ameliorate a phenotype. (Bauman et al., 2009)

Antisense-mediated exon skipping strategy is based on masking of ESE and ISE in order to interfere with the constitutive exon definition forcing the spliceosome to remove a targeted exon together with its neighboring introns. (Aartsma-Rus and van Ommen, 2007; Mann et al., 2001) Short synthetic oligonucleotides are used for masking the trans-acting elements in pre-mRNA. The nucleic acid analogs are capable of hybridizing to RNA following Watson-Crick base paring. There is a range of chemistries available for producing antisense oligonucleotides (AONs): 2' O-methyl RNA, morfolinos (PMO), locked nucleic acid (LNA), peptide nucleic acid (PNA) or tricyclo-DNA (Figure 24). They differ in their binding affinity to RNA, efficiency in penetrating cells, availability and survival in the cell nucleus and production costs. (reviewed in (Havens and Hastings, 2016))

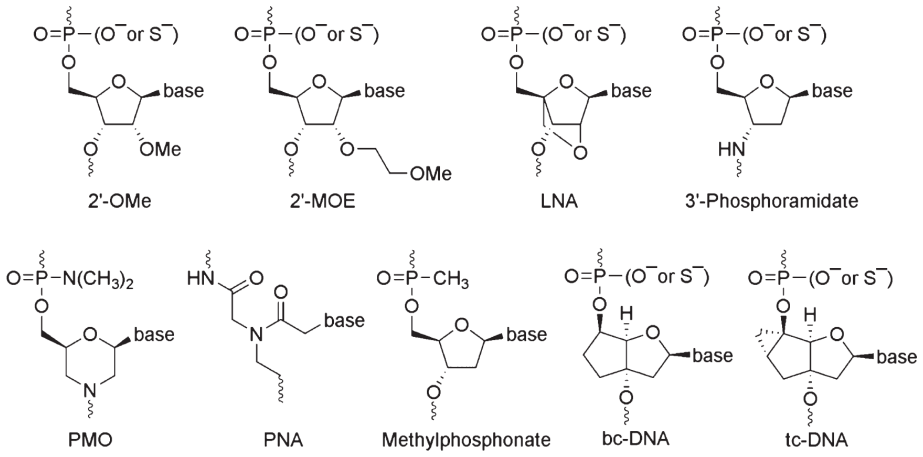

Figure 24 Nucleic acid analogs and their chemical structure.

2'-OMe: 2'-OMethyl, 2'-MOE: 2'OMethoxyethyl, LNA: Locked nucleic acid, PMO: Phosphorodiamidate morpholino oligomer, PNA: Peptide nucleic acid, bc-DNA: Bicyclo-DNA, tc-DNA: Tricyclo-DNA. The graphic was reproduced from (Goyenvalle et al., 2016).

In the in vitro screening experiments of this thesis the 2′-*O*-methyl-modified phosphorothioate RNA was used. The substitution of a sulfur atom in the phosphodiester linkage and addition of a methly group at 2’ position of the ribose in these oligonucleotides offer an improved stability of RNA-AONs complex and higher resistance to endo- and exonucleases in comparison to RNA. (Kurreck, 2003; Stein et al., 1988) Furthermore, these oligonucleotides are characterized by good solubility and easy synthesis. This simplifies handling and decreases experimental costs.

The phosphorothioate-modified 2’OMe oligonucleotide is one of the most widely used chemistries in the antisense research. (Uhlmann et al., 2002) An antisense oligonucleotide with phosphorothioate linkage called Fomivirsen was the first antisense antiviral drug for cytomegalovirus retinitis approved by FDA. (Marwick, 1998) The earliest clinical trials that used 2′-*O*-methyl-modified phosphorothioate oligonucleotides as a splice switching instrument were performed for Duschenne muscular dystrophy (DMD). (van Deutekom et al., 2007; Goemans et al., 2011) Numerous pre-clinical studies in the field of DMD proved the efficacy of skipping mutation-carrying exons of dystrophin pre-mRNA using 2-*O*-methylated and phosphothioated antisense oligonucleotides in vivo in the MDX mouse model (Lu et al., 2003) and in vitro in both MDX myoblasts (Dunckley et al., 1998) and in DMD patient myoblasts. (Aartsma-Rus et al., 2003; van Deutekom et al., 2001)

Antisense-mediated modulation of splicing was also used in the field of dysferlinopathy. The splice switching based approach was used by Aartsma-Rus et al. who was able to trigger skipping of exons 19, 24, 30 and 34 of the human dysferlin pre-mRNA in human primary myoblasts using 2′-*O*-methyl RNA with a phosphorothioate backbone. (Aartsma-Rus et al., 2010a) The information about the secondary structure of dysferlin pre-mRNA and the location of potential ESEs was fed into the design process of the splice switching AONs. The secondary structure of the dysferlin pre-mRNA was predicted by the m-fold algorithm (Zuker, 2003) and the location of the predicted ESEs by the RESCUE-ESE tool (Fairbrother, 2002) was verified with Human Splicing Finder (HSF) (Desmet et al., 2009). Wein et. al managed to skip dysferlin exon 32 in human fibroblast-derived myoblasts using 2′-*O*-methyl RNA with a phosphorothioate backbone. (Wein et al., 2010) Also in this case the rational design of AONs was supported by a bioinformatic analysis performed with HSF and ESEfinder. The skipping of dysferlin exon 32 was further improved by designing an AON which targeted both 3’end of the exon and its donor splice site. (Barthélémy et al., 2015) The splice switching approach was also successfully used to skip dysferlin pseudoexon 44.1 that is included in the mRNA transcripts because of a mutation that leads to creation of a cryptic splice site. Applying HSF and RESCUE-ESE algorithms the AONs were designed in order to mask ESEs in the pseudoexon 44.1 and increase chances of skipping. (Dominov et al., 2014)

1.5.2. U7-based exon skipping in pre-mRNA

Small nuclear RNAs (snRNAs) are short RNA molecules that are associated with ribonucleoproteins localized in the cell nucleus. Small nuclear ribonucleoproteins (snRNP) are involved in pre-mRNA splicing (Lührmann et al., 1990) and pre-mRNA 3'end processing (Krieg and Melton, 1984). One can distinguish two classes of snRNAs in mammalian cells. Highly abundant (10^5-10^6 copies/nucleus) major snRNAs that include U1-U6 and less abundant (10^3-10^4 copies/nucleus) minor snRNAs represented by U7-U12. (Zieve and Sauterer, 1990) The minor snRNAs contain trimethylguanosine 5' caps and can be immunoprecipitated by anti-Sm antibodies. The snRNPs are assembled in the cytoplasm, where snRNA is loaded on snRNP afterwards transported back to the nucleus. (Zieve and Feeney, 1990) The snRNA is associated with a doughnut-shaped multiprotein complex (Sm) consisting of seven proteins B/B', D1, D2, D3, E, F, G. (Kambach et al., 1999; Lerner and Steitz, 1979) These core proteins were called "smith Antigen" (Sm) from the patient's name Stephanie Smith, who was affected by the autoimmune disease systemic lupus erythematosus (SLE) and whose serum antibodies were precipitating the snRNPs core proteins. (Tan and Kunkel, 1966)

The U7 snRNP, a member of minor snRNAs, is involved in the processing of 3'end of histone pre-mRNA. (Galli et al., 1983) The structure and the three functional domains of the U7 snRNA: antisense sequence for binding histone's RNA, Sm-protein binding region and the palindromic region forming stem-loop structure were characterized for both human and mouse species (Figure 25, panel A & B). (Mowry and Steitz, 1987; Soldati and Schümperli, 1988)

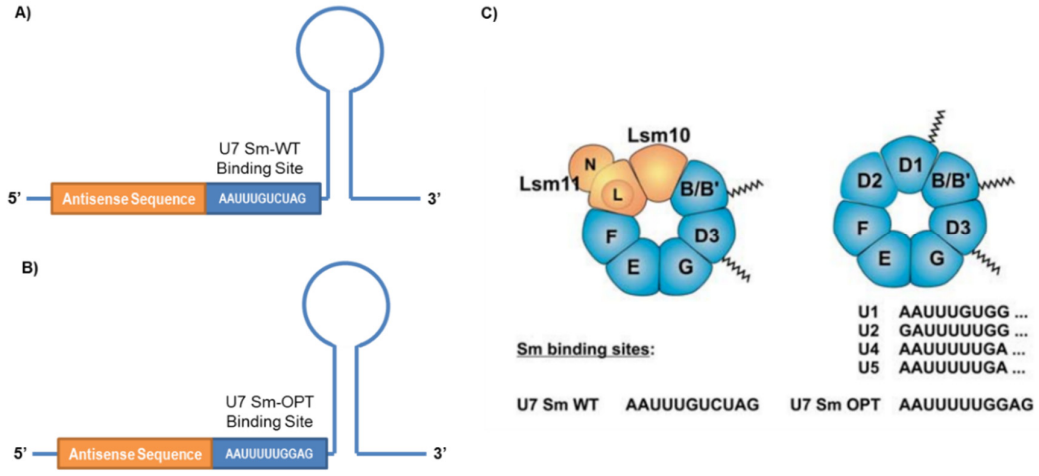

Figure 25 Schematic structure of the U7 snRNA and of the Sm-core protein complex.

Panel A and B is a schematic representation of the U7 snRNA structure with an antisense sequence, the stem-loop structure at the 3'end and the Sm binding site containing the U7 wild type Sm-WT (Panel A) sequence and the canonical Sm-OPT (Panel B) sequence. Panel C represents the seven core proteins constituting the U7 Sm complex with the Lsm10 and 11 proteins and the standard Sm complex with the D1 and D2 proteins. The Sm

binding sequences of U1, U2, U4, U5 were shown to visualize the consensus sequence for the U7 Sm-OPT. The image in panel C was reproduced from Schümperli et al. (Schümperli and Pillai, 2004)

It is worth mentioning that the U7 snRNP Sm core contains the four standard proteins: B/B', E, F, G and two U7 specific peptides known as Sm-like proteins: Lsm10, Lsm11, which replace the D1 and D2 elements from the standard heptamer (Figure 25, panel C). (Pillai et al., 2001, 2003)

It tuned out that the native Sm-protein binding site (5'-AAUUUGUCUAG-3') of the U7 snRNA differs from the consensus sequence (SmOPT: 5'- AAUUUUUGGAG -3') available in the major snRNAs. (Gruber et al., 1991) Furthermore, Grimm et al. showed that the native U7 Sm binding site is the factor that limits the accumulation of U7 snRNP in the nucleus. (Grimm et al., 1993) If the Sm-binding region is completely mutated the U7 snRNP is not enriched in the nucleus. However, if the sequence is replaced with the SmOPT consensus sequence from the major snRNAs then high level of the U7 snRNP is accumulated in the nucleus. (Stefanovic et al., 1995) This discovery was later used for the design of therapeutic U7 molecules.

U7 snRNP recognizes the 3'UTR of histone transcripts trough an antisense sequence embedded in the snRNA. (Müller and Schümperli, 1997; Smith et al., 1991) It was shown that this antisense sequence can be replaced with a sequence recognizing other pre-mRNA transcripts like β-globin or dystrophin (De Angelis et al., 2002; Brun et al., 2003; Gorman et al., 1998; Goyenvalle, 2004) turning the U7 snRNAs into an effective splice-switching instrument (Figure 26).

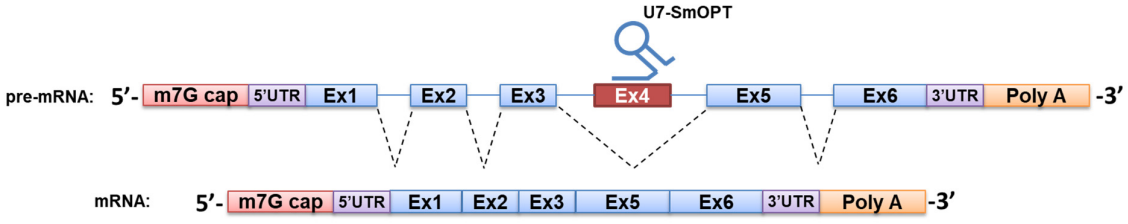

Figure 26 Mode of action of U7 snRNA-based exon skipping.

U7 snRNA contains an antisense sequence specific for exon 4 of a given pre-mRNA. The U7 snRNA masks an ESE leading to splicing modulation and removal of the targeted exon from the mRNA transcript.

The U7-Sm-OPT gene with an appropriate antisense sequence can be delivered into cell where it can be expressed in the nucleus and modulate the splicing of targeted pre-mRNA. A major advantage of U7-based exon skipping over AONs is that the antisense sequence is embedded in the U7 snRNA thus protected from degradation by nucleases. Furthermore, it accumulates in the cell nucleus where splicing takes place and finally the SmOPT modification and the substituted antisense sequence ensure that the U7 snRNP is not processing the

histone pre-mRNA but is used for the splice-switching activity at the targeted pre-mRNA. If U7 snRNAs are delivered via viral vectors one gets a reliable tool for a long term expression of an antisense sequences in the mitotic tissue.

Using U7-SmOPT-based exon skipping and AAV-mediated delivery, Goyenvalle et al. managed to rescue the severe DMD phenotype of dKO mice. A single dose of the U7 constructs packaged in AAV9 and administered via an intravenous injection (i.v.) was enough to restore dystrophin expression in skeletal muscle and heart, improve the muscle histology and function, reduce the CK levels in blood and extend the lifespan of the treated mice. (Goyenvalle et al., 2012) Also improvement of the dystrophic phenotype in skeletal muscle and heart was reported for the golden retriever muscular dystrophy dog (GRMD) model treated with U7-SmOPT constructs which were delivered by either AAV1 or AAV6. (Bish et al., 2012; Vulin et al., 2012)

The U7-strategy can be also modified to create a bifunctional snRNA carrying not only the antisense sequence that targets a specific region of pre-mRNA but also having a nonhybridizing tail with the binding sites for the hnRNPA1 repressor protein. Combined with the lentiviral or AAV delivery this approach improved the level of exon skipping in dystrophin exon 51 both in vitro and in vivo (Goyenvalle et al., 2009). Although, it was demonstrated that the bifunctional U7 snRNA is able to skip exon independently of available ESEs, however, the masking of a potent ESE further improves the overall skipping effect caused by the hnRNPA1.

1.6. Vectors

1.6.1. Adeno-associated virus (AAV)

Adeno-associated virus (AAV) serotype 2 was discovered in 1965 in the negatively stained preparations of simian adenovirus. (ATCHISON et al., 1965) It is a replication-dependent, non-enveloped, single stranded DNA virus belonging to the *Dependovirus* genus of the *Parvoviridae* family. The virus contains ssDNA of either plus or minus polarity that are equally infectious. (Berns and Rose, 1970; Samulski et al., 1987) It has icosahedral capsid of approximately 24 nm that contains viral genome of 4,7kb with two genes rep and cap. (Atchison et al., 1966) They encode four replication proteins: Rep78, Rep68, Rep52, Rep40 (Mendelson et al., 1986), three capsid proteins: VP1, VP2, VP3 (Rose et al., 1971; Srivastava et al., 1983) and one assembly-activating protein (APP) necessary for transport of VP proteins and capsid assembly (Sonntag et al., 2010) (Figure 27). The genome starts and terminates with palindromic sequences called inverted terminal repeat (ITR), which forms a T-like structure (Koczot et al., 1973; Lusby et al., 1980). The ITRs are used for viral replication to prime the leading strand synthesis (Hauswirth and Berns, 1979; LeFebvre and Berns, 1984), for virus encapsidation (Wu et al., 2010), for viral integration (Linden et al., 1996) and finally for virus rescue from a host genome (Hong et al., 1992).

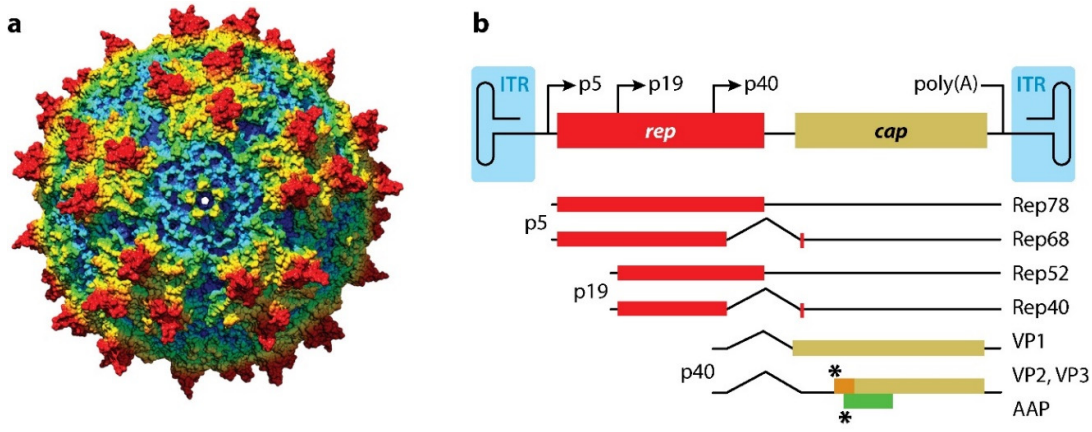

Figure 27 Capsid and genetic map of an AAV.

Panel A represents capsid surface as a depth-cued space-filling model. Amino acids that are close to the core of the virus are colored blue and those farther away are in red. Panel B shows the elements of the AAV genome: ITRs, rep and cap genes and the promoters. Below the genome, three open reading frames (ORFs) coding for 8 proteins were shown. The asterisk represents a weak codon upstream of AUG codon. The orange rectangle is an additional N-Terminal residue included in the VP2 protein and the green rectangle shows the assembly-activating protein (APP) necessary for assembly and maturation of the capsid. The image was reproduced from (Samulski and Muzyczka, 2014).

After infection the AAV virus enters either a lytic cycle or a latent phase. (Handa et al., 1977; Hoggan et al., 1972) The virus follows the lytic cycle if cell is co-infected with a helper virus like adenovirus (Ad) (Parks et al., 1967) or herpes simplex virus (HSV) (Buller et al., 1981). The productive infection can be also triggered in the absence of a helper virus by genotoxic effect like UV irradiation or carcinogens, however, only a small portion of cells (3%) is able to support AAV replication under these conditions (Yakobson et al., 1987; Yalklnoglu et al., 1988). The viral genome is replicated by the single strand displacement mechanism. (Berns, 1990; Egan et al., 1992; Hauswirth and Berns, 1979; Tattersall and Ward, 1976) It was demonstrated that adenovirus provides important early function genes (E1, E4) that enhance this process. (Fisher et al., 1996) If helper virus is not available AAV causes a latent infection and it integrates preferentially into the AAVS1 locus of human chromosome 19 (19q13-qter) (Cheung et al., 1980; Kotin et al., 1990) by replication mediated model (Linden et al., 1996) and remains in the latent phase until an infection with a helper virus takes place. Approximately 0,1% of viral genomes that reach nucleus integrate into AAVS1. (Deyle and Russell, 2009; Hüser et al., 2002)

The virons infect wide range of mammalian dividing (Flotte et al., 1992; Kaplitt et al., 1994; Lebkowski et al., 1988) and nondividing (Flotte et al., 1994) cells. The current research on shows AAV uses a variety of receptors to dock and enter the cell depending on the serotype. (Asokan et al., 2012) The docking on cell surface takes place via heparan sulphate proteoglycans (Summerford and Samulski, 1998) or alpha2,3 and alpha2,6 sialic acids (Wu et al., 2006) and their internalization is supported by co-receptors $\alpha_v\beta_5$ integrin heterodimers (Summerford et al., 1999), fibroblast growth factor receptor type 1 (Qing et al., 1999), platelet-derived growth factor receptor PDGFR-α (Pasquale et al., 2003) or epidermal growth factor receptor (EGFR) (Weller et al., 2010). In 2016 Pillay et al. discovered another transmembrane protein (AAVR) acting as a crucial receptor for the AAV2 infection. The experiments with the AAVR knock-out cell line further proved potent inhibitory effect on infectivity of a broad range of AAVs 1, 2, 3B, 5, 6, 8 and 9. The effect was also observed in the AAVR knock-out mice infected with AAV9. (Pillay et al., 2016) The AAV infection takes place relatively quickly after contact with a cell. The half-time clearance of AAV particles from cell surface was estimated by Bartlett et all. to 8 minutes. (Bartlett et al., 2000) Although, the internalization pathways are still to be elucidated it is already known that one route for the virus entry is receptor-mediated endocytosis leading to the formation of clathrin-coated vesicles. Following endosomal acidification (Douar et al., 2001), the AAV particles are released into the cytoplasm within 30 minutes after the initial infection. Within 2h post infection AAV particles accumulate in the perinuclear region and enter nucleus through the nuclear pore complex (Bartlett et al., 2000)

Although, the data on seroprevalence of IgG against AAV-2 varies between age groups the percentage of seropositive individuals is relatively high in various parts of the world and ranges 40-80%. Using samples from Germany, Switzerland, Japan and Brazil, Erles et al. estimated that 40- 60% of people below age of 40 and over 70% of adults over 59 years of age was exposed to AAV2 virus and carries IgG antibodies against it. (Erles et al., 1999) So far no disease was associated with an infection of AAV, hence AAV is a good candidate for delivery vehicle in gene therapy.

1.6.2. Recombinant adeno-associated virus (rAAV)

The recombinant adeno-associated virus (rAAV) is a modified version of the native AAV. rAAV is also called “gutless” because it does not contain the genes coding for the rep and cap proteins, which prevents it from self-replication (Hermonat and Muzyczka, 1984; Lebkowski et al., 1988; McLaughlin et al., 1988; Samulski et al., 1982, 1989). It carries only a promotor, transgene and a polyA signal cloned between the viral ITRs. The rep and cap genes are provided in trans during the viral production using a tri-transfection method (Xiao et al., 1998). The size of the transgenic constructs including the ITRs should not exceed 5 kbp, otherwise the packaged ssDNA is being truncated and results in heterogeneous size. Wu et al. suggested that the packaging mechanism of AAV introduces the first 5.050 bp from the 3’ end of either plus or minus strand and truncates the genome if it exceeds this size. (Wu et al., 2010)

rAAV maintains its capability of infecting cells, trafficking to nucleus and uncoating, however, its genome is not directed for an integration into the AAVS1 locus. It has been postulated that rAAV integrates at random at a low rates in an nasopharyngeal carcinoma cell (Ponnazhagan et al., 1997) or in immortalized epithelial cell line. (Kearns et al., 1996) The random integrations takes place preferentially in intergenic regions, transcription start sites, CpG islands, DNA palindromes (Inagaki et al., 2007; Kaeppel et al., 2013; Nakai et al., 2003, 2005) and at sites of double-strand DNA breaks via cell own non-homologous end joining repair mechanism (Miller et al., 2003). Recchia et al. demonstrated that the rescue of site specific integrations of rAAV can be achieved both in vitro and in vivo if rep78 protein expression is guaranteed in trans during the infection (Recchia et al., 2004).

The current model of rAAV infection states that the rAAV genome persists in nucleus in circular intermediated which can form larger episomal concatemers. This phenomenon was observed in muscle tissue where circular monomers of rAAV genome were slowly forming multimers larger than 12 kbp within 80 days after intramuscular injection of rAAV2 into C57BL/6 mice. (Duan et al., 1998) Also Vincent-Lacaze et al. confirmed in the in vivo experiments involving

intramuscular injection of rAAV in BALB/c mice that high-molecular-weight concatemers are templates for stable transgene expression in muscle. (Vincent-Lacaze et al., 1999) Both Nakai et al. and Thomas et al. suggest that the concatemerization process most probably starts by recruitment of plus and minus strands of rAAV genomes in order to form linear dsDNA and subsequently circular monomers (Figure 28). (Nakai et al., 2000; Thomas et al., 2004) Next the concatemerization process takes place through intramolecular recombination of independent monomer circular viral genomes and results in large multimers that accumulate over time of 120 days post-infection. (Yang et al., 1999) The concatemerization can, however, start with the synthesis of the complementary strand synthesis because both Zhou et al. and Zhong et al. were able to show that rAAV carrying only a single polarity strand was able to transduce cells in an in vivo and in vivo experiment. (Zhong et al., 2008; Zhou et al., 2008)

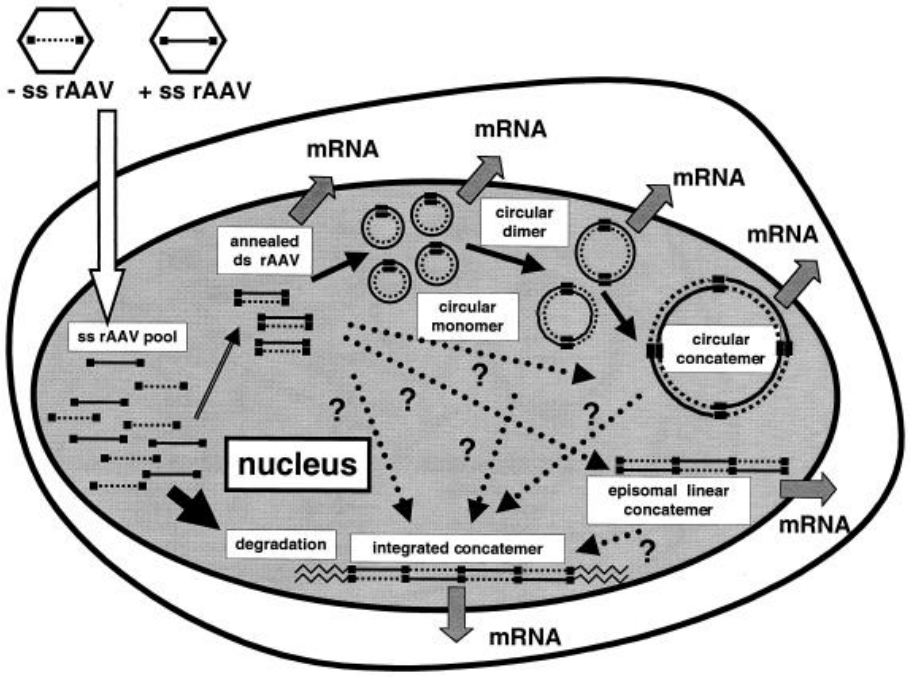

Figure 28 Model of AAV concatemerization and persistence in a transduced nucleus suggested by Nakai et. al.

The scheme was reproduced from (Nakai et al., 2000).

1.6.3. rAAV as a delivery vehicle in skeletal muscle

rAAVs exhibit a very broad tropism depending on the serotype of the virus. For example, rAAV4 and rAAV5 have a superior transduction efficiency for central nervous system over rAAV2 (Davidson et al., 2000). rAAV5 and rAAV6 reach highest transduction rate of lung (Limberis et al., 2009). Gregorevic et al. showed high transduction efficiency of skeletal muscle with AAV6 (Gregorevic et al., 2004), however, later studies demonstrated that rAAV8 and

rAAV9 are the most potent serotypes infecting skeletal muscle and heart tissue after either intramuscular or systemic injections (Inagaki et al., 2006; Wang et al., 2005). Finally the most recent study of AAV mediated gene expression and tissue tropism after systemic injection in mice showed that AAV9 is superior over AAV1-8 for muscle delivery (Figure 29). (Zincarelli et al., 2008)

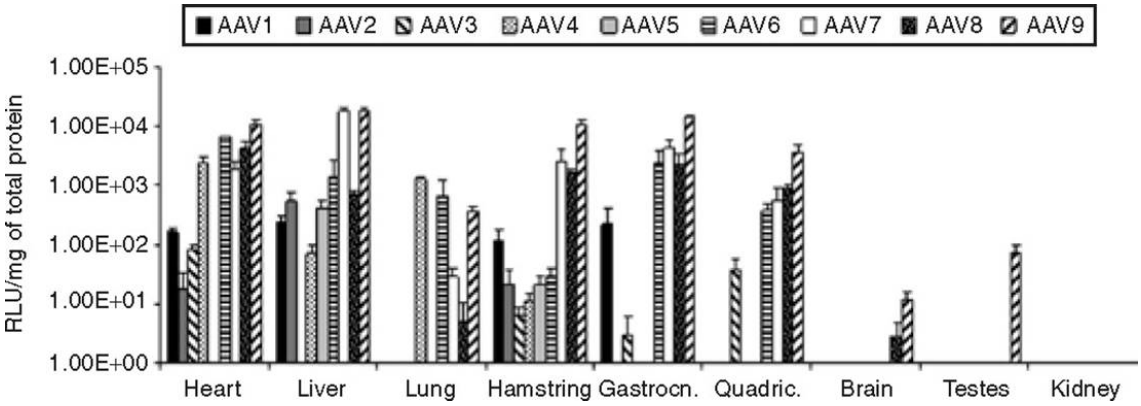

Figure 29 Transduction efficiency of AAV serotypes 1-9 measured by luciferase expression profile in mouse tissues.

The quantification was performed 100 days after an intravenous injection of 10^{11} VG into adult mice. The chart was reproduced from (Zincarelli et al., 2008)

As previously mentioned, rAAV is maintained in episomal form outside the genome of transduced cells. In slowly dividing cells this is a huge advantage because reduces the chances of interference with the host genome. Furthermore, a long term expression of transgenes delivered by rAAV can assured. It has been demonstrated that rAAV can express a transgene in the muscle tissue of healthy immunocompetent mice for 10 months (Kessler et al., 1996), 1 year (Rivière et al., 2006) or even over 1,5 years.(Xiao et al., 1996) The concatemerization, lack of integration and long-term transgene expression (22 months) in skeletal muscle was also observed in nonhuman primates infected with rAAV1 and rAAV8. (Penaud-Budloo et al., 2008) Penaud-Budloo also showed that this high molecular weight concatemers associate with cell histones to form a chromatin like structure. This long persistence was further enhanced by the fact that healthy skeletal muscle is a postmitotic tissue with little turnover rate. However, the episomal nature of rAAV genome can become a significant drawback if mitotically active cells or tissue with high cell turnover is targeted. For instance, the dystrophic muscle usually undergoes a continuous regeneration process in which necrotic fibers are replaced by newly formed myotubes. Pacak et al. demonstrated that intravenous injection of therapeutic vector expressing sarcoglycan in alpha sarcoglycan knockout mice (*sgca*$^{-/-}$) led to prolonged gene expression, reduction of muscle fiber necrosis and lower loss of average AAV genome number over a period of 12 months as compared to

the muscle injected with the beta galactosidase reporter gene. (Pacak et al., 2008) Also Le Hir et al. reported time-dependent loss of the therapeutic effect in dystrophic muscle injected with an AAV delivering U7 snRNA to rescue the mdx or dystrophin/utrophin double-knockout (dKO) phenotype. (Le Hir et al., 2013)

1.6.4. Lentivirus

Lentivirus is a genus of retrovirus family (Retroviridae). (Fauquet et al., 2005) It is an enveloped RNA virus that is able to infect both dividing and non-dividing cells (Naldini et al., 1996). It is characterized by its reverse transcriptase and integrase that are necessary for the reverse transcription of the viral RNA genome into DNA (a provirus form) and integration into the genome of an infected cell. Human (HIV), simian (SIV) or feline (FIV) immunodeficiency virus belong to this family. Since the lentivirus vectors are based on HIV-1 virus I am going to focus on this genus. (Durand and Cimarelli, 2011; Weiss et al., 2006)

HIV genome contains two identical positive-sense ssRNA molecules closed in a conical capsid made of capsid protein p24 (Figure 30). The capsid contains also virus essential proteins integrase, protease and reverse transcriptase. The capsid is surrounded by matrix protein p17 and a lipid bilayer called enveloped. The ssRNAs genome code for three structural genes: group specific antigen (gag), replication proteins (pol) that include reverse transcriptase, protease and integrase, envelope protein (env), two regulatory genes: regulator of expression of virion proteins (rev), HIV transactivator protein (tat) and four accessory genes: vif, vpr, vpu, nef. Furthermore, the genome contains primer binding site (PBS), tat-activation region (tar) and the psi packaging signal (Ψ). The genome is enclosed between two long terminal repeats (LTRs). (Coffin et al., 1997)

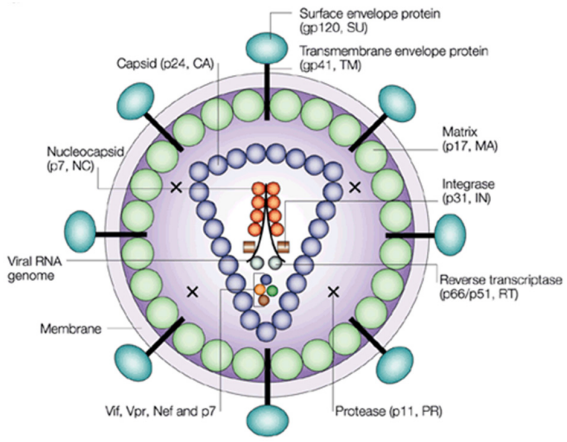

Figure 30 Schematic representation of a HIV-1 particle.

The graphics was reproduced from (Robinson, 2002).

For the purpose of gene transfer, the replication-defective lentiviruses based on the human immunodeficiency virus type HIV-1 were created. Because the HIV-1 is very pathogenic and is categorized as biosafety level 3 hazard it was important to modify the original virus to produce replication incompetent vectors. The safety of these vectors is guaranteed by the physical separation of selected virus coding proteins on different plasmids so called non-overlapping split-genome packaging constructs. This reduces the chances of producing replication competent lentivirus (RCL).

The third generation lentivector system (Figure 31) uses four plasmids delivered in quadritransfection into virus producing HEK 293T cells. (Dull et al., 1998a) The transfer vector (pRRL.SIN) carries the transgene under control of a heterologous promoter and cis-acting elements PBS, Ψ, RRE, the central polypurine tract (cPPT), Woodchuck hepatitis virus posttranscriptional regulatory element (WPRE) enclosed between the LTRs. The WPRE was shown to increase the level of transgene expression in lentivirus system (Zufferey et al., 1999) and cPPT was demonstrated to be essential for transduction of non-dividing cells because of improved nuclear transport of the pre-integration complex (Barry et al., 2001; Zennou et al., 2000). The RRE element is bound by HIV-1 Rev protein and is responsible for nuclear export of RNA transcripts into cytoplasm. (Pollard and Malim, 1998)

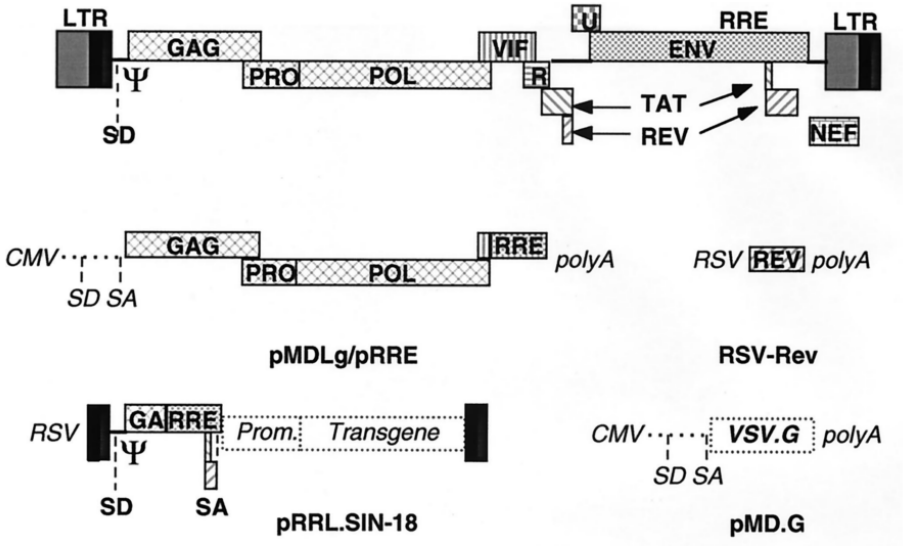

Figure 31 Schematic view on wild type HIV-1 provirus and the 3rd generation lenti vector plasmids.

The scheme at the top represents the genome organization of the wild type HIV-1 provirus. The third generation lentivirus vector system is based non-overlapping split-genome packaging constructs that were depicted below the HIV-1 provirus. The names of the plasmids are written in bold under the cDNA schemes. The 5'LTR depicted on pRRL.SIN-18 plasmid contains a chimeric LTR meaning that the transcription of viral RNA is driven by heterologous promotor from Rous sarcoma virus. CMV- cytomegalovirus promoter, RSV- Rous sarcoma virus promoter, SD- splice donor site, SA- splice acceptor site. The graphics was reproduced from (Dull et al., 1998b). pMDLg/pRRE RSV-Rev pMD.G

The accessory genes vif, vpr, vpu and nef and the regulatory tat gene were removed from the lentivector. The packaging/replication and envelope proteins are delivered on three other plasmids: pMDLg/pRRE, RSV-Rev, pMD.G. This trans-complementation approach assures that the virus can be produced only in cells supplied with the necessary plasmids and the gutless virus delivers only the transgene and is not able to replicate. This approach reduced the chances of reconstituting replication-competent recombinants through the recombination process. (Durand and Cimarelli, 2011; Sakuma et al., 2012)

The system was further improved by creation of self-inactivating vectors (SIN). (Zufferey et al., 1998) The lenti 3'LTR contains both binding sites for host transcription factors and weak promoter region. By introducing a deletion in the U3 region of the 3′ long terminal repeat (LTR) the TATA box and binding site for transcriptional factors Sp1 and NF-κB are removed and the potential transcriptional activity of the LTR is stopped. (Sakuma et al., 2012) Consequently, if RCL is produced the SIN reduces the probability of RCL propagation. This also diminishes the risk that genes of the host genome in the proximity of the integrated transgene will be unintentionally expressed activating for instance protooncogenes. Furthermore, SIN also diminishes the interference between the weak LTR promotor activity with a promotor regulating a transgene.

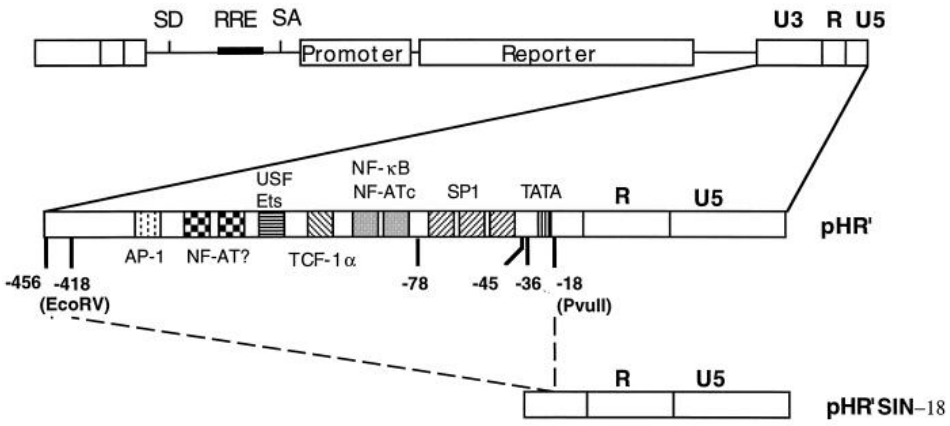

Figure 32 Scheme of SIN HIV-derived vector.

The enlarged 3'LTR of HIV-1 lentiviral vector presents the binding sites for different transcription factors in the region that was removed in a self-inactivating vector (SIN). The graphics was reproduced from (Zufferey et al., 1998)

1.6.5. Lentivirus as a delivery vehicle

The HIV-1 virus targets only cells expressing human CD4 receptor. In order to broaden lentivirus tropism for numerous mammalian tissues pseudotyping with vesicular stomatitis virus G glycoprotein (VSV-G) is used. (Burns et al., 1993) The modified vectors were shown

to transduce liver or muscle tissue in vivo. (Kafri et al., 1997; Seppen et al., 2001) VSV-G was also proved to be effective for transducing both dividing MDX primary myoblasts and terminally differentiated myotubes. (Pichavant and Tremblay, 2012) Additionally, VSV-G-pseudotyped lenti vectors were much stable during centrifugation that allowed achieving higher virus titers during a production process. The payload of a lentivirus based vector is 9–10 kb in total. However, the highest titer is reached for genome size of less than 5kb and the drop of 100 fold in virus titer is observed for genomes between 6-12 kb. (Kumar et al., 2001)

2. AIMS OF THE STUDY

This PhD thesis project had two major objectives. The first one was to develop an exon-skipping-based therapeutic strategy for LGMD2B caused by the homozygous mutation c.4022T>C in exon 38 of the dysferlin gene. The second one was to investigate if the removal of the mutated exon has any detrimental effect on the membrane repair function of dysferlin protein.

The motivation for the project was our access to patients with the described mutation and additionally availability of a corresponding mouse model (MMex38) that could be used for studying the effect of any therapeutic approach in vivo.

3. RESULTS

3.1. Bioinformatic analysis of human dysferlin cDNA

The aim of the bioinformatic analysis was to investigate the secondary structure of RNA around the dysferlin exon 38 and to identify the potential ESE and ESS available in this region. The results of the analysis were used to design the antisense sequences for an exon skipping strategy.

A detailed study of the region around exon 38 of the human dysferlin gene showed that the exon targeted for an excision is surrounded by a very short intron 37-38 of only 118 nt at its 5‘ end and a midsize intron 38-39 of 1.014 nt at its 3’end (Figure 33).

Figure 33 A schematic representation of human dysferlin pre-mRNA from exon 38 to exon 39.

The exons are represented as rectangles and the introns as solid lines. Exons which removal would result in frame shift are depicted as rectangles with sharp ends. The values in italics represent the length of exons and introns expressed as number of nucleotides. An approximate position of the mutation (DYSF p.L1341P, c4022T>C) in exon 38 is marked with the red vertical line and the mutation carrying exon is highlighted in red.

Further investigation of the short distance between exon 37 and 38 was necessary because any possible secondary structure in this area may have had an impact on the feasibility of removing exon 38. Folding of this short intronic sequence produced a stable hairpin secondary structure for both prediction algorithms: minimum free energy structure and centroid secondary structure (Figure 34).

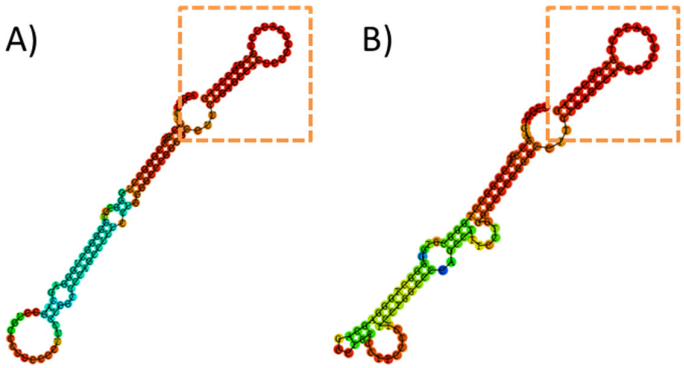

Figure 34 RNA secondary structure predicted for the intron 37-38 of human dysferlin gene.

(**A**) Minimum free energy structure. (**B**) Centroid secondary structure. The hairpin structure was marked by the orange rectangle.

Next I was interested if folding of a larger piece of pre-mRNA which included the human exon 37, intron 37-38 and exon 38 would also reveal a stable hairpin situated at the 3‘ end of the intron 37-38. The result of simulation confirmed that the previously observed hairpin is also detected in the larger piece of analyzed pre-mRNA (Figure 35, left panel). Furthermore, the folding algorithm predicted another hairpin next to the previously detected structure. The two hairpins can further reduce the spatial distance between the exon 37 and 38 (Figure 35, right panel). Consequently, removing both exons simultaneously might be easier than the excision of just exon 38.

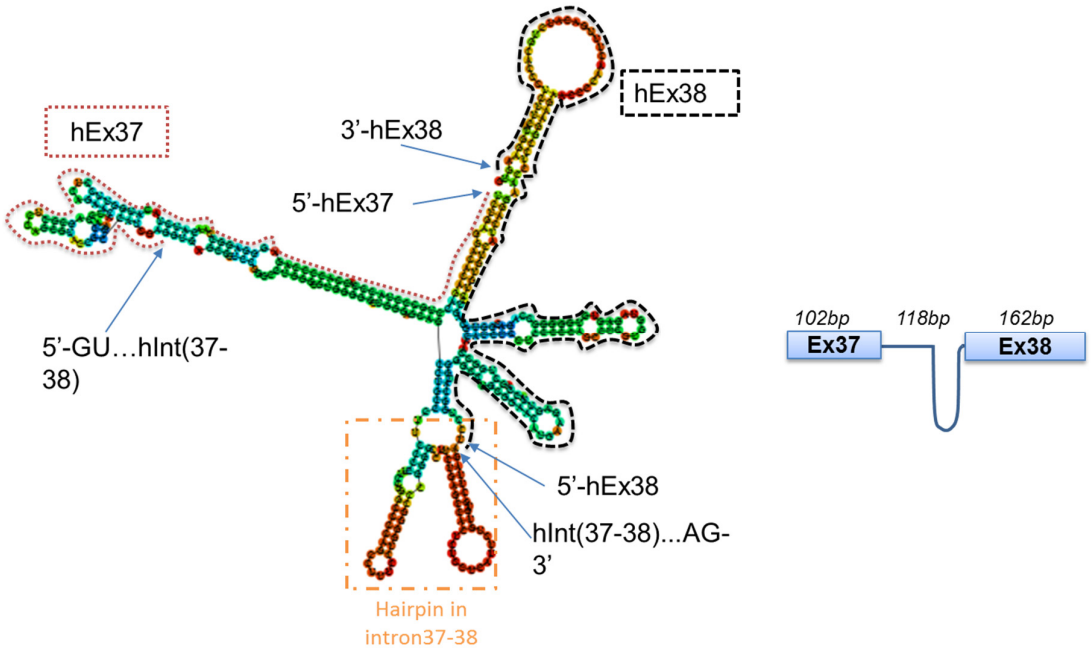

Figure 35 RNA secondary structure of human dysferlin exon 37, intron 37-38, exon 38.

The dotted orange rectangle point out the hairpins formed at the 3‘ end of the intron 37-38. The dotted red and black lines mark the sequences belonging to exon 37 and exon 38 respectively. The beginning and the end of each exon and intron were pinpointed with blue arrows. On the right a schematic representation of possible distance reduction between exon 37 and 38 caused by the predicted secondary structure.

The bioinformatic analysis included also a search for potential ESE and ESS. Exon 37 is very rich in ESEs and they can be grouped into four blocks with visible spatial separations (Figure 36, upper panel). Exon 38 has less ESEs than exon 37. They aggregate into six distinguishable blocks (Figure 36, lower panel).

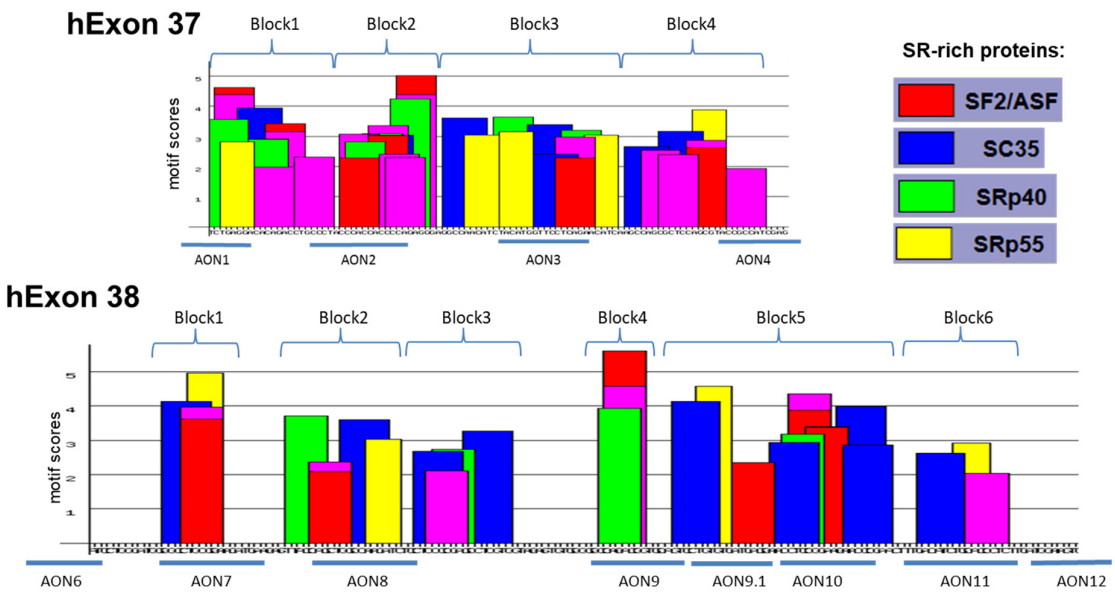

Figure 36 ESEs predicted with ESEfinder for human dysferlin exon 37 and 38.

The X-axis represents the nucleotide sequence of exons and the Y-axis the motif score predicted by the ESEfinder algorithm. The horizontal bares under the sequences represent the localization of AONs that mask ESE in the exons.

In order to skip exon 38 or both exons 37 and 38, I designed thirteen AONs (Figure 36 and Table 4). The proposed AONs covered the largest possible number of ESE-blocks with the highest motif scores estimated by ESEfinder. Furthermore, the AONs were selected in such a way that masking the silencing motifs: hnRNP A1 (Table 2) with scores predicted by Human Splice Finder (HSF) above 75 and the Sironi's motifs (Table 3) with scores above 80 was avoided.

A)

Sequence Position	cDNA Position	Linked Protein Type	Motif	Value 0-100	
4	+4	hnRNP A1	GAGGAC	78.33 (+37.24 %)	⇦
34	+34	hnRNP A1	CAGAGG	70.48 (+14.48 %)	
36	+36	hnRNP A1	GAGGGA	88.57 (+66.90 %)	⇦
40	+40	hnRNP A1	GAGCGC	76.67 (+32.42 %)	⇦
77	+77	hnRNP A1	CAGCGC	67.62 (+6.21 %)	
85	+85	hnRNP A1	CAGCGT	68.57 (+8.97 %)	

B)

Sequence Position	cDNA Position	Linked Protein Type	Motif	Value 0-100	
28	+28	hnRNP A1	AAGAGT	72.38 (+20.00 %)	
71	+71	hnRNP A1	TAGAGT	87.62 (+64.14 %)	⇦
73	+73	hnRNP A1	GAGTGT	72.38 (+20.00 %)	
87	+87	hnRNP A1	GACGGT	68.33 (+8.28 %)	
108	+108	hnRNP A1	CAGGAA	76.43 (+31.73 %)	⇦
153	+153	hnRNP A1	CATGGA	65.48 (+0.00 %)	

Table 2 List of hnRNP A1 motifs predicted by HSF.

The motifs were predicted for A) exon 37 and B) exon38 of human dysferlin. Arrows mark the motifs whose score exceed 75.

A)

Sequence Position	cDNA Position	Sironi's motif	Silencer motif	
+1	Motif 1 - CTAGAGGT	TCTGAGGA	62.94	
+1	Motif 2 - [T/G]G[T/A]GGGG	TCTGAGGA	66.35	
+3	Motif 2 - [T/G]G[T/A]GGGG	TGAGGACA	70.18	
+10	Motif 1 - CTAGAGGT	ACAGACCT	63.97	
+15	Motif 3 - TCTCCCAA	CCTGCCCT	64.26	
+16	Motif 3 - TCTCCCAA	CTGCCCTA	62.15	
+20	Motif 3 - TCTCCCAA	CCTACCCA	71.15	
+21	Motif 3 - TCTCCCAA	CTACCCAC	68.27	
+24	Motif 3 - TCTCCCAA	CCCACCAC	63.64	
+28	Motif 3 - TCTCCCAA	CCACCCCA	73.01	
+29	Motif 3 - TCTCCCAA	CACCCCAG	66.96	
+33	Motif 1 - CTAGAGGT	CCAGAGGG	88.24	⇦
+35	Motif 2 - [T/G]G[T/A]GGGG	AGAGGGAG	79.45	⇦
+37	Motif 1 - CTAGAGGT	AGGGAGGC	68.14	
+37	Motif 2 - [T/G]G[T/A]GGGG	AGGGAGGC	63.88	
+39	Motif 2 - [T/G]G[T/A]GGGG	GGAGGCCA	67.10	
+61	Motif 3 - TCTCCCAA	CCTCAGAA	65.08	
+76	Motif 1 - CTAGAGGT	CCAGCGCT	72.10	
+81	Motif 3 - TCTCCCAA	GCTCCAGC	63.78	

B)

Sequence Position	cDNA Position	Sironi's motif	Silencer motif	
+7	Motif 2 - [T/G]G[T/A]GGGG	GCATGGGG	69.17	
+8	Motif 1 - CTAGAGGT	CATGGGGC	61.17	
+8	Motif 2 - [T/G]G[T/A]GGGG	CATGGGGC	73.38	
+10	Motif 2 - [T/G]G[T/A]GGGG	TGGGGCCT	60.69	
+26	Motif 2 - [T/G]G[T/A]GGGG	TGAAGAGT	65.06	
+27	Motif 1 - CTAGAGGT	GAAGAGTT	75.88	⇦
+32	Motif 3 - TCTCCCAA	GTTACCAG	64.41	
+38	Motif 2 - [T/G]G[T/A]GGGG	AGCTGGCC	62.80	
+50	Motif 3 - TCTCCCAA	TCTCCTCC	73.67	
+53	Motif 3 - TCTCCCAA	CCTCCCCC	85.05	⇦
+54	Motif 3 - TCTCCCAA	CTCCCCCA	60.45	
+55	Motif 3 - TCTCCCAA	TCCCCCAG	86.22	⇦
+64	Motif 1 - CTAGAGGT	CTCGTGGT	68.80	
+66	Motif 2 - [T/G]G[T/A]GGGG	CGTGGTAG	62.55	
+69	Motif 2 - [T/G]G[T/A]GGGG	GGTAGAGT	65.03	
+70	Motif 1 - CTAGAGGT	GTAGAGTG	68.59	
+72	Motif 2 - [T/G]G[T/A]GGGG	AGAGTGTG	61.32	
+74	Motif 2 - [T/G]G[T/A]GGGG	AGTGTGGG	76.43	⇦
+76	Motif 2 - [T/G]G[T/A]GGGG	TGTGGGGG	100.16	⇦
+77	Motif 2 - [T/G]G[T/A]GGGG	GTGGGGGC	67.64	
+78	Motif 2 - [T/G]G[T/A]GGGG	TGGGGGCC	77.59	⇦
+84	Motif 1 - CTAGAGGT	CCAGACGG	71.33	
+86	Motif 2 - [T/G]G[T/A]GGGG	AGACGGTG	63.07	
+90	Motif 2 - [T/G]G[T/A]GGGG	GGTGCAGT	63.28	
+114	Motif 3 - TCTCCCAA	CCTCCGGA	68.65	
+124	Motif 3 - TCTCCCAA	AACCCCAA	67.83	
+125	Motif 3 - TCTCCCAA	ACCCCAAC	60.79	
+143	Motif 3 - TCTCCCAA	GCACCCTC	69.84	
+152	Motif 2 - [T/G]G[T/A]GGGG	TCATGGAA	61.41	
+154	Motif 1 - CTAGAGGT	ATGGAAGT	60.67	

Table 3 List of Sironi's motifs predicted by HSF.

The motifs were predicted for A) exon 37 and B) exon38 of human dysferlin. Arrows mark the motifs whose score exceed 75.

Additionally, AON1, AON6 and AON2, AON12 were designed to mask intronic acceptor and donor splice sites. All antisense sequences were analyzed for their secondary structure using the RNAfold algorithm. Only oligonucleotides that didn't create energetically stable hairpin were selected as candidates for an experimental validation (Table 4, last column).

Exon	Name	Target 5' -3'	AON sequence 5'-3'	Length	Secondary Structure
37	AON1 (Acceptor site, -7,+8)	actgcagTCTGAGGA	TCCTCAGACTGCAGT	15	
37	AON2 (+18,+35)	GCCCTACCCACCACCCCA	TGGGGTGGTGGGTAGGGC	18	
37	AON3 (+51,+68)	CTACATGGTTCCTCAGAA	TTCTGAGGAACCATGTAG	18	
37	AON4 (Donor Site, +91,-3)	ACCGCCATCGAGgtg	CACCTCGATGGCGGT	15	
Intron 37-38	AON(37-38)_1 (+22,+36)	GTGGGGGCTGGGAGC	GCTCCCAGCCCCCAC	15	
38	AON6 (Acceptor site, -16,+2)	cattctgtgtgcttagAT	ATctaagcacacagaatg	18	
38	AON7 (+12,+29)	GGGCCTGCGGAACATGAA	TTCATGTTCCGCAGGCCC	18	
38	AON8 (+36,+53)	CCAGCTGGCCAACATCTC	GAGATGTTGGCCAGCTGG	18	
38	AON9 (+81,+95)	GGGCCAGACGGTGCA	TGCACCGTCTGGCCC	15	
38	AON9.1 (+95,+110)	GTCCTGTGTCATCAG	CTGATGACACAGGAC	15	
38	AON10 (+112,+126)	AACCTCCGGAAGAAC	GTTCTTCCGGAGGTT	15	
38	AON11 (+133,+150)	TTTGACATCTGCACCCTC	GAGGGTGCAGATGTCAAA	18	
38	AON12 (Donor site, +152,-7)	TCATGGAAGTGgtgagcc	ggctcacCACTTCCATGA	18	

Table 4 The list of designed AONs and their targets in human dysferlin pre-mRNA.

The position of AONs was defined by a start and an end nucleotide position relative to the first nucleotide of the targeted exon. Small letters in AONs sequence depict parts of AONs that cover the intronic sequence whereas capital letters the exonic sequence. The length of AONs is expressed in nt and the results of secondary structure analysis are presented as pictures in the last column.

The short intron 37-38 was also investigated for potential targets that could be used in the exon skipping strategy. Sasaki-Haraguchi et al. showed that ultra-short introns (<65nt) contain the G-rich intronic sequence: CAGGGGCTGGG which is enhancing the intron splicing. (Sasaki-Haraguchi et al., 2012) It has been also reported that GGGGCUG, (A/U)GGG, GGG and GGGG sequence functions as intronic splice enhancers (ISEs) and facilitate inclusion of exons following these sequences. (Carlo et al., 1996; Sirand-Pugnet et al., 1995) Although the human dysferlin intron 37-38, which is 118nt long, doesn't belong to the group of ultra-short introns, however, I was able to find the major part (GGGGCTGGG) of the G-rich intronic sequence that was studied by Sasaki-Haraguchi et al. in the intron 37-38 (Figure 37). Consequently, I designed AON5 to block this ESS and hopefully to force skipping of both exon 37 and 38 as one large exon.

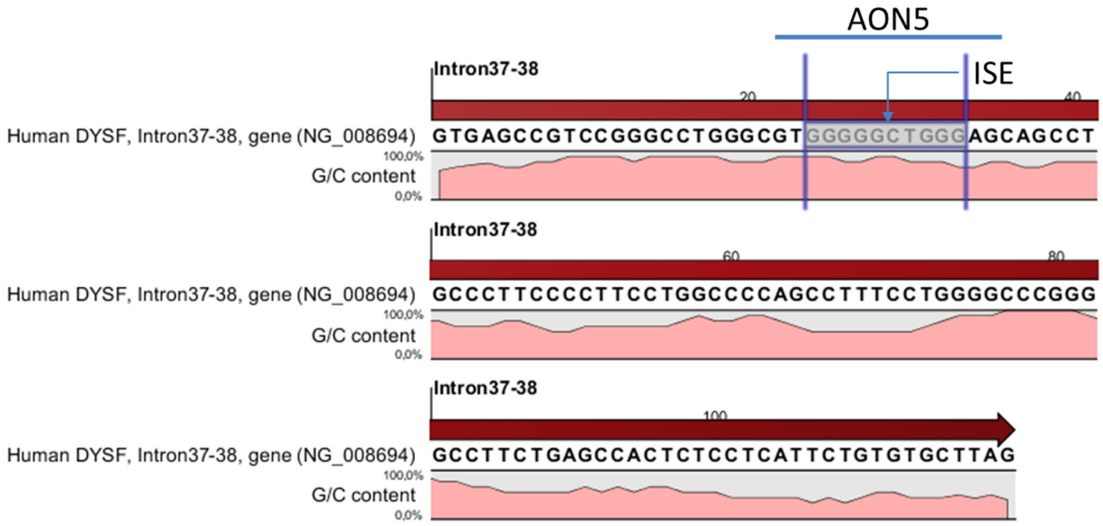

Figure 37 Sequence of intron 37-38, G/C content and the position of AON5 masking ISE.

The ISE in the intron 37-38 of human dysferlin pre-mRNA was highlighted. The level of GC is represented in the plot below the intronic sequence. The AON5 position is marked by the blue horizontal line.

3.2. In vitro exon skipping using AONs in human immortal myoblasts

Human immortalized myoblasts c25 (Mamchaoui et al., 2011) that were derived from a 25-year-old healthy donor were used for the screening of 12 AONs designed to skip exon 38 of human dysferlin gene. For this purpose, the myoblasts were transfected with the AON using lipofectamin LTX and next they were differentiated into myotubes. After 3 days of differentiation the exon skipping effect was detected using RT-PCR and visualized on an agarose gel (Figure 38). The AON4, masking 3'end of exon 37 and the donor site of intron 37-38 triggered skipping of exon 37, whereas AON6, AON7, AON9 and AON12 skipped exon 38. The level of skipping was between 2,7% and 13,8%.

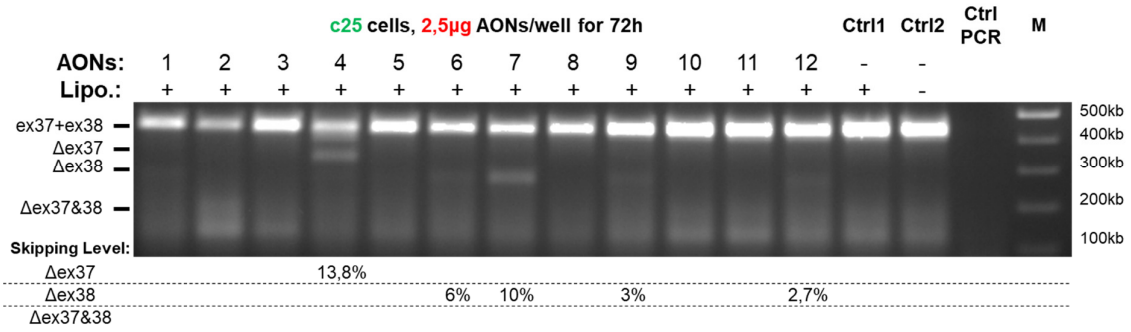

Figure 38 Detection of exon skipping using RT-PCR in c25 cell treated with 2,5 µg of 2'OMe AONs.

Results of the RT-PCR for the dysferlin mRNA region spanning the exons 36, 37, 38 and 39. The cells were transfected using lipofectamin LTX reagent. Lanes 1-12 represent AONs treatments, lanes 13 and 14 are negative controls, lane 15 is a water control for the RT-PCR and lane 16 is a ladder.

The increase of the AON dose to 5 µg increased also the skipping effect in the case of AON4, AON5 and AON7 reaching the level between 14% and 23% (Figure 39). The AON9 and AON12 improved the skipping performance only minimally by 1-2 percentage points.

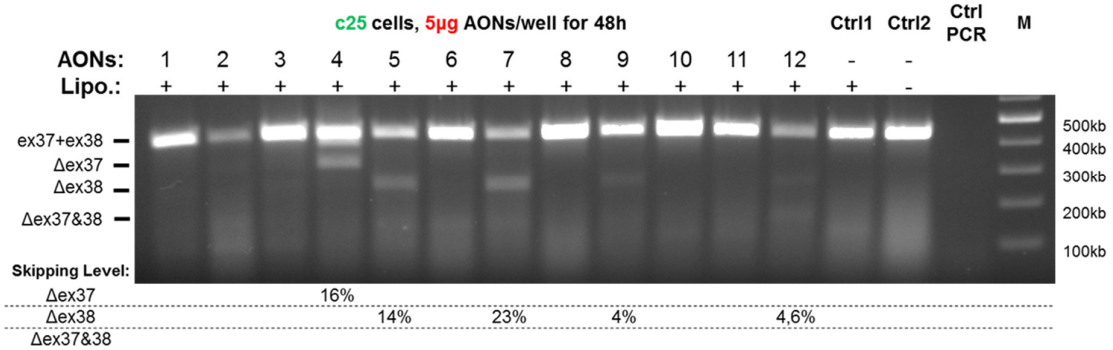

Figure 39 Detection of exon skipping using RT-PCR in c25 cell treated with 5 µg of 2'OMe AONs.

Results of RT-PCR for the dysferlin mRNA region spanning the exons 36, 37, 38 and 39. The cells were transfected using lipofectamin LTX reagent. Lanes 1-12 represent AONs treatments, lanes 13 and 14 are negative controls, lane 15 is a water control for the RT-PCR and lane 16 is a ladder.

The AONs were also screened for exon skipping in immortalized human myoblasts (i814) (Philippi et al., 2012) which were derived from a 60-year-old patient carrying the investigated homozygous mutation (DYSF p.L1341P, c4022T>C) in exon 38 of the dysferlin gene. The myoblasts were transfected with 2,5µg of AONs using lipofectamin LTX and next they were differentiated into myotubes. After 3 days of differentiation the exon skipping effect was detected using RT-PCR and visualized on an agarose gel (Figure 40). In the case of i814 cells the AON4 skipped the exon 37 and AONs 5, 6, 7, 9, 9.1 and 12 skipped the exon 38.

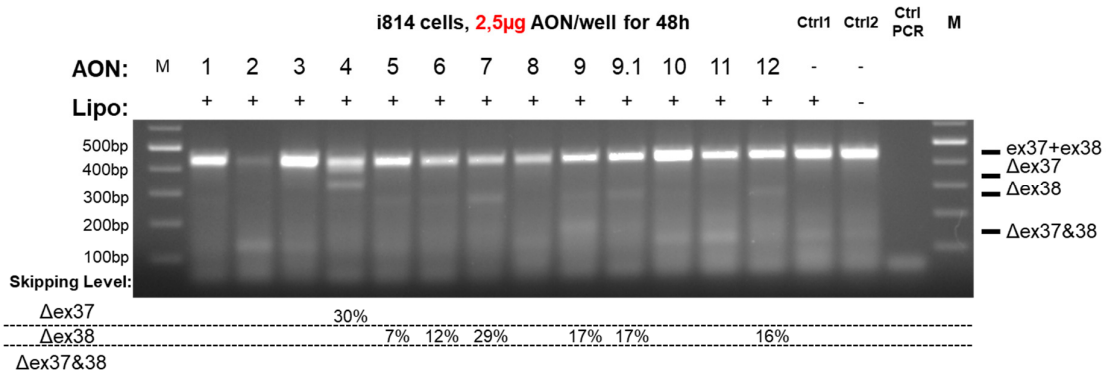

Figure 40 Detection of exon skipping using RT-PCR in i814 cells treated with 2,5 µg of 2'OMe AONs.

Results of RT-PCR for the dysferlin mRNA region spanning the exons 36, 37, 38 and 39. The cells were transfected using lipofectamin LTX reagent. Lanes 2-14 represent AONs treatments, lanes 15 and 16 are negative controls, lane 17 is a water control for the RT-PCR and lane 18 is a ladder.

3.3. In vivo exon skipping using AON

Based on the screening of AONs in c25 and i814 cells I decided to study the exon skipping effect in vivo in WT BL10 mice. For this purpose, five best performing AONs from the in vitro study were selected. They included AON4, AON7, AON9, AON9.1 and AON12. Their distribution over human dysferlin pre-mRNA was represented in the Figure 41.

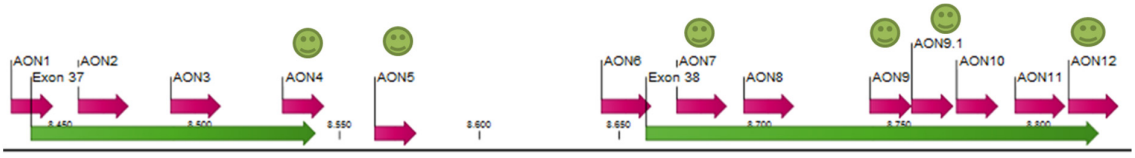

Figure 41 Diagram representing distribution of AON covering exon 37, intron 37-38 and exon 38 of human dysferlin pre-mRNA.

The AONs are represented by the red and exons by the green arrows. The green smiles mark the AONs that successfully triggered exon skipping in the in vitro test.

The AONs that were tested in the in vitro phase of the project were designed for the human dysferlin sequence. Hence, it was necessary to perform a comparative study of human and mouse dysferlin in order to find out which of the successful AONs could be directly used in an vivo experiment. The mouse dysferlin sequence in comparison to human has only minor nucleotide differences within the exons 37 and 38. There are 13 mismatches in exon 37 and 16 mismatches in exon 38. (Figure 42) The substitutions of cytosine to thymine are negligible because during the transcription to pre-mRNA thymine is converted to uracil that can base pair with both A and G from AONs. This alternative base paring was described as the wobble hypothesis by Crick in 1966. (Crick, 1966) Consequently, exon 37 differs only in 6 nt and exon 38 in 10 nt.

Figure 42 Sequence alignment of exon 37 and 38 of the human and mouse dysferlin gene.

The mismatches are highlighted in pink and the matching nucleotides are represented as dots in the lower sequence. The yellow bar chart represents the level of conservation across the sequence.

The mouse intron 37-38, however, exhibits a smaller degree of homology to the human one because it is shorter by 21 nt and has 32 mismatching nucleotides. Hence, the mouse intron 37-38 is identical in 67% with the respective human intron. The base-by-base comparison of the introns was represented in the Figure 43.

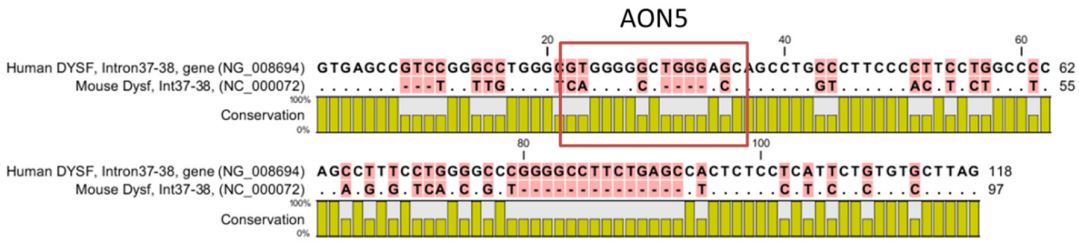

Figure 43 Sequence alignment of human and mouse dysferlin intron 37-38.

The mismatches are highlighted in pink and the matching nucleotides are represented as dots in the lower sequence, the sequence gaps as dashes. The yellow bar chart represents the level of conservation across the sequence. The red rectangle shows the position of AON5.

In order to perform exon skipping experiment in vivo using the AONs tested in the human immortalized myoblasts it was necessary to verify sequence compatibility between AONs designed for human and their targets in the mouse mRNA. The sequences of the best in vitro performing AONs: 4, 5, 7, 9, and 12 were analyzed to predict if they can be used in the in vivo mouse experiment (Figure 44).

The target of AON4 has two mismatches in the mouse pre-mRNA. The human sequence contains two cytosine bases whereas the mouse sequence has two uracil bases at the positions 3 and 9. This discrepancy, however, should not hinder AON4 from binding its target because both cytosine and uracil are able to base pair with guanine available at the corresponding positions in the antisense sequence. The comparison of the intronic target of AON5 showed too many differences between the species and the antisense sequence had to be excluded for the in vivo experiments. The target for AON7 is exactly the same in both species. The targeted mouse sequence for AON9 has 3 mismatches and none of them is capable of wobble base pairing, hence, this oligonucleotide was disqualified from the in vivo experiment. In exchange, a mouse specific sequence called AON9m was used. Finally, the AON12 targeted the same sequence in both mouse and human pre-mRNA. Additionally, AON9.1 was added for a test in the mouse model in order to mask the ESEs at the beginning of the block 5 in exon 38 (Figure 36).

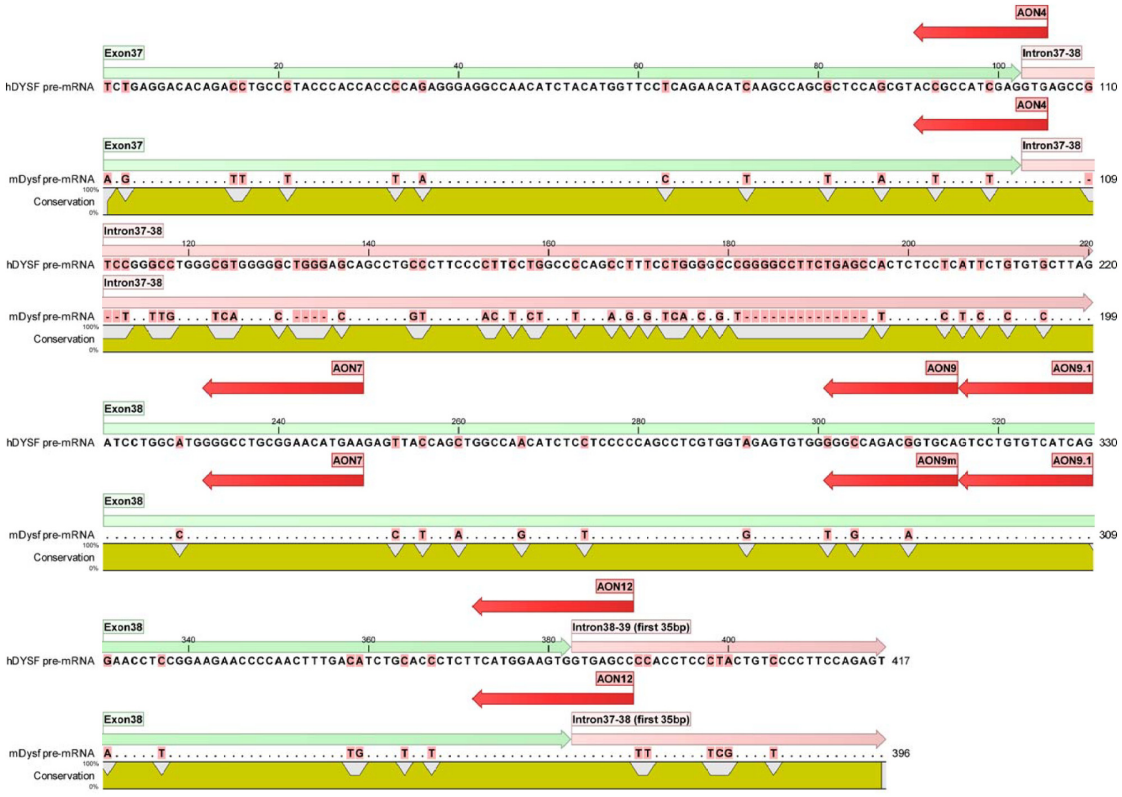

Figure 44 Alignment of human and mouse dysferlin exon 37, intron 37-38 and exon 38 and localization of AONs selected for the in vivo test.

The mismatching nucleotides are highlighted in pink and the gaps in sequence are marked with a dash '-'. The level of conservation between the human and mouse sequence is represented by the graph below the alignment.

The in vivo exon skipping experiment was performed in 5-week-old BL10 WT mice. 30µg of AONs: 4/7/9m/9.1/12 were injected intramuscularly into tibialis anterior (TA). For every AON three biological repeats were done and the animals were sacrificed three weeks after the injection. The exon skipping was detected by means of reverse transcription and nested PCR (Figure 45). The band at 750bp corresponds to the full dysferlin transcript and the band at 486 bp represents the mRNA without exons 37 and 38. The skipping results are ambiguous because PBS control samples contain very thin bands around 486 bp. Hence, one cannot tell if the thin bands visible at 486 bp in the AON7, AON9.1 and AON12 represent skipped product. The bands at 486 bp are not visible in the tcDNA negative control. The tcDNA is a synthetic analog of DNA that was designed to skip exon 51 of the human dystrophin gene.

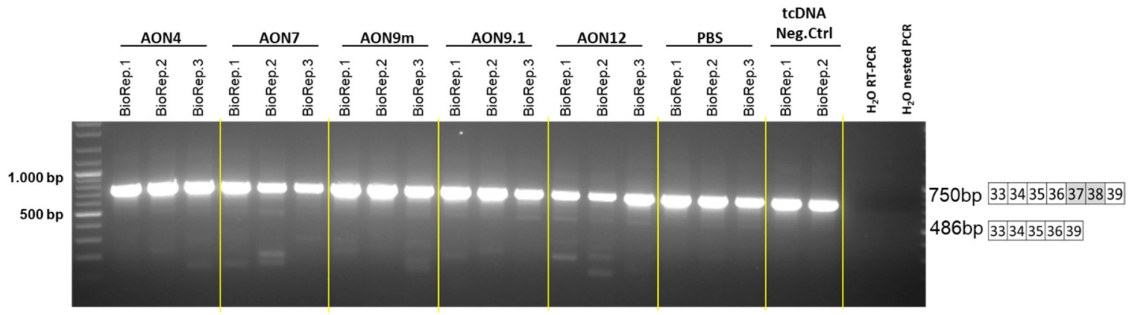

Figure 45 Detection of exon skipping in dysferlin pre-mRNA in vivo using 2'OMe AONs.

Results of RT-PCR and nested PCR for the dysferlin mRNA spanning the region between exon 33 and 39. The transcript expression was detected in the TA muscle of BL10 WT mice after intramuscular administration of 30µg of 2'OMe AON. Lanes 2-15 represent treatment with the mU7 constructs, lanes 16-18 are a PBS negative control, lanes 19-20 are tcDNA negative control, lane 21 is a water control for the RT-PCR and lane 22 is a water control for the nested PCR, lane 1 is ladder.

3.4. In vivo exon skipping using U7 small nuclear RNA.

In order to skip mouse exon 38 in dysferlin pre-mRNA twelve long antisense sequences that span the targeted exon were designed (Figure 46). Their secondary structure was modeled in RNAfold in order to exclude these antisense sequences that had high probability of forming a hairpin (Table 5, last column).

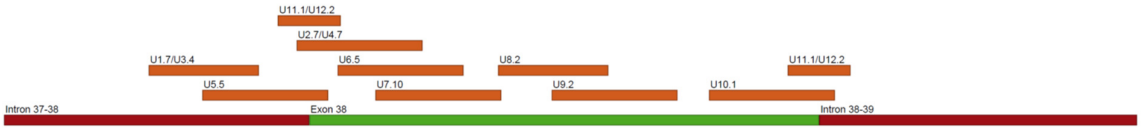

Figure 46 Antisense sequences of U7 constructs mapped on the intron 37-38, exon 38 and intron38-39 of mouse dysferlin pre-mRNA.

Introns are represented by red and exons by green solid lines. U7 constructs are shown in orange.

Seven antisense sequences (U2.7, U4.7, U6.5, U7.10, U8.2, U9.2 and U10.1) covered almost the whole exon 38. Additionally, three sequences (U1.7, U3.4, U5.5) were targeting the branching point in the intron 37-38. Five sequences (U2.7, U4.7, U5.5) were masking the acceptor site of intron 37-38 and one (U10.1) targeted the donor site of intron 38-39. The sequences U11.1 and U12.2 masked both the acceptor of intron 37-38 and the donor site of intron 38-39. The sequence pairs U1.7/U3.4, U2.7/U4.7 and U11.1/U12.2 masked the same regions, however, the first member of every pair targeted exactly the same sequence as in the mouse dysferlin pre-mRNA, whereas the second member of the pair contained a single nucleotide mutation in a ‘kiss domain’. The kiss domain comprises the area of 3-4 nucleotides at the distance between 15-21 nucleotides from the 3’ of the antisense sequence. (Garcia et al., 2013) Garcia et al. showed in their patent from 2013 that correct folding of U7 construct is required for the efficient antisense activity. For the correct conformation of U7 construct the interaction between the U7 loop and part of the antisense sequence, called kiss domain, is essential (Figure 47). It causes a change in conformation of the whole construct in such a way, that the attached Sm proteins do not block any hydrogen bonding of antisense sequence with the target (Figure 47b). The Sm proteins are snRNPs which form a seven-membered ring structure, called Sm core, that can bind to appropriate snRNA and transport it to the splicosome. (Schümperli and Pillai, 2004)

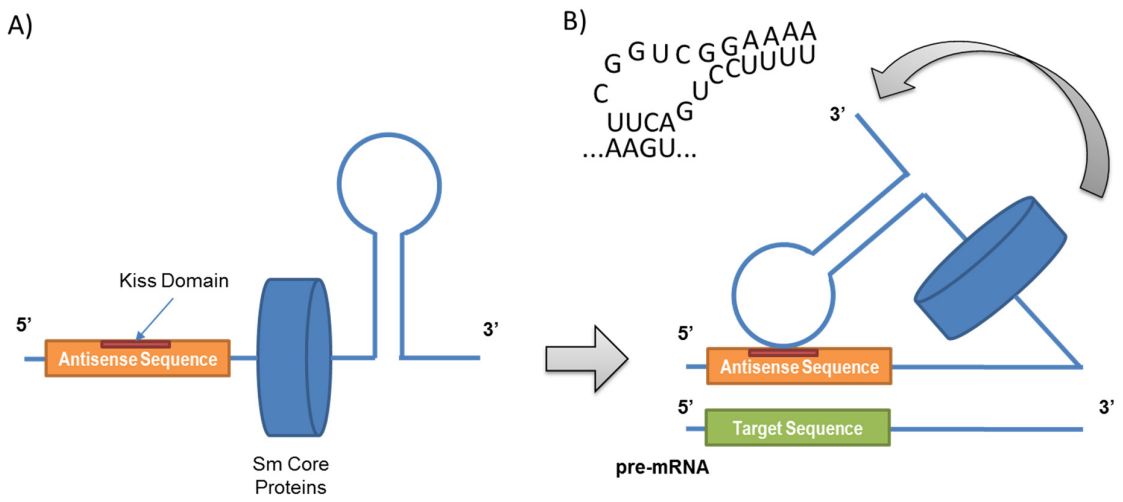

Figure 47 A schematic representation of U7 structure and the mode of action via the antisense sequence and the kissing domain.

Panel A is a schematic representation of the U7 construct. Panel B represents the probable conformation change of U7 construct that is necessary for a correct binding of antisense sequence to its pre-mRNA target. The scheme was based on the image from the patent file of (Garcia et al., 2013).

The mutations inserted in the kiss domain were limited only to C>T substitutions (Table 5). This approach allowed to increase the probability of U7 construct adopting the correct conformation while limiting the detrimental effect on the binding efficiency of modified antisense sequence to its mRNA target.

U7 Name	U7 Size	U7 Target	Target Sequence 5'-3'	Antisense Sequence 5'-3'	Kissing Domain (AAGT/ AGGT/ GAGT/ GGGT)
U1.7	35	BP in int37-38	TCCTGCCTCAGACGTGCTCAGCGGCTCT CTCTCCC	GGGAGAGAGAGCCGCTGAGCACGTCTGA GGCAGGA	No
U3.4				GGGAGAGAGAGCCGCTGAGTACGTCTGA GGCAGGA	Yes but forced by a mutation
U5.5	40	BP and AS in int37-38	TCAGCGGCTCTCTCTCCCCTTCCTCTGTC CTTAGATCCTG	CAGGATCTAAGGACAGAGGAAGGGGAG AGAGAGCCGCTGA	No
U2.7	40	AS in int37-38 and exon 38	TTAGATCCTGGCCTGGGGCCTGCGGAA CATGAAGAGCTAT	*ATAGCTCTTCATGTTCCGCAGGCCCCAGGC CAGGATCTAA*	No
U4.7				*ATAGCTCTTCATGTTCCGCAGGTCCCAGGC CAGGATCTAA*	Yes but forced by a mutation
U6.5	40	exon 38	TGGGGCCTGCGGAACATGAAGAGCTAT CAGATGGCCAGCA	TGCTGGCCATCTGATAGCTCTTCATGTTCC GCAGGCCCCA	No
U7.10	40	exon 38	AACATGAAGAGCTATCAGATGGCCAGC ATCTCTTCCCCCA	TGGGGGAAGAGATGCTGGCCATCTGATA GCTCTTCATGTT	No
U8.2	35	exon 38	AGCCTCGTGGTGGAGTGTGGTGGGCA GACAGTGCA	TGCACTGTCTGCCCACCACACTCCACCACG AGGCT	No
U9.2	40	exon 38	TGGTGGGCAGACAGTGCAGTCCTGTGT CATCAGAAACCTT	AAGGTTTCTGATGACACAGGACTGCACTG TCTGCCCACCA	No
U10.1	40	exon38 and DS of int38-39	CCAACTTTGATGTCTGTACTCTCTTCATG GAAGTGGTGAG	CTCACCACTTCCATGAAGAGAGTACAGAC ATCAAAGTTGG	Yes
U11.1	40	AS of int37-38 and DS of int38-39	CTGTCCTTAGATCCTGGCCTCATGGAAG TGGTGAGCCTTA	TAAGGCTCACCACTTCCATGAGGCCAGGA TCTAAGGACAG	No
U12.2				TAAGGCTCACCACTTCCATGAGGTCAGGA TCTAAGGACAG	Yes but forced by a mutation
Scram	28	none	none	GGTGTATTGCATGATAGTAATTTTTGG	No

Table 5 List of mU7 constructs and their targets.

The table includes the information about constructs' size in nt, targeted sequence in mouse dysferlin pre-mRNA, antisense sequence and note about existence of kissing domain. The bold and underlined sequence defines the boundaries in which 4-nucleotide-long kissing domain should be localized. The green nucleotides represent 4-nucleotide-long kissing domain that was present in the original antisense sequence. The red nucleotide represents mutation introduced in the antisense sequence in order to create the 4-nucleotide-long kissing domain. The blue nucleotides represent the 3-nucleotide-long kissing domain.

The U7 constructs were screened for exon skipping activity in the MDX mouse model. Every construct packed in AAV was injected into three TA muscles, which were harvested one month later. The results of the RT-PCR were presented in Figure 48. The band at 750bp represents the full PCR product and the band at 484bp the skipped version missing exon 37 and 38. The band between the full and skipped product represents the combination of both products that takes place during the annealing step of the PCR reaction. Only constructs U7.10, U8.2 and U9.2 presented detectable skipping level of both exon 37 and 38. The remaining constructs triggered none or negligible skipping. The skipping was also validated by sequencing of the main and skipped product (Figure 49).

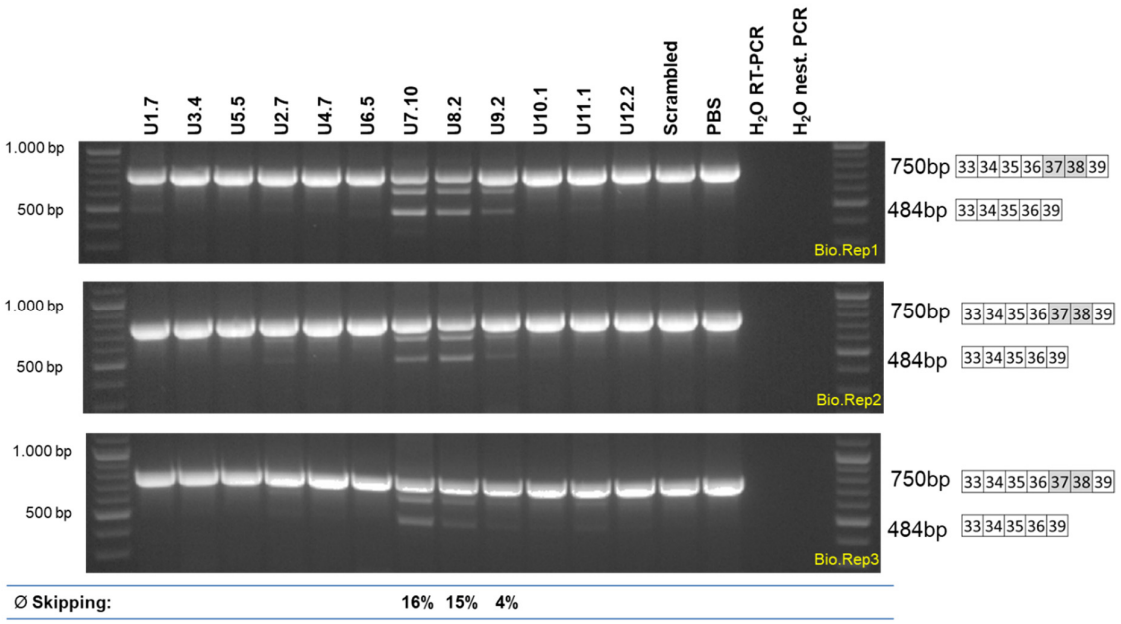

Figure 48 Screening of mU7 constructs for exon skipping in the MDX mouse model.

Results of RT-PCR and nested PCR for dysferlin mRNA spanning the region between exon 33 and 39. The transcript expression was detected in the TA muscle of MDX mice after intramuscular administration of $1{,}3*10^{11}$ VGs/TA. Lanes 2-14 represent treatment with the U7 constructs, lane 15 is a PBS negative control, lane 16 is water control for the RT-PCR and lane 17 is water control for the nested PCR, lanes 1 and 18 ladder.

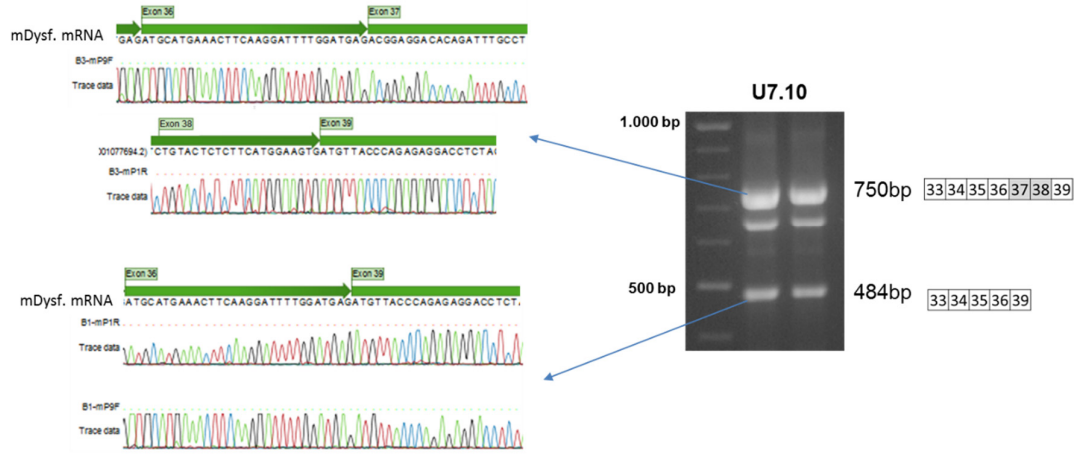

Figure 49 Sequencing of full and skipped product of nested PCR performed for the U7.10 construct.

The band at 750bp corresponds to the full dysferlin containing both exons 37 and 38. The sequencing of this band verifies the presence of the junction between the exon 36 and 37 and the junction between exon 38 and 39. The band at 484bp represents the truncated dysferlin without exons 37 and 38. The sequencing of this band in both forward and reverse direction verifies the presence the junction between exons 37 and 39.

The exon skipping level was measured for the three constructs: U7.10, U8.2 and U9.2 by densitometric quantification from the gel pictures or by a qPCR method. According to the

readout from the gel the best skipping was triggered by U7.10 and U8.2 reaching the level of 15-16%. The construct U9.2 performed at the level of only 4%.

Densitometry	ex37&38 Skipping Level		
	U7.10	U8.2	U9.2
Repeat 1	29%	24%	6%
Repeat 2	8%	15%	3%
Repeat 3	12%	6%	2%
	16%	15%	4%

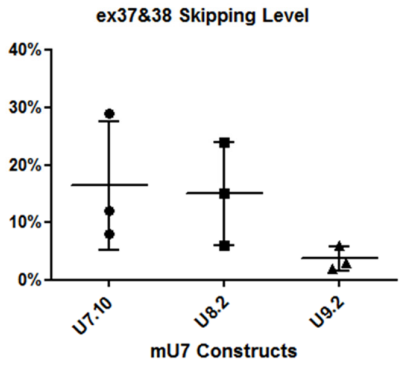

Figure 50 Densitometric quantification of exon skipping using mU7 antisense constructs in MDX mice.

The table on the left represents exon skipping level for U7.10, U8.2 and U9.2 constructs determined for every biological repeat. The graph on the right represents the mean values and standard deviation of exon skipping level for three biological repeats.

Exon skipping level was also quantified by qPCR. Using this approach, the amount of the skipped transcript was compared to the total amount of full dysferlin transcripts. The highest skipping level was archived by U7.10 followed by U8.2. The construct U9.2 triggered skipping at the level of negative control (U7 scrambled).

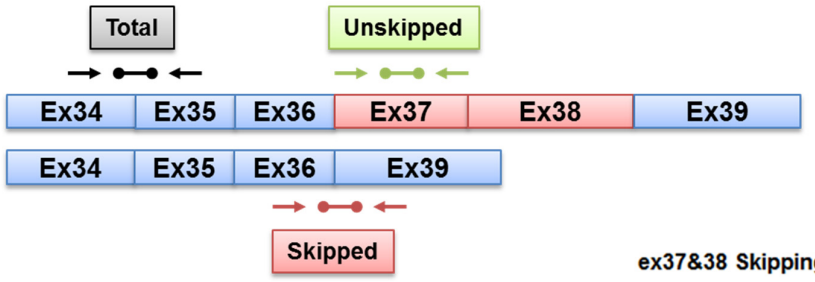

qPCR	Level of ex37&38 Skipping			
	U7.10	U8.2	U9.2	Scrambled
Repeat 1	0,11%	0,07%	0,02%	0,02%
Repeat 2	0,14%	0,03%	0,02%	0,01%
Repeat 3	0,16%	0,03%	0,00%	0,01%
	0,14%	0,04%	0,01%	0,02%

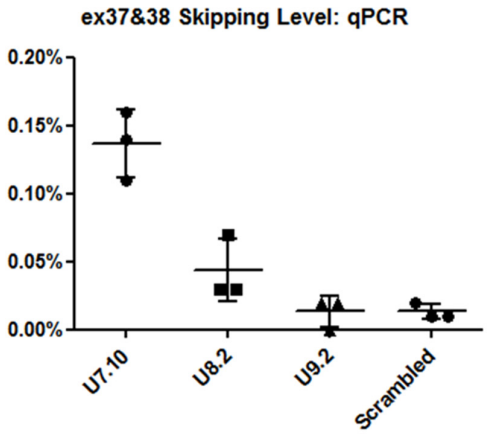

Figure 51 qPCR quantification of exon skipping using mU7 antisense constructs in MDX mice.

The qPCR assay setup was depicted in the top panel. Primers are represented by arrows and molecular probe by lines with dots at both ends. The individual levels of exon skipping for every biological repeat are presented in the table at the left. The graph on the right represents the mean levels of skipping for the mU7 constructs. The error bares represent SEM for the three biological repeats.

The therapeutic efficacy of U7 strategy was also assessed in the MMex38 dysferlinopathy mouse model. A large batch of AAVs containing the selected U7 constructs (U7.10, U8.2, U9.2 and Scrambled) was produced using the baculovirus system. $1{,}56*10^{12}$ VGs were injected intramuscularly into TA muscle of 4-6,5 month old MMex38 mice. After 4 weeks the mice were sacrificed and the TA muscle was extracted for an RNA and protein analysis. The nested PCR allowed detection of very low exon skipping of both exon 37 and 38 for the construct U7.10 in all four biological replicates and U8.2 for three replicates (Figure 52). The construct 9.2 triggered very little skipping detected only in the replicate number 4. No skipping was detected in U7 Scrambled construct, PBS and WT controls.

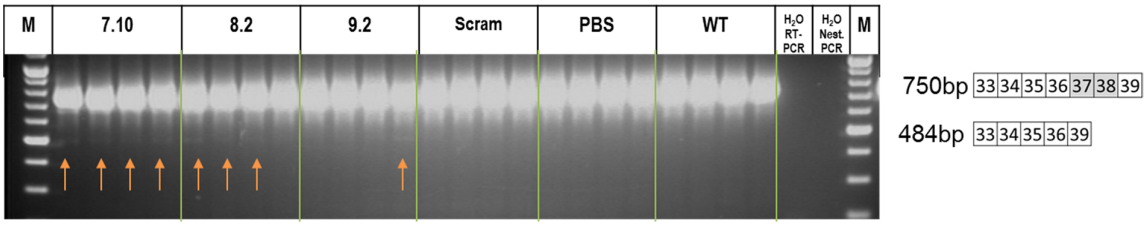

Figure 52 Detection of exon skipping at the RNA level triggered by the selected U7 constructs in the MMex38 mouse model.

The RT-PCR and the nested PCR for dysferlin mRNA spanning the region between exon 33 and 39. The transcript expression was detected in the TA muscle of MMex38 mice after intramuscular administration of $1{,}56*10^{12}$ VGs/TA. Lanes 2-17 represent treatment with the mU7 constructs: U7.10/U8.2/U9.2/Scrambled, lanes 18-21 is a PBS negative control, lanes 22-25 is wild type control (BL6 mice), lane 26 is a water control for the RT-PCR and lane 27 is a water control for the nested PCR, lane 1 and 28 is ladder.

The TAs of MMex38 mice injected with the mU7 constructs packed in AAV were analyzed for dysferlin expression using the western blot analysis (Figure 53). For none of the three mU7 constructs a significant increase in the amount of protein could be detected (Figure 54).

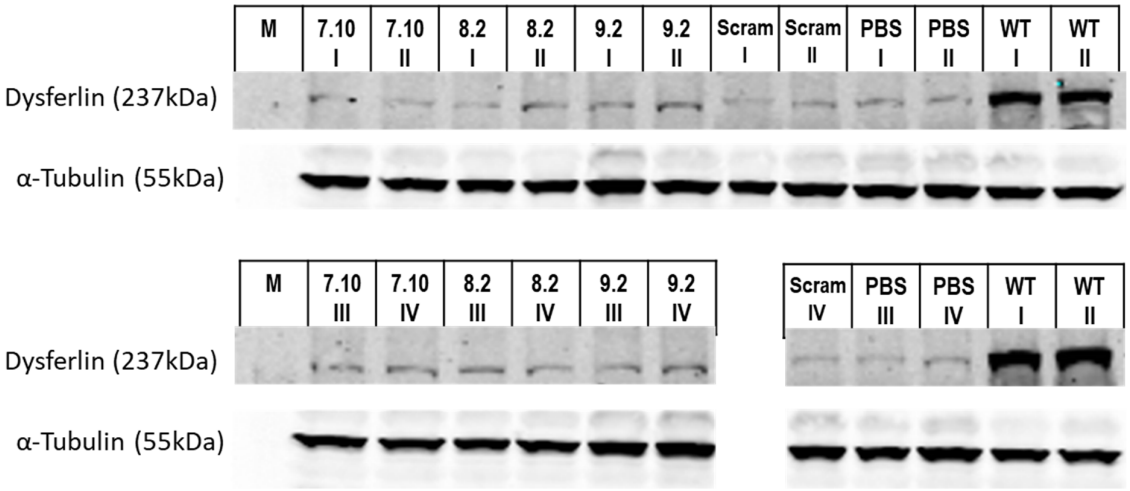

Figure 53 Detection of dysferlin protein level rescued by the selected mU7 constructs in the TAs of MMex38 mouse model.

Results of western blot analysis of TA muscle after intramuscular injection of $1{,}56*10^{12}$ VGs/TA. Membrane developed with the Lycor system for dysferlin and α-tubulin: lane 1 ladder, lanes 2-9 represent treatment with the mU7 constructs: U7.10/U8.2/U9.2/Scrambled, lanes 10-11 is a PBS negative control, lanes 12-13 wild type control (BL6 mice). The numbers I, II, III and IV represent the biological repeats.

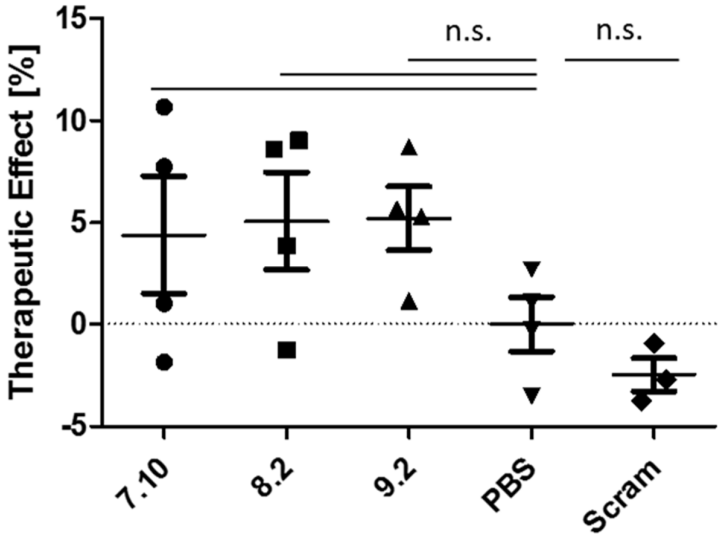

Figure 54 Quantification of the therapeutic effect at the protein level after intramuscular injection of the selected mU7 constructs into TA of MMex38 mice.

The densitometric quantification of individual lanes from the Figure 53 was performed using ImageJ software. The values were first normalized to the WT control and the mean values were calculated from four b. The Therapeutic Effect for every construct was calculated as follows: (Average Amount of dysferlin for mU7 treated TAs) – (Average Amount of dysferlin for PBS injected TAs). The error bares represent SEM.

3.5. In vitro exon skipping using U7 small nuclear RNA

Due to low exon skipping efficiency of mU7 constructs delivered with AAV vector I decided to verify the therapeutic potential of the therapy in vitro using C2C12 cell model. For this purpose, C2C12 cells were infected with either 10^{11} or 10^{12} VGs that corresponded to MOI of 10^6 or 10^7 respectively. Next the cells were differentiated to myotubes for 5 days and their RNA was isolated to detect exon skipping. The analysis showed that the exon skipping was triggered by mU7 constructs when delivered at MOI of 10^7. The constructs U7.10 and U8.2 triggered exon skipping of both exon 37 and 38 at the level of 9,5% and 12,9% respectively. The skipping caused by U9.2 was low and was estimated at the level of 1,3%. U7 constructs delivered to C2C12 cells at MOI 10^6 did not caused detectable exon skipping.

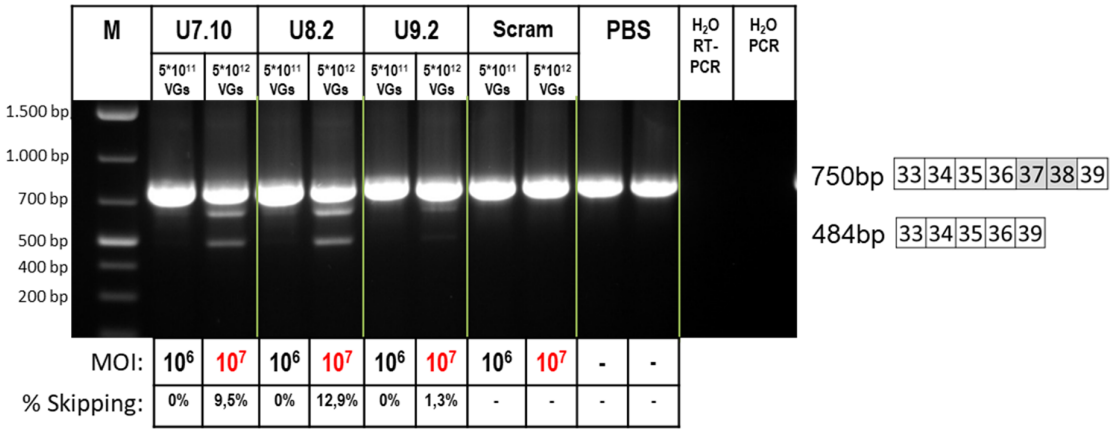

Figure 55 Detection of exon skipping triggered by the selected mU7 constructs delivered by AAV in vitro in C2C12 myotubes.

The results of the RT-PCR and the nested PCR: lanes 2-9 represent treatment with the selected U7 constructs: U7.10, U8.2 and U9.2, lane 10 and 11 is a PBS negative control, lane 12 is a water control for the RT-PCR and lane 13 is a water control for the nested PCR, lane 1 is ladder. The MOI and the percentage of exon skipping was marked at the bottom of the gel.

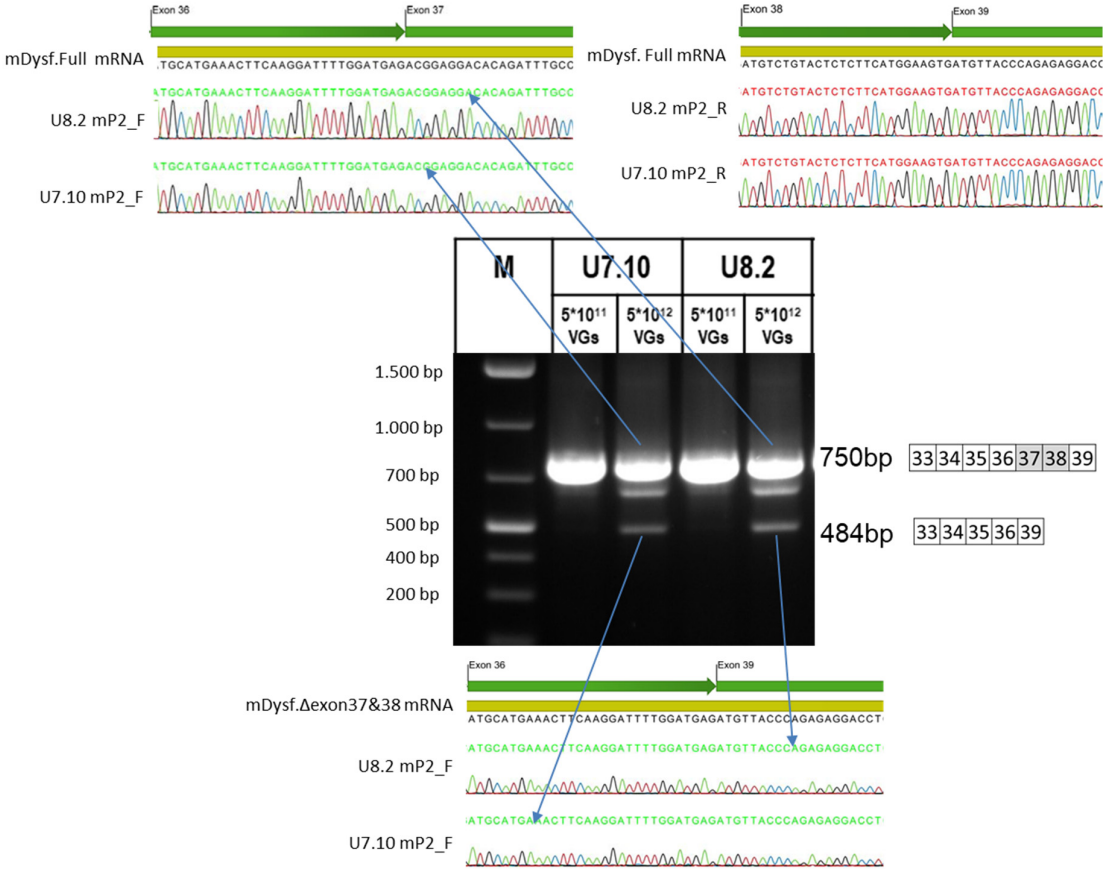

Figure 56 Sequencing of full and skipped product of nested PCR performed for the U7.10 and U8.2 construct used in C2C12 cells.

The band at 750bp corresponds to the full dysferlin containing both exons 37&38. The sequencing of this band with the primer mP2_F verifies the presence of the junction between the exon 36 and 37 and with the primer mP2_R verifies the existence of the junction between exon 38 and 39. The band at 484bp represents the truncated dysferlin without exons 37 and 38. The sequencing in of this band in both forward and reverse direction verifies the presence of the junction between exons 36 and 39.

After the successful in vitro exon skipping with U7 and AAVs in C2C12 cells the experiment was repeated in the dysferlin deficient mouse myoblasts obtained from MMex38 mice. The cells were isolated from 8 weeks old mice. The population was enriched for VCAM1 surface marker using FACS. The quality of isolated myoblasts was verified by desmin and PAX7 staining (Figure 57). The FACS-based isolation protocol allowed to isolate 98-100% desmin positive cells and 49-67% PAX7 positive cells.

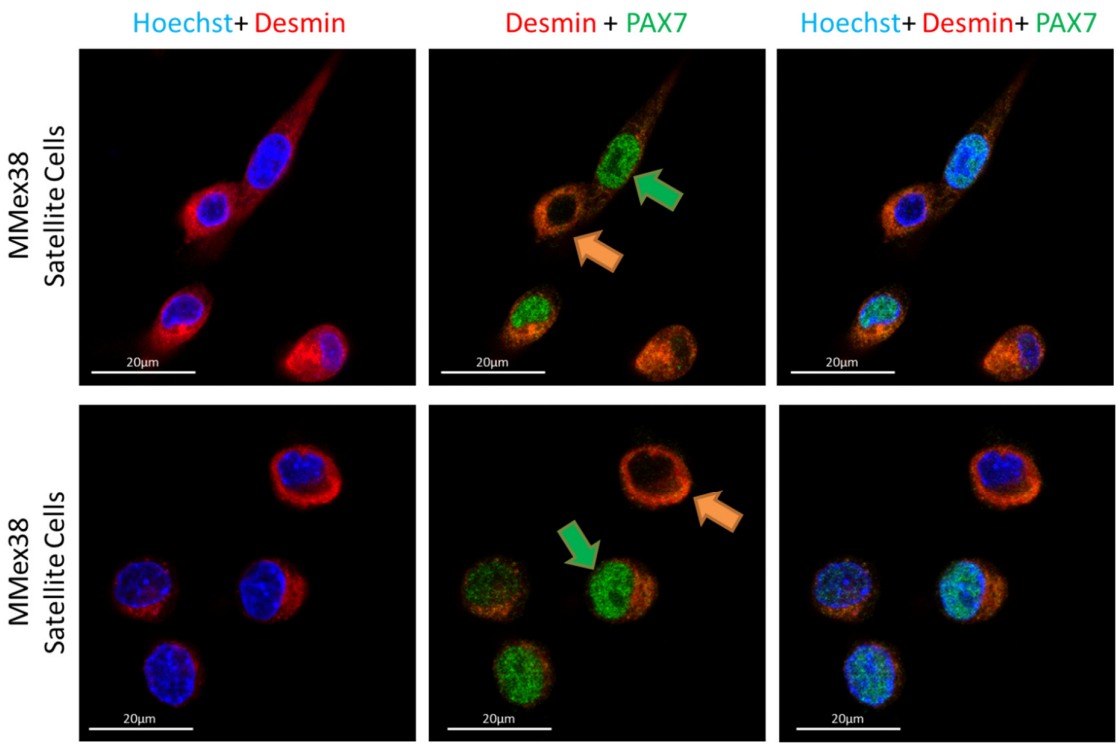

Figure 57 Immunofluorescent staining of MMex38 satellite cells used for the in vitro exon skipping with mU7.

Confocal microscopic image of immunostaining of PAX7 (green), desmin (red) and nuclei (blue). The orange arrows point at PAX7 negative cells and the green ones at PAX7 positive cells. The scale bar has 20 µm.

The isolated satellite cells were amplified for 2 passages and seeded at matrigel coated wells at density of 50.000 cells per well of a 12-well-plate. Before the infections the majority of cells exhibited a round morphology typical for the undifferentiated myoblasts (Figure 58).

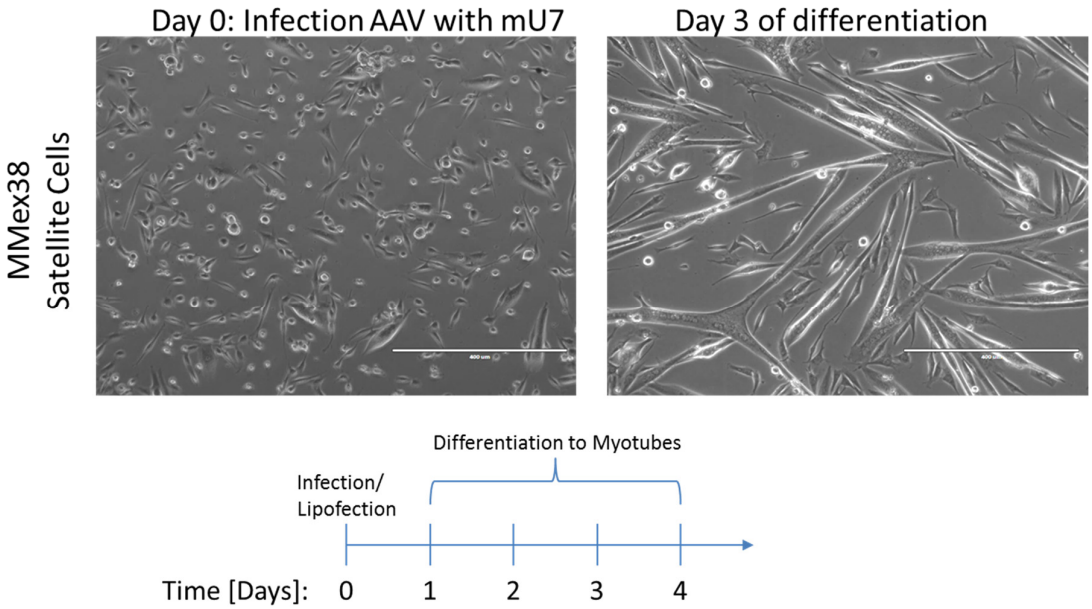

Figure 58 Morphology of MMex38 satellite cells at the day of infection and after 3 days of differentiation into myotubes.

Bright field images of MMex38 satellite cells cultured on Matrigel at the day of infection using AAV2/9 containing mU7 construct and after formation of myotubes at the day 3 of differentiation using DMEM with 2% horse serum. The scale bar has 400µm. The time axis at the bottom describes the experimental protocol.

The cells were either infected with AAVs containing mU7 constructs at MOI 107 or transfected with lipofectamin 3000 and a pRRLSIN.cPPT.PGK-MCS.WPRE plasmid carrying mU7 construct. After 24h the medium was changed to DMEM+2% horse serum and the myoblasts were differentiated to myotubes for three days. At the end of the differentiation the multinucleated myotubes were visible under the light microscope (Figure 58). The RNA was isolated and nested RT-PCR was performed. In none of the samples obtained after lipofection (Figure 59) or after AAV transduction (Figure 60) exon skipping could be detected. The RT-PCR and nested PCR assay performed correctly because the main product for full dysferlin was properly amplified and the skipping was detected with RNA obtain from the previous experiment on C2C12 cells transduced with AAV containing the selected mU7 constructs.

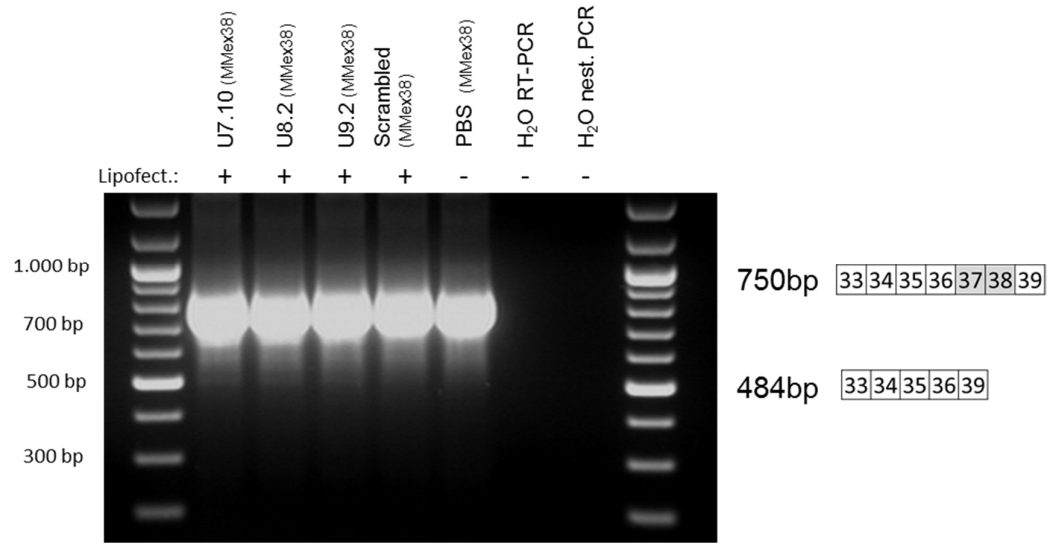

Figure 59 Detection of exon skipping triggered in vitro by mU7 constructs delivered as plasmid using lipofection into mouse satellite cells (MMex38).

The results of the RT-PCR and the nested PCR: lanes 2-5 represent treatment with the mU7 constructs: U7.10, U8.2 and U9.2, lane 6 is a PBS negative control, lane 7 is a water control for the RT-PCR and lane 8 is a water control for the nested PCR, lane 1 and 9 is ladder.

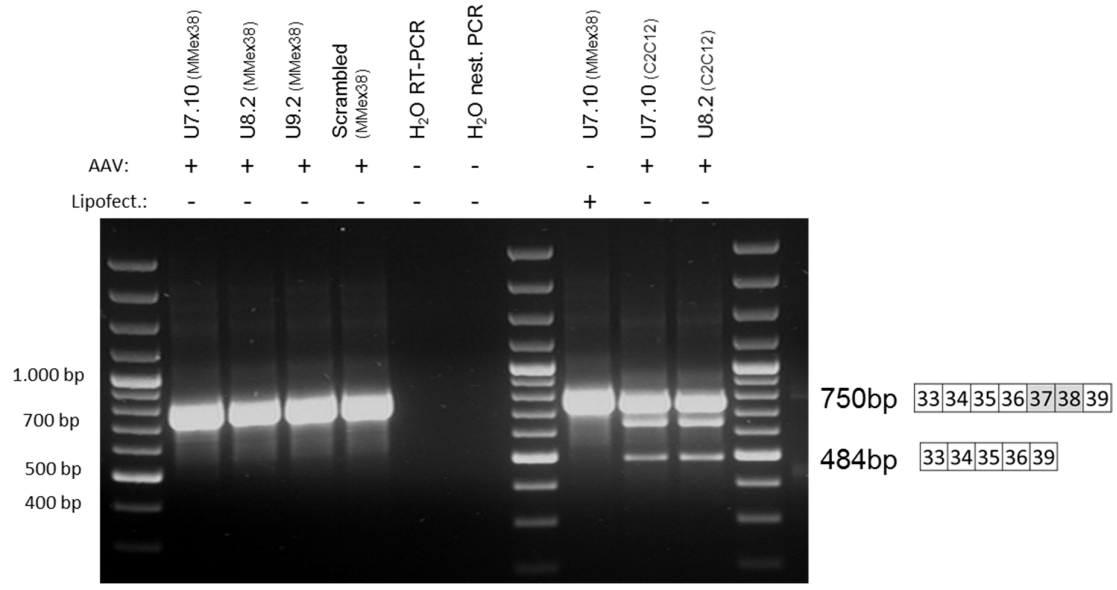

Figure 60 Detection of exon skipping triggered in vitro by mU7 constructs delivered by AAV and lipofection into mouse satellite cells (MMex38).

The results of the RT-PCR and nested PCR: lanes 2-5 represent treatment with the mU7 constructs: U7.10, U8.2 and U9.2 delivered by AAV2/9 at MOI 10^7, lane 6 is a water control for the RT-PCR and lane 7 is a water control for the nested PCR, lane 9 is the sample treated with the mU7 construct (U7.10) delivered by lipofection, lane 10 and 11 represent a positive control for the RT-PCR and the nested PCR performed with the RNA from the C2C12 previously transduced with AAV2/9 mU7 constructs: U7.10 and U8.2, lane 1, 8 and 12 is ladder. The MOI was 10^7.

3.6. In vitro functional study of dysferlin variants

Dysferlin is a modular protein that contains calcium binding domains (C2 domains). Removal of exons from the C2 domains may turn out to be detrimental for the function of the protein. Exon 37 has only three nucleotides that code the beginning of the C2E domain whereas the whole Exons 38 codes for a large part of the C2E domain (Figure 70). Consequently, it was important to investigate the outcome of exon removal on the dysferlin membrane repair ability.

3.6.1. Microinjections as a delivery method of dysferlin variants

In order to assess the impact of exon skipping on the function of dysferlin five dysferlin variants were created: full dysferlin, dysferlin without exon 37, without exon 38 and without both exon 37 and 38 (Figure 61). The constructs under control of CMV promotor were cloned into the pIRES2-EGFP plasmid.

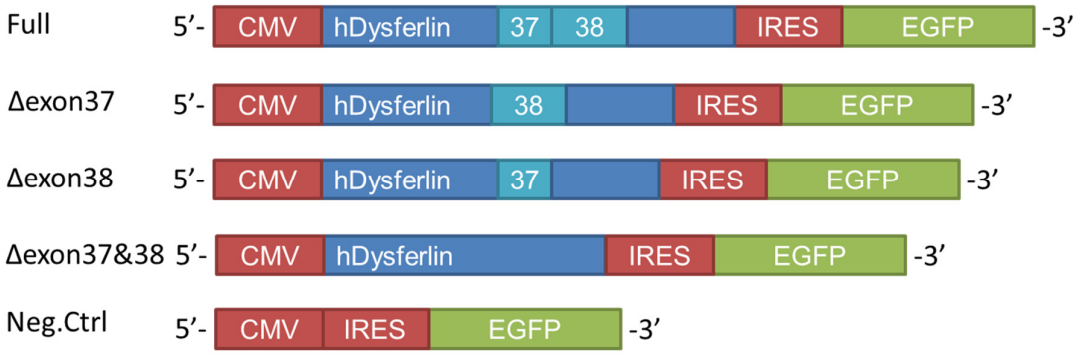

Figure 61 Dysferlin constructs cloned into the pIRES2-EGFP plasmid and used for the microinjections.

The plasmids were microinjected into differentiated myotubes derived from dysferlin deficient immortalized myoblasts i379 (Philippi et al., 2012), AB320 (provided by P. Laforet & N. Levy and stored at Jain Foundation) and myotubes derived from the human primary myoblasts 379. For details of myoblasts mutations please consult the Table 6 in the "Material and Methods" section.

Figure 62 presents the behavior of a dysferlin deficient myotube before and after the microinjection. When the needle enters into the cytoplasm the plasmid is delivered and the myotube slightly increases in size. Shortly after the needle retraction the myotube starts to stretch, gets large holes in the cytoplasm and tears apart at the place of the injection. This behavior was observed for almost all of the microinjected myotubes. Few surviving myotubes were very large in size, hence not suitable for further investigation with the laser wounding assay. Thus, the microinjection was not the method of choice for delivering transgene into dysferlin deficient myotubes and a less invasive approach had to be applied.

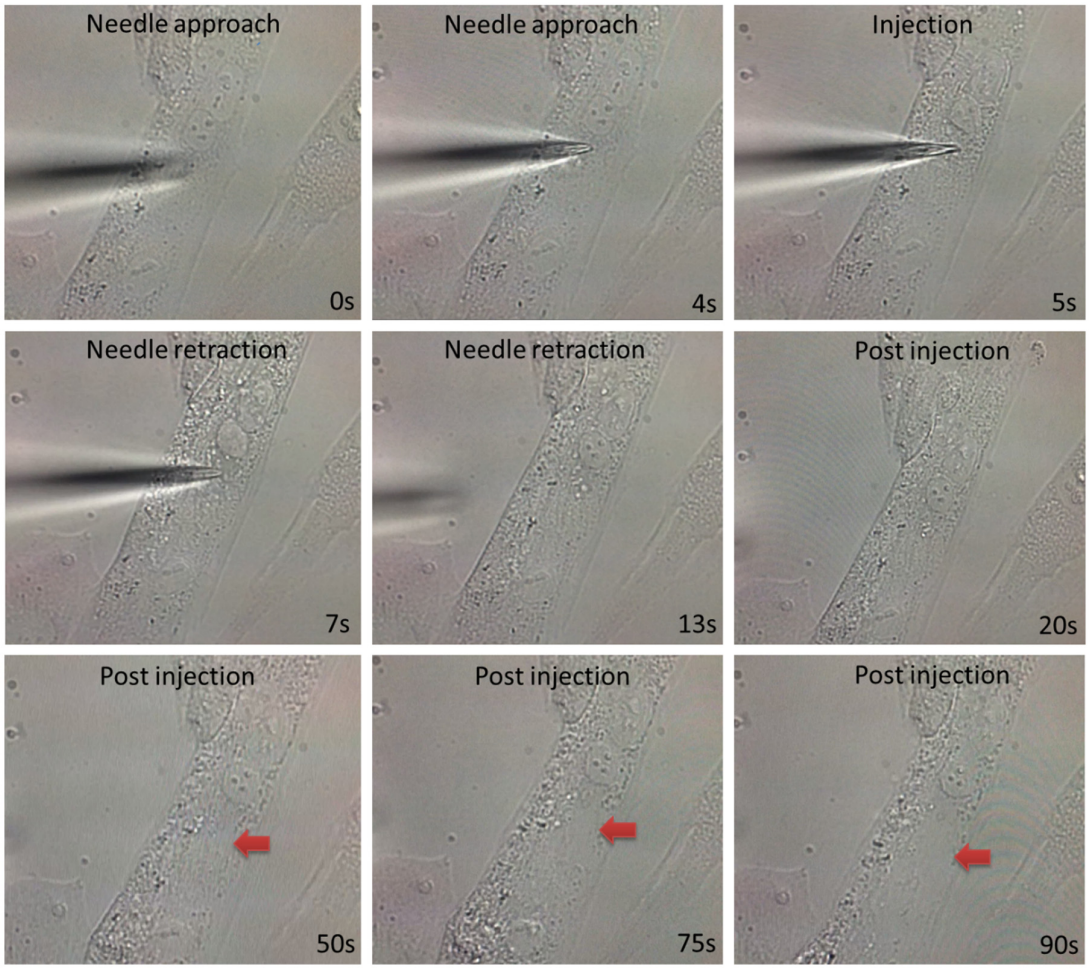

Figure 62 Behavior of a myotube derived from the human primary myoblasts 379 in the three phases of microinjections.

The red arrow indicates the position where a hole in the cytoplasm is formed. The time is expressed in seconds [s].

3.6.2. Lentiviral delivery of dysferlin variants

The microinjections of plasmids were not a successful means of delivery into the dysferlin deficient myotubes, hence I decided to use lentiviral vectors as an alternative means of transport. For this purpose, the full and truncated dysferlin constructs under control of phosphoglycerate kinase (PGK) promoter were cloned into a lentiviral plasmid pRRLSIN.cPPT.PGK-MCS.WPRE (Figure 63). The EGFP reporter was connected to dysferlin by the P2A self-cleaving peptide.

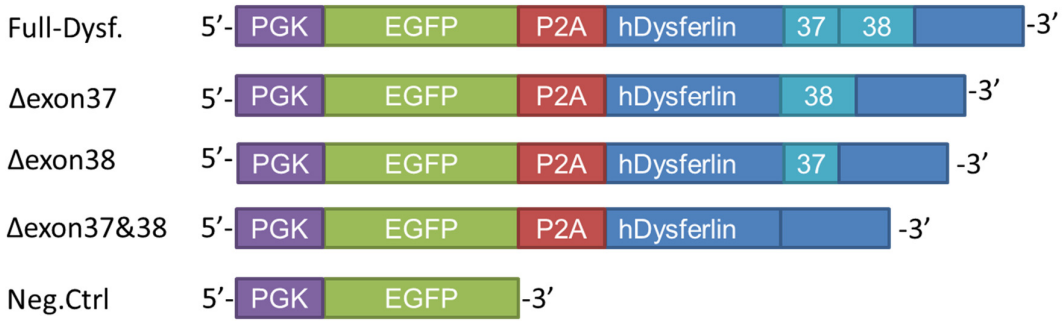

Figure 63 Dysferlin constructs cloned into the pRRLSIN.cPPT.PGK-MCS.WPRE plasmid and used for the lentivirus productions.

The optimal infection conditions were tested using the full dysferlin lentivirus in dysferlin deficient immortalized human myoblasts i379 and AB320. The efficiency of infections was estimated for four different viral dilutions: 1:10, 1:50, 1:100 and 1:300 by measuring the EGFP signal by flow cytometer (Figure 64). The optimal transduction conditions turned out to be at the dilution 1:50 that allowed to obtain 40-67% of EGFP positive cells. Although the concentration of 1:10 led to higher transduction efficiency, however, it also resulted in high cell toxicity, slower proliferation rate and abnormal cell morphology that could be observed by creation of cytoplasmic vacuoles. Consequently, the highest virus concentration was not used for further experiments.

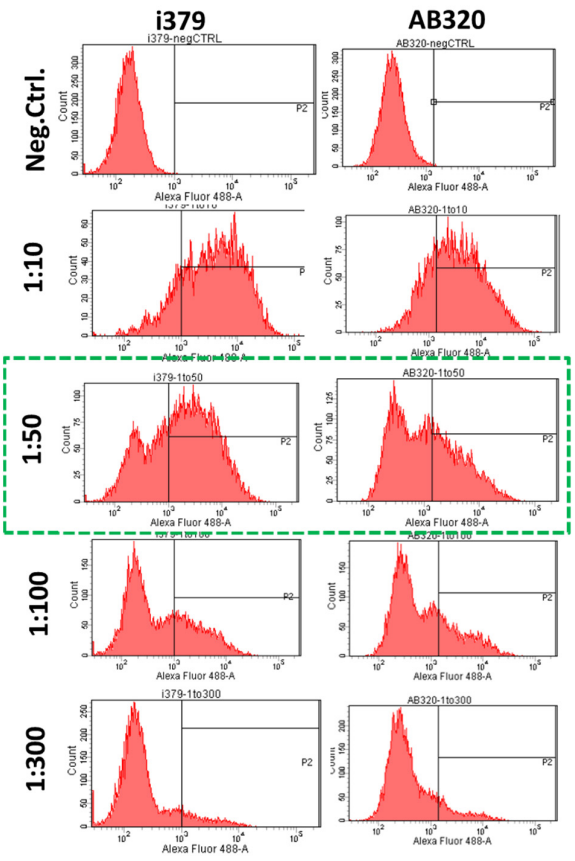

Virus Dilutions	i379 at Day 7		AB320 at Day 7	
	%EGFP	Mean Intensity	%EGFP	Mean Intensity
Neg. Ctrl.	0,2%	1128	0,2%	1623
1:10	81,4%	7762	73,1%	8410
1:50	63,7%	5773	40,7%	6180
1:100	33,6%	4388	28,3%	6035
1:300	12%	3755	13,4%	5183

Figure 64 Flow cytometry analysis of immortalized myoblasts i379, AB320 infected with the lentivirus containing the cassette with full dysferlin and EGFP.

The panel on the left presents the relationship between the count of EGFP positive cells and the concentration of the virus used for the transduction. The percentage of EGFP positive cells was presented in the table on the right. The green box represents the virus dilution that was considered as optimal for the further experiments.

The strength of EGFP signal was stretching over two orders of magnitude so it was necessary to verify by immunostaining if the increasing EGFP signal correlates with the increasing expression of dysferlin. The i379 myoblasts were infected with the lentivirus at the dilution 1:10 and expanded in culture to obtain 10 million cell. The cells were FACS sorted for the EGFP signal strength into three categories: weak, medium and strong (Figure 65).

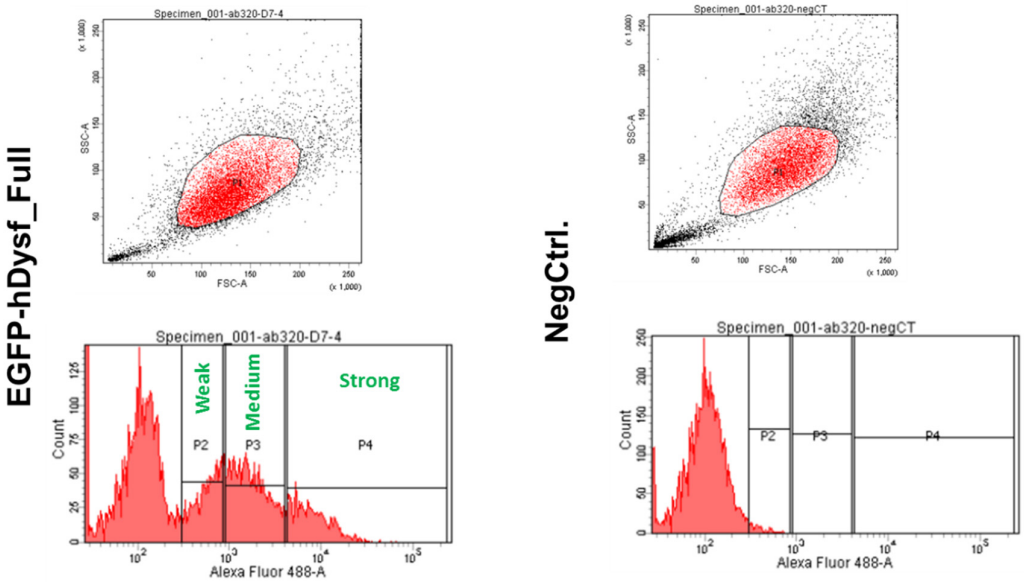

Figure 65 The FACS sorting of i379 myoblasts infected with lentivirus containing the cassette with full dysferlin and EGFP.

The upper panels represent the forward and side scatter gating of the i379 population. The cells were sorted for the strength of EGFP signal and were divided into the three categories: weak, medium and strong.

Next the myoblasts were immunostained for dysferlin. The results confirmed that the cells with the strongest EGFP signal exhibited also the strongest dysferlin signal in the immunostaining (Figure 66). To assure proper overexpression of the transgene, I decided to use only the myoblast that had strong EGFP signal for the laser wounding analysis.

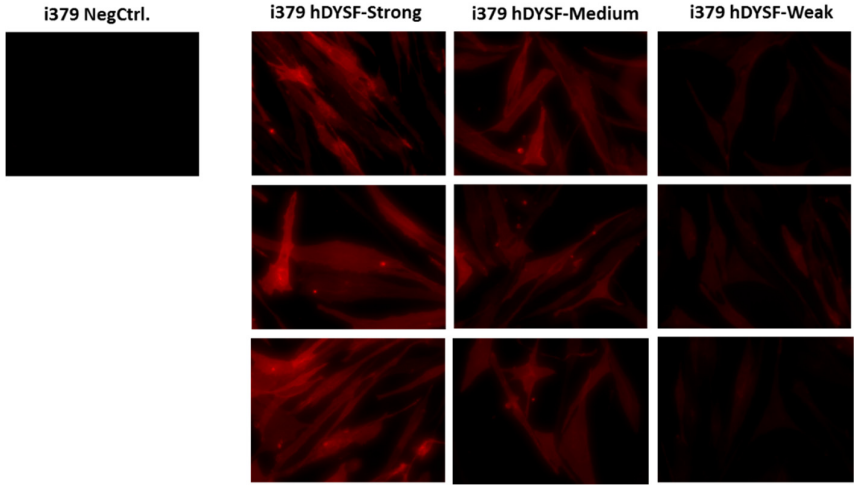

Figure 66 Immunostaining of immortalized myoblasts (i379) transduced with the lentivirus containing the EGFP-DYSF Full construct and FACS sorted for the strength of EGFP signal into the three groups: strong, medium and weak.

Fluorescent microscopy image of immunostaining for full dysferlin (red) using ROMEO antibody.

The functional study of truncated dysferlin was performed using laser wounding assay. The dysferlin deficient human primary myoblasts 1524A derived from a 28-year-old female patient carrying a homozygous dysferlin mutation in Exon 44: c.4872delG were transduced with lentiviruses containing previously described dysferlin constructs (Figure 63). The cells were immunostained for myoblast marker CD56 coupled to Alexa 647 in order to enrich the myoblast population and sort out the contaminating fibroblasts. The stained cells were FACS sorted for both strong EGFP and strong Alexa 647 signals (Figure 67). Next the myoblasts were amplified and finally differentiated for 5 days into myotubes, which were used in the laser wounding assay.

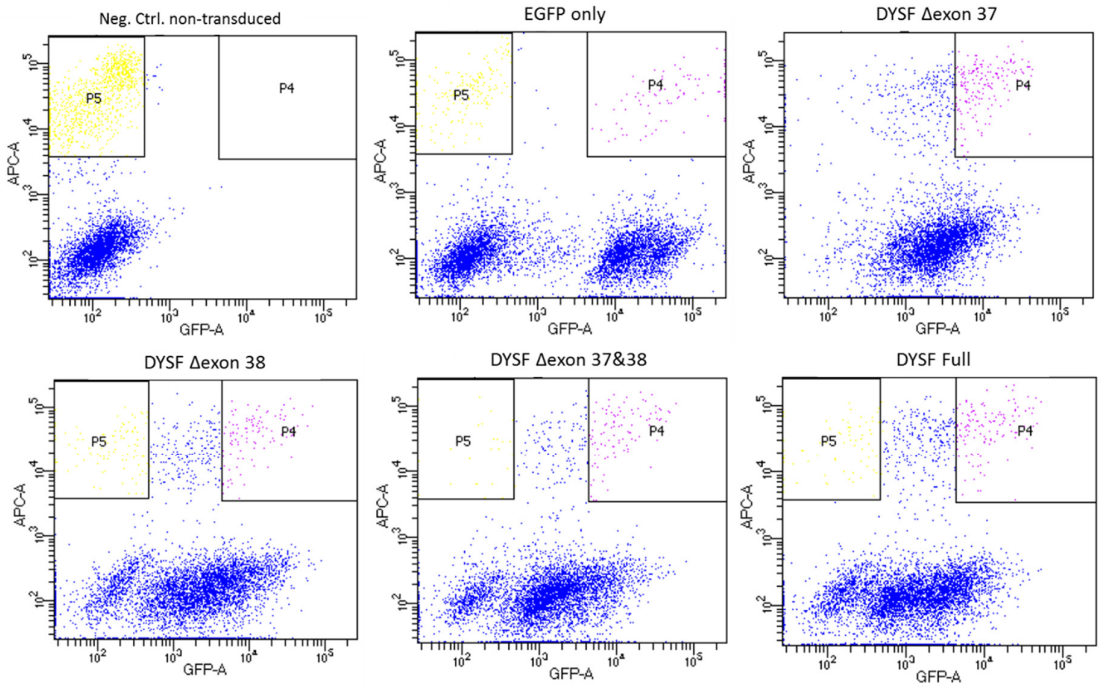

Figure 67 FACS sort of 1524A myoblasts transduced with the lentivirus containing the dysferlin constructs: Δexon37, Δexon38, Δexon37&38, DYSF-Full, only EGFP.

The P4 gate was used to enrich the myoblast 1524A population positive for both CD56 marker and a strong EGFP signal.

3.6.3. Membrane repair capability of dysferlin variants

Shortly before the wounding experiment the differentiation medium was exchanged to Tyrode solution supplemented with red fluorescent dye FM-4-64. The myotubes were wounded using a laser beam from a confocal microscope. After the membrane disruption, the influx of fluorescent dye FM-4-64 was measured over a period of 280s (Figure 68). The strongest fluorescent signal was measured for the non-transduced myotubes (Figure 69). The lowest influx was observed for myotubes containing full dysferlin, dysferlin without exon 37 and

dysferlin without exons 37&38. Removal of exon 38 had some detrimental effect on the membrane repair of myotubes because they performed worse than the myotubes with the full dysferlin but at the same time significantly better than the non-transduced myotubes. The cells that were transduced with only EGFP exhibited higher fluorescent influx than full dysferlin and truncated version without exon 37 and without both exon 37 and 38.

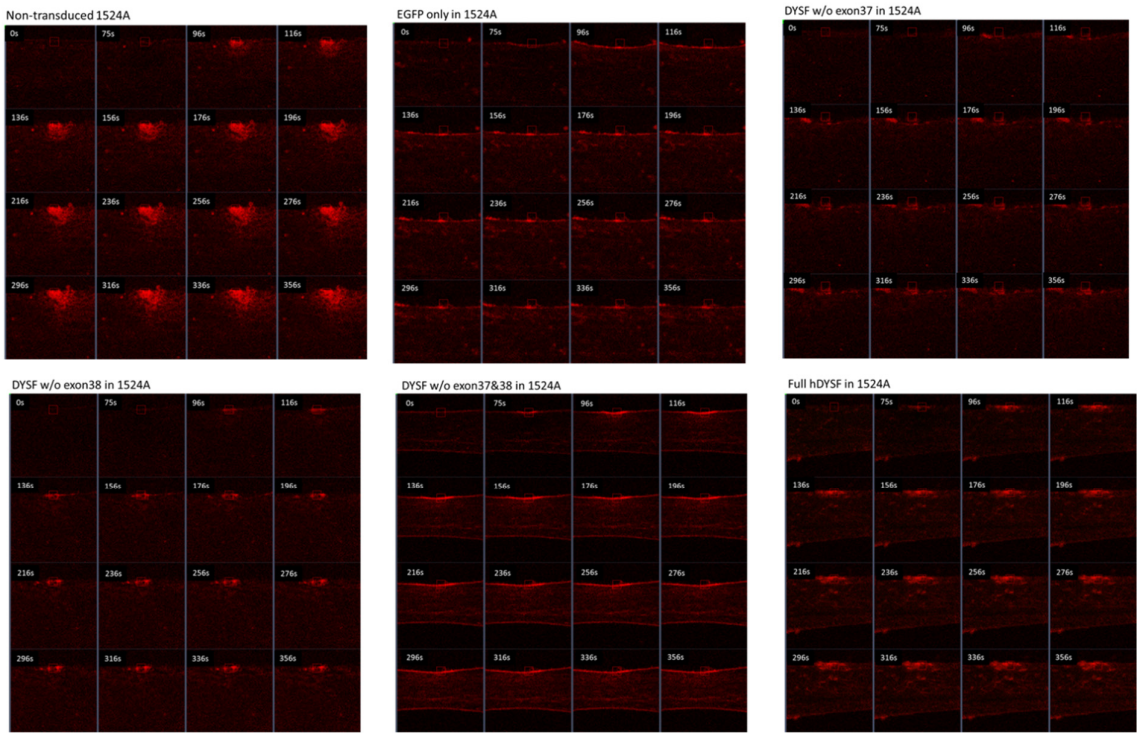

Figure 68 Time dependent influx of the red fluorescent dye FM-4-64 into wounded myotubes (1524A) that were transduced with the lentivirus containing full and truncated dysferlin gene.

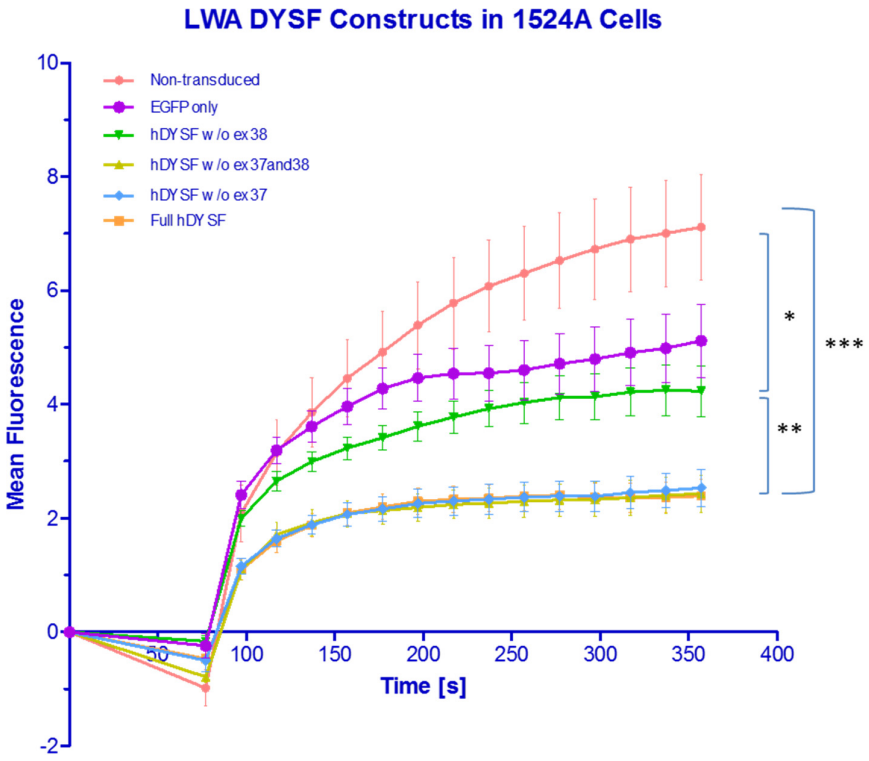

Figure 69 Quantification of the results from laser wounding assay performed in the dysferlin deficient myotubes (1524A) transduced with the lentivirus containing full and truncated dysferlin gene.

For each construct the following number of myotubes was wounded: Δexon37: n=11, Δexon38: n=16, Δexon37&38: n=16, Full: n=15, Non-transduced: n=15, EGFP: n=8.

3.6.4. Homology-based modeling of full and truncated dysferlin protein

The laser wounding assay demonstrated that truncated dysferlin without exon 37 and dysferlin without exons 37 and 38 are able to repair sarcolemma as effectively as the full version of the protein. However, dysferlin without exon 38 performed worse membrane resealing than the full dysferlin. I was interested to find out what structural implications does the removal of exon 38 and both exon 37 and 38 might have. To study this question, the C2E domain of human dysferlin was modeled by homology modeling approach at automated protein structure homology-modelling server SWISS-MODEL.

The primary structure of human dysferlin protein was found in UniProt and according to the database annotation the C2E domain is encoded by exon 38 and part of exon 39. In order to investigate the role of exon 37 in the protein structure, the algorithm was feed with the amino acid sequence encoded by all three dysferlin exons: 37, 38 and 39. Dysferlin C2Avar1 domain (4iqh.1.A) was chosen as a template for building the C2E domain model. The alignment of the

two domain primary structures and the prediction of secondary structures was presented in the Figure 70.

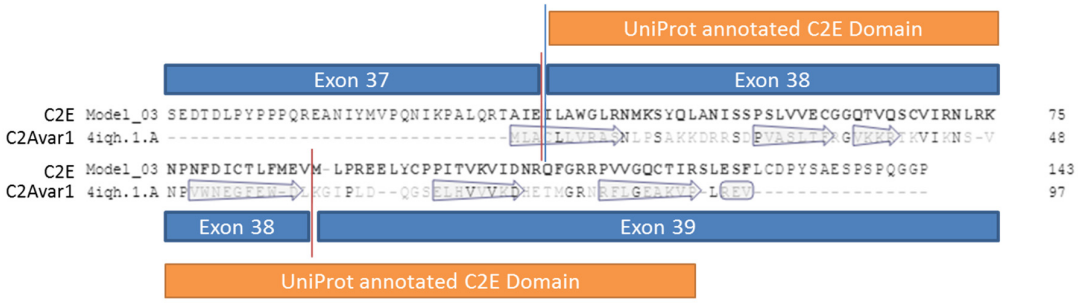

Figure 70 Primary structure alignment of dysferlin C2E and C2Ava1 domains.

The amino acids sequences of C2E (Mode_03) and C2Ava1 (4iqh.1.A) domains are represented by capital letters. The beta sheets of the secondary structure were annotated as arrows. The UniProt annotated C2E domain was represented as an orange rectangle and its end was marked by a blue horizontal line. Exons were represented as blue rectangles and the exon boundaries were marked by the vertical red lines.

According to the homology model, the C2E domain starts at the end of exon 37 and encloses its three last amino acids: AIE. It spans throughout exon 38 and stops at the amino acid sequence: SLESF of exon 39. This region of the C2E domain differs from the UniProt annotated C2E domain, which is shorter by 8 amino acids because it starts at the beginning of exon 38 with the amino acid sequence: ILA and finishes in exon 39 with the sequence: TIR (Figure 70). The homology-based model predicts that the C2E domain consists of 6 β-sheets. The tertiary structure of C2E domain modeled with SWISS-MODEL was depicted in 3D in the Figure 71.

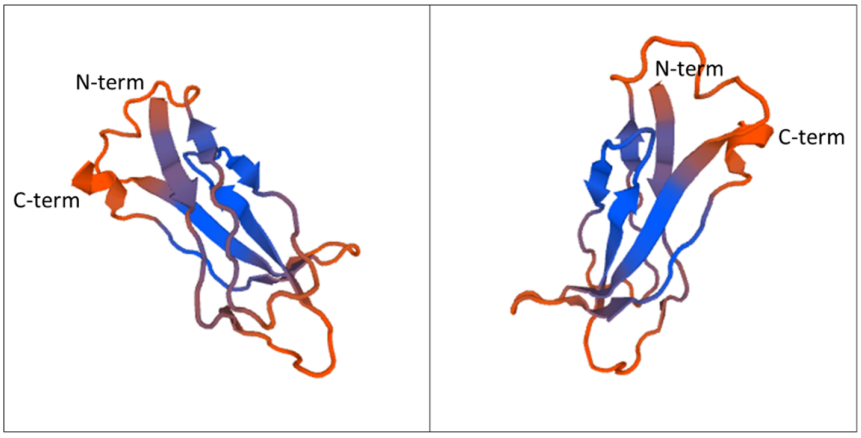

Figure 71 Tertiary protein structure of human dysferlin C2E domain depicted in a 3D model.

The model was created using homology-modelling server SWISS-MODEL. The images represent a front and a back perspective of the human dysferlin C2E domain.

According to the hydrophobicity analysis of the amino acid sequence encoded by the dysferlin exons 37, 38 ad 39 the β-sheets of C2E domain are located in the hydrophobic regions of the protein (Figure 72). Hence, the modeled tertiary structure (Figure 71) represents the conformation of the β-strands that minimizes the exposure of the hydrophobic amino acids from the polar environment of the cell.

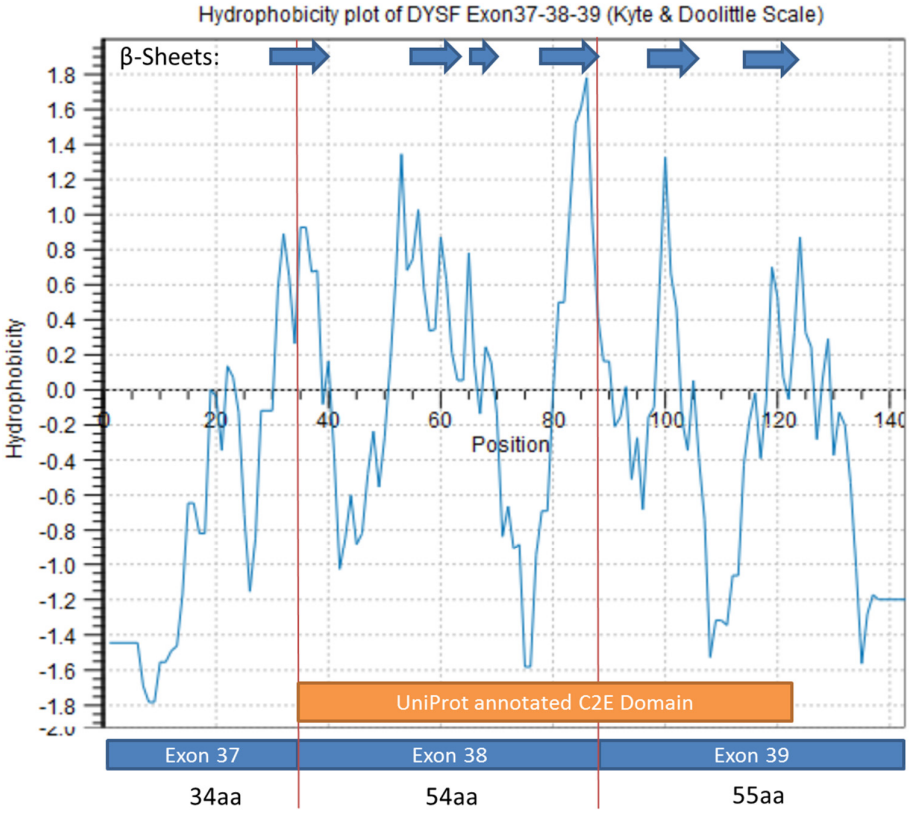

Figure 72 Hydrophobicity plot for the amino acid sequence encoded by human dysferlin exons 37, 38 and 39.

The impact on C2E domain after removing both exon 37 and 38 from the dysferlin coding sequence was presented in the Figure 72. The truncated C2E domain consists of only two β-sheets, which are exposed to direct interaction with the polar environment inside a cell.

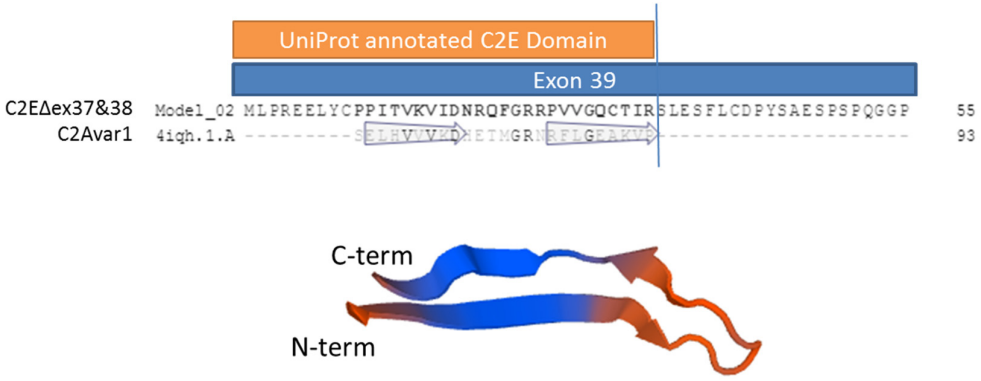

Figure 73 Primary structure alignment of dysferlin C2E_Δex37&38 and C2Avar1 domains and the tertiary structure of C2E_Δex37&38 domain in 3D view.

The amino acids sequences of C2E_Δex37&38 (Mode_02) and C2Ava1 (4iqh.1.A) domains are represented by capital letters. The beta sheets of the secondary structure were annotated as arrows. The UniProt annotated C2E domain was represented as an orange rectangle and its end was marked by a blue horizontal line. Exons were represented as blue rectangles and the exon boundaries were marked by the vertical red lines.

The removal of only exon 37 leads to large truncation of the first β-strand, which is now modeled with only two amino acids: LR (Figure 74).

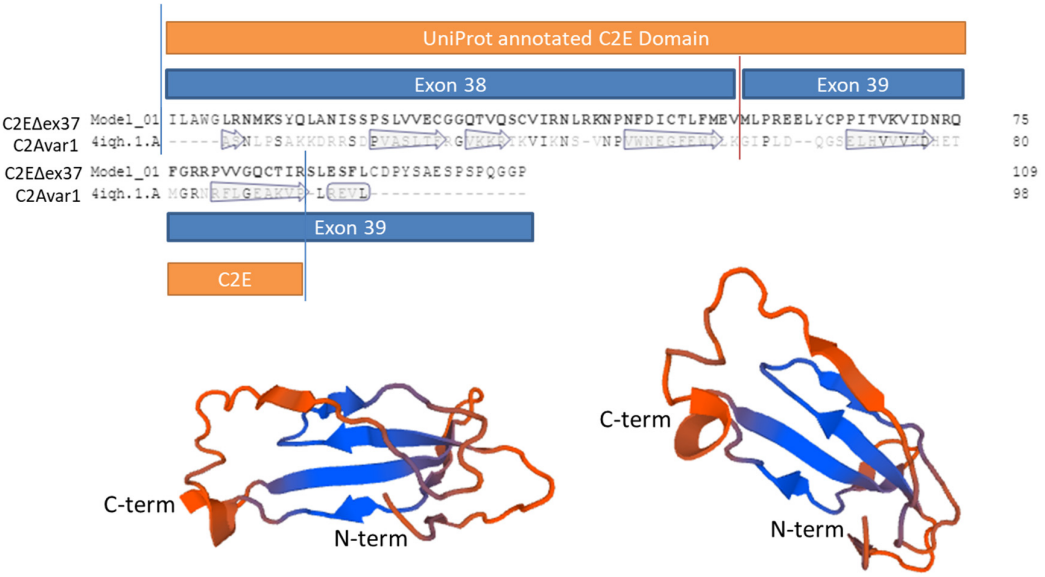

Figure 74 Primary structure alignment of dysferlin C2E_Δex37 and C2Avar1 domains and tertiary structure of C2E_Δex37 domain in a 3D view.

The amino acids sequences of C2E_Δex37 (Mode_01) and C2Ava1 (4iqh.1.A) domains are represented by capital letters. The beta sheets of the secondary structure were annotated as arrows. The UniProt annotated C2E domain was represented as an orange rectangle and its end was marked by a blue horizontal line. Exons were represented as blue rectangles and the exon boundaries were marked by the vertical red lines.

The removal of exon 38 has the same effect on C2E domain as the removal of both exon 37&38. The model predicted that the remaining amino acid sequence forms two β-strands whose conformation resembles the tertiary structure of C2E domain without exons 37&38 (Figure 75).

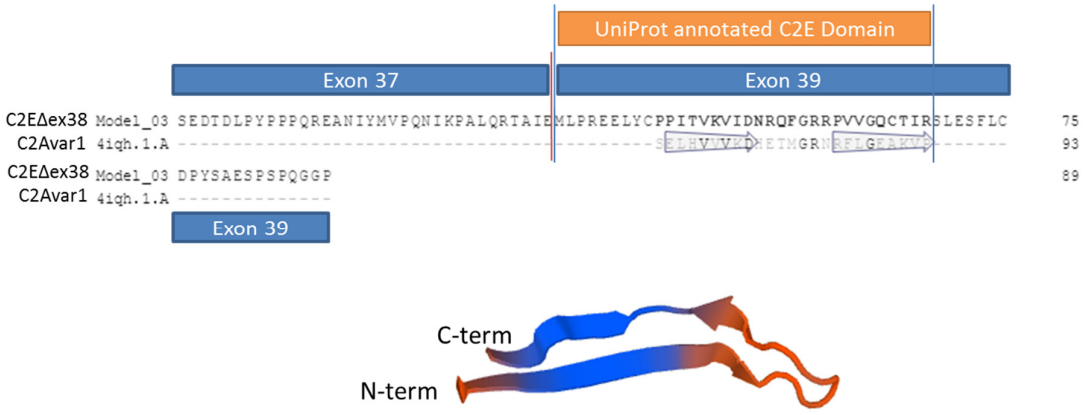

Figure 75 Primary structure alignment of dysferlin C2E_Δex38 and C2Avar1 domain and the tertiary structure of C2E_Δex38 domain in a 3D view.

The amino acids sequences of C2E_Δex38 (Mode_03) and C2Ava1 (4iqh.1.A) domains are represented by capital letters. The beta sheets of secondary structure were annotated as arrows. The UniProt annotated C2E domain was represented as orange rectangle and its end was marked by a blue horizontal line. Exons were represented as blue rectangles and the exon boundaries were marked by the vertical red lines.

3.6.5. PEST-motif localization in the skipped exons

After modeling the dysferlin C2E domain, I wanted to verify if the removal of targeted exons also impacts the PEST motif that was previously annotated for mentioned region by Wein et al. According to their bioinformatic analysis using ScanProsite and Pfam the PEST motif is encoded by exon 38. (Wein et al., 2010) The PEST sequence is a signal for a proteolytic cleavage, thus it decreases the half-lifetime of protein. (Rechsteiner and Rogers, 1996) Hence, removal of this motif from the protein could increase its availability. Using epestfind online tool, I analyzed the amino acid sequence encoded by dysferlin exons 37, 38 and 39 (Figure 76).

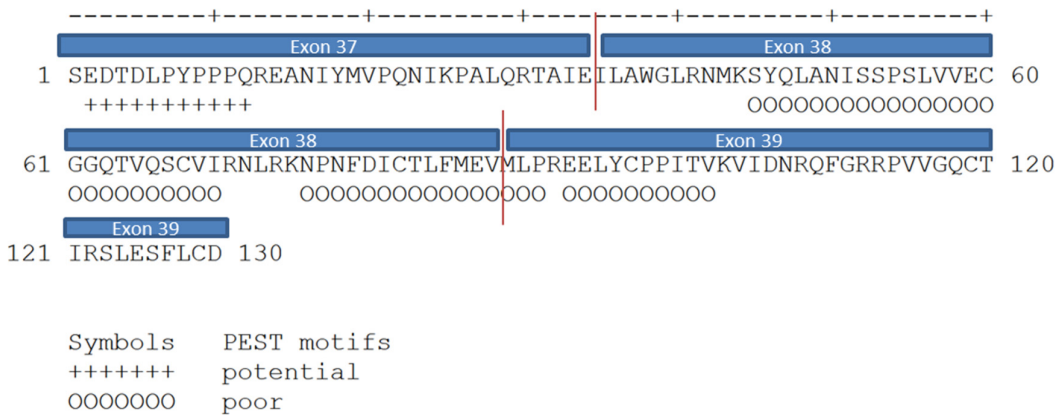

Figure 76 Annotation of PEST motifs predicted by epestfind tool for the human dysferlin sequence encoded by exons 37, 38 and 39.

The predicted PEST motifs are represented either by “+” or “o” symbols. Exons were represented as blue rectangles and the exon boundaries were marked by the vertical red lines.

The predicted PEST motifs found in the amino acid sequences encoded by exon 38 and 39 were qualified as ‘poor’ meaning they did not meet the threshold criteria for the PEST score of 5.0. These motifs are considered as unlikely to lead a given protein for degradation. The motif that was qualified as ‘potential’ is encoded at the beginning of exon 37 sequence and is not included in the C2E domain.

3.6.6. Localization of dysferlin variants in human myoblast and myotubes

The localization study of full and truncated dysferlin was performed in the dysferlin deficient myotubes derived from the human primary myoblast 1525 obtained from a 26-year-old dysferlinopathy female patient carrying a homozygous mutation in dysferlin Exon 44: c.4872delG. First, the myoblasts were infected with the lentiviruses containing previously created versions of the dysferlin gene. Next the cells were differentiated into myotubes and finally stained with an antibody against dysferlin and desmin.

The WT human primary myoblasts (1552) obtained from a healthy 49-year-old female donor were used as a positive control. The immunostaining with the anti-dysferlin ROMEO antibody revealed the proper localization pattern of dysferlin. The native dysferlin is enriched mainly at the membrane of myotubes (Figure 77). Dysferlin is also detected inside the cytoplasm and it is represented by patches of fluorescent signal on the 2D images. The 3D reconstruction of stacked confocal images shows that intracellular dysferlin localizes in the vicinity of nuclei, surrounding them from all sides (Figure 78).

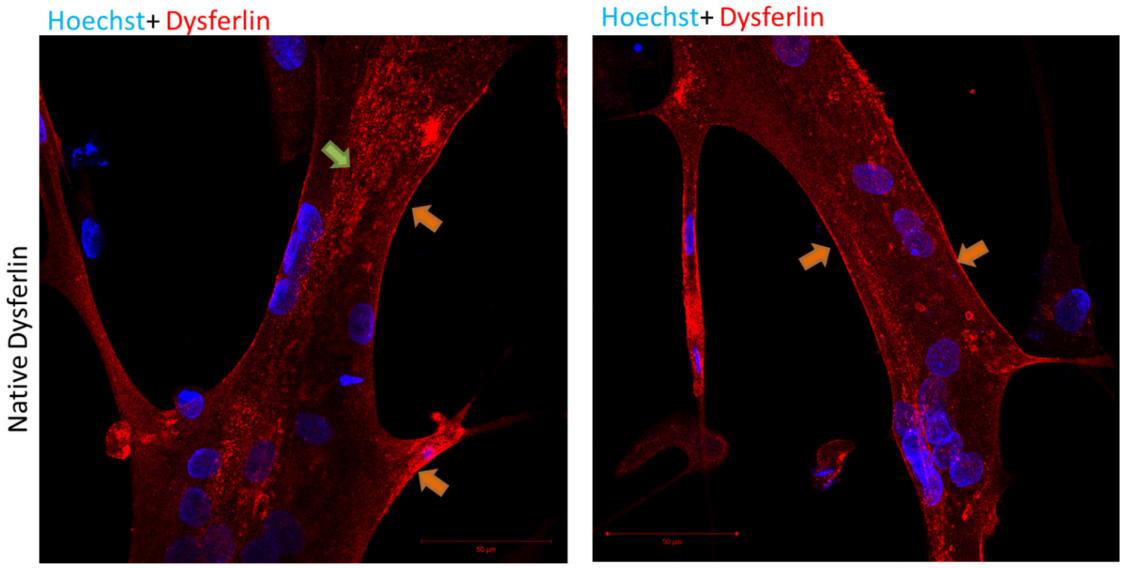

Figure 77 Dysferlin localization in healthy myotubes derived from the primary human myoblasts (1552).

Confocal microscopic image of immunostaining of native dysferlin (red) using ROMEO antibody and Hoechst staining of nuclei (blue). The orange arrows pinpoint dysferlin localized at sarcolemma and the green arrows indicate patches of dysferlin in cytosol. The size bar has 50 µm.

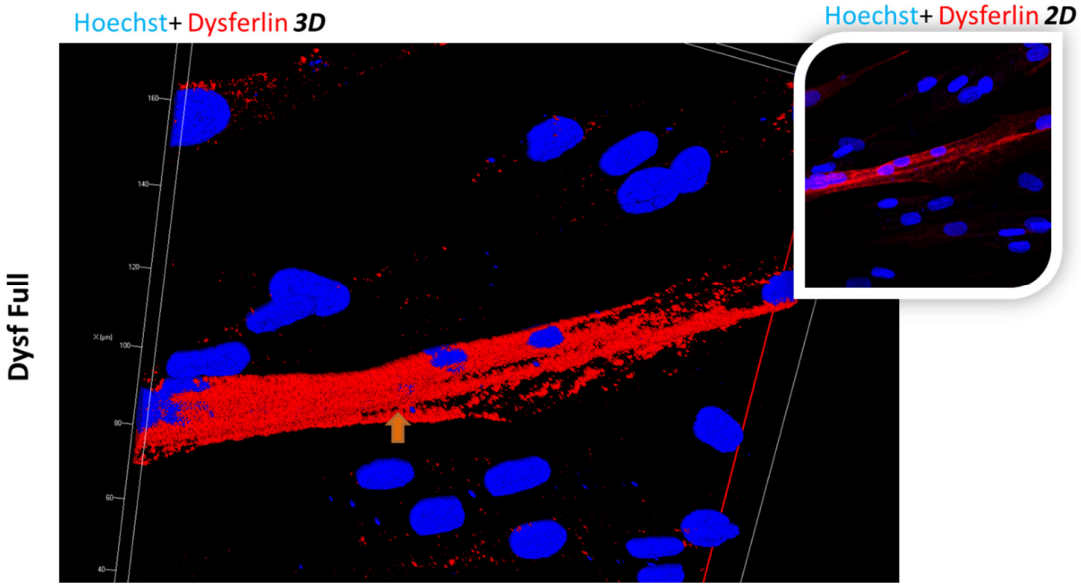

Figure 78 3D localization of dysferlin in healthy myotubes derived from primary human myoblasts (1552).

Confocal microscopic image of immunostaining of dysferlin (red) immunostaining using ROMEO antibody and Hoechst staining of nuclei (blue). The panel on the top right corner is the 2D view of the myotubes. The orange arrow points at the area where dysferlin localizes above the nucleus.

Comparison of immunostaining of dysferlin deficient myotubes (1525) transduced with the full dysferlin construct and with only EGFP was illustrated in the Figure 79. There is no dysferlin

signal in negative control cells that were transduced with the lentivirus containing only the EGFP cassette. The myotubes transduced with full dysferlin exhibit a strong cytoplasmic signal and a correct membrane localization of dysferlin (Figure 80). Myotubes were also positively stained for desmin.

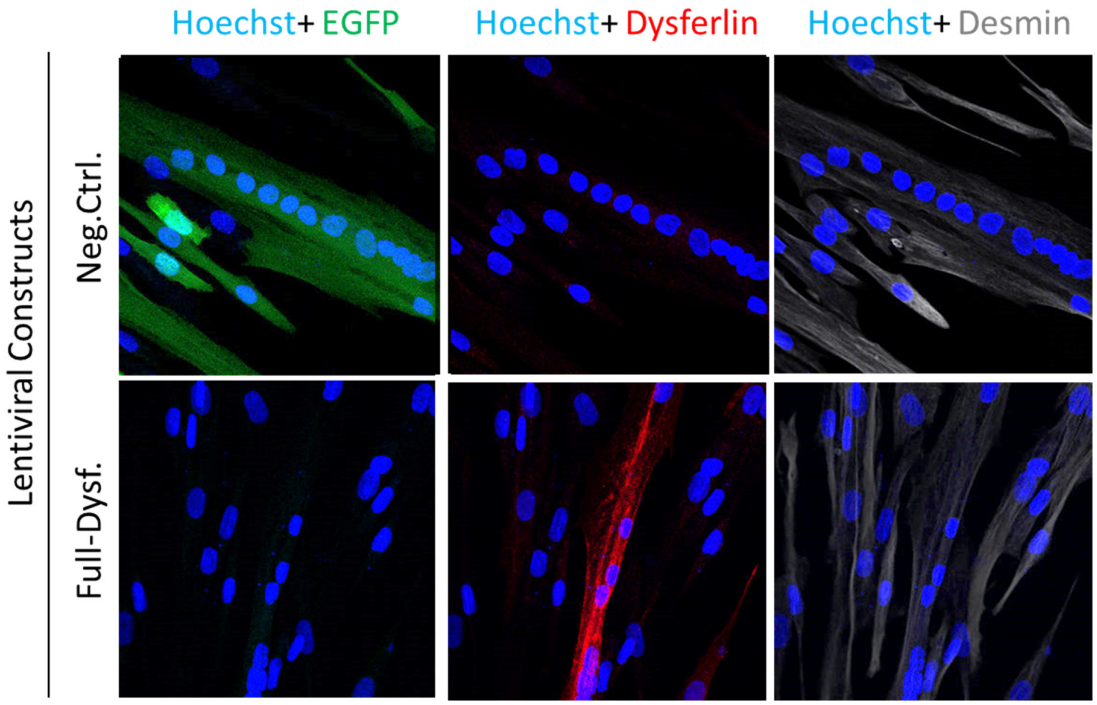

Figure 79 Localization of full dysferlin construct in myotubes derived from dysferlin deficient human primary myoblasts (1525).

Confocal microscopic image of immunostaining of dysferlin (red) using ROMEO antibody, desmin staining (grey) and Hoechst staining of nuclei (blue). The EGFP signal (green) comes from the integrated lentiviral cassette.

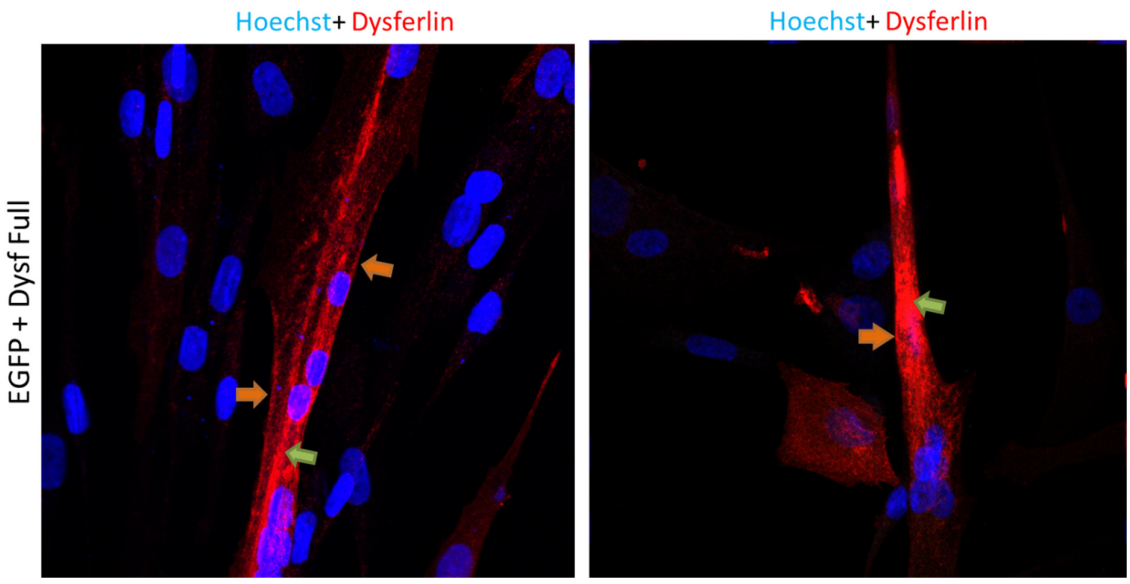

Figure 80 Localization of full dysferlin construct in myotubes derived from dysferlin deficient human primary myoblasts (1525).

Confocal microscopic image of immunostaining of dysferlin (red) using ROMEO antibody and Hoechst staining of nuclei (blue). The orange arrows pinpoint dysferlin localized at the sarcolemma and the green arrows indicate patches of dysferlin in cytosol.

In the case of truncated dysferlin none of the myotubes expressing Δexon 37, Δexon 38 and Δexon 37&38 constructs showed proper membrane localization (Figure 81). The signal coming from the dysferlin antibody concentrated mainly around the nuclei and was fading out when moving away from the center of a myotube (Figure 82, Figure 83, Figure 84). The 3D reconstruction of the dysferlin localization demonstrated enrichment of the dysferlin signal around nuclei of myotubes transduced with the constructs Δexon 37 (Figure 82) and Δexon 37&38 (Figure 84). The myotubes expressing the construct Δexon 38 (Figure 83) demonstrated the lowest enrichment of 3D dysferlin signal in the vicinity of nuclei.

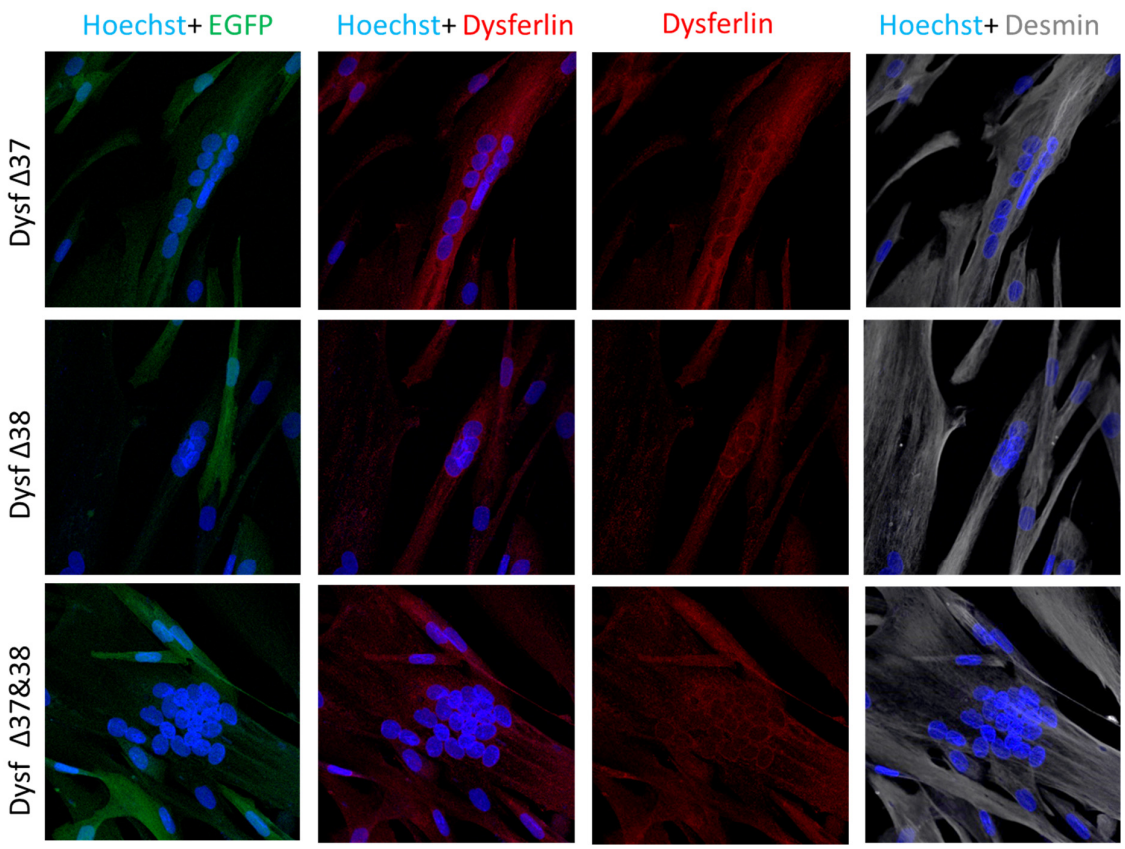

Figure 81 Localization of dysferlin Δexon 37, Δexon 38 and Δexon 37&38 constructs in myotubes derived from dysferlin deficient human primary myoblasts (1525).

Confocal microscopic image of immunostaining of dysferlin constructs (red) using ROMEO antibody, desmin staining (grey) and Hoechst staining of nuclei (blue). The EGFP signal (green) comes from the integrated lentiviral cassette.

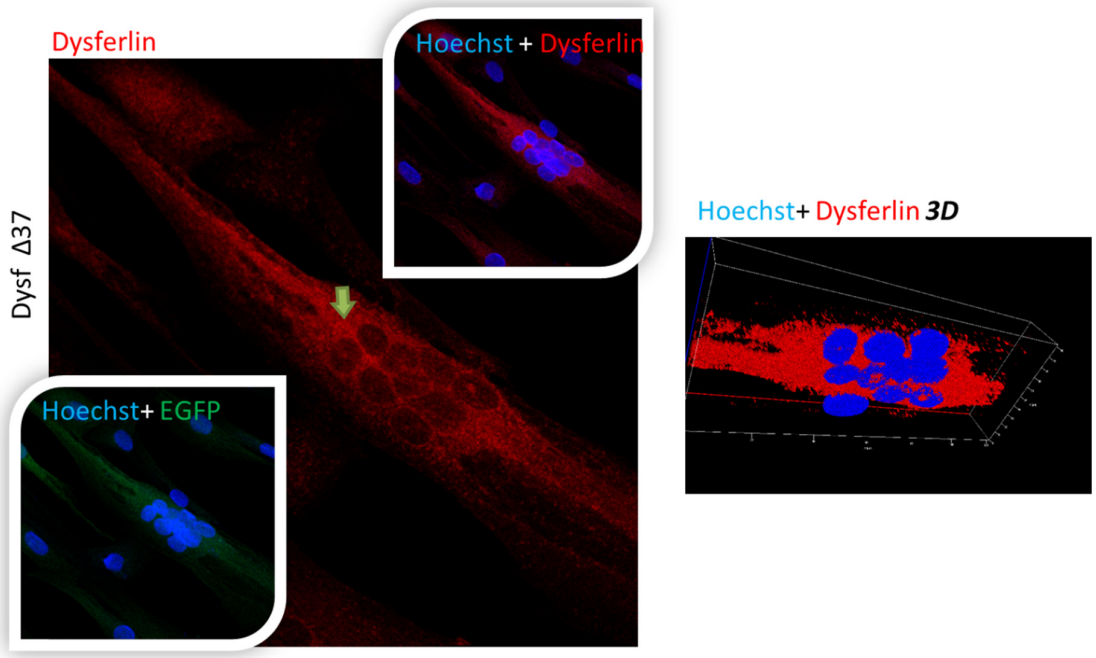

Figure 82 3D localization of dysferlin Δexon 37 construct in myotubes derived from dysferlin deficient human primary myoblasts (1525).

Confocal microscopic image of immunostaining of dysferlin constructs (red) using ROMEO antibody and Hoechst staining of nuclei (blue). The EGFP signal (green) comes from the integrated lentiviral cassette. The green arrow pinpoints the cytoplasmic dysferlin around nucleus.

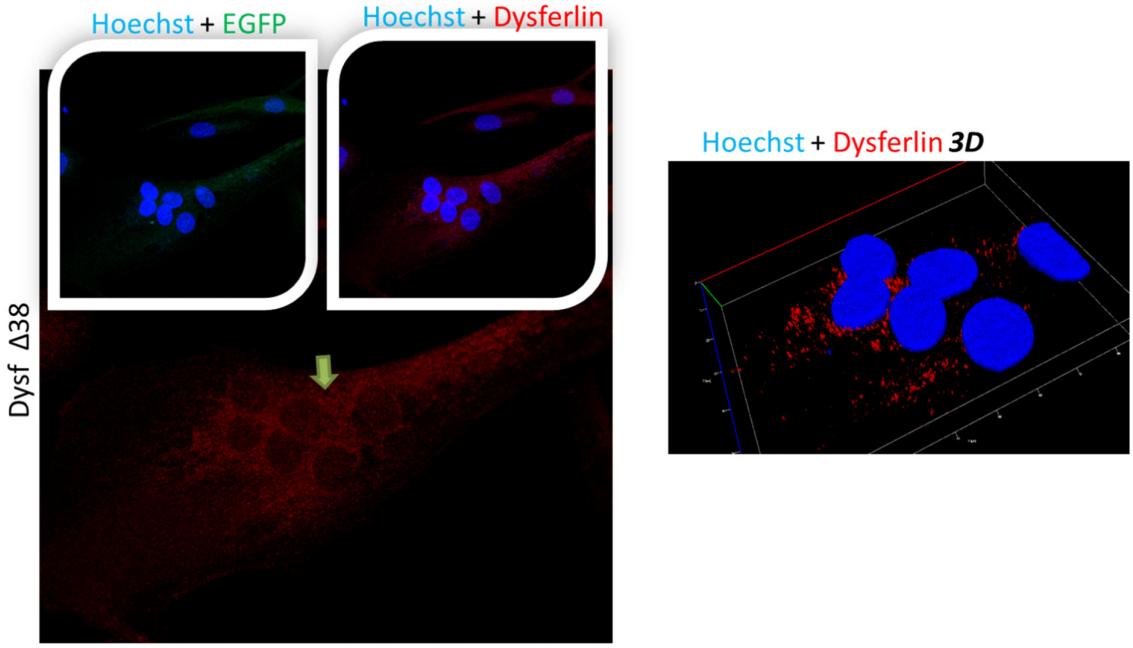

Figure 83 3D localization of dysferlin Δexon 38 construct in myotubes derived from dysferlin deficient human primary myoblasts (1525).

Confocal microscopic image of immunostaining of dysferlin constructs (red) using ROMEO antibody and Hoechst staining of nuclei (blue). The EGFP signal (green) comes from the integrated lentiviral cassette. The green arrow pinpoints the cytoplasmic dysferlin around nucleus.

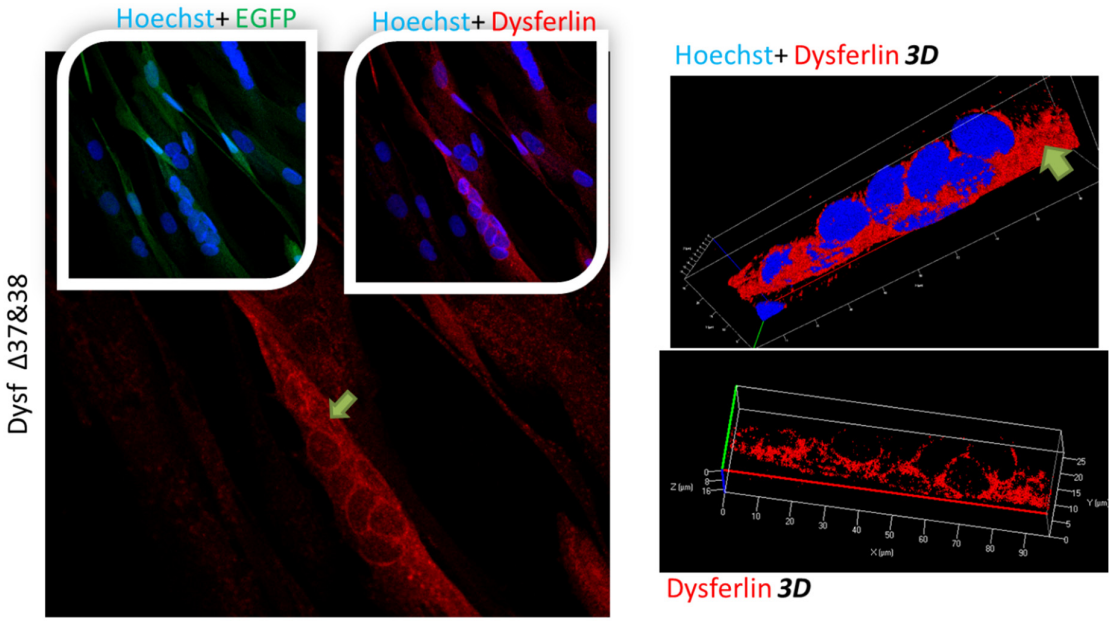

Figure 84 3D localization of dysferlin Δexon 37&38 construct in myotubes derived from dysferlin deficient human primary myoblasts (1525).

Confocal microscopic image of immunostaining of dysferlin constructs (red) using ROMEO antibody and Hoechst staining of nuclei (blue). The EGFP signal (green) comes from the integrated lentiviral cassette. The green arrow pinpoints the cytoplasmic dysferlin around nucleus.

Dysferlin is also detected in the undifferentiated myoblasts that were transduced with the lentiviral constructs (Figure 85). The highest expression of dysferlin was observed for the full length protein, which localizes mainly in the cell cytoplasm. The truncated dysferlin is expressed less in comparison to its full version. It is also detected in the cytoplasm, however, the 3D images suggest that the highest amount of dysferlin without exon 37 and without exon 38 concentrates mainly in the vicinity of nucleus.

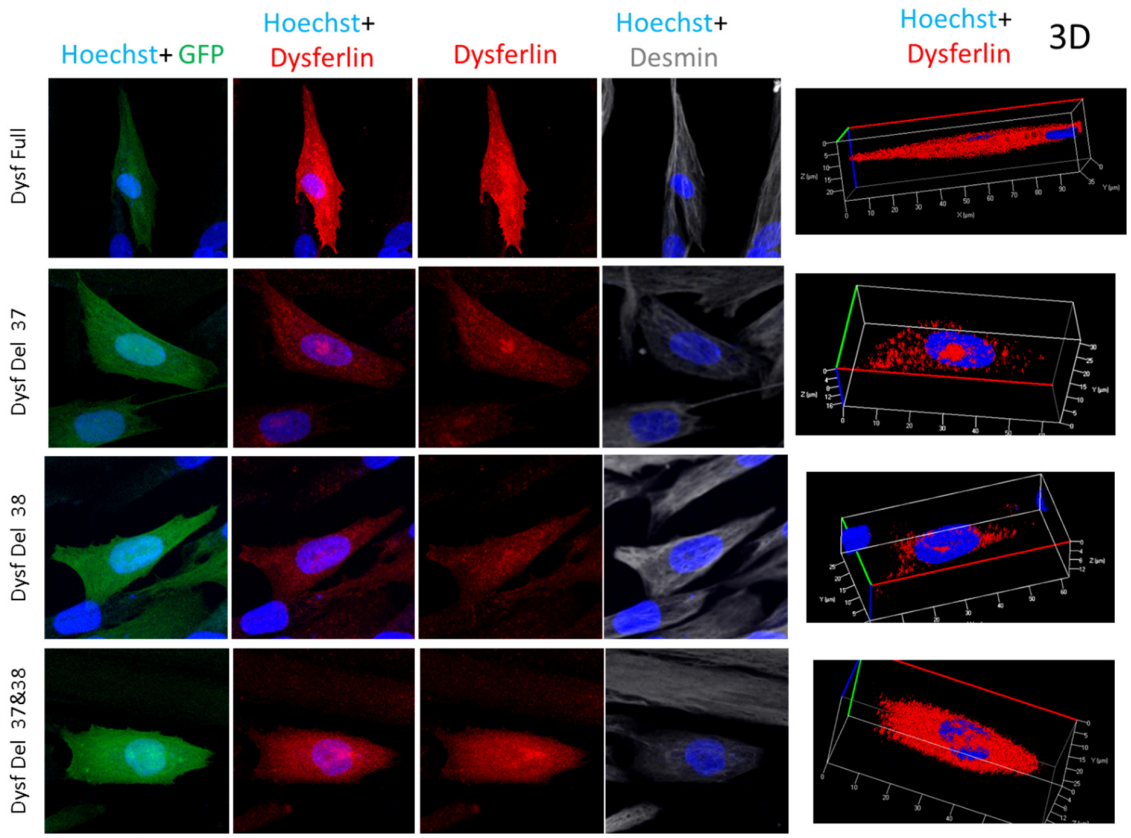

Figure 85 Localization of dysferlin Δexon 37, Δexon 38 and Δexon 37&38 constructs in dysferlin deficient human primary myoblasts (1525).

Confocal microscopic image of immunostaining of dysferlin constructs (red) using ROMEO antibody, desmin staining (grey) and Hoechst staining of nuclei (blue). The EGFP signal (green) comes from the integrated lentiviral cassette.

4. MATERIAL AND METHODS

4.1. Bioinformatic analysis of dysferlin pre-mRNA

Search for probable exonic splice enhancers (ESE) targeted by the set of human serine-arginine-rich (SR) proteins: SF2/ASF, SC35, SRp40 and SRp55 in human dysferlin pre-mRNA was performed using the online tool ESEfinder v.3.0 (http://krainer01.cshl.edu/cgi-bin/tools/ESE3/esefinder.cgi). (Cartegni et al., 2003). Default values of thresholds were used for the analysis of dysferlin exons 37 and 38.

	Matrices (select one or more)	Threshold
☑	**SRSF1** (SF2/ASF round 3 winner)	1.956
☑	**SRSF1 (IgM-BRCA1)** (Smith06-HMG-matrix)	1.867
☑	**SRSF2** (SC35 round 3 winner)	2.383
☑	**SRSF5** (SRp40 round 3 winner)	2.67
☑	**SRSF6** (SRp55 round 3 winner)	2.676
		Reset thresholds

Figure 86 Table of threshold values used for the analysis of ESE with ESEfinder.

For the analysis of exonic splice silencers (ESS) Human Splicing Finder HSF v.2.4.1 (http://www.umd.be/HSF) was used (Azakir et al., 2012)(Desmet et al., 2009). Sironi silencing motifs (Sironi et al., 2004) and sequences that exhibit high binding efficiency for the heterogeneous nuclear ribonucleoprotein A1 (hnRNP A1) (Del Gatto-Konczak et al., 1999) were taken into account.

RNA secondary structure of dysferlin exons and introns or of antisense sequences was predicted using the RNAfold web server (http://rna.tbi.univie.ac.at/cgi-bin/RNAWebSuite/RNAfold.cgi) (Gruber et al., 2008). For the antisense oligonucleotides and mU7 constructs only sequences not building a hairpin were selected for the verification of their exon skipping activity in the experimental part.

4.2. Analysis of dysferlin secondary and tertiary structure.

The structure of human dysferlin C2E domain was analyzed with the homology-modelling server SWISS-MODEL (https://swissmodel.expasy.org/). (Arnold et al., 2006; Biasini et al., 2014; Guex et al., 2009; Kiefer et al., 2009) For this purpose, the amino acid sequence encoded by exon 37, 38 and 39 of human dysferlin gene was obtained from Uniprot database

(accession number O75923). (Consortium, 2017) The sequence was used in SWISS-MODEL to predict the secondary and tertiary structure of C2E domain in the full dysferlin and dysferlin without exon38. As a homology template the dysferlin C2Avar1 domain (4iqh.1.A) was chosen. (Fuson et al., 2014)

The hydrophobicity plots were made in CLC Main Workbench (version 7.7.3) applying the amino acid scale values from the Kyte and Doolittle hydrophobicity scale. (Kyte and Doolittle, 1982). The analysis of potential proteolytic cleavage sites (PEST motifs) was performed with epestfind (http://emboss.bioinformatics.nl/cgi-bin/emboss/epestfind). (Rice et al., 2000)

4.3. Characterization of human primary and immortalized myoblasts

Cell Name	Type	Donor Age	Donor Sex	Muscle	Mutation in Dysferlin	Dysferlin Deficiency
c25	immortal	25	-	Semitendinosus	healthy	no
i379	immortal	43	female	Vastus lateralis	Exon 16: c.1448C>A HTZ, p.S483X; Exon 55: c.*107T>A HTZ, (3'UTR)	yes
i814	immortal	60	-	Vastus lateralis	Exon 38: c.4022T>C HMZ, p.L1341P	yes
AB320	immortal	29	female	Quadriceps	Intron 4: c.342-1G>A HTZ; Exon 32: c.3516_3517delTT HTZ, p.Ser1173X	yes
379	primary	43	female	Vastus lateralis	Exon 16: c.1448C>A HTZ, p.S483X; Exon 55: c.*107T>A HTZ, (3'UTR)	yes
1524A	primary	28	female	Triceps	Exon 44: c.4872delG HMZ	yes
1525	primary	25	female	Vastus lateralis	Exon 44: c.4872delG HMZ	yes
1552	primary	49	female	Vastus lateralis	healthy	no

Table 6 List of human primary and immortalized myoblasts used for the experiments.

4.4. Cell culture

Dysferlin deficient human immortalized myoblasts i814, i379, AB320 and healthy immortalized myoblasts c25, dysferlin deficient human primary myoblasts 379, 1524 and 1525, human

primary myoblasts 1552 and murine C2C12 cell line were cultured in humidified incubator at 37ºC with 5% CO_2 in Skeletal Muscle Cell Growth Medium SMCGM (Provitro) supplemented with the manufacturer mix of 5% fetal calf serum (FCS), fetuin, human recombinant epidermal growth factor (hEGF), human recombinant fibroblast growth factor (bFGF), insulin, dexamethasone, gentamicin and amphothericin B. The medium was additionally enriched with 10% FCS (Biochrom) and 1x glutamax (Life Technologies). For differentiation cells were grown up to 70% confluency and the medium was changed to Opti-MEM reduced serum medium (Life Technologies) supplemented with 2% horse serum (Lonza).

The MMex38 satellite cells were cultured in humidified incubator at 37ºC with 5% CO_2 on laminin (Millipore) coated plates in the satellite cell growth medium (DMEM/F12, 15% FBS, 1% gentamycin) supplemented with bFGF (Sigma) 1:1.000 and LIF 1:1.000 and B27 without vitamin A (Gibco) 1:50. The medium was changed every day. For the differentiation into myotubes cells were seeded at 1% Matrigel (Corning) coated plates and cultured in the DMEM medium (Gibco) supplemented with 2% horse serum (Lonza).

4.5. Cloning

4.5.1. Cloning of dysferlin constructs for microinjections and lentiviral productions

The starting material for producing the four versions of dysferlin protein (full, Δex37, Δex38, Δex37&38) connected to EGFP via PTA peptide were the following plasmids: pIRES2-EFGP, pRRLSIN.cPPT.PGK-MCS.WPRE, full-length human dysferlin cDNA pUC57-Kan-DysfFull, truncated human dysferlin cDNA pUC57-Kan-DysfΔex37 and pUC57-Kan-DysfΔex38 obtained as a gift from the Jain Foundation Inc., lentiCRISPR v2 was a gift from Feng Zhang (Addgene plasmid #52961) (Sanjana et al., 2014).

First the pUC57-Kan-DyfΔex37&38 plasmid was constructed. For this purpose, the pUC57-Kan-DysfFull was used as a template and circular PCR was done using Phusion Master Mix (Thermo Fisher Scientific) and P11c_F, P11a_R primers, which were designed to excise exon 37 and 38. The PCR product was gel purified and digested with the DpnI (NEB) enzyme to remove the original circular template plasmid. Next the free ends of pUC57-Kan-DyfΔex37&38 were ligated with Quick Ligase T4 (NEB) and transformed using heat shock method into XL-10 Gold Ultracompetent E.Coli (Agilent). The positive clone was verified by restriction digest and sequencing.

Before cloning of dysferlin constructs into the pIRES2-EGFP plasmid, the backbone was modified at two positions to introduce the EcoRV, NsiI, SpeI, MluI restriction sites in the MCS and the SwaI, AgeI restriction sites at the end of the EGFP cassette. A pair of complementary oligonucleotide strands carrying the four restriction sites and appropriate overhangs was ordered at Eurogentech (top strand: 5'-CTAGAgatatcatgcatactagtacgcgtG-3', bottom strand: 3'-TctatagtacgtatgatcatgcgcaCGATC-5'). The MCS was digested with NheI (NEB) enzyme, the two oligos were annealed and cloned into the pIRES2-EGFP plasmid. Next the SwaI and AgeI sites were introduced. Also in this case, a pair of complementary oligonucleotides with the two restriction sites and overhangs was ordered at Eurogentech (top strand: 5'-GGCCAatttaaataccggtGC-3', bottom strand: 3'- TtaaatttatggccaCGCCGG-5'). The pIRES2-EGFP_EcoRV-NsiI-SpeI-MluI was digested with NotI (NEB) and the two oligos were annealed and cloned into the plasmid. The modified plasmid pIRES2-EGFP_EcoRV-NsiI-SpeI-MluI_SwaI-AgeI was digested with SpeI (NEB) and XhoI (NEB) enzymes. Using the same enzymes, the first 3.241 nt of dysferlin cDNA, which are the same for all the dysferlin constructs, were cut out from the pUC57-Kan-DysfFull. The fragment was gel purified and cloned into the pIRES2-EGFP_EcoRV-NsiI-SpeI-MluI_SwaI-AgeI plasmid. In the next step the remaining part of dysferlin cDNA (part B) was cut out with XhoI (NEB) and BmtI (NEB) enzymes from the following plasmids pUC57-Kan-DyfFull, pUC57-Kan-DysfΔex37, pUC57-Kan-DysfΔex38, pUC57-Kan-DysfΔex37&38 and gel purified. The plasmid with the first part of dysferlin pIRES2-EGFP_EcoRV-NsiI-SpeI-MluI_SwaI-AgeI-DysfPartA was digested with XhoI (NEB) and BmtI (NEB) enzymes and the part B fragments were cloned individually into separate plasmid. The positive clones were verified by restriction analysis and sequencing.

Cloning of dysferlin constructs into the lentiviral plasmid pRRLSIN.cPPT.PGK-MCS.WPRE took place in 4 steps. First the EGFP cDNA (756nt) was amplified from pIRES-EGFP plasmid using cP23F and cP24R primers. The P2A fragment (113nt) was copied from the lentiCRISPR v2 plasmid using cP24F and cP24R primers. The first 625nt of human dysferlin (hDYSFsh) was amplified using cP25F and DYSF-Seq1R primers from the pIRES-EGFP-hDYSF_Full. The first 3.289nt of human dysferlin hDYSFa was also amplified using cP25F and cP25R primers from the pIRES-EGFP-hDYSF_Full plasmid, whereas the remaining part of human dysferlin containing the exon modifications (hDYSFb) was amplified from the pIRES-EGFP-hDYSF_Full, pIRES-EGFP-hDYSF_Δex37, pIRES-EGFP-hDYSF_Δex38, pIRES-EGFP-hDYSF_ Δex37&38 plasmids. The fragments were gel purified. In the second step the amplicons EGFP and P2A were combined in a PCR reaction with cP23F and cP24R primers. The EGFP_P2A fragment was gel purified. In the fourth step the amplicons EGFP_P2A and hDYSFsh were combined in a PCR reaction with cP23F and DYSF-Seq1R primers. The EGFP_P2A_hDYSFsh fragment was gel purified and cloned into pRRLSIN.cPPT.PGK-

MCS.WPRE using restriction enzymes BmtI and XbaI. Next the hDYSFa fragment was cloned into pRRLSIN.cPPT.PGK-EGFP_P2A_hDYSFsh.WPRE using the restriction sites XbaI and SalI. The positive clone was verified by sequencing. Finally, the fragment hDYSFb was introduced into pRRLSIN.cPPT.PGK-EGFP_P2A_hDYSFsh.WPRE using the enzymes PspXI and MluI to obtain the full construct pRRLSIN.cPPT.PGK-EGFP_P2A_hDYSFa_hDYSFb.WPRE. The clones with the correct constructs were verified by sequencing, amplified in XL-10 Gold Ultracompetent E.Coli (Agilent) and plasmids were isolated with the NucleoBond Xtra EF MaxiPrep (Macherey-Nagel).

Primer Name	Primer Sequence 5´-3´
P11c_F	ATGCTGCCCAGGGAGGAGCTCTACTGCCCCCCCATCACC
P11a_R	CTCATCCAGGATCCTTGATGTCTCCTGCACCTCAAAACC
cP23F	ATTATTGCTAGCATGGTGAGCAAGGGCGAGG
cP23R	AAGTTTGTTGCGCCGGATCCCATATGCTTGTACAGCTCGTCCATGC
cP24F	GGCATGGACGAGCTGTACAAGCATATGGGATCCGGCGCAACAAACTT
cP24R	AGGATGAAGACCCTCAGCATCGGTCCAGGATTCTCTTCGA
cP25F	TCGAAGAGAATCCTGGACCGATGCTGAGGGTCTTCATCCTCTATGC
cP25R	ATCATTGTCGACACGCGTACTACTCGAGGTGGAACTTCCAGC
DYSF-Seq1R	TAAAGATGGGCTCATCAAAC

Table 7 List of primers used for cloning of human dysferlin cDNA into the pIRES2-EFGP, pRRLSIN.cPPT.PGK-MCS.WPRE plasmids.

4.5.2. Cloning of mU7 antisense constructs for small scale AAV production using 293T cells

The antisense sequences of mU7 constructs were defined (Table 5). Before cloning the antisense sequences into the pSMD2-U7 vector, the plasmid was modified in order to introduce the BbsI and EcoRI restriction site within the U7 construct. First the U7 construct was amplified in two separate PCR rounds using Phusion Master Mix (Thermo Fisher Scientific). For the first PCR reaction XbaI_F and cP21_R primers were used. For the second reaction cP21_F and NheI_R primers were used. The PCR products were purified with a NucleoSpin Gel and PCR Clean-up (Macherey-Nagel). Next an aliquot of the first and second PCR product were used as a template for a third PCR with XbaI_F and NheI_R primers. The modified U7 construct was gel purified and cloned into the pSMD2 plasmid with XbaI and NheI primers. The modified plasmid was amplified in XL-10 Gold Ultracompetent E.Coli (Agilent) and the positive clone for pSMD2-U7-BbsI was verified by a restriction digest and sequencing.

The mU7 antisense sequences were ordered at Eurogentech as two complementary single stranded oligonucleotides with BbsI overhangs at 5' and 3' ends. The pSMD2-U7-BbsI plasmid was digested with BbsI restriction enzyme (NEB) and the annealed antisense oligonucleotides of U7 construct were cloned into the vector. Every mU7 construct was sequenced to verify the correct placement in the full mU7 sequence. The clones with the correct mU7 constructs were amplified in XL-10 Gold Ultracompetent E.Coli (Agilent) and plasmids were isolated with NucleoBond Xtra EF MaxiPrep (Macherey-Nagel). The correctness of mU7 antisense sequence was verified by sequencing.

Primer Name	Primer Sequence 5´-3´
cP21_F	tcgaGAATTCatGAAGACaattgcggaagtgcgtctgtag
cP21_R	TCatGAATTCtcGAAGACctaatttttggagcaggttttctgac
XbaI_F	TTATTAGCTAGCcacatacgcgtttcctaggaaaccagagaaggatc
NheI_R	TAATAATCTAGAtaacaacataggagctgtgattggctgttttcagccaatc

Table 8 List of primers used for cloning of mU7 constructs into the pSMD2 plasmid.

4.5.3. Cloning of mU7 antisense constructs for large scale AAV production using baculovirus

The mU7 constructs (U7.10, U8.2, U9.2) were cut out from pSMD2-U7-BbsI plasmid using SnaBI (NEB) restriction enzyme. The fragments were gel purified and cloned into the pFBD plasmid with SnaBI (NEB) restriction enzyme. The XL-10 Gold Ultracompetent E.Coli (Agilent) were heat shock transformed with the ligation reaction and plated on LB agar plates with ampicillin. The clones carrying the U7 insert were detected by means of miniprep amplification and restriction analysis with XbaI (NEB) and SnaBI (NEB) enzymes. Next the pFBD-U7 plasmids were transformed into MAX Efficiency DH10Bac (Invitrogen) chemically competent E.coli carrying baculovirus genome (bacmid) and a helper for transposition of U7 constructs into the bacmid. The bacteria were plated on LB agar plates containing kanamycin, gentamicin and tetracycline, Bluo-gal and IPTG. White colonies were selected for 5 mL liquid culture and plasmid extraction using NucleoSpin Plasmid Miniprep Kit (Macherey-Nagel). The presence of positive transposition was verified using M13F/R and Gent(FR) primers. The positive clones were amplified in 250 mL liquid culture and the bacmid was isolated with NucleoBond Xtra EF MaxiPrep (Macherey-Nagel).

Primer Name	Primer Sequence 5´-3´
M13F	CCCAGTCACGACGTTGTAAAACG
M13R	AGCGGATAACAATTTCACACAGG

Gent(FR)	CGTAACATCGTTGCTGCTGCGTAA

Table 9 List of primers used for verification of transposition of the mU7 constructs into the bacmid.

4.5.4. Cloning of mU7 antisense constructs for in vitro exon skipping

The mU7 constructs were amplified using Phusion polymerase (NEB) and C1_F and C1a_R primers. The fragments were gel purified and cloned into the pRRLSIN.cPPT.PGK-MCS.WPRE plasmid using XhoI and BamHI restriction sites. The positive clones were verified by a restriction digest and sequencing and amplified in 250 mL liquid culture. The plasmid was isolated with NucleoBond Xtra EF MaxiPrep (Macherey-Nagel).

Primer Name	Primer Sequence 5´-3´
C1_F	AAACTCGAGtctagataacaacataggagct
C1a_R	ATTGGATCCcacatacgcgtttcctagga

Table 10 List of primers used for cloning of the mU7 constructs into the pRRLSIN.cPPT.PGK-MCS.WPRE plasmid.

4.6. Lentiviral production

Third generation (Dull et al., 1998c), self-inactivating lentiviral vectors (Zufferey et al., 1998) were produced at UVSQ at Luis Garcia Lab using quadri-transfection of 293T cells. Sequences encoding Gag, Pol and Rev proteins were delivered on pMDLg/pRRE and pRSV-Rev packaging plasmids, whereas the vesicular stomatitis virus envelope glycoprotein (VSV-G) on pMD2.G plasmid. The viral LTRs with dysferlin gene connected to EGFP and control of human phosphoglycerate kinase-1 (PGK-1) promoter were delivered on the pRRLSIN.cPPT.PGK-MCS.WPRE plasmid. Three days after transfection the supernatant was collected and centrifuged at 3.500 g for 30 minutes and filtered via 0,3 µm filter. The filtered supernatant was further concentrated using tangential flow filtration system from Specturm Labs. The concentrate was centrifuged for 2 hrs at 20.000 rpm with Beckmann ultracentrifuge and the viral pallet was resuspended in PBS, aliquoted and frozen at -80ºC. Viral titer was estimated by means of Lenti-X qRT-PCR Titration Kit (Clontech) and titration by infection.

4.7. Recombinant adeno-associated virus (rAAV) production

The rAAVs were produced in Luis Garcia Lab at UVSQ. A low scale production of rAAVs was done using tri-transfection method (Xiao et al., 1998) combined with the downstream detergent treatment according to the (Dias Florencio et al., 2015) protocol. A large scale rAAV

production for animal experiments was performed with the baculovirus expression system in SF9 insect cells according to (Buclez et al., 2016) protocol. The produced AAV2 was pseudotyped with an AAV9 capsid resulting in the recombinant rAAV2/9. For tri-transfection a plasmid pAAV2/9 encoding replication and capsid proteins, a helper plasmid pXX6 and a transgene encoding plasmid pSMD2 were used. For the baculovirus system the U7 transgene was cloned into the pFBD plasmid. The transgene was transposed into the baculovirus genome and functional baculoviral particles were produced. The rAAV2/9 particles were produced by coinfection of SF9 cells with three baculoviral constructs encoding for the mU7 transgene, rAAv2/9 capsid and replication proteins. The rAAV2/9 titers were estimated by qPCR and were between $2*10^{12}$ and $1,5*10^{13}$ VG/mL.

4.8. Transfections and transductions

Immortalized human myoblasts were transfected with 2'-O-methyl phosphorothioate antisense oligonucleotides (2'OM-S-oligos) and Lipofectamine LTX with Plus Reagent (Invitrogen). The day before experiment 150.000 cells per well were seeded in 12-well-plates. Next day cells were washed with PBS and 900 µL of Opti-MEM were added. A 1:1 mix of Plus Reagent with 2'OM-S-oligos in total of 105 µL of Opti-MEM was prepared. A dilution of Lipofectamine LTX in total of 105 µL Opti-MEM was made. For every µg of oligonucleotides 1 µL of Plus Reagent and 2 µL of Lipofectamine LTX were used. Both solutions were combined and incubated for 5 minutes. 100 µL of the mix was added to cells. 24 hrs later the medium was replaced with 1 mL of fresh Opti-MEM and cells were differentiated for 3 days.

C2C12 cells and MMex38 satellite cells were transfected with U7 constructs cloned into the pRRLSIN.cPPT.PGK-MCS.WPRE plasmid by means of Lipofectamin 3000 (Invitrogen). The day before experiment 50.000 cells per well were seeded in 12-well-plates. Next day cells were washed with PBS and 600 µL of fresh SMCGM or satellite cell growth medium (DMEM/F12, 15% FBS, 1% gentamycin) supplemented with bFGF (Sigma), LIF and B27 without vitamin A (Gibco) was added. 500 ng of plasmid and 1 µL of P3000 Reagent (Invitrogen) were diluted in 50µL of OptiMEM medium (Gibco). Next 1 µL of Lipofectamin 3000 was diluted in 50µL of OptiMEM medium. Afterwards, the diluted lipofectamin was added to the diluted plasmid and incubated for 5 min in room temperature. 100 µL of the mix was added to cells. 24 hrs later the medium was changed to the differentiation medium (DMEM, 2% horse serum, 1% PenStrep). The medium was changed every day and the cells were differentiated for 3 days in the case of satellite cells and 5 days in the case of C2C12 cells.

Human primary myoblasts were transduced with Lentivirus at MOI of 2. The cells were seeded at density of 50.000 cells per well in 12-well-plate in SMCGM. Next day the cells were washed

with PBS and medium was changed to 600 µL of fresh SMCGM. Appropriate amount of virus was added. The cells were inoculated with the virus for 24 hrs and afterwards the medium was changed. 72 hrs post transduction the cells were passed to a 10 cm dish for further expansion. Differentiation was induced with Opti-MEM with 2% horse serum and was continued for 4-5 days.

C2C12 cells or MMex38 mouse satellite cells were transduced with AAV2/9 at MOI of 10^6 or 10^7. The C2C12 cells were seeded at the density of 500.000 cells per well in 6-well-plate in SMCGM and the mouse satellite cell were seeded at the density of 50.000 in 12-well-plate in the growth medium (DMEM/F12, 15% FBS, 1% gentamycin) supplemented with bFGF (Sigma), LIF and B27 without vitamin A (Gibco). Next day the cells were washed with PBS and medium was changed to fresh medium. Appropriate amount of virus was added. The cells were inoculated with the virus for 24hrs and afterwards the medium was changed to a differentiation medium (DMEM, 2% horse serum, 1% PenStrep). The medium was changed every day and the cells were differentiated for 3 days in the case of satellite cells and 5 days in the case of C2C12 cells

4.9. Quantitative real time PCR (qPCR)

Prior qPCR the isolated RNA was treated with Turbo DNAse (Ambion) for 30 min at 37ºC to remove any trances of DNA. The reaction was stopped by adding 2 µl of the DNAse inhibitor mix. For the reverse transcription the SuperScript VILO cDNA Synthesis Kit (Invitrogen) with random hexamers was used. 2,5 µg of RNA was revers transcribed to cDNA for 60 min at 42ºC. To detect skipped, unskipped and total dysferlin transcripts a qPCR TaqMan assay was designed using the Custom TaqMan Assays Design Tool (Life Technolgoies). For quantification of unskipped product FAM probe (MEX3637_M) in exon 37 was used. Detection of the skipped transcript (Δex37&38) was made with a FAM probe (MEX3639_M) placed at the junction of exon 36 and 39. The total amount of dysferlin transcript was estimated with a FAM probe (MEX3435_M) situated at the junction of exon 34 and 35. The qPCR was performed with iTaq Universal Probes supermix (Biorad) on Biorad CFX96™ Touch System for 40 cycles (95ºC for 30 s followed by 40 cycles of 95ºC for 5 s and 60ºC for 30 s). The samples were measured in triplicates. 50 ng of RNA was used per reaction. Data were analyzed using Biorad Precision Melt Analysis Software. For every analyzed sample (mU7.10, mU8.2, mU9.2, SCRAM, PBS) the ΔCt of all the replicates was calculated by subtracting the mean Ct of the endogenous control 18S from each of the replicates of the skipped/unskipped/total dysferlin assays. The abundance of every transcript was calculated using the formula $(1+\text{qPCR Efficiency}/100\%)^{-\Delta Ct}$. The percentage of skipped transcript was

calculated by dividing the abundance of the skipped product by the abundance of the total transcript. The background level caused by non-specific amplification was determined by calculating the level of skipping for a PBS sample and subtracting this value from the percentage of skipped transcripts determined for every mU7 sample (mU7.10, mU8.2, mU9.2, SCRAM). The average level of skipping was calculated from the triplicates and the significance was calculated with unpaired two-tailed student test.

Primer/Probe Name	Primer/Probe Sequence 5´-3´
MEX3637_F	GGAGGCCAACATCTACATGGTT
MEX3637_R	GGCAGTACGTTGGAGAGCT
MEX3637_M	CCCCAGAACATTAAGCC
MEX3639_F	ATGCATGAAACTTCAAGGATTTTGGA
MEX3639_R	GACCACAATAGGTGGACAGTAGAG
MEX3639_M	CTCTCTGGGTAACATCTCA
MEX3435_F	GCAGCGTTCGAGCTTATCC
MEX3435_R	AGCCAGGGATGTGATGG
MEX3435_M	ATGGCTGGCTTCTCTC

Table 11 List of primers used for qPCR.

4.10. Flow cytometry and FACS sorting of lentivirus transduced primary myoblasts

The cells were detached from culture plates with trypsin and centrifuged at 200g for 5 min. The supernatant was removed and the pellet was resuspended in 2 mL of ice cold staining buffer (1% BSA in 1x PBS). The cells were filtered through a 70 µm nylon mesh and spun again at 200g for 5 min. Next the cells were suspended in 400 µL of staining buffer with primary antibody mouse monoclonal anti-CD56-NCAM (Milteny) 1:200 and incubated for 15 min at 4ºC. Afterwards, 1 mL of cold staining buffer was added and the cells were centrifuged at 200g for 5 min. The supernatant was removed cells were washed 2 more times with 1 mL of cold staining buffer. The pellet was resuspended in 400 µL of cold staining buffer containing secondary antibody Alexa 647 goat anti-mouse (Invitrogen) 1:500 and incubated for 15 min at 4ºC. Afterwards, 1 mL of cold staining buffer was added and the cells were centrifuged at 200 g for 5 min. The supernatant was removed cells were washed 2 more times with 1 mL of cold staining buffer. Finally, the cells were resuspended in PBS and FACS sorted using BD FACSaria F cell sorter according to the gating presented in the Figure 67.

4.11. Microinjections

The plasmids dilutions (250 ng/µL) were prepared and centrifuged with 12.000 g at 4°C for 45 min. The clarified solution was loaded on Femtotip II capillaries from Eppendorf. The FemtoJet system combined with the InjectMan NI 2 (Eppendorf) was used for microinjections. The injections were done into myotubes differentiated from immortalized myoblasts i379, AB320 and myotubes derived from human primary myoblasts 379. The injection was performed with a continuous flow under the pressure of 80 to 120 hPa. About 50 myotubes were injected per cell type. The expression of EGFP was verified 24 hours later using a fluorescent microscope.

4.12. Membrane wounding assay

The myoblasts were grown and differentiated in 3,5 cm glass bottom dishes (Ibidi). Before the laser wounding assay myotubes were washed twice with Tyrode solution (5 mM KCl, 140 mM NaCl, 2 mM $MgCl_2$, 2,5 mM $CaCl_2$, 10 mM HEPES, pH 7,2). (Marg et al., 2012a) The assay was performed in 1mL of Tyrode solution supplemented with 2,5 µL of 1 mM FM 4-64 fluorophore (Invitrogen) using Zeiss LSM 510 META confocal microscope. Myotubes were wounded with 30 mW argon-laser by irradiating area of 2,5x2,5 µm for 60 s. A single image was taken before irradiation and further pictures were recorded in time series every 20 s after wounding to observe the changes in the fluorescence intensity over time. Fluorescent intensities were measured using ImageJ software and plotted against the time axis. The significance was calculated with unpaired two-tailed student test.

4.13. RNA Isolation, RT-PCR and nested PCR

RNA was isolated from cells or mouse TA muscle using TRIzol Reagent (Life Technologies) according to the manufacturer protocol. The cells were harvested directly from culture dish with 1 mL of TRIzol and stored at -80ºC. The isolated TA muscle was harvested and stored in homogenization tubes with ceramic beads in TIRzol at -80ºC. For the RNA isolation the muscle samples were thawed and homogenized in Precellys24 (Bertin Instruments) at 5.000 rpm for 45 s and at 6.800 rpm for 15 s. The downstream steps followed the manufacturer protocol. RNA was resuspended in RNAse free water, incubated in heat block at 55ºC for 15 min and finally stored at -80ºC. RNA concentration was measured by NanoVue Plus spectrophotometer (Biochrome).

1 µg of total RNA was used in a reverse transcription reaction. For the detection of exon skipping the reverse transcription and PCR reactions were done in one tube using

AccessQuick™ RT-PCR System (Promega) for 40 cycles. In the case of cell-based experiments a pair of primers P1_F/P1_R primers was used in the RT-PCR reaction. 10 µl of the PCR product were analyzed for the skipped exons on 1,5% agarose gel. The level of exon skipping was estimated by densitometry method. In the case of in vivo mouse and in vitro C2C12, MMex38 satellite cells experiment the nested RT-PCR strategy with a pair of external primers mP3/mP3R and a pair of internal primers mP2F/mP2R was applied to screen samples for exon skipping. For this purpose, 500 ng of total RNA was used in the RT-PCR reaction for 35 cycles and 1µl of the its product was taken for the nested PCR reaction using GoTaq Master Mix (Promega) for 25 cycles. 5-7 µl of the nested PCR product were analyzed for the skipped exons on 1,5% agarose gel.

Primer Name	Primer Sequence 5´-3´
P1_F	CCTGGTTTTGAGGTGCAGGA
P1_R	GTAGGGGTCACACAGGAAGC
mP2F	AAGCCAGAAGACAGTGGTGG
mP2R	GAGTATGGGTCGCACAGGAA
mP3F	TCTTTGACTATGGGAACCGCT
mP3R	CTGTGGGGATGGACTCTCTG

Table 12 List of primers used for the RT-PCR and the nested PCR.

4.14. SDS-page and western blot

For the protein isolation form TA muscles an extraction buffer (50 mM Tris, 150 mM NaCl, 0,5% Triton X-100, 0,5% Na-Deoxycholat, 1 mM EDTA, 50 mM NaF, 1 mM sodium orthovanadate) with the pH of 7,4 was used. Before the tissue lysis the buffer was supplemented with the protease inhibitors 1 mM PMSF and 1x Complete (Roche). The tissue was minced with a manual homogenization pistil in 400 µl of full lysis buffer and incubated for 30 min on ice. Next the samples were centrifuged at 1.500 g in 4ºC and the supernatant was recovered for protein concentration measurement with BCA Protein Assay Kit™ (Thermo Scientific). For SDS-Page 50 µg of protein lysate was mixed with 6xSDS- sample buffer and incubated at 95ºC for 5 min. Proteins were run on Novex™ WedgeWell™ 8-16% Tris-Glycine Mini Gels 1mm, 15well (Invitrogen) in the XCell SureLock™ Mini Cell Electrophoresis System (Invitrogen) for 60min at 200V. The separated proteins were transferred to a nitrocellulose membrane using semi-dry-blot (Trans-Blot® SD Semi-Dry Electrophoretic Transfer Cell, Biorad) at 18 V for 60 min. Membranes were blocked in 4% milk dissolved in TBS-T. The membrane was incubated overnight at 4ºC with two primary antibodies diluted in 4% milk and TBS-T: mouse monoclonal antibody anti alpha-tubulin (Sigma-Aldrich) 1:3.000 and rabbit monoclonal antibody Hamlet anti-Dysferlin (Novocastra) 1:500. Next the membrane was

washed thee times with TBS-T for 15 min and a secondary antibody IRDye 800 anti-mouse (Rockland) 1:5.000 diluted in 4% milk and TBS-T was added and incubated for 60 min at room temperature. Next the membrane was washed three times with TBS-T for 15 min. The fluorescent signal was detected using Odyssey Infrared Imager (LI-COR).

4.15. Immunostainings of myoblast, myotubes and satellite cells

Cells were seeded on glass cover slips or in glass bottomed plates (ibidi) and fixed with 3,7% formaldehyde for 10 min at room temperature. Next they were washed three times with 1xPBS. Afterwards the cells were permeabilized with 0,2% Triton-X100 in 1xPBS for 5 min at room temperature and washed three times with 1xPBS. Next the cells were blocked with 1%BSA in 1xPBS for 1h at room temperature. For dysferlin localization study the blocked cells were incubated overnight at 4ºC with two primary antibodies diluted in 1% BSA in 1xPBS: mouse monoclonal antibody anti-Desmin (DAKO) 1:100 and rabbit monoclonal antibody ROMEO anti-Dysferlin (Abcam) 1:150. For satellite cell quality control the cells were incubated overnight at 4ºC with two primary antibodies diluted in 1% BSA in 1xPBS: mouse monoclonal antibody anti-Desmin (DAKO) 1:100 and mouse monoclonal antibody anti-PAX7 (DSHB) 1:150. Next day the cells were washed three times with 1xPBS and incubated for 1 h at room temperature with the secondary antibody diluted 1:500 in 1% BSA in 1xPBS: polyclonal Alexa 568 donkey anti-rabbit (Life Technologies) and polyclonal Alexa 647 goat anti-mouse (Life Technologies). For the satellite cell quality control the secondary antibodies included: polyclonal Alexa 488 goat anti-mouse (Invitrogen) and Alexa 568 donkey anti-rabbit (Life Technologies). Next the cells were stained for 10 min with Hoechst 1:5000 in 1xPBS. Finally, the cells were washed three times with 1xPBS and the cover slips were mounted on glass plates using aquamount medium (Polyscience).

4.16. Animal experiments

The in vivo verification of antisense activity of AONs was made in 1-2 months old BL10 wild type mice. The AONs were delivered by an intramuscular injection into the TA muscle at the concentration of 30 µg/TA. The mice were sacrificed 3 weeks after the injection. 2,5-3 months old mice of MDX strain were used for the in vivo screening of the mU7 constructs delivered with AAV2/9 virus. $1{,}32*10^{11}$ VGs containing mU7 constructs were delivered by an intramuscular injection into every TA muscle. The mice were sacrificed 4 weeks after the injection. In both experiments the animals were anesthetized by inhalation of isoflurane before the injections were made. The mice were sacrificed by cervical dislocation. The experiments were made in the laboratory of Dr. Luis Garcia at the UFR des sciences de la santé Simone

Veil, Université de Versailles Saint-Quentin-en-Yvelines, 2 Avenue de la Source de la Bièvre, 78180 Montigny-le-Bretonneux, France.

Dysferlinopathy caused by human mutation DYSF p.L1341P in dysferlin was modeled with the MMex38 mice, which carry an equivalent homozygous mutation in the exon 38 of the dysferlin gene (Dysf p.L1360P). 4-6 months old mice were used for the pilot phase testing the exon skipping efficiency of the selected mU7 constructs. The animals were anesthetized by inhalation of isoflurane and the selected mU7 constructs were delivered as an intramuscular injection into the TA muscle at the concentration of $1,56*10^{12}$ VG/TA. The mice were sacrificed by cervical dislocation 4 weeks after the injection. For the isolation of dysferlin deficient myoblasts 5-8 weeks old MMex38 mice were used. The animals were kept at the Animal Facility of Max-Delbrück Center für Molekulare Medizin, Robert Rössle Str. 10, 13125 Berlin. The experiments were performed under the license number G0145/16 and X9001/17 in the laboratory of Prof. Simone Spuler at the Experimental and Clinical Research Center, Lindenberger Weg 80, 13125 Berlin, Germany.

4.17. Isolation and culturing of mouse satellite cells

The MMex38 mice of 5-8 weeks were sacrificed by cervical dislocation. The muscle tissue from both hind limbs was extracted and placed in 10 mL of digestion medium (DMEM, 25 mM Hepes pH 7,0, Gentamycin 1:100, Amphotericin) supplemented with NB4 300 ng/µL (Serva) and dispase II 2,5 ng/µL enzymes (Roche). The samples underwent three digestion rounds of 15min at 37ºC in a shaking incubator (120 rpm). After each round the tissue slurry was dissociated by pipetting 20-30 times up-and-down. Before the final pipetting 500 µL of 0,25% trypsin (Gibco) was added. The digested tissue was filtered through a tissue bag, subsequently through 100 µm, 70 µm and 40 µm cell strainer and ultimately spun at 500g for 10 min at room temperature. The supernatant was removed and cell pellet was resuspended in 10mL of cold staining buffer (HBSS, 25 mM Hepes, 0,5% BSA, 2mM EDTA, Gentamycin 1:200). The cells were centrifuged again at 500 g for 10 min at room temperature and the pellet was resuspended in 1 mL of cold staining buffer containing four primary antibodies: polyclonal IgG goat-anti-VCAM1 (R&D) 1:100, monoclonal IgG PE-rat-anti-CD31 (BD Parmingen) 1:200, monoclonal IgG PE-rat-anti-CD45 (BD Parmingen) 1:200, monoclonal IgG PE-rat-anti-Sca1 (BD Parmingen) 1:200. The cells were incubated on ice for 15 min and washed two times with 1 mL of cold staining buffer. Next the cell pellet was resuspended stained for 15 min on ice with a secondary antibody: polyclonal donkey anti-goat Alexa-488 (Invitrogen) and the cells were subsequently washed three times and resuspended in the staining buffer for FACS sorting. During sorting the cells were collected into tubes filled with

the satellite cell growth medium (DMEM/F12, 15% FBS, 1% gentamycin) supplemented with bFGF (Sigma) 1:1.000 and LIF 1:1.000.

5. DISCUSSION

5.1. Dysferlin exon 37 and 38 are separated by a short intron that contains a hairpin secondary structure

It is essential to perform a bioinformatic analysis before undertaking any exon skipping tries because it provides basic information for the rational design of an antisense strategy. Aartsma-Rus demonstrated that successful exon skipping has to take into consideration both location of cis-acting elements and possible RNA secondary structures, which influence accessibility of ESEs and ESSs for the SR proteins. (Aartsma-Rus et al., 2009)

My analysis of the dysferlin cDNA secondary structure revealed that exon 37 and 38 are located close to each other. The separating intron 37-38 with 118 nt is relatively short, considering that introns in human genome have on average 5.419 bp and some of them can exceed even 100.000 bp. (Sakharkar et al., 2004) Moreover, the analysis provided information about the secondary structure available in the human but not in the mouse dysferlin intron 37-38. The intron is likely to build a hairpin at its 3' end. This structure reduces additionally the intron's length and consequently shortens the distance between exons 37 and 38. It is noteworthy that the 3'ss of intron 37-38 is enclosed in the hairpin structure so the AG nucleotides do not seem to be easily accessible to the splicing machinery. This conformation is likely to weaken the definition of the exon. The impact on splicing outcome of pre-RNA secondary structure near a splice site has been already described in the pre-mRNA of tau protein in which the stem-loop structure sequesters the 5'ss of intron 10-11 and leads to natural skipping of exon 10 (Figure 23). Mutations that disrupt the hairpin increase the availability of the splice site and increase the rate of exon 10 inclusion. (Jiang et al., 2000) Similar inhibitory effect of a hairpin on 5'ss was described for the SMN2 pre-mRNA (Singh et al., 2007). In the case of dysferlin exon 38 the stem-loop structure does not have such a pronounced modifying effect on the native splicing of exon 38. Nevertheless, assuring proper splicing of exon 38 might be dependent on the interaction between SR proteins and ESEs compensating/loosening the unfavorable RNA secondary structure. These facts led me to a hypothesis that a simultaneous skipping of both exon 37 and 38 could be easier than skipping just exon 38.

Despite of the fact that RNAfold detected a hairpin in the intron, it is important to keep in mind that RNA folding takes place co-transcriptionally in a cell. (Kramer and Mills, 1981) Hence, the transcribed RNA is folded shortly after being synthesized and the resulting structures can be

influenced by the speed of transcription, intermediate forms that are formed during elongation and processing of a transcript and by attaching proteins to a freshly synthesized RNA strand. These events can influence the secondary structure but are not reflected by the algorithms like RNAfold that use thermodynamic parameters and assume that RNA is always able to reach the most energetically stable structure. (Gruber et al., 2008) A possible improvement in the accuracy of predicting the RNA secondary structure could provide the CoFold algorithm. (Proctor and Meyer, 2013) It takes into account the kinetics of the co-transcriptional folding process and combines it with the thermodynamic information. Nevertheless, the algorithm is currently not used for the development of exon skipping strategies.

5.2. Masking ESEs with AONs in dysferlin exon 38 triggers low levels of skipping of exon 38 in WT human immortalised myoblasts but not in WT mouse

When deciding about the antisense strategy, one should also answer the question which parts of the targeted exon should be masked with antisense oligonucleotides or snRNAs. The best method for predicting potential cis-acting elements is an in silico search for ESEs and ESSs using online tools like ESEfinder or HSF. This approach was already successfully used in the design of antisense sequences for the exon skipping in the dystrophin pre-mRNA (Aartsma-Rus et al., 2009) and for the removal of exon 32 in the dysferlin pre-mRNA (Barthélémy et al., 2015).

The authors of ESEfinder pinpoint, however, some limitations to this methodology that should be taken into account before interpreting the results. (Cartegni et al., 2003) Firstly, the algorithm does not consider the native context of the predicted ESEs whose activity is normally modulated or hindered by SR proteins binding to neighboring ESSs. In other words, a predicted ESE may turn out to be inactive in the context of the living cell if, for instance, trans-acting hnRNPs mask the predicted enhancer. Secondly, the authors underline that there is only a rough correlation between the numerical score and the splicing effectivity. Hence, the highest score does not necessarily describe the most effective ESE motif. Thirdly, the algorithms work only with a subset of all known SR proteins so one has to keep in mind that there are other trans-acting proteins that are also likely to influence the final splicing pattern and whose binding sequences were not represented in the prediction. Fourthly, the ESEfinder predicts the ESEs for the human SR proteins and it cannot be extrapolated to other species without considering the level of conservation between the trans-acting elements: SRSF1(SF2/ASF), SRSF2 (SC35), SRSF5 (SRp40), SRSF6 (SRp55).

In the case of exon 37 and 38 of human dysferlin there were many ESEs predicted by ESEfinder with the database of the consensus binding sequences for SF2/ASF, SC35, SRp40 and SRp55 proteins. Taking into account the large amount of possible ESEs, I decided to group them into six blocks (Figure 87 upper panel) that were masked using antisense 2′-*O*-methyl-modified phosphorothioate RNA. Additionally, one ISE was added to the in vitro screening test in human immortalized myoblasts. The best AONs that removed exon 38 were: AON5 covering an ISE in intron 37-38, AON7 masking the second best ESE (block 1) in exon 38, AON9 covering the best ESE (block 4) in exon 38, AON9.1 masking selected ESEs of the block 5 and AON12 targeting the junction between exon 38 and intron 38-39 (3'ss). Interestingly, the AON7 was the best performing antisense oligonucleotide, although it was masking the second best ESE predicted by the ESEfinder (Figure 87). This confirms the limitation of the ESEfinder predicting algorithm that the highest score of an ESE does not necessarily tell if it is the most active enhancer. (Cartegni et al., 2003) The experiments confirmed also the importance of the ISE for the inclusion of the exon 38. AON5 masking this sequences managed to trigger skipping of exon 38 and confirmed the role of the intronic enhancer predicted by Carlo et al. (Carlo et al., 1996)

The antisense activity of AON7, AON9m, AON9.1, AON12 was also tested intramuscularly in C57BL10 mouse model at the concentration of 30 µg/TA. None of the oligonucleotides provided detectable exon skipping. It is unlikely that the lack of exon skipping was caused by an insufficient dose of the injected 2′-*O*-methyl-modified phosphorothioate per TA muscle. Heemskerk et al. compared activity of 2'OMe PS and PMOs and injected 20 µg of 2'OMe PS per gastrocnemius in order to skip exon 23 of mouse dystrophin. The exon skipping results were fluctuating from 2% for the 25mer and 20% for the 20mer oligonucleotide. (Heemskerk et al., 2009) In a comparative study of three AON chemistries: PMO, PNA, 2'OMe PS Cao et al. used 5 µg of 2'OM PS per TA in C57BL6 and MDX mice to induce exon skipping of exon 23 in dystrophin pre-mRNA at the level of 7,7%. (Cao et al., 2014) Interestingly, this study proved that PMO and PNA based AONs were much more efficient than 2'OMe PS because they were able to skip dystrophin exon 23 with the efficiency of 53% and 25% respectively, while 2'OMe PS reached the maximum of 7-9%. (Cao et al., 2014) Hence, changing chemistry to PMO might also address exon skipping efficiency of dysferlin exon 38 in both in vitro and in vivo experiments.

Also the time point of three weeks that was chosen for the exon skipping of dysferlin does not seem to impact the result. Cao et al. showed that time points of 2 and 4 weeks did not exhibit any significant differences in the level of skipped exon when 2'OMe PS were injected. (Cao et al., 2014)

A possible reason for the lack of skipping in vivo might be a different distribution of exonic splice enhancers in the human and mouse genome. Answering this question remains challenging because there are no online tools available that would allow a comprehensive comparison of know cis-acting elements between species. The limited comparison between human and mouse ESEs can be made by means of the RESCUE-ESE algorithm. (Fairbrother, 2002; Fairbrother et al., 2004) Aligning the distribution of the ESEs in the exon 38 of human and mouse pre-mRNA one can observe that generally ESEs group in similar way in both species (Figure 87). Only few minor differences around nucleotides 30-40, 115-125, 135-140 can be recorded. However, it is impossible to state how important are these differences because the RESCUE-ESE tool does not provide information about the relative strength of the predicted enhancers.

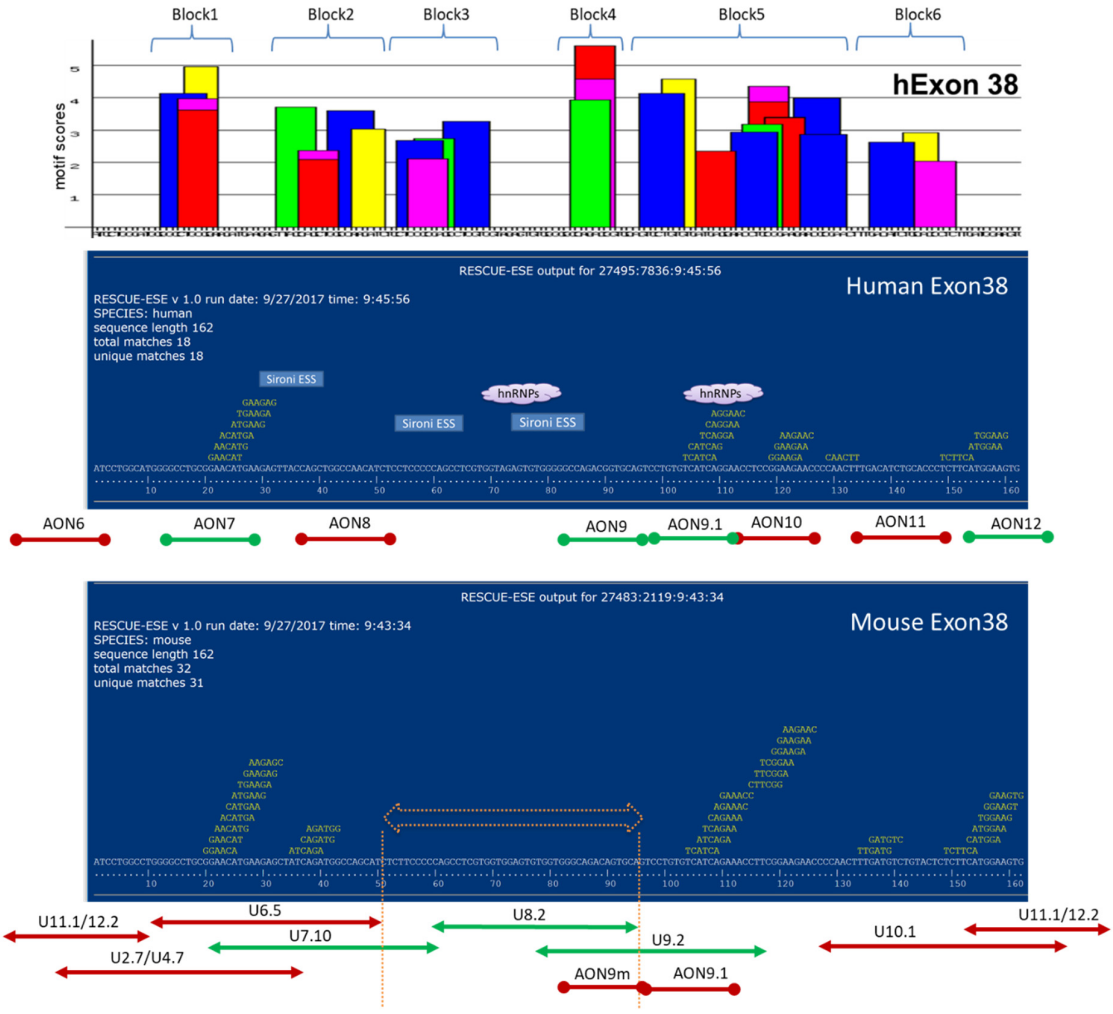

Figure 87 Comparison of ESE predicted by ESEfinder and RESCUE-ESE in human and mouse dysferlin exon 38.

The upper panel represents ESEs in human dysferlin exon 38 predicted by ESEfinder (red: SF2/ASF, blue: SC35, green: SRp40, yellow: SRp55). The middle panel is a collection of ESEs in human dysferlin exon 38 predicted by

RESCUE-ESE. The cloud represents position of highly scored ESS targeted by hnRNPs and predicted with HSF. The lower panel represents the ESEs in the mouse dysferlin exon 38 predicted by RESCUE-ESE. The Sironi ESS and hnRNPs predicted for human exon 38 by HSF with scores >75 were depicted with blue rectangles and violet clouds respectively. Below panels with the predicted ESEs there is a mapping of antisense sequences of 2'OMe PS AON (lines ended with circles) and U7 snRNA (lines ended with arrows). Green color depicts antisense sequences triggering exon skipping and red ones the non-functioning sequences. The orange vertical lines and the orange horizontal line depict the area in the mouse exon 38 that is critical for removing exon 37 and 38.

Furthermore, one should keep in mind that the ESE predicted by the RESCUE-ESE algorithm were derived by a computational comparison of sequences of weak and strong exons in order to find potential hexamers corresponding to the enhancer sequences. Consequently, RESCUE-ESE does not provide a holistic picture of all possible ESEs targeted by the wide range of SR proteins and it does not put them in the context of silencing element.

5.3. Antisense U7 snRNAs targeting dysferlin exon 38 trigger simultaneous skipping of exon 37 and 38 in MDX mouse

In the case of the U7 snRNA-based approach twelve antisense sequences were designed, cloned in the U7 backbone, packaged into AAV2/9 and screened in vivo in the MDX mouse model. The antisense sequences were distributed across the whole mouse exon 38 and included also the intronic sequences like BP, 3'ss and 5'ss. Out of twelve U7 snRNA only three (U7.10, U8.2 and U9.2) caused simultaneous skipping of both exon 37 and 38. U11.1 and U12.2 snRNAs that were masking the 3'ss and 5'ss did not evoke any skipping of exon 38 although AON12 targeting 3'ss of human intron 38-39 managed to skip exon 38. Surprisingly, U6.5 snRNAs masked exactly the same ESE region like 2'OMe PS AON7 in the human myoblast, however, it did not have any impact on splicing in the mouse model (Figure 87). Furthermore, U6.5 snRNA also overlapped in 70% with the most efficient snRNA U7.10. Also U2.7 and U4.7 were masking both 3'ss of intron 37-38 and the sequence corresponding to the AON7 and did not trigger skipping in the mouse model (Figure 87). The U7.10, however, didn't mask the whole first block of ESEs predicted for the human exon 38 (Figure 87). Hence, it seems that the key mouse ESEs are situated in the location corresponding to human ESE block 2 or 3 of exon 38. Because U2.7 and U4.7 covered block 1 and 2 and didn't modify splicing the most influential seems to be the area corresponding to the block 3 (Figure 87). The ESEs from the block 3 are partially masked by U7.10 and U8.2 snRNAs, which had the best exon skipping activity from all twelve candidates. The experimentally determined area crucial for triggering simultaneous exon skipping of both exon 37 and 38 was marked by the orange arrow in the Figure 87.

The questions why do masking ESE in block 3 of exon 38 with U7.10 and U8.2 snRNAs removes both exon 37 and 38 remains unanswered. The analysis of the 5'ss and 3'ss of introns 36-37, 37-38, 38-39 with MaxEntScan online tool (Yeo and Burge, 2004) did not show any substantial differences in the scores of the splice sites (Figure 88). It seems plausible to think that the DS of intron 37-38 (MAXENT: 8,70) would not recognize the AS of intron 37-38 (MAXENT: 8,63) because its definition is probably weaker by masking of ESE in the exon 38 with the antisense U7.10/U8.2 snRNA. In this case the DS of intron 37-38 should pair with the next available strong AS which in this case is the AS of intron 38-39 (MAXENT: 9,48). This would result in skipping of exon 38 (Figure 88 gray bow). However, both exons 37 and 38 are removed what implicates that the DS of intron 36-37 (MAXENT: 8,70) pairs with the AS of intron 38-39 (MAXENT: 9,48) and causes skipping of the two exons simultaneously (Figure 88 orange bow).

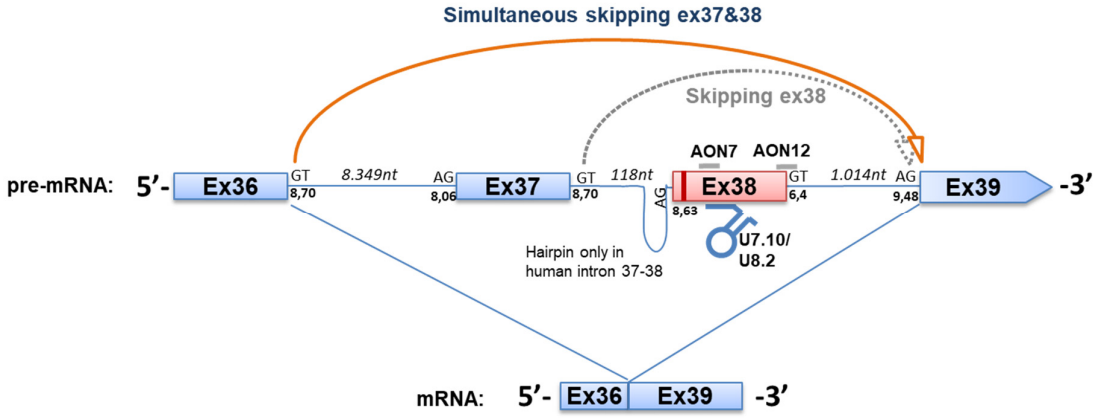

Figure 88 Theoretical paring model of splice sites in dysferlin pre-mRNA.

The exons were depicted as blue rectangle and mutated exon as a red rectangle. The vertical line in exon 38 depicts the position of the mutation: c4022T>C.The horizontal lines between exons are introns. A 5'ss with GT nucleotides and 3'ss with AG nucleotides were depicted on the left and right of every intron. Below every splice site the MAXENT score is provided. The length of introns is written in italics. The orange bow with an arrow demonstrated possible paring of 5'ss with 3'ss caused by U7 snRNAs, which trigger skipping of both exon 37 and 38. Dotted gray bow with an arrow shows possible pairing of 5'ss with 3'ss that can be expected by the use of AONs triggering skipping of exon 38.

We learn how complex the splicing code is and the integration of the current knowledge for the applicative purposes is still a challenge. The currently available online tools lack highly reliable algorithms which would integrate the knowledge about majority of know trans-acting elements in the prediction process. Furthermore, a more straightforward interpretation of the outcome would facilitate the rational design process of an antisense strategy. Finally, one cannot rely on theoretical predictions, hence a systematic verification of possible targets has to be undertaken experimentally.

5.4. U7 snRNA-based exon skipping was poorly detectable in the dysferlin deficient mouse model (MMex38)

The best performing U7 snRNAs (U7.10, U8.2, U9.2) were injected intramuscularly into the TA muscle of dysferlin deficient mice (MMex38) carrying the mutation in exon 38. Although, the analysis of skipping at the RNA level showed some simultaneous skipping of exon 37 and 38 by U7.10 and U8.2, the result was read from the very faint bands on the agarose gel (Figure 52), hence at the detection limit of the nested PCR method. The analysis at the protein level did not show any increase in the amount of dysferlin so no therapeutic effect was reached. In order to verify if the problem of poorly detectable exon skipping could have been caused by a specific batch of AAV virus that was produced for the purpose of the in vivo experiment, the in vitro test using the same virus in C2C12 and primary mouse myoblasts isolated from MMex38 was performed. Interestingly, simultaneous skipping of exon 37 and 38 was reproduced in C2C12 cells at high MOI of 10^7 but not in the myotubes derived from the primary MMex38 myoblasts.

A possible problem of U7 snRNA being active in C2C12 cells and not in the MMex38 primary myoblast is the delivery of AAV. Stitelman et al. demonstrated that satellite cells migrating during embryonal myogenesis can be transduced by AAV whereas the quiescent satellite cells cannot. (Stitelman et al., 2014) However, one cannot consider the isolated MMex38 satellite cells as being in a quiescent state because they divide over time in cell culture. Importantly, Arnett et al. showed that AAV particles are transducing efficiently differentiated myotubes, less efficiently proliferating myoblasts and are not transducing the quiescent satellite cells. (Arnett et al., 2014) The authors noticed a clear preference of AAV to infect multinucleated cells in comparison to proliferating myoblasts in cell culture. Furthermore, they also discovered that Pax7 positive satellite cells undergo transduction in vivo with AAV8. Taken together the facts that proliferating primary myoblasts are more difficult to be transduced than myotubes and that the successful transduction of CC12 cells with AAV2/9 required MOI of 10^7 one can assume that the amount of virus was not sufficient for generation of exon skipping effect in MMEx38 primary myoblasts. Interestingly, Arnett et al. used for their experiments MOI of 100 to infect C2C12. This is 100.000 times less than I used in my U7 snRNA experiment in C2C12 cells. This fact poses a question about the reasons for the low infectivity of AAV virus used the in vivo experiments. The loss in infectivity cannot be only attributed to the nature of the MMex38 satellite cells because large amounts of AAV2/9 were also necessary for the infection of my C2C12 cells. Thus, an issue with AAV quality seems to be the most plausible explanation for the observed low infectivity.

5.5. Human dysferlin without exon 37 or exon 38 or both exon 37 and 38 maintains its membrane repair function

The results of the membrane wounding assay demonstrated that the truncated dysferlin is capable of maintaining its membrane resealing function. In the first try to test the function of truncated dysferlin, the constructs were delivered via microinjections to myotubes derived from dysferlin deficient human primary and immortalized myoblasts. Although this approach was successfully applied by Marg et al. (Marg et al., 2012b) in healthy human primary myoblasts, the microinjections performed in dysferlin deficient myotubes failed. The needle penetrating sarcolemma was disrupting the sarcolemma and resulting in complete myotubes destruction within couple of minutes after the injection. The dysferlin deficiency made the membrane too fragile for this type of DNA delivery. Hence, it was necessary to switch to a less invasive method.

In the second try the truncated dysferlin was delivered using the VSV-G pseudotyped lenitiviral vectors. However, also this method had its limitations. It was shown that the genomes between 6 -10 kb are packaged less efficiently into the lenti particles. (Kumar et al., 2001) Because dysferlin gene together with a promotor and the EGFP marker approach the packaging limit of the vector, the virus had to be produced in high titer to assure enough of infectious particles. The dysferlin constructs were combined with the EGFP marker by means of a P2A peptide in order to cleave the marker and assure availability of the native form of the protein during the laser wounding assay. The critical step in the cell preparation was FACS sorting and cell expansion. FACS sorting was reducing the amount of viable cells and the infected cells had a limited number of passages for the population expansion. With each passage primary human myoblasts lose their proliferative capacity and tend to undergo morphologic changes (increase in size, elongation and vacuolization) caused by senescence. The phenomenon of replicative aging has been already described for human (Decary et al., 1997), rat (Schultz and Lipton, 1982) and chicken (Wright, 1985) satellite cells. In cell culture, healthy human myoblasts obtained at birth are able to perform about 60 divisions, at the age of 9 years this potential drops to about 30 and in the adulthood remains at the level of 15 divisions. (Renault et al., 2000) However, this potential can be exploited much earlier if muscle undergoes continuous regeneration. This is the case in the DMD patients whose satellite cells undergo many divisions and lose telomeres 14 times faster than the healthy controls. (Decary et al., 2000)

The results of the laser wounding assay exhibited high standard deviation between individual myotubes of expressing given dysferlin construct. The myotubes derived from aging myoblasts are shorter, thinner and contain less nuclei than myotubes derived from younger

myoblasts (Figure 89). (Mouly et al., 2005) The myoblasts derived from our dysferlin deficient patient were already near the limit of their proliferative capacity because of patient's age and the fact that the patient suffered from dystrophic phenotype where a regenerative rate is higher than in healthy individuals.

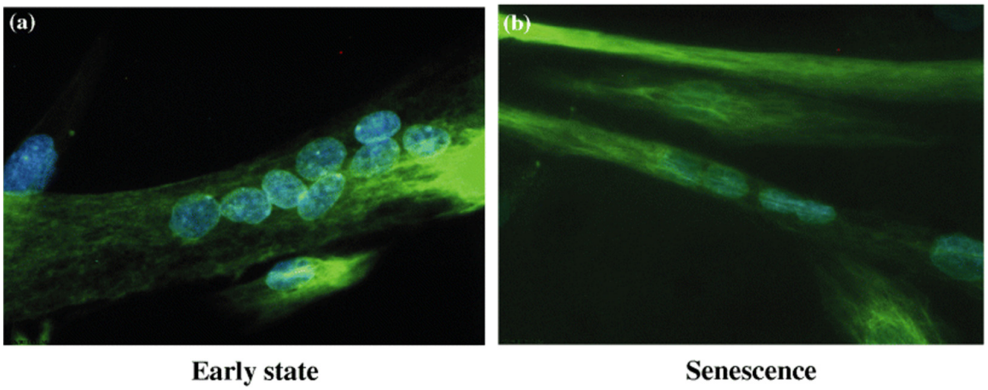

Figure 89 Phenotype difference between myotubes of early state and senescent myoblasts.

The myotubes were stained with desmin (green). Panel a) shows a myotube formed from young myoblasts and panel b) a myotube derived from ageing myoblasts. The picture was adapted from (Mouly et al., 2005).

Although there is no data on membrane resealing properties of myotubes made from myoblasts in the early or late proliferative stage, a question remains open how a letnivirus infection and the replicative senescence contribute to this variability.

It was previously reported that skipping of exons 37 or 38 of dysferlin might be possibly pathogenic because exons contain the coding sequence of C2E domain. (Aartsma-Rus et al., 2010b) Interestingly, dysferlin without exon 37, without exon 37 and 38 performed in my laser wounding assay as well as the full dysferlin. Although the excision of exon 37 and 38 led to removal of half of the C2E domain, the membrane resealing properties of the truncated dysferlin did not deteriorate. Possibly because C2E domain is not coordinating Ca^{2+} atoms (Fuson et al., 2014), hence is probably not critical for the membrane repair activity. The dispensability of C2E domain was demonstrated indirectly using naturally occurring mini-dysferlin in a patient with less severe dysferlinopathy phenotype. The truncated protein contains only two calcium binding domains: C2F, C2G and the transmembrane domain. (Krahn et al., 2010) Using the laser wounding assay, Krahn et al. showed that mini-dysferlin delivered via AAV into the dysferlin-deficient mice is able to retain its membrane resealing function. (Krahn et al., 2010)

There is still an ongoing debate if the improvement of membrane repair ability measured by the laser wounding assay is sufficient to claim an improvement in the dystrophic phenotype. The mini-dystrophin experiments performed by Krahn et al. led to a partial improvement of

muscle histology. Lostal et al. demonstrated that neither overexpression of mini-dysferlin nor myoferlin are able alleviate dystrophic changes in vivo, although they rescue the resealing functionality measured by the laser wounding assay. (Lostal et al., 2012) On the other hand, Grose et al. demonstrated full functional recovery of diaphragm of dysferlin deficient mice treated with full dysferlin delivered in two recombining parts by a rAAV5. (Grose et al., 2012) Efficient recovery was reported also by Lostal et al. who delivered full dysferlin in dual AAV system to dysferlin deficient mice. In this case, the level of rescued dysferlin was at 1-4% of endogenous protein, what might explain not a full recovery of the histological and functional parameters. (Lostal et al., 2010) Nevertheless, in both Grose et al. and Lostal et al. studies the membrane wounding abilities of muscle fibers was fully recovered.

5.6. Human dysferlin without exon 37 or exon 38 or both exon 37 and 38 does not localize at sarcolemma

The immunostainings of myotubes derived from human primary myoblasts and transduced with the truncated dysferlin constructs show that dysferlin is localized mainly in the cytoplasm near nuclei and not at the membrane. A possible explanation for the perinuclear localization could provide the homology modeling of the C2E domain, which showed that exon 38 codes for almost four beta sheets of the domain. Hence, the removal of exon 38 is likely to expose the hydrophobic amino acids of the remaining two beta sheets to the cellular environment. Such exposure could lead to misfolding of the protein and result in aggregation of dysferlin in endoplasmic reticulum (ER). Lack of dysferlin in the immunostainings of myotubes overexpressing truncated dysferlin could be also associated with the model of accelerated endocytosis. Evesson et al. proposed that decreased expression of dysferlin at the membrane of myotubes carrying some dysferlin missense mutations can be attributed to increased protein lability due to accelerated endocytosis and endosomally driven proteolysis. Their experiments confirmed that not only missense mutations but also large deletion of C2B-FerI-C2C or C2A-C2B-C2C-C2D-C2E lead to 2,5 times increased reduction of dysferlin expression at sarcolemma. (Evesson et al., 2010)

Lack of detectable dysferlin in the sarcolemma makes the interpretation of my positive laser wounding assay data complicated. The literature provides numerous proofs that lack of dysferlin in sarcolemma is associated with the impaired membrane repair process. (Bansal et al., 2003; Grose et al., 2012; Schoewel et al., 2012) It is worth pinpointing that also in the case of gene therapy with mini-dysferlin the transfected human fibroblasts and AAV transduced mice myofibers exhibited not only sarcolemma localization of mini-dysferlin but also a strong

signal from the cytoplasmic compartments. Hence, a question if cytoplasmic dysferlin is able to mediate membrane resealing process remains to be answered.

The immunostaining of transduced myoblasts show strong, patchy staining of dysferlin constructs in the cytoplasm. Also in the case of myoblasts a perinuclear accumulation of dysferlin was observed, however, it is not as pronounced as in the myotubes (Figure 85). Similar pattern can be observed in the myoblasts transduced with the full dysferlin. Moreover, the over expressed full dysferlin does not localize at the membrane of myoblasts. In contrary mini-dysferlin transfected into human primary fibroblasts showed both patchy cytoplasmic and correct membrane localization. (Krahn et al., 2010) Also full length dysferlin transfer into dysferlin deficient B6.A/J-*Dysf*^{prmd} mice using dual AAV vector system showed both membrane and cytoplasmic localization. (Lostal et al., 2010) The question arises if the patchy form of dysferlin found in the cytoplasm is a result of dysferlin overexpression. Lostal et al. explain the cytoplasmic localization with co-localization of overexpressed dysferlin with ryanodin-receptor (RyR1) in T-tubules. (Lostal et al., 2010) Glover et al. produced transgenic mice overexpressing dysferlin at low (2 times endogenous), medium and high level (30 times endogenous) and noticed that at high level mice exhibited non-necrotic, progressive dystrophic phenotype, which was not associated with compromised sarcolemma integrity like in the case of dysferlinopathy (Glover et al., 2010) Furthermore, both membrane and perinuclear staining of dysferlin in the muscle cross sections was observed. Also cytoplasmic aggregates of dysferlin were discovered in some muscle fibers. The authors suggested that perinuclear staining and the increased expression of ER chaperon 78-kDa glucose-regulated protein (GRP78) (Wang et al., 2009) and calreticulin (Saito, 1999) are signs of endoplasmic reticulum stress caused by overexpression of dysferlin and accumulation of unfolded or misfolded protein in ER. (Glover et al., 2010) Hence, it seems that appropriate level of dysferlin is crucial for proper functioning of muscle and this fact should be taking into account when developing a gene therapeutic strategy for dysferlinopathy.

6. ATTACHMENTS

6.1. Maps of plasmids containing human dysferlin cDNA variants

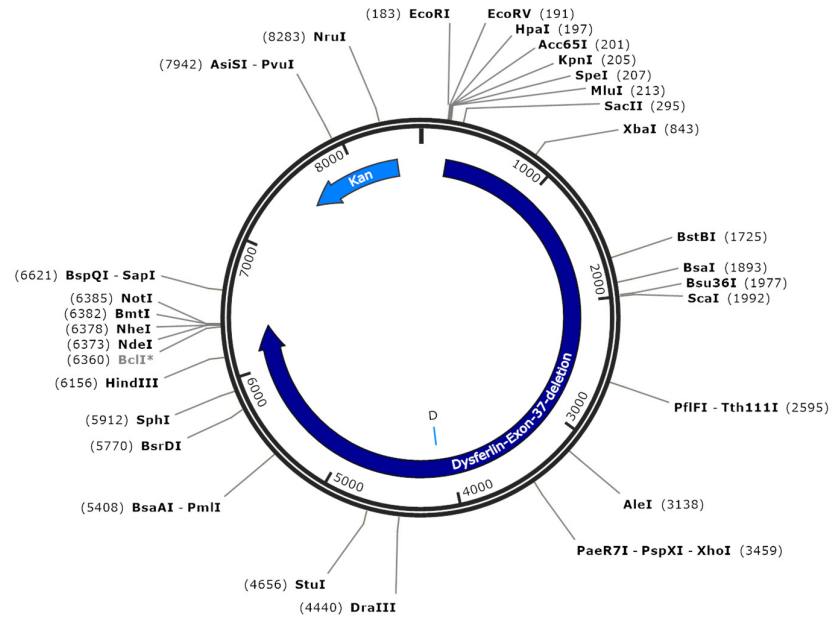

Dysferlin-Exon-37-deletion_in_pUC57-Kan
8572 bp

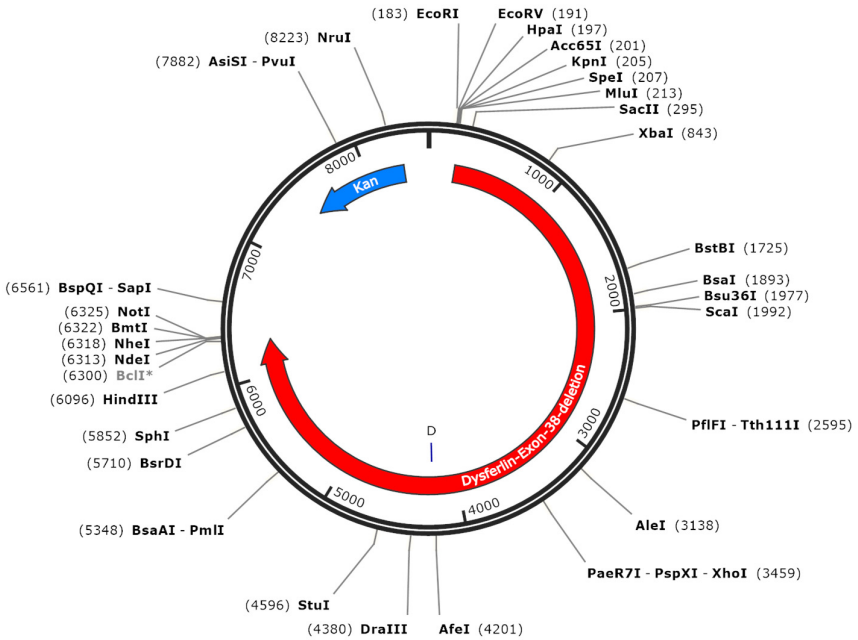

Dysferlin-Exon-38-deletion_in_pUC57-Kan
8512 bp

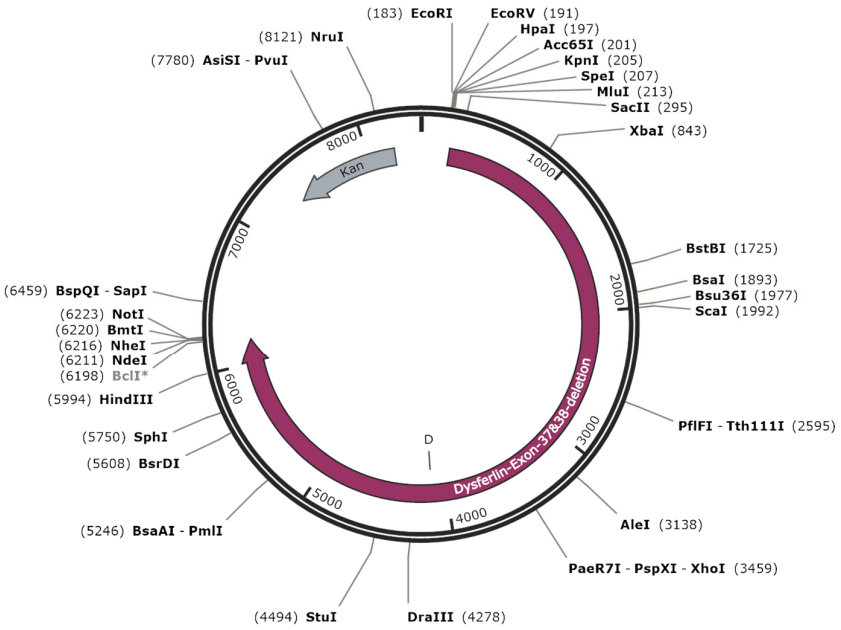

Dysferlin-Exon-37-38-deletion_in_pUC57-Kan
8410 bp

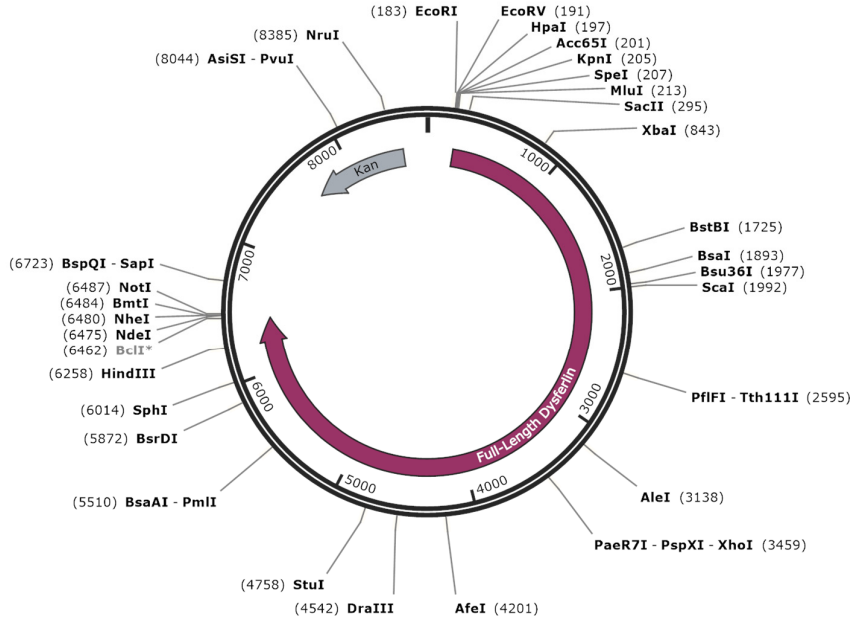

Full-Length_Dysferlin_in_pUC57-Kan
8674 bp

6.2. Maps of plasmids based on pIRES2-EGFP

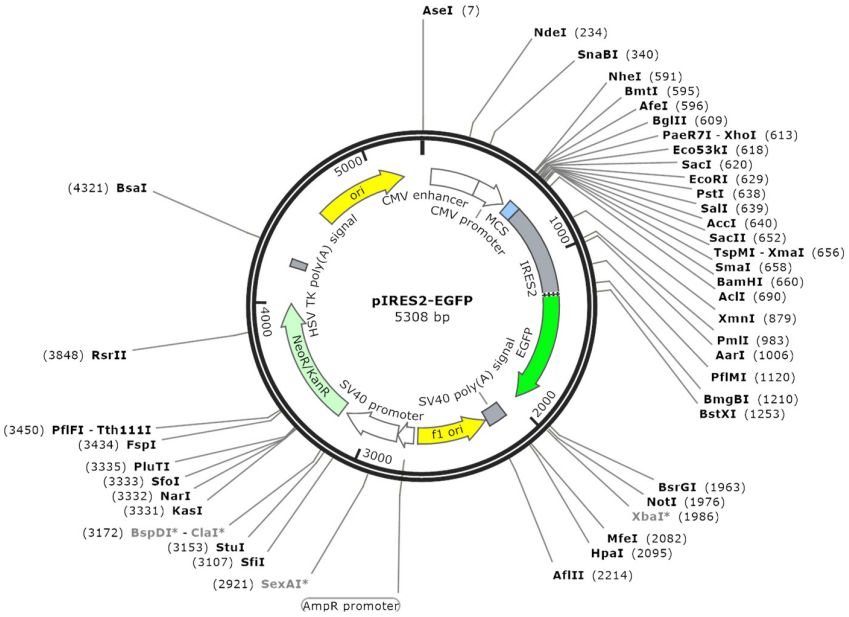

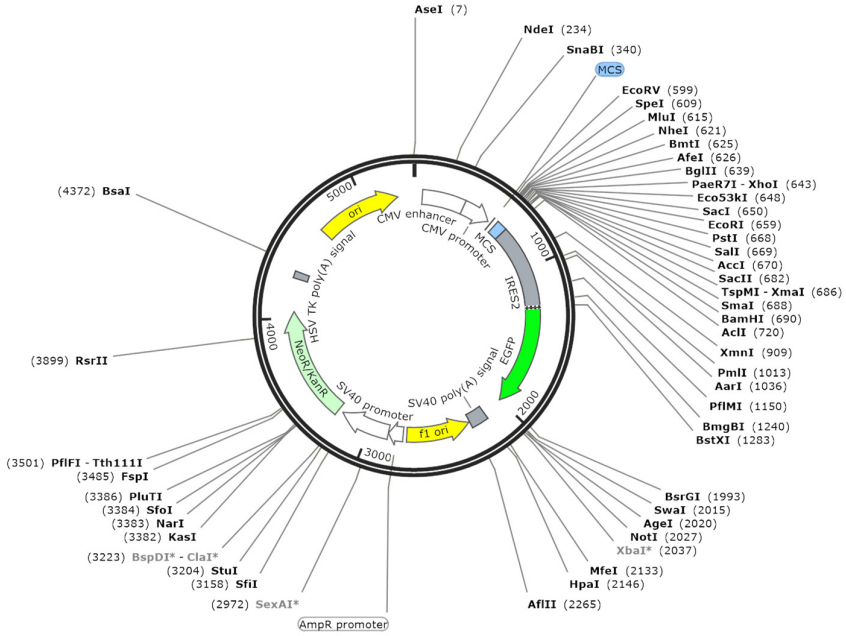

pIRES2-EGFP_NheI-EcoRV_NsiI_SpeI_MluI-NheI_NotI_SwaI_AgeI
5359 bp

6.3. Maps of plasmids based on pRRLSIN.cPPT.PGK-MCS.WPRE

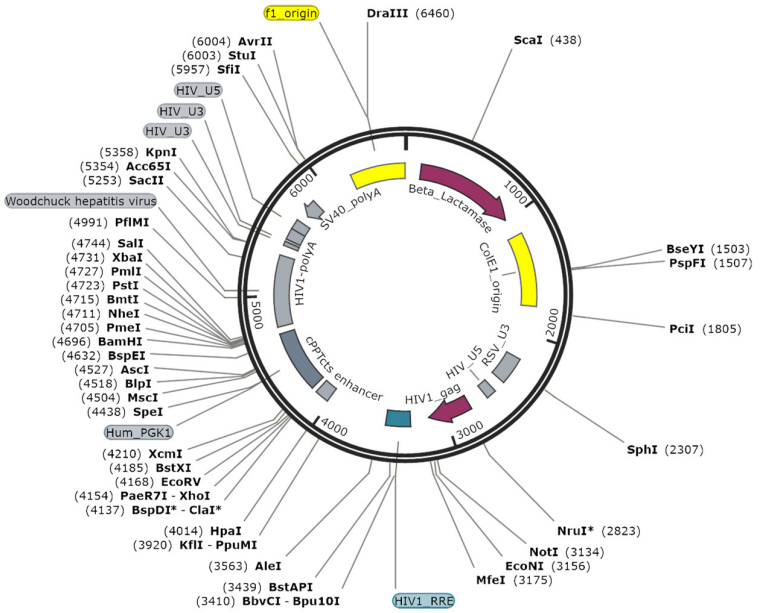

pRRLSINPPTPGK_MCS_WPRE
6684 bp

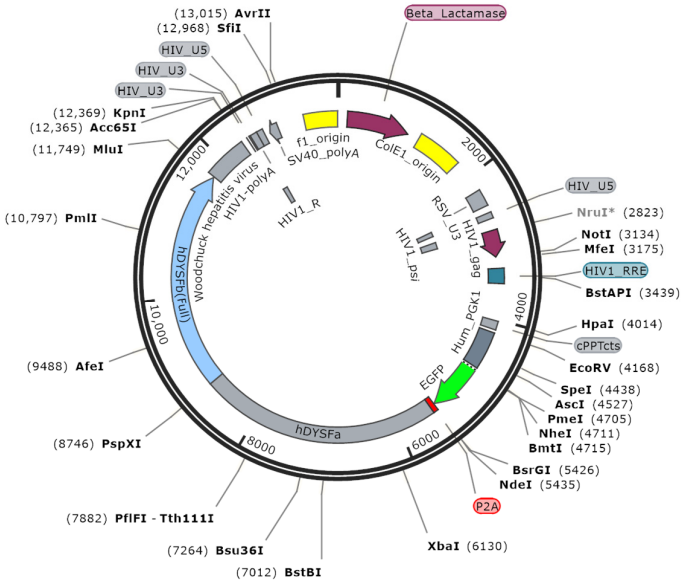

Vector_pRRL_EGFPwoStop_GSG-P2A_hDYSFa_hDYSFb(Full)_v1
13,695 bp

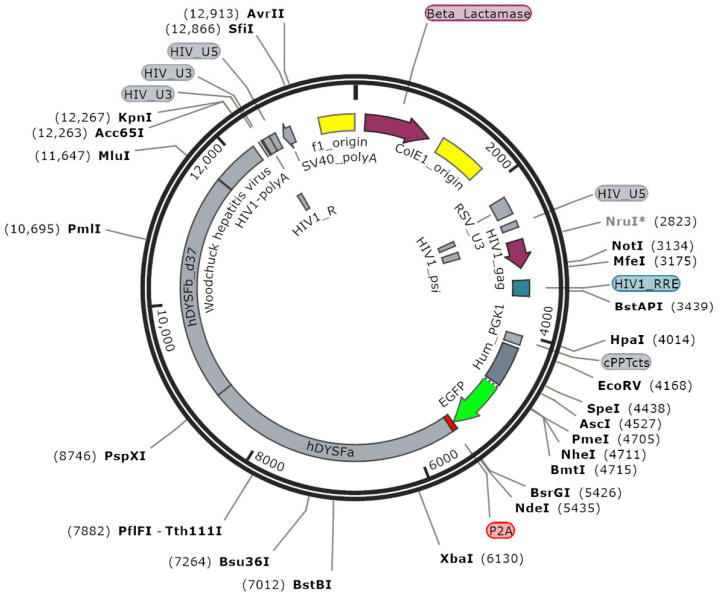

Vector_pRRL_EGFPwoStop_GSG-P2A_hDYSFa_hDYSFb(d37)
13,593 bp

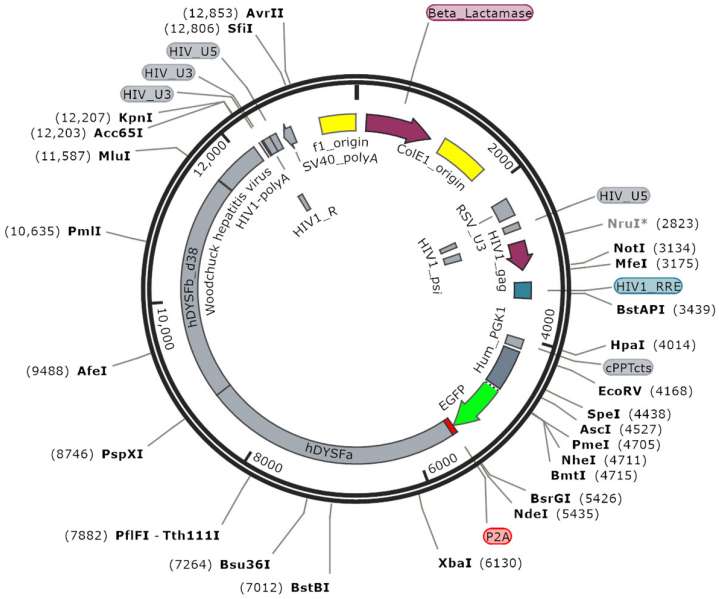

Vector_pRRL_EGFPwoStop_GSG-P2A_hDYSFa_hDYSFb(d38)
13,533 bp

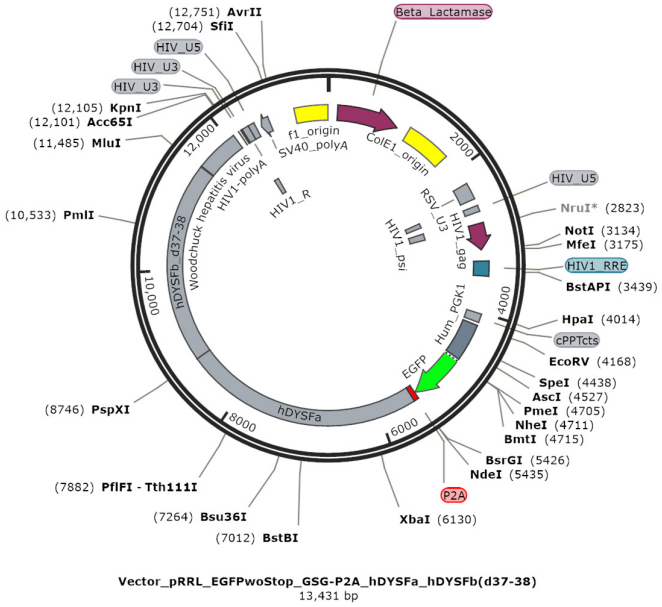

Vector_pRRL_EGFPwoStop_GSG-P2A_hDYSFa_hDYSFb(d37-38)
13,431 bp

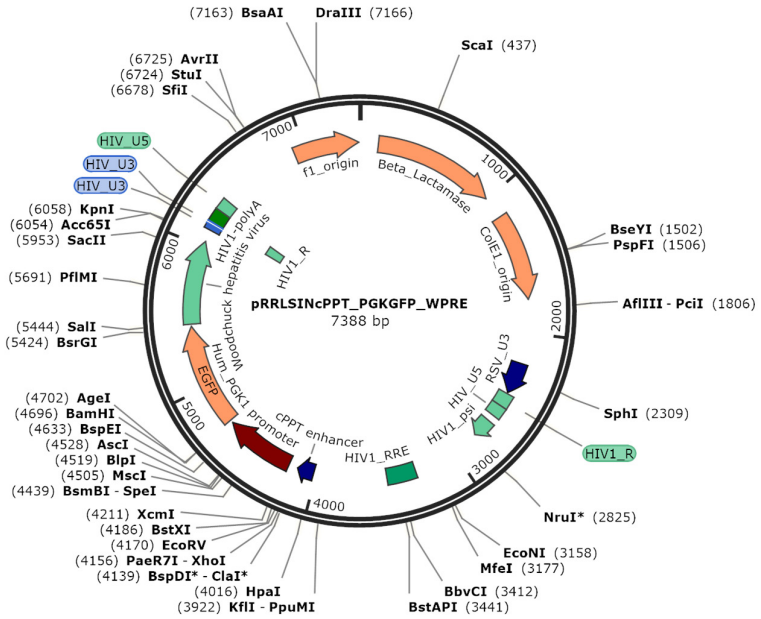

6.4. Maps of plasmids based on pSMD2 plasmid

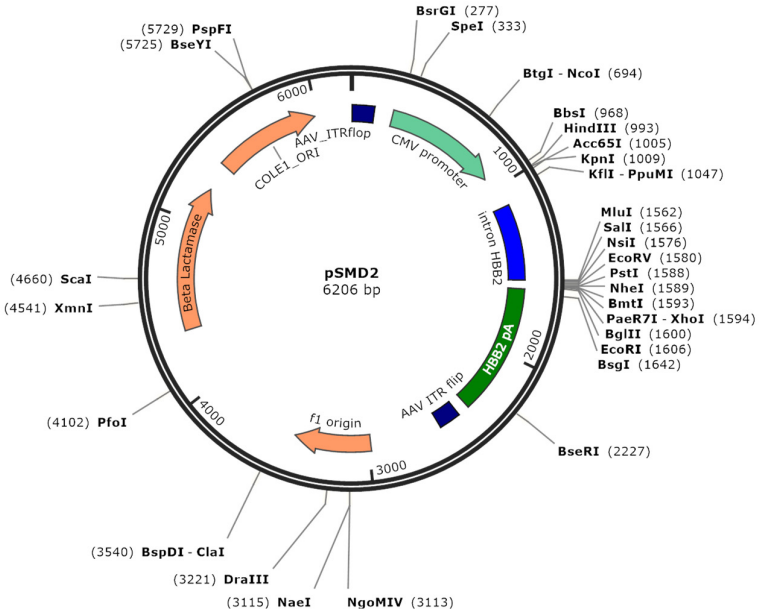

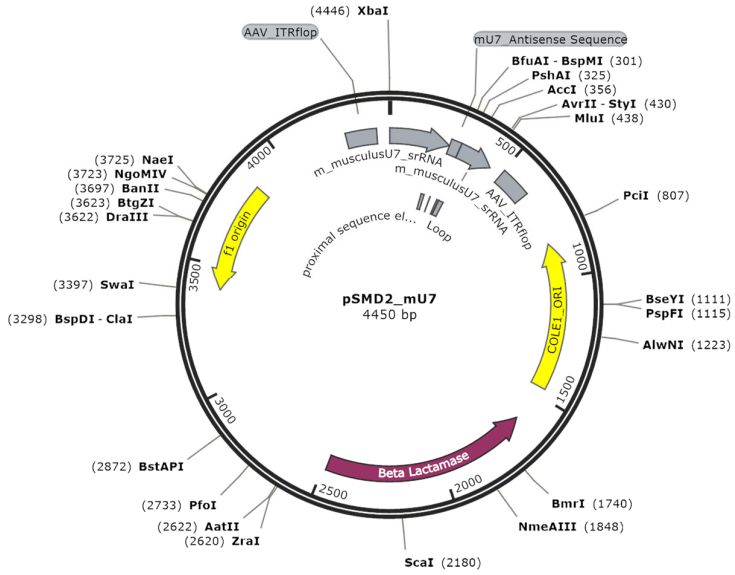

6.5. Other plasmids

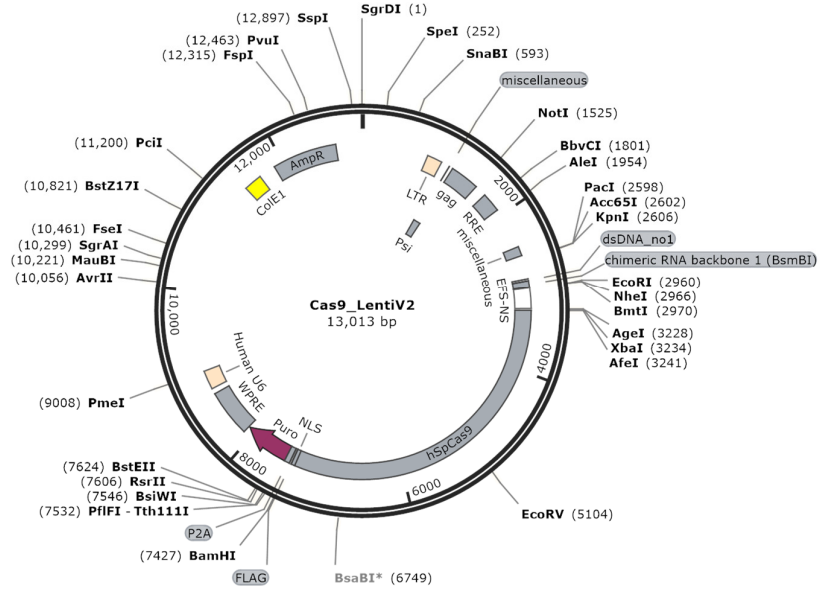

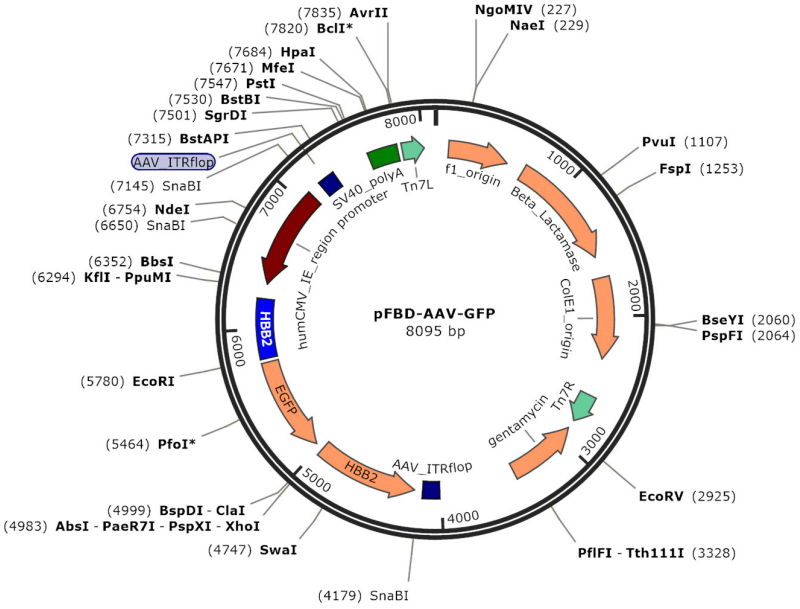

7. BIBLIOGRAPHY

Aartsma-Rus, A., and van Ommen, G.-J.B. (2007). Antisense-mediated exon skipping: a versatile tool with therapeutic and research applications. RNA *13*, 1609–1624.

Aartsma-Rus, A., Janson, A.A.M., Kaman, W.E., Bremmer-Bout, M., den Dunnen, J.T., Baas, F., van Ommen, G.-J.B., and van Deutekom, J.C.T. (2003). Therapeutic antisense-induced exon skipping in cultured muscle cells from six different DMD patients. Hum. Mol. Genet. *12*, 907–914.

Aartsma-Rus, A., van Vliet, L., Hirschi, M., Janson, A.A., Heemskerk, H., de Winter, C.L., de Kimpe, S., van Deutekom, J.C., 't Hoen, P.A., and van Ommen, G.-J.B. (2009). Guidelines for Antisense Oligonucleotide Design and Insight Into Splice-modulating Mechanisms. Mol. Ther. *17*, 548–553.

Aartsma-Rus, A., Singh, K.H.K., Fokkema, I.F.A.C., Ginjaar, I.B., van Ommen, G.-J., den Dunnen, J.T., and van der Maarel, S.M. (2010a). Therapeutic exon skipping for dysferlinopathies? Eur. J. Hum. Genet. *18*, 889–894.

Aartsma-Rus, A., Singh, K.H.K., Fokkema, I.F.A.C., Ginjaar, I.B., van Ommen, G.-J., den Dunnen, J.T., and van der Maarel, S.M. (2010b). Therapeutic exon skipping for dysferlinopathies? Eur. J. Hum. Genet. *18*, 889–894.

Anderson, L. V, Davison, K., Moss, J.A., Young, C., Cullen, M.J., Walsh, J., Johnson, M.A., Bashir, R., Britton, S., Keers, S., et al. (1999). Dysferlin is a plasma membrane protein and is expressed early in human development. Hum. Mol. Genet. *8*, 855–861.

De Angelis, F.G., Sthandier, O., Berarducci, B., Toso, S., Galluzzi, G., Ricci, E., Cossu, G., and Bozzoni, I. (2002). Chimeric snRNA molecules carrying antisense sequences against the splice junctions of exon 51 of the dystrophin pre-mRNA induce exon skipping and restoration of a dystrophin synthesis in Delta 48-50 DMD cells. Proc. Natl. Acad. Sci. U. S. A. *99*, 9456–9461.

Aoki, M., Liu, J., Richard, I., Bashir, R., Britton, S., Keers, S.M., Oeltjen, J., Brown, H.E., Marchand, S., Bourg, N., et al. (2001). Genomic organization of the dysferlin gene and novel mutations in Miyoshi myopathy. Neurology *57*, 271–278.

Argon, Y., and Ward, S. (1980). Caenorhabditis elegans fertilization-defective mutants with abnormal sperm. Genetics *96*, 413–433.

Argov, Z., Sadeh, M., Mazor, K., Soffer, D., Kahana, E., Eisenberg, I., Mitrani-Rosenbaum, S., Richard, I., Beckmann, J., Keers, S., et al. (2000). Muscular dystrophy due to dysferlin deficiency in Libyan Jews. Clinical and genetic features. Brain A J. Neurol. *123 (Pt 6*, 1229–1237.

Arnett, A.L., Konieczny, P., Ramos, J.N., Hall, J., Odom, G., Yablonka-Reuveni, Z., Chamberlain, J.R., and Chamberlain, J.S. (2014). Adeno-associated viral vectors do not efficiently target muscle satellite cells. Mol. Ther. - Methods Clin. Dev. *1*, 14038.

Arnold, K., Bordoli, L., Kopp, J., and Schwede, T. (2006). The SWISS-MODEL workspace: a web-based environment for protein structure homology modelling. Bioinformatics *22*, 195–201.

Asokan, A., Schaffer, D. V, and Jude Samulski, R. (2012). The AAV Vector Toolkit: Poised at the Clinical Crossroads. Mol. Ther. *20*, 699–708.

Atchison, R.W., Casto, B.C., and Hammon, W.M. (1966). Electron microscopy of adenovirus-associated virus (AAV) in cell cultures. Virology *29*, 353–357.

ATCHISON, R.W., CASTO, B.C., and HAMMON, W.M. (1965). ADENOVIRUS-ASSOCIATED DEFECTIVE VIRUS PARTICLES. Science *149*, 754–756.

Azakir, B.A., Di Fulvio, S., Salomon, S., Brockhoff, M., Therrien, C., and Sinnreich, M. (2012). Modular dispensability of dysferlin C2 domains reveals rational design for mini-dysferlin molecules. J. Biol. Chem. *287*, 27629–27636.

Bansal, D., and Campbell, K.P. (2004). Dysferlin and the plasma membrane repair in muscular dystrophy. Trends Cell Biol. *14*, 206–213.

Bansal, D., Miyake, K., Vogel, S.S., Groh, S., Chen, C.-C., Williamson, R., McNeil, P.L., and Campbell, K.P. (2003). Defective membrane repair in dysferlin-deficient muscular dystrophy. Nature *423*, 168–172.

Barry, S.C., Harder, B., Brzezinski, M., Flint, L.Y., Seppen, J., and Osborne, W.R.A. (2001). Lentivirus Vectors Encoding Both Central Polypurine Tract and Posttranscriptional Regulatory Element Provide Enhanced Transduction and Transgene Expression. Hum. Gene Ther. *12*, 1103–1108.

Barthélémy, F., Blouin, C., Wein, N., Mouly, V., Courrier, S., Dionnet, E., Kergourlay, V., Mathieu, Y., Garcia, L., Butler-Browne, G., et al. (2015). Exon 32 Skipping of Dysferlin Rescues Membrane Repair in Patients' Cells. J. Neuromuscul. Dis. *2*, 281–290.

Bartlett, J.S., Wilcher, R., and Samulski, R.J. (2000). Infectious Entry Pathway of Adeno-Associated Virus and Adeno-Associated Virus Vectors. J. Virol. *74*, 2777–2785.

Bashir, R., Strachan, T., Keers, S., Stephenson, A., Mahjneh, I., Marconi, G., Nashef, L., and Bushby, K.M. (1994). A gene for autosomal recessive limb-girdle muscular dystrophy maps to chromosome 2p. Hum. Mol. Genet. *3*, 455–457.

Bashir, R., Keers, S., Strachan, T., Passos-Bueno, R., Zatz, M., Weissenbach, J., Le Paslier, D., Meisler, M., and Bushby, K. (1996). Genetic and physical mapping at the limb-girdle muscular dystrophy locus (LGMD2B) on chromosome 2p. Genomics *33*, 46–52.

Bashir, R., Britton, S., Strachan, T., Keers, S., Vafiadaki, E., Lako, M., Richard, I., Marchand, S., Bourg, N., Argov, Z., et al. (1998). A gene related to Caenorhabditis elegans spermatogenesis factor fer-1 is mutated in limb-girdle muscular dystrophy type 2B. Nat. Genet. *20*, 37–42.

Bauman, J., Jearawiriyapaisarn, N., and Kole, R. (2009). Therapeutic potential of splice-switching oligonucleotides. Oligonucleotides *19*, 1–13.

Bejaoui, K., Hirabayashi, K., Hentati, F., Haines, J.L., Ben Hamida, C., Belal, S., Miller, R.G., McKenna-Yasek, D., Weissenbach, J., Rowland, L.P., et al. (1995). Linkage of Miyoshi myopathy (distal autosomal recessive muscular dystrophy) locus to chromosome 2p12-14. Neurology *45*, 768–72.

Berg, J.M. (Jeremy M., Tymoczko, J.L., Stryer, L., and Stryer, L. (2002). Biochemistry (W.H. Freeman).

Berns, K.I. (1990). Parvovirus replication. Microbiol. Rev. *54*, 316–329.

Berns, K.I., and Rose, J.A. (1970). Evidence for a single-stranded adenovirus-associated virus genome: isolation and separation of complementary single strands. J. Virol. *5*, 693–699.

Beyer, A.L., and Osheim, Y.N. (1988). Splice site selection, rate of splicing, and alternative splicing on nascent transcripts. Genes Dev. *2*, 754–765.

Bi, G.Q., Alderton, J.M., and Steinhardt, R.A. (1995). Calcium-regulated exocytosis is required for cell membrane resealing. J. Cell Biol. *131*, 1747–1758.

Biasini, M., Bienert, S., Waterhouse, A., Arnold, K., Studer, G., Schmidt, T., Kiefer, F., Cassarino, T.G., Bertoni, M., Bordoli, L., et al. (2014). SWISS-MODEL: Modelling protein tertiary and quaternary structure using evolutionary information. Nucleic Acids Res. *42*, W252–W258.

Bish, L.T., Sleeper, M.M., Forbes, S.C., Wang, B., Reynolds, C., Singletary, G.E., Trafny, D., Morine, K.J., Sanmiguel, J., Cecchini, S., et al. (2012). Long-term restoration of cardiac dystrophin expression in golden retriever muscular dystrophy following rAAV6-mediated exon skipping. Mol. Ther. *20*, 580–589.

Black, D.L., Chabot, B., and Steitz, J.A. (1985). U2 as well as U1 small nuclear ribonucleoproteins are involved in premessenger RNA splicing. Cell *42*, 737–750.

Blandin, G., Beroud, C., Labelle, V., Nguyen, K., Wein, N., Hamroun, D., Williams, B., Monnier, N., Rufibach, L.E., Urtizberea, J.A., et al. (2012). UMD-DYSF, a novel locus specific database for the compilation and interactive analysis of mutations in the dysferlin gene. Hum. Mutat. *33*, E2317–E2331.

Blencowe, B.J. (2000). Exonic splicing enhancers: Mechanism of action, diversity and role in human genetic diseases. Trends Biochem. Sci. *25*, 106–110.

Breathnach, R., Benoist, C., O'Hare, K., Gannon, F., and Chambon, P. (1978). Ovalbumin gene: evidence for a leader sequence in mRNA and DNA sequences at the exon-intron boundaries. Proc. Natl. Acad. Sci. U. S. A. *75*, 4853–4857.

Britton, S., Freeman, T., Vafiadaki, E., Keers, S., Harrison, R., Bushby, K., and Bashir, R. (2000). The third human FER-1-like protein is highly similar to dysferlin. Genomics *68*, 313–321.

Brun, C., Suter, D., Pauli, C., Dunant, P., Lochmüller, H., Burgunder, J.M., Schümperli, D., and Weis, J. (2003). U7 snRNAs induce correction of mutated dystrophin pre-mRNA by exon skipping. Cell. Mol. Life Sci. *60*, 557–566.

Buclez, P.-O., Dias Florencio, G., Relizani, K., Beley, C., Garcia, L., and Benchaouir, R. (2016). Rapid, scalable, and low-cost purification of recombinant adeno-associated virus produced by baculovirus expression vector system. Mol. Ther. — Methods Clin. Dev. *3*, 16035.

Buller, R.M., Janik, J.E., Sebring, E.D., and Rose, J.A. (1981). Herpes simplex virus types 1 and 2 completely help adenovirus-associated virus replication. J. Virol. *40*, 241–247.

Buratti, E., and Baralle, F.E. (2004). MINIREVIEW Influence of RNA Secondary Structure on the Pre-mRNA Splicing Process. Mol. Cell. Biol. *24*, 10505–10514.

Burns, J.C., Friedmann, T., Drievert, W., Burrascano, M., and Yee, J.-K. (1993). Vesicular stomatitis virus G glycoprotein pseudotyped retroviral vectors: Concentration to very high titer and efficient gene transfer into mammalian and nonmammalian cells (gene therapy/zebrafish). Genetics *90*, 8033–8037.

Caceres, J., Stamm, S., Helfman, D., and Krainer, A. (1994). Regulation of alternative splicing in vivo by overexpression of antagonistic splicing factors. Science (80-.). *265*, 1706–1709.

Cai, C., Weisleder, N., Ko, J.K., Komazaki, S., Sunada, Y., Nishi, M., Takeshima, H., and Ma, J. (2009a). Membrane repair defects in muscular dystrophy are linked to altered interaction between MG53, caveolin-3, and dysferlin. J. Biol. Chem. *284*, 15894–15902.

Cai, C., Masumiya, H., Weisleder, N., Matsuda, N., Nishi, M., Hwang, M., Ko, J.-K., Lin, P., Thornton, A., Zhao, X., et al. (2009b). MG53 nucleates assembly of cell membrane repair machinery. Nat. Cell Biol. *11*, 56–64.

Cao, L., Han, G., Gu, B., and Yin, H.F. (2014). Wild-type mouse models to screen antisense oligonucleotides for exon-skipping efficacy in Duchenne muscular dystrophy. PLoS One *9*, e111079.

Carlo, T., Sterner, D.A., and Berget, S.M. (1996). An intron splicing enhancer containing a G-rich repeat facilitates inclusion of a vertebrate micro-exon. RNA *2*, 342–353.

Cartegni, L., Wang, J., Zhu, Z., Zhang, M.Q., and Krainer, A.R. (2003). ESEfinder: A web resource to identify exonic splicing enhancers. Nucleic Acids Res. *31*, 3568–3571.

Chandradas, S., Deikus, G., Tardos, J.G., and Bogdanov, V.Y. (2010). Antagonistic roles of four SR proteins in the biosynthesis of alternatively spliced tissue factor transcripts in monocytic cells. J. Leukoc. Biol. *87*, 147–152.

Cheung, A.K., Hoggan, M.D., Hauswirth, W.W., and Berns, K.I. (1980). Integration of the adeno-associated virus genome into cellular DNA in latently infected human Detroit 6 cells. J. Virol. *33*, 739–748.

Coffin, J.M., Hughes, S.H., and Varmus, H.E. (1997). Retroviruses (Cold Spring Harbor Laboratory Press).

Consortium, T.U. (2017). UniProt : the universal protein knowledgebase. Nucleic Acids Res. *45*, 158–169.

Crick, F.H.C. (1966). Codon—anticodon pairing: The wobble hypothesis. J. Mol. Biol. *19*, 548–555.

Davidson, B.L., Stein, C.S., Heth, J.A., Martins, I., Kotin, R.M., Derksen, T.A., Zabner, J., Ghodsi, A., and Chiorini, J.A. (2000). Recombinant adeno-associated virus type 2, 4, and 5 vectors: transduction of variant cell types and regions in the mammalian central nervous system. Proc. Natl. Acad. Sci. U. S. A. *97*, 3428–3432.

Davis, D.B., Delmonte, A.J., Ly, C.T., and McNally, E.M. (2000). Myoferlin, a candidate gene and potential modifier of muscular dystrophy. Hum. Mol. Genet. *9*, 217–226.

Davis, D.B., Doherty, K.R., Delmonte, A.J., and McNally, E.M. (2002). Calcium-sensitive phospholipid binding properties of normal and mutant ferlin C2 domains. J. Biol. Chem. *277*, 22883–22888.

Decary, S., Mouly, V., Hamida, C. Ben, Sautet, A., Barbet, J.P., and Butler-Browne, G.S. (1997). Replicative Potential and Telomere Length in Human Skeletal Muscle: Implications for Satellite Cell-Mediated Gene Therapy. Hum. Gene Ther. *8*, 1429–1438.

Decary, S., Ben Hamida, C., Mouly, V., Barbet, J.P., Hentati, F., and Butler-Browne, G.S. (2000). Shorter telomeres in dystrophic muscle consistent with extensive regeneration in young children. Neuromuscul. Disord. *10*, 113–120.

Demonbreun, A.R., Rossi, A.E., Alvarez, M.G., Swanson, K.E., Deveaux, H.K., Earley, J.U., Hadhazy, M., Vohra, R., Walter, G.A., Pytel, P., et al. (2014). Dysferlin and myoferlin regulate transverse tubule formation and glycerol sensitivity. Am. J. Pathol. *184*, 248–259.

Desmet, F.-O., Hamroun, D., Lalande, M., Collod-Béroud, G., Claustres, M., and Béroud, C. (2009). Human Splicing Finder: an online bioinformatics tool to predict splicing signals. Nucleic Acids Res. *37*, e67.

van Deutekom, J.C., Bremmer-Bout, M., Janson, A.A., Ginjaar, I.B., Baas, F., den Dunnen, J.T., and van Ommen, G.J. (2001). Antisense-induced exon skipping restores dystrophin expression in DMD patient derived muscle cells. Hum. Mol. Genet. *10*, 1547–1554.

van Deutekom, J.C., Janson, A.A., Ginjaar, I.B., Frankhuizen, W.S., Aartsma-Rus, A., Bremmer-Bout, M., den Dunnen, J.T., Koop, K., van der Kooi, A.J., Goemans, N.M., et al. (2007). Local Dystrophin Restoration with Antisense Oligonucleotide PRO051. N. Engl. J. Med. *357*, 2677–2686.

Deyle, D.R., and Russell, D.W. (2009). Adeno-associated virus vector integration. Curr. Opin. Mol. Ther. *11*, 442–447.

Dias Florencio, G., Precigout, G., Beley, C., Buclez, P.-O., Garcia, L., and Benchaouir, R. (2015). Simple downstream process based on detergent treatment improves yield and in vivo transduction efficacy of adeno-associated virus vectors. Mol. Ther. Methods Clin. Dev. *2*, 15024.

Doherty, K.R., Cave, A., Davis, D.B., Delmonte, A.J., Posey, A., Earley, J.U., Hadhazy, M., and McNally, E.M. (2005). Normal myoblast fusion requires myoferlin. Development *132*, 5565–5575.

Dominov, J.A., Uyan, Ö., Sapp, P.C., McKenna-Yasek, D., Nallamilli, B.R.R., Hegde, M., and Brown, R.H. (2014). A novel dysferlin mutant pseudoexon bypassed with antisense oligonucleotides. Ann. Clin. Transl. Neurol. *1*, 703–720.

Douar, A.-M., Poulard, K., Stockholm, D., and Danos, O. (2001). Intracellular Trafficking of Adeno-Associated Virus Vectors: Routing to the Late Endosomal Compartment and Proteasome Degradation. J. Virol. *75*, 1824–1833.

Duan, D., Sharma, P., Yang, J., Yue, Y., Dudus, L., Zhang, Y., Fisher, K.J., and Engelhardt, J.F. (1998). Circular intermediates of recombinant adeno-associated virus have defined structural characteristics responsible for long-term episomal persistence in muscle tissue. J. Virol. *72*, 8568–8577.

Dull, T., Zufferey, R., Kelly, M., Mandel, R.J., Nguyen, M., Trono, D., and Naldini, L. (1998a). A third-generation lentivirus vector with a conditional packaging system. J. Virol. *72*, 8463–8471.

Dull, T., Zufferey, R., Kelly, M., Mandel, R.J., Nguyen, M., Trono, D., and Naldini, L. (1998b). A third-generation lentivirus vector with a conditional packaging system. J. Virol. *72*, 8463–8471.

Dull, T., Zufferey, R., Kelly, M., Mandel, R.J., Nguyen, M., Trono, D., and Naldini, L. (1998c). A third-generation lentivirus vector with a conditional packaging system. J. Virol. *72*, 8463–8471.

Dunckley, M.G., Manoharan, M., Villiet, P., Eperon, I.C., and Dickson, G. (1998). Modification of splicing in the dystrophin gene in cultured Mdx muscle cells by antisense oligoribonucleotides. Hum. Mol. Genet. *7*, 1083–1090.

Durand, S., and Cimarelli, A. (2011). The Inside out of Lentiviral Vectors. Viruses *3*, 132–159.

Egan, M., Flotte, T., Afione, S., Solow, R., Zeitlin, P.L., Carter, B.J., and Guggino, W.B. (1992). Defective regulation of outwardly rectifying Cl− channels by protein kinase A corrected by insertion of CFTR. Nature *358*, 581–584.

Erles, K., Sebökovà, P., and Schlehofer, J.R. (1999). Update on the prevalence of serum antibodies (IgG and IgM) to adeno- associated virus (AAV). J. Med. Virol. *59*, 406–411.

Evesson, F.J., Peat, R.A., Lek, A., Brilot, F., Lo, H.P., Dale, R.C., Parton, R.G., North, K.N., and Cooper, S.T. (2010). Reduced plasma membrane expression of dysferlin mutants is attributed to accelerated endocytosis via a syntaxin-4-associated pathway. J. Biol. Chem. *285*, 28529–28539.

Fairbrother, W.G. (2002). Predictive Identification of Exonic Splicing Enhancers in Human Genes. Science (80-.). *297*, 1007–1013.

Fairbrother, W.G., Yeo, G.W., Yeh, R., Goldstein, P., Mawson, M., Sharp, P.A., and Burge, C.B. (2004).

RESCUE-ESE identifies candidate exonic splicing enhancers in vertebrate exons. Nucleic Acids Res. *32*, W187-90.

Fauquet, C., International Committee on Taxonomy of Viruses., and International Union of Microbiological Societies. Virology Division. (2005). Virus taxonomy : classification and nomenclature of viruses : eighth report of the International Committee on the Taxonomy of Viruses (Elsevier Academic Press).

Fisher, K.J., Gao, G.P., Weitzman, M.D., DeMatteo, R., Burda, J.F., and Wilson, J.M. (1996). Transduction with recombinant adeno-associated virus for gene therapy is limited by leading-strand synthesis. J. Virol. *70*, 520–532.

Flotte, T.R., Solow, R., Owens, R.A., Afione, S., Zeitlin, P.L., and Carter, B.J. (1992). Gene expression from adeno-associated virus vectors in airway epithelial cells. Am. J. Respir. Cell Mol. Biol. *7*, 349–356.

Flotte, T.R., Afione, S.A., and Zeitlin, P.L. (1994). Adeno-associated virus vector gene expression occurs in nondividing cells in the absence of vector DNA integration. Am. J. Respir. Cell Mol. Biol. *11*, 517–521.

Fridén, J., Sjöström, M., and Ekblom, B. (1983). Myofibrillar Damage Following Intense Eccentric Exercise in Man. Int. J. Sports Med. *4*, 170–176.

Fu, X.D., and Ares Jr., M. (2014). Context-dependent control of alternative splicing by RNA-binding proteins. Nat. Rev. Genet. *15*, 689–701.

Fuson, K., Rice, A., Mahling, R., Snow, A., Nayak, K., Shanbhogue, P., Meyer, A.G., Redpath, G.M.I., Hinderliter, A., Cooper, S.T., et al. (2014). Alternate splicing of dysferlin C2A confers Ca2+-dependent and Ca2+-independent binding for membrane repair. Structure *22*, 104–115.

Gallardo, E., Rojas-García, R., de Luna, N., Pou, A., Brown, R.H., and Illa, I. (2001). Inflammation in dysferlin myopathy: immunohistochemical characterization of 13 patients. Neurology *57*, 2136–2138.

Galli, G., Hofstetter, H., Stunnenberg, H.G., and Birnstiel, M.L. (1983). Biochemical complementation with RNA in the Xenopus oocyte: a small RNA is required for the generation of 3' histone mRNA termini. Cell *34*, 823–828.

Garcia, L., Furling, D., Beley, C., and Voit, T. (2013). Modified U7 snRNAs for treatment of neuromuscular diseases.

Del Gatto-Konczak, F., Olive, M., Gesnel, M.C., and Breathnach, R. (1999). hnRNP A1 recruited to an exon in vivo can function as an exon splicing silencer. Mol. Cell. Biol. *19*, 251–260.

Geuens, T., Bouhy, D., and Timmerman, V. (2016). The hnRNP family: insights into their role in health and disease. Hum. Genet. *135*, 851–867.

Glover, L.E., Newton, K., Krishnan, G., Bronson, R., Boyle, A., Krivickas, L.S., and Brown, R.H. (2010). Dysferlin overexpression in skeletal muscle produces a progressive myopathy. Ann. Neurol. *67*, 384–393.

Goemans, N.M., Tulinius, M., van den Akker, J.T., Burm, B.E., Ekhart, P.F., Heuvelmans, N., Holling, T., Janson, A.A., Platenburg, G.J., Sipkens, J.A., et al. (2011). Systemic Administration of PRO051 in Duchenne's Muscular Dystrophy. N. Engl. J. Med. *364*, 1513–1522.

Gorman, L., Suter, D., Emerick, V., Schümperli, D., and Kole, R. (1998). Stable alteration of pre-mRNA splicing patterns by modified U7 small nuclear RNAs. Proc. Natl. Acad. Sci. U. S. A. *95*, 4929–4934.

Goyenvalle, A. (2004). Rescue of Dystrophic Muscle Through U7 snRNA-Mediated Exon Skipping. Science (80-.). *306*, 1796–1799.

Goyenvalle, A., Babbs, A., van Ommen, G.-J.B., Garcia, L., and Davies, K.E. (2009). Enhanced Exon-skipping Induced by U7 snRNA Carrying a Splicing Silencer Sequence: Promising Tool for DMD Therapy. Mol. Ther. *17*, 1234–1240.

Goyenvalle, A., Babbs, A., Wright, J., Wilkins, V., Powell, D., Garcia, L., and Davies, K.E. (2012). Rescue of severely affected dystrophin/utrophin-deficient mice through scAAV-U7snRNA-mediated exon skipping. Hum. Mol. Genet. *21*, 2559–2571.

Goyenvalle, A., Leumann, C., and Garcia, L. (2016). Therapeutic Potential of Tricyclo-DNA antisense oligonucleotides. J. Neuromuscul. Dis. *3*, 157–167.

Grabowski, P.J., and Sharp, P.A. (1986). Affinity chromatography of splicing complexes: U2, U5, and U4 + U6 small nuclear ribonucleoprotein particles in the spliceosome. Science (80-.). *233*, 1294–1299.

Green, M.R. (1991). Biochemical mechanisms of constitutive and regulated pre-mRNA splicing. Annu. Rev. Cell Biol. *7*, 559–599.

Gregorevic, P., Blankinship, M.J., Allen, J.M., Crawford, R.W., Meuse, L., Miller, D.G., Russell, D.W., and Chamberlain, J.S. (2004). Systemic delivery of genes to striated muscles using adeno-associated viral vectors. Nat. Med. *10*, 828–834.

Grimm, C., Stefanovic, B., and Schümperli, D. (1993). The low abundance of U7 snRNA is partly determined by its Sm binding site. EMBO J. *12*, 1229–1238.

Grose, W.E., Clark, K.R., Griffin, D., Malik, V., Shontz, K.M., Montgomery, C.L., Lewis, S., Brown, R.H., Janssen, P.M.L., Mendell, J.R., et al. (2012). Homologous recombination mediates functional recovery of dysferlin deficiency following AAV5 gene transfer. PLoS One *7*, e39233.

Gruber, A., Soldati, D., Burri, M., and Schümperli, D. (1991). Isolation of an active gene and of two pseudogenes for mouse U7 small nuclear RNA. BBA - Gene Struct. Expr. *1088*, 151–154.

Gruber, A.R., Lorenz, R., Bernhart, S.H., Neuböck, R., and Hofacker, I.L. (2008). The Vienna RNA websuite. Nucleic Acids Res. *36*, W70-4.

Guex, N., Peitsch, M.C., and Schwede, T. (2009). Automated comparative protein structure modeling with SWISS-MODEL and Swiss-PdbViewer: A historical perspective. Electrophoresis *30*, S162–S173.

Hall, S.L., and Padgett, R.A. (1996). Requirement of U12 snRNA for in vivo splicing of a minor class of eukaryotic nuclear pre-mRNA introns. Science (80-.). *271*, 1716–1718.

Hanamura, A., Cáceres, J.F., Mayeda, A., Franza, B.R., and Krainer, A.R. (1998). Regulated tissue-specific expression of antagonistic pre-mRNA splicing factors. RNA *4*, 430–444.

Handa, H., Shiroki, K., and Shimojo, H. (1977). Establishment and characterization of KB cell lines latently infected with adeno-associated virus type 1. Virology *82*, 84–92.

Harris, E., Bladen, C.L., Mayhew, A., James, M., Bettinson, K., Moore, U., Smith, F.E., Rufibach, L., Cnaan, A., Bharucha-Goebel, D.X., et al. (2016). The Clinical Outcome Study for dysferlinopathy. Neurol. Genet. *2*, e89.

Hauswirth, W.W., and Berns, K.I. (1979). Adeno-associated virus DNA replication: nonunit-length molecules. Virology *93*, 57–68.

Havens, M.A., and Hastings, M.L. (2016). Splice-switching antisense oligonucleotides as therapeutic drugs. Nucleic Acids Res. *44*, 6549–6563.

Heemskerk, H.A., de Winter, C.L., de Kimpe, S.J., van Kuik-Romeijn, P., Heuvelmans, N., Platenburg, G.J., van Ommen, G.J.B., van Deutekom, J.C.T., and Aarstsma-Rus, A. (2009). In vivo comparison of 2'-O-methyl phosphorothioate and morpholino antisense oligonucleotides for Duchenne muscular dystrophy exon skipping. J. Gene Med. *11*, 257–266.

Hermonat, P.L., and Muzyczka, N. (1984). Use of adeno-associated virus as a mammalian DNA cloning vector: transduction of neomycin resistance into mammalian tissue culture cells. Proc. Natl. Acad. Sci. U. S. A. *81*, 6466–6470.

Le Hir, M., Goyenvalle, A., Peccate, C., Précigout, G., Davies, K.E., Voit, T., Garcia, L., and Lorain, S. (2013). AAV genome loss from dystrophic mouse muscles during AAV-U7 snRNA-mediated exon-skipping therapy. Mol. Ther. *21*, 1551–1558.

Ho, M., Gallardo, E., McKenna-Yasek, D., De Luna, N., Illa, I., and Brown, R.H. (2002). A novel, blood-based diagnostic assay for limb girdle muscular dystrophy 2B and miyoshi myopathy. Ann. Neurol. *51*, 129–133.

Hoggan, M.D., Thomas, G.F., and Johnson, F.B. (1972). Continuous carriage of adenovirus-associated virus genome in cell culture in the absence of helper adenovirus. Proc. Fourth Lepetit Colloquium, North-Holland, Amsterdam 41–47.

Hong, G., Ward, P., and Berns, K.I. (1992). In vitro replication of adeno-associated virus DNA. Proc. Natl. Acad. Sci. U. S. A. *89*, 4673–4677.

Huang, Y., Laval, S.H., van Remoortere, A., Baudier, J., Benaud, C., Anderson, L.V.B., Straub, V., Deelder, A., Frants, R.R., den Dunnen, J.T., et al. (2007). AHNAK, a novel component of the dysferlin protein complex, redistributes to the cytoplasm with dysferlin during skeletal muscle regeneration. FASEB J. *21*, 732–742.

Hüser, D., Weger, S., and Heilbronn, R. (2002). Kinetics and frequency of adeno-associated virus site-specific integration into human chromosome 19 monitored by quantitative real-time PCR. J. Virol. *76*, 7554–7559.

Illa, I., Serrano-Munuera, C., Gallardo, E., Lasa, A., Rojas-Garca, R., Palmer, J., Gallano, P., Baiget, M., Matsuda, C., and Brown, R.H. (2001). Distal anterior compartment myopathy: A dysferlin mutation causing a new muscular dystrophy phenotype. Ann. Neurol. *49*, 130–134.

Illarioshkin, S.N., Ivanova-Smolenskaya, I.A., Greenberg, C.R., Nylen, E., Sukhorukov, V.S., Poleshchuk, V. V, Markova, E.D., and Wrogemann, K. (2000). Identical dysferlin mutation in limb-girdle muscular dystrophy type 2B and distal myopathy. Neurology *55*, 1931–1933.

Inagaki, K., Fuess, S., Storm, T.A., Gibson, G.A., Mctiernan, C.F., Kay, M.A., and Nakai, H. (2006). Robust systemic transduction with AAV9 vectors in mice: efficient global cardiac gene transfer superior to that of AAV8. Mol. Ther. *14*, 45–53.

Inagaki, K., Lewis, S.M., Wu, X., Ma, C., Munroe, D.J., Fuess, S., Storm, T.A., Kay, M.A., and Nakai, H. (2007). DNA palindromes with a modest arm length of greater, similar 20 base pairs are a significant target for recombinant adeno-associated virus vector integration in the liver, muscles, and heart in mice. J. Virol. *81*, 11290–11303.

Jiang, Z., Cote, J., Kwon, J.M., Goate, A.M., and Wu, J.Y. (2000). Aberrant splicing of tau pre-mRNA caused by intronic mutations associated with the inherited dementia frontotemporal dementia with

parkinsonism linked to chromosome 17. Mol. Cell. Biol. *20*, 4036–4048.

Kaeppel, C., Beattie, S.G., Fronza, R., van Logtenstein, R., Salmon, F., Schmidt, S., Wolf, S., Nowrouzi, A., Glimm, H., von Kalle, C., et al. (2013). A largely random AAV integration profile after LPLD gene therapy. Nat. Med. *19*, 889–891.

Kafri, T., Blömer, U., Peterson, D.A., Gage, F.H., and Verma, I.M. (1997). Sustained expression of genes delivered directly into liver and muscle by lentiviral vectors. Nat. Genet. *17*, 314–317.

Kambach, C., Walke, S., Young, R., Avis, J.M., De La Fortelle, E., Raker, V.A., Lührmann, R., Li, J., and Nagai, K. (1999). Crystal structures of two Sm protein complexes and their implications for the assembly of the spliceosomal snRNPs. Cell *96*, 375–387.

Kanopka, A., Mühlemann, O., and Akusjärvi, G. (1996). Inhibition by SR proteins of splicing of a regulated adenovirus pre-mRNA. Nature *381*, 535–538.

Kaplitt, M.G., Leone, P., Samulski, R.J., Xiao, X., Pfaff, D.W., O'Malley, K.L., and During, M.J. (1994). Long-term gene expression and phenotypic correction using adeno-associated virus vectors in the mammalian brain. Nat. Genet. *8*, 148–154.

Kearns, W.G., Afione, S.A., Fulmer, S.B., Pang, M.C., Erikson, D., Egan, M., Landrum, M.J., Flotte, T.R., and Cutting, G.R. (1996). Recombinant adeno-associated virus (AAV-CFTR) vectors do not integrate in a site-specific fashion in an immortalized epithelial cell line. Gene Ther. *3*, 748–755.

Kessler, P.D., Podsakoff, G.M., Chen, X., McQuiston, S.A., Colosi, P.C., Matelis, L.A., Kurtzman, G.J., and Byrne, B.J. (1996). Gene delivery to skeletal muscle results in sustained expression and systemic delivery of a therapeutic protein. Proc. Natl. Acad. Sci. *93*, 14082–14087.

Khodor, Y.L., Rodriguez, J., Abruzzi, K.C., Tang, C.H.A., Marr, M.T., and Rosbash, M. (2011). Nascent-seq indicates widespread cotranscriptional pre-mRNA splicing in Drosophila. Genes Dev. *25*, 2502–2512.

Kiefer, F., Arnold, K., Kunzli, M., Bordoli, L., and Schwede, T. (2009). The SWISS-MODEL Repository and associated resources. Nucleic Acids Res. *37*, D387–D392.

Klinge, L., Laval, S., Keers, S., Haldane, F., Straub, V., Barresi, R., and Bushby, K. (2007). From T-tubule to sarcolemma: damage-induced dysferlin translocation in early myogenesis. FASEB J. *21*, 1768–1776.

Klinge, L., Harris, J., Sewry, C., Charlton, R., Anderson, L., Laval, S., Chiu, Y.H., Hornsey, M., Straub, V., Barresi, R., et al. (2010). Dysferlin associates with the developing T-tubule system in rodent and human skeletal muscle. Muscle and Nerve *41*, 166–173.

Koczot, F.J., Carter, B.J., Garon, C.F., and Rose, J.A. (1973). Self-complementarity of terminal sequences within plus or minus strands of adenovirus-associated virus DNA. Proc. Natl. Acad. Sci. U. S. A. *70*, 215–219.

Kornblihtt, A.R., Schor, I.E., Alló, M., Dujardin, G., Petrillo, E., and Muñoz, M.J. (2013). Alternative splicing: a pivotal step between eukaryotic transcription and translation. Nat. Rev. Mol. Cell Biol. *14*, 153–165.

Kotin, R.M., Siniscalco, M., Samulski, R.J., Zhu, X.D., Hunter, L., Laughlin, C.A., McLaughlin, S., Muzyczka, N., Rocchi, M., and Berns, K.I. (1990). Site-specific integration by adeno-associated virus. Proc. Natl. Acad. Sci. U. S. A. *87*, 2211–2215.

Kozak, M. (1987). An analysis of 5'-noncoding sequences from 699 vertebrate messenger rNAS.

Nucleic Acids Res. *15*, 8125–8148.

Krahn, M., Béroud, C., Labelle, V., Nguyen, K., Bernard, R., Bassez, G., Figarella-Branger, D., Fernandez, C., Bouvenot, J., Richard, I., et al. (2009). Analysis of the DYSF mutational spectrum in a large cohort of patients. Hum. Mutat. *30*, E345-75.

Krahn, M., Wein, N., Bartoli, M., Lostal, W., Courrier, S., Bourg-Alibert, N., Nguyen, K., Vial, C., Streichenberger, N., Labelle, V., et al. (2010). A naturally occurring human minidysferlin protein repairs sarcolemmal lesions in a mouse model of dysferlinopathy. Sci. Transl. Med. *2*, 50ra69.

Kramer, F.R., and Mills, D.R. (1981). Secondary structure formation during RNA synthesis. Nucleic Acids Res. *9*, 5109–5124.

Krieg, P.A., and Melton, D.A. (1984). Formation of the 3' end of histone mRNA by post-transcriptional processing. Nature *308*, 203–206.

Kumar, M., Keller, B., Makalou, N., and Sutton, R.E. (2001). Systematic Determination of the Packaging Limit of Lentiviral Vectors. Hum. Gene Ther. *12*, 1893–1905.

Kurreck, J. (2003). Antisense technologies: Improvement through novel chemical modifications. Eur. J. Biochem. *270*, 1628–1644.

Kyte, J., and Doolittle, R.F. (1982). A simple method for displaying the hydropathic character of a protein. J. Mol. Biol. *157*, 105–132.

Lander, E.S., Linton, L.M., Birren, B., Nusbaum, C., Zody, M.C., Baldwin, J., Devon, K., Dewar, K., Doyle, M., FitzHugh, W., et al. (2001). Initial sequencing and analysis of the human genome. Nature *409*, 860–921.

Lebkowski, J.S., McNally, M.M., Okarma, T.B., and Lerch, L.B. (1988). Adeno-associated virus: a vector system for efficient introduction and integration of DNA into a variety of mammalian cell types. Mol. Cell. Biol. *8*, 3988–3996.

LeFebvre, R.B., and Berns, K.I. (1984). Unique events in parvovirus replication. Microbiol Sci *1*, 163–167.

Lek, A., Evesson, F.J., Sutton, R.B., North, K.N., and Cooper, S.T. (2012). Ferlins: regulators of vesicle fusion for auditory neurotransmission, receptor trafficking and membrane repair. Traffic *13*, 185–194.

Lennon, N.J., Kho, A., Bacskai, B.J., Perlmutter, S.L., Hyman, B.T., and Brown, R.H. (2003). Dysferlin Interacts with Annexins A1 and A2 and Mediates Sarcolemmal Wound-healing. J. Biol. Chem. *278*, 50466–50473.

Lerner, M.R., and Steitz, J.A. (1979). Antibodies to small nuclear RNAs complexed with proteins are produced by patients with systemic lupus erythematosus. Proc. Natl. Acad. Sci. U. S. A. *76*, 5495–5499.

Leshinsky-Silver, E., Argov, Z., Rozenboim, L., Cohen, S., Tzofi, Z., Cohen, Y., Wirguin, Y., Dabby, R., Lev, D., and Sadeh, M. (2007). Dysferlinopathy in the Jews of the Caucasus: A frequent mutation in the dysferlin gene. Neuromuscul. Disord. *17*, 950–954.

Limberis, M.P., Vandenberghe, L.H., Zhang, L., Pickles, R.J., and Wilson, J.M. (2009). Transduction Efficiencies of Novel AAV Vectors in Mouse Airway Epithelium In Vivo and Human Ciliated Airway Epithelium In Vitro. Mol. Ther. *17*, 294–301.

Linden, R.M., Ward, P., Giraud, C., Winocour, E., and Berns, K.I. (1996). Site-specific integration by adeno-associated virus. Proc Natl Acad Sci U S A *93*, 11288–11294.

Listerman, I., Sapra, A.K., and Neugebauer, K.M. (2006). Cotranscriptional coupling of splicing factor recruitment and precursor messenger RNA splicing in mammalian cells. TL - 13. Nat. Struct. Mol. Biol. *13 VN-r*, 815–822.

Liu, H.X., Zhang, M., and Krainer, A.R. (1998a). Identification of functional exonic splicing enhancer motifs recognized by individual SR proteins. Genes Dev. *12*, 1998–2012.

Liu, J., Aoki, M., Illa, I., Wu, C., Fardeau, M., Angelini, C., Serrano, C., Urtizberea, J.A., Hentati, F., Hamida, M. Ben, et al. (1998b). Dysferlin, a novel skeletal muscle gene, is mutated in Miyoshi myopathy and limb girdle muscular dystrophy. Nat. Genet. *20*, 31–36.

Lostal, W., Bartoli, M., Bourg, N., Roudaut, C., Bentaïb, A., Miyake, K., Guerchet, N., Fougerousse, F., McNeil, P., and Richard, I. (2010). Efficient recovery of dysferlin deficiency by dual adeno-associated vector-mediated gene transfer. Hum. Mol. Genet. *19*, 1897–1907.

Lostal, W., Bartoli, M., Roudaut, C., Bourg, N., Krahn, M., Pryadkina, M., Borel, P., Suel, L., Roche, J.A., Stockholm, D., et al. (2012). Lack of correlation between outcomes of membrane repair assay and correction of dystrophic changes in experimental therapeutic strategy in dysferlinopathy. PLoS One *7*, e38036.

Lu, Q.L., Mann, C.J., Lou, F., Bou-gharios, G., Morris, G.E., Xue, S., Fletcher, S., Partridge, T.A., Wilton, S.D., Lou, F., et al. (2003). Functional amounts of dystrophin produced by skipping the mutated exon in the mdx dystrophic mouse.

Lührmann, R., Kastner, B., and Bach, M. (1990). Structure of spliceosomal snRNPs and their role in pre-mRNA splicing. BBA - Gene Struct. Expr. *1087*, 265–292.

Lusby, E., Fife, K.H., and Berns, K.I. (1980). Nucleotide sequence of the inverted terminal repetition in adeno-associated virus DNA. J. Virol. *34*, 402–409.

Macpherson, P.C., Schork, M.A., and Faulkner, J.A. (1996). Contraction-induced injury to single fiber segments from fast and slow muscles of rats by single stretches. Am. J. Physiol. *271*, C1438-46.

Mamchaoui, K., Trollet, C., Bigot, A., Negroni, E., Chaouch, S., Wolff, A., Kandalla, P.K., Marie, S., Di Santo, J., St Guily, J.L., et al. (2011). Immortalized pathological human myoblasts: towards a universal tool for the study of neuromuscular disorders. Skelet. Muscle *1*, 34.

Maniatis, T., and Tasic, B. (2002). Alternative pre-mRNA splicing and proteome expansion in metazoans. Nature *418*, 236–243.

Mann, C.J., Honeyman, K., Cheng, A.J., Ly, T., Lloyd, F., Fletcher, S., Morgan, J.E., Partridge, T.A., and Wilton, S.D. (2001). Antisense-induced exon skipping and synthesis of dystrophin in the mdx mouse. Proc. Natl. Acad. Sci. U. S. A. *98*, 42–47.

Marg, A., Schoewel, V., Timmel, T., Schulze, A., Shah, C., Daumke, O., and Spuler, S. (2012a). Sarcolemmal Repair Is a Slow Process and Includes EHD2. Traffic *13*, 1286–1294.

Marg, A., Schoewel, V., Timmel, T., Schulze, A., Shah, C., Daumke, O., and Spuler, S. (2012b). Sarcolemmal repair is a slow process and includes EHD2. Traffic *13*, 1286–1294.

Marwick, C. (1998). First “antisense” drug will treat CMV retinitis. JAMA *280*, 871.

Matera, A.G., and Wang, Z. (2014). A day in the life of the spliceosome. Nat. Rev. Mol. Cell Biol. *15*, 108–121.

Matsuda, C., Aoki, M., Hayashi, Y.K., Ho, M.F., Arahata, K., and Brown, R.H. (1999). Dysferlin is a surface

membrane-associated protein that is absent in Miyoshi myopathy. Neurology *53*, 1119–1119.

Matsuda, C., Hayashi, Y.K., Ogawa, M., Aoki, M., Murayama, K., Nishino, I., Nonaka, I., Arahata, K., and Brown Jr., R.H. (2001). The sarcolemmal proteins dysferlin and caveolin-3 interact in skeletal muscle. Hum. Mol. Genet. *10*, 1761–1766.

Mayeda, A., and Krainer, A.R. (1992). Regulation of alternative pre-mRNA splicing by hnRNP A1 and splicing factor SF2. Cell *68*, 365–375.

Mayeda, A., Munroe, S.H., Cáceres, J.F., and Krainer, A.R. (1994). Function of conserved domains of hnRNP A1 and other hnRNP A/B proteins. EMBO J. *13*, 5483–5495.

Mayorga, L.S., Berón, W., Sarrouf, M.N., Colombo, M.I., Creutz, C., and Stahl, P.D. (1994). Calcium-dependent fusion among endosomes. J. Biol. Chem. *269*, 30927–30934.

McLaughlin, S.K., Collis, P., Hermonat, P.L., and Muzyczka, N. (1988). Adeno-associated virus general transduction vectors: analysis of proviral structures. J. Virol. *62*, 1963–1973.

McNeil, P.L. (1993). Cellular and molecular adaptations to injurious mechanical stress. Trends Cell Biol. *3*, 302–307.

McNeil, P.L., and Khakee, R. (1992). Disruptions of muscle fiber plasma membranes. Role in exercise-induced damage. Am J Pathol *140*, 1097–1109.

McNeil, P.L., and Terasaki, M. (2001). Coping with the inevitable: how cells repair a torn surface membrane. Nat. Cell Biol. *3*, E124–E129.

McNeil, A.K., Rescher, U., Gerke, V., and McNeil, P.L. (2006). Requirement for annexin A1 in plasma membrane repair. J. Biol. Chem. *281*, 35202–35207.

McNeil, P.L., Vogel, S.S., Miyake, K., and Terasaki, M. (2000). Patching plasma membrane disruptions with cytoplasmic membrane. J. Cell Sci. *113 (Pt 1*, 1891–1902.

Mendelson, E., Trempe, J.P., and Carter, B.J. (1986). Identification of the trans-acting Rep proteins of adeno-associated virus by antibodies to a synthetic oligopeptide. J. Virol. *60*, 823–832.

Miller, D.G., Petek, L.M., and Russell, D.W. (2003). Human gene targeting by adeno-associated virus vectors is enhanced by DNA double-strand breaks. Mol. Cell. Biol. *23*, 3550–3557.

Miyoshi, K., Kawai, H., Iwasa, M., Kusaka, K., and Nishino, H. (1986). Autosomal recessive distal muscular dystrophy as a new type of progressive muscular dystrophy. Seventeen cases in eight families including an autopsied case. Brain *109 (Pt 1*, 31–54.

Mouly, V., Aamiri, A., Bigot, A., Cooper, R.N., Di Donna, S., Furling, D., Gidaro, T., Jacquemin, V., Mamchaoui, K., Negroni, E., et al. (2005). The mitotic clock in skeletal muscle regeneration, disease and cell mediated gene therapy. Acta Physiol. Scand. *184*, 3–15.

Mowry, K.L., and Steitz, J.A. (1987). Identification of the human U7 snRNP as one of several factors involved in the 3' end maturation of histone premessenger RNA's. Science *238*, 1682–1687.

Mueller, W., and Hertel, K. (2011). The role of SR and SR-related proteins in pre-mRNA splicing. RNA Bind. Proteins 1–21.

Müller, B., and Schümperli, D. (1997). The U7 snRNP and the hairpin binding protein: Key players in histone mRNA metabolism. Semin. Cell Dev. Biol. *8*, 567–576.

Nakagawa, M., Matsuzaki, T., Suehara, M., Kanzato, N., Takashima, H., Higuchi, I., Matsumura, T., Goto, K., Arahata, K., and Osame, M. (2001). Phenotypic variation in a large Japanese family with Miyoshi myopathy with nonsense mutation in exon 19 of dysferlin gene. J. Neurol. Sci. *184*, 15–19.

Nakai, H., Storm, T.A., and Kay, M.A. (2000). Recruitment of Single-Stranded Recombinant Adeno-Associated Virus Vector Genomes and Intermolecular Recombination Are Responsible for Stable Transduction of Liver In Vivo. J. Virol. *74*, 9451–9463.

Nakai, H., Montini, E., Fuess, S., Storm, T.A., Grompe, M., and Kay, M.A. (2003). AAV serotype 2 vectors preferentially integrate into active genes in mice. Nat. Genet. *34*, 297–302.

Nakai, H., Wu, X., Fuess, S., Storm, T.A., Munroe, D., Montini, E., Burgess, S.M., Grompe, M., and Kay, M.A. (2005). Large-Scale Molecular Characterization of Adeno-Associated Virus Vector Integration in Mouse Liver. J. Virol. *79*, 3606–3614.

Naldini, L., Blömer, U., Gallay, P., Ory, D., Mulligan, R., Gage, F.H., Verma, I.M., and Trono, D. (1996). In vivo gene delivery and stable transduction of nondividing cells by a lentiviral vector. Science *272*, 263–267.

Norwood, F.L.M., Harling, C., Chinnery, P.F., Eagle, M., Bushby, K., and Straub, V. (2009). Prevalence of genetic muscle disease in Northern England: in-depth analysis of a muscle clinic population. Brain *132*, 3175–3186.

Pacak, C.A., Conlon, T., Mah, C.S., and Byrne, B.J. (2008). Relative persistence of AAV serotype 1 vector genomes in dystrophic muscle. Genet Vaccines Ther *6*, 14.

Padgett, R.A., Konarska, M.M., Grabowski, P.J., Hardy, S.F., and Sharp, P.A. (1984). Lariat RNA's as intermediates and products in the splicing of messenger RNA precursors. Science *225*, 898–903.

Pan, Q., Shai, O., Lee, L.J., Frey, B.J., and Blencowe, B.J. (2008). Deep surveying of alternative splicing complexity in the human transcriptome by high-throughput sequencing. Nat. Genet. *40*, 1413–1415.

Pandit, S., Zhou, Y., Shiue, L., Coutinho-Mansfield, G., Li, H., Qiu, J., Huang, J., Yeo, G.W., Ares, M., and Fu, X.D. (2013). Genome-wide Analysis Reveals SR Protein Cooperation and Competition in Regulated Splicing. Mol. Cell *50*, 223–235.

Parks, W.P., Melnick, J.L., Rongey, R., and Mayor, H.D. (1967). Physical assay and growth cycle studies of a defective adeno-satellite virus. J. Virol. *1*, 171–180.

Pasquale, G. Di, Davidson, B.L., Stein, C.S., Martins, I., Scudiero, D., Monks, A., and Chiorini, J.A. (2003). Identification of PDGFR as a receptor for AAV-5 transduction. Nat. Med. *9*, 1306–1312.

Patel, A.A., and Steitz, J.A. (2003). Splicing double: insights from the second spliceosome. Nat. Rev. Mol. Cell Biol. *4*, 960–970.

Penaud-Budloo, M., Le Guiner, C., Nowrouzi, A., Toromanoff, A., Chérel, Y., Chenuaud, P., Schmidt, M., von Kalle, C., Rolling, F., Moullier, P., et al. (2008). Adeno-associated virus vector genomes persist as episomal chromatin in primate muscle. J. Virol. *82*, 7875–7885.

Philippi, S., Bigot, A., Marg, A., Mouly, V., Spuler, S., and Zacharias, U. (2012). Dysferlin-deficient immortalized human myoblasts and myotubes as a useful tool to study dysferlinopathy. PLoS Curr. *4*, RRN1298.

Piccolo, F., Moore, S.A., Ford, G.C., and Campbell, K.P. (2000). Intracellular accumulation and reduced sarcolemmal expression of dysferlin in limb-girdle muscular dystrophies. Ann. Neurol. *48*, 902–912.

Pichavant, C., and Tremblay, J.P. (2012). Generation of lentiviral vectors for use in skeletal muscle research. Methods Mol. Biol. *798*, 285–295.

Pillai, R.S., Will, C.L., Lührmann, R., Schümperli, D., and Müller, B. (2001). Purified U7 snRNPs lack the Sm proteins D1 and D2 but contain Lsm10, a new 14 kDa Sm D1-like protein. EMBO J. *20*, 5470–5479.

Pillai, R.S., Grimmler, M., Meister, G., Will, C.L., Lührmann, R., Fischer, U., and Schümperli, D. (2003). Unique Sm core structure of U7 snRNPs: assembly by a specialized SMN complex and the role of a new component, Lsm11, in histone RNA processing. Genes Dev. *17*, 2321–2333.

Pillay, S., Meyer, N.L., Puschnik, A.S., Davulcu, O., Diep, J., Ishikawa, Y., Jae, L.T., Wosen, J.E., Nagamine, C.M., Chapman, M.S., et al. (2016). An essential receptor for adeno-associated virus infection. Nature *530*, 108–112.

Pollard, V.W., and Malim, M.H. (1998). THE HIV-1 REV PROTEIN. Annu. Rev. Microbiol. *52*, 491–532.

Pollard, A.J., Krainer, A.R., Robson, S.C., and Nicholas Europe-Finner, G. (2002). Alternative splicing of the adenylyl cyclase stimulatory G-protein Gαs is regulated by SF2/ASF and heterogeneous nuclear ribonucleoprotein A1 (hnRNPA1) and involves the use of an unusual TG 3'-splice site. J. Biol. Chem. *277*, 15241–15251.

Ponnazhagan, S., Erikson, D., Kearns, W.G., Zhou, S.Z., Nahreini, P., Wang, X.S., and Srivastava, A. (1997). Lack of site-specific integration of the recombinant adeno-associated virus 2 genomes in human cells. Hum.Gene Ther *8*, 275–284.

Pramono, Z.A.D., Lai, P.S., Tan, C.L., Takeda, S., and Yee, W.C. (2006). Identification and characterization of a novel human dysferlin transcript: Dysferlin_v1. Hum. Genet. *120*, 410–419.

Pramono, Z.A.D., Tan, C.L., Seah, I.A.L., See, J.S.L., Kam, S.Y., Lai, P.S., and Yee, W.C. (2009). Identification and characterisation of human dysferlin transcript variants: Implications for dysferlin mutational screening and isoforms. Hum. Genet. *125*, 413–420.

Proctor, J.R., and Meyer, I.M. (2013). CoFold: An RNA secondary structure prediction method that takes co-transcriptional folding into account. Nucleic Acids Res. *41*, e102–e102.

Qing, K., Mah, C., Hansen, J., Zhou, S., Dwarki, V., and Srivastava, A. (1999). Human fibroblast growth factor receptor 1 is a co-receptor for infection by adeno-associated virus 2. Nat Med *5*, 71–77.

Rahimov, F., and Kunkel, L.M. (2013). Cellular and molecular mechanisms underlying muscular dystrophy. J. Cell Biol. *201*, 499–510.

Recchia, A., Perani, L., Sartori, D., Olgiati, C., and Mavilio, F. (2004). Site-specific integration of functional transgenes into the human genome by adeno/AAV hybrid vectors. Mol. Ther. *10*, 660–670.

Rechsteiner, M., and Rogers, S.W. (1996). PEST sequences and regulation by proteolysis. Trends Biochem. Sci. *21*, 267–271.

Reed, R. (1996). Initial splice-site recognition and pairing during pre-mRNA splicing. Curr. Opin. Genet. Dev. *6*, 215–220.

Renault, V., Piron-Hamelin, G., Forestier, C., DiDonna, S., Decary, S., Hentati, F., Saillant, G., Butler-Browne, G.S., and Mouly, V. (2000). Skeletal muscle regeneration and the mitotic clock. In Experimental Gerontology, (Pergamon), pp. 711–719.

Rice, P., Longden, I., and Bleasby, A. (2000). EMBOSS: the European Molecular Biology Open Software Suite. Trends Genet. *16*, 276–277.

Rivière, C., Danos, O., and Douar, A.M. (2006). Long-term expression and repeated administration of AAV type 1, 2 and 5 vectors in skeletal muscle of immunocompetent adult mice. Gene Ther. *13*, 1300–1308.

Robberson, B.L., Cote, G.J., and Berget, S.M. (1990). Exon definition may facilitate splice site selection in RNAs with multiple exons. Mol. Cell. Biol. *10*, 84–94.

Robinson, H.L. (2002). Vaccines: New Hope for an Aids Vaccine. Nat. Rev. Immunol. *2*, 239–250.

Roostalu, U., and Strähle, U. (2012). In Vivo Imaging of Molecular Interactions at Damaged Sarcolemma. Dev. Cell *22*, 515–529.

Rose, J.A., Maizel, J. V, Inman, J.K., Shatkin, A.J., and Shatkin, A.J. (1971). Structural proteins of adenovirus-associated viruses. J. Virol. *8*, 766–770.

Ruskin, B., Krainer, A.R., Maniatis, T., and Green, M.R. (1984). Excision of an intact intron as a novel lariat structure during pre-mRNA splicing in vitro. Cell *38*, 317–331.

Saito, Y. (1999). Calreticulin functions in vitro as a molecular chaperone for both glycosylated and non-glycosylated proteins. EMBO J. *18*, 6718–6729.

Sakharkar, M.K., Chow, V.T.K., and Kangueane, P. (2004). Distributions of exons and introns in the human genome. In Silico Biol. *4*, 387–393.

Sakuma, T., Barry, M.A., and Ikeda, Y. (2012). Lentiviral vectors: basic to translational. Biochem J *443*, 603–618.

Samulski, R.J., and Muzyczka, N. (2014). AAV-Mediated Gene Therapy for Research and Therapeutic Purposes. Annu. Rev. Virol. *1*, 427–451.

Samulski, R.J., Berns, K.I., Tan, M., and Muzyczka, N. (1982). Cloning of adeno-associated virus into pBR322: rescue of intact virus from the recombinant plasmid in human cells. Proc. Natl. Acad. Sci. U. S. A. *79*, 2077–2081.

Samulski, R.J., Chang, L.S., and Shenk, T. (1987). A recombinant plasmid from which an infectious adeno-associated virus genome can be excised in vitro and its use to study viral replication. J. Virol. *61*, 3096–3101.

Samulski, R.J., Chang, L.S., and Shenk, T. (1989). Helper-free stocks of recombinant adeno-associated viruses: normal integration does not require viral gene expression. J. Virol. *63*, 3822–3828.

Sanjana, N.E., Shalem, O., and Zhang, F. (2014). Improved vectors and genome-wide libraries for CRISPR screening. Nat. Methods *11*, 783–784.

Sasaki-Haraguchi, N., Shimada, M.K., Taniguchi, I., Ohno, M., and Mayeda, A. (2012). Mechanistic insights into human pre-mRNA splicing of human ultra-short introns: Potential unusual mechanism identifies G-rich introns. Biochem. Biophys. Res. Commun. *423*, 289–294.

Schoewel, V., Marg, A., Kunz, S., Overkamp, T., Siegert Carrazedo, R., Zacharias, U., Daniel, P.T., and Spuler, S. (2012). Dysferlin-Peptides Reallocate Mutated Dysferlin Thereby Restoring Function. PLoS One *7*, e49603.

Schultz, E., and Lipton, B.H. (1982). Skeletal muscle satellite cells: Changes in proliferation potential as a function of age. Mech. Ageing Dev. *20*, 377–383.

Schümperli, D., and Pillai, R.S. (2004). The special Sm core structure of the U7 snRNP: Far-reaching

significance of a small nuclear ribonucleoprotein. Cell. Mol. Life Sci. *61*, 2560–2570.

Selcen, D., Stilling, G., and Engel, A.G. (2001). The earliest pathologic alterations in dysferlinopathy. Neurology *56*, 1472–1481.

Seppen, J., Barry, S.C., Harder, B., and Osborne, W.R.A. (2001). Lentivirus administration to rat muscle provides efficient sustained expression of erythropoietin. Blood *98*, 594–596.

Singh, N.N., Singh, R.N., and Androphy, E.J. (2007). Modulating role of RNA structure in alternative splicing of a critical exon in the spinal muscular atrophy genes. Nucleic Acids Res. *35*, 371–389.

Sirand-Pugnet, P., Durosay, P., Brody, E., and Marie, J. (1995). An intronic (A/U)GGG repeat enhances the splicing of an alternative intron of the chicken beta-tropomyosin pre-mRNA. Nucleic Acids Res. *23*, 3501–3507.

Sironi, M., Menozzi, G., Riva, L., Cagliani, R., Comi, G.P., Bresolin, N., Giorda, R., and Pozzoli, U. (2004). Silencer elements as possible inhibitors of pseudoexon splicing. Nucleic Acids Res. *32*, 1783–1791.

Smith, H.O., Tabiti, K., Schaffner, G., Soldati, D., Albrecht, U., and Birnstiel, M.L. (1991). Two-step affinity purification of U7 small nuclear ribonucleoprotein particles using complementary biotinylated 2'-O-methyl oligoribonucleotides. Proc. Natl. Acad. Sci. U. S. A. *88*, 9784–9788.

Soldati, D., and Schümperli, D. (1988). Structural and functional characterization of mouse U7 small nuclear RNA active in 3' processing of histone pre-mRNA. Mol. Cell. Biol. *8*, 1518–1524.

Solis, A.S., Peng, R., Crawford, J.B., Phillips, J.A., and Patton, J.G. (2008). Growth hormone deficiency and splicing fidelity: Two serine/arginine-rich proteins, ASF/SF2 and SC35, act antagonistically. J. Biol. Chem. *283*, 23619–23626.

Sonntag, F., Schmidt, K., and Kleinschmidt, J.A. (2010). A viral assembly factor promotes AAV2 capsid formation in the nucleolus. Proc. Natl. Acad. Sci. U. S. A. *107*, 10220–10225.

Sontheimer, E.J., and Steitz, J.A. (1993). The U5 and U6 small nuclear RNAs as active site components of the spliceosome. Science *262*, 1989–1996.

Sperling, J., Azubel, M., and Sperling, R. (2008). Structure and Function of the Pre-mRNA Splicing Machine. Structure *16*, 1605–1615.

Spuler, S., Carl, M., Zabojszcza, J., Straub, V., Bushby, K., Moore, S.A., Bähring, S., Wenzel, K., Vinkemeier, U., and Rocken, C. (2008). Dysferlin-deficient muscular dystrophy features amyloidosis. Ann. Neurol. *63*, 323–328.

Srebrow, A., and Kornblihtt, A.R. (2006). The connection between splicing and cancer. J. Cell Sci. *119*, 2635–2641.

Srivastava, A., Lusby, E.W., and Berns, K.I. (1983). Nucleotide sequence and organization of the adeno-associated virus 2 genome. J. Virol. *45*, 555–564.

Stefanovic, B., Hackl, W., Lührmann, R., and Schümperli, D. (1995). Assembly, nuclear import and function of U7 snRNPs studied by microinjection of synthetic U7 RNA into Xenopus oocytes. Nucleic Acids Res. *23*, 3141–3151.

Stein, C.A., Subasinghe, C., Shinozuka, K., and Cohen, J.S. (1988). Physicochemical properties of phosphorothioate oligodeoxynucleotides. Nucleic Acids Res. *16*, 3209–3221.

Stitelman, D.H., Brazelton, T., Bora, A., Traas, J., Merianos, D., Limberis, M., Davey, M., and Flake, A.W.

(2014). Developmental stage determines efficiency of gene transfer to muscle satellite cells by in utero delivery of adeno-associated virus vector serotype 2/9. Mol. Ther. Methods Clin. Dev. *1*, 14040.

Summerford, C., and Samulski, R.J. (1998). Membrane-associated heparan sulfate proteoglycan is a receptor for adeno-associated virus type 2 virions. J. Virol. *72*, 1438–1445.

Summerford, C., Bartlett, J.S., and Samulski, R.J. (1999). AlphaVbeta5 integrin: a co-receptor for adeno-associated virus type 2 infection. Nat. Med. *5*, 78–82.

Suzuki, N., Aoki, M., Takahashi, T., Takano, D., Asano, M., Shiga, Y., Onodera, Y., Tateyama, M., and Itoyama, Y. (2004). Novel dysferlin mutations and characteristic muscle atrophy in late-onset miyoshi myopathy. Muscle and Nerve *29*, 721–723.

Tan, E.M., and Kunkel, H.G. (1966). Characteristics of a soluble nuclear antigen precipitating with sera of patients with systemic lupus erythematosus. J. Immunol. (Baltimore, Md 1950) *96*, 464–471.

Tarn, W.Y., and Steitz, J.A. (1996). A novel spliceosome containing U11, U12, and U5 snRNPs excises a minor class (AT-AC) intron in vitro. Cell *84*, 801–811.

Tatei, K., Takemura, K., Mayeda, A., Fujiwara, Y., Tanaka, H., Ishihama, A., and Ohshima, Y. (1984). U1 RNA-protein complex preferentially binds to both 5’ and 3’ splice junction sequences in RNA or single-stranded DNA. Proc Natl Acad Sci U S A *81*, 6281–6285.

Tattersall, P., and Ward, D.C. (1976). Rolling hairpin model for replication of parvovirus and linear chromosomal DNA. Nature *263*, 106–109.

Terasaki, M., Miyake, K., and McNeil, P.L. (1997). Large plasma membrane disruptions are rapidly resealed by Ca2+- dependent vesicle-vesicle fusion events. J. Cell Biol. *139*, 63–74.

Therrien, C., Dodig, D., Karpati, G., and Sinnreich, M. (2006). Mutation impact on dysferlin inferred from database analysis and computer-based structural predictions. J. Neurol. Sci. *250*, 71–78.

Thomas, C.E., Storm, T.A., Huang, Z., and Kay, M.A. (2004). Rapid uncoating of vector genomes is the key to efficient liver transduction with pseudotyped adeno-associated virus vectors. J. Virol. *78*, 3110–3122.

Ueyama, H., Kumamoto, T., Horinouchi, H., Fujimoto, S., Aono, H., and Tsuda, T. (2002). Clinical heterogeneity in dysferlinopathy. Intern. Med. *41*, 532–536.

Uhlmann, E., Peyman, A., and Will, D.W. (2002). Antisense: Medicinal Chemistry. In Encyclopedia of Cancer, pp. 103–117.

Venter, J.C., Adams, M.D., Myers, E.W., Li, P.W., RJ, M., Sutton, G.G., Smith, H.O., Yandell, M., A, E.C., Holt, R.A., et al. (2001). The Sequence of the Human Genome. Science (80-.). *291*, 1304–1351.

Vincent-Lacaze, N., Snyder, R.O., Gluzman, R., Bohl, D., Lagarde, C., and Danos, O. (1999). Structure of adeno-associated virus vector DNA following transduction of the skeletal muscle. J. Virol. *73*, 1949–1955.

Vulin, A., Barthélémy, I., Goyenvalle, A., Thibaud, J.-L., Beley, C., Griffith, G., Benchaouir, R., le Hir, M., Unterfinger, Y., Lorain, S., et al. (2012). Muscle function recovery in golden retriever muscular dystrophy after AAV1-U7 exon skipping. Mol. Ther. *20*, 2120–2133.

Waddell, L.B., Lemckert, F.A., Zheng, X.F., Tran, J., Evesson, F.J., Hawkes, J.M., Lek, A., Street, N.E., Lin, P., Clarke, N.F., et al. (2011). Dysferlin, annexin A1, and mitsugumin 53 are upregulated in muscular dystrophy and localize to longitudinal tubules of the T-system with stretch. J. Neuropathol. Exp.

Neurol. *70*, 302–313.

Wang, M., Wey, S., Zhang, Y., Ye, R., and Lee, A.S. (2009). Role of the Unfolded Protein Response Regulator GRP78/BiP in Development, Cancer, and Neurological Disorders. Antioxid. Redox Signal. *11*, 2307–2316.

Wang, Z., Zhu, T., Qiao, C., Zhou, L., Wang, B., Zhang, J., Chen, C., Li, J., and Xiao, X. (2005). Adeno-associated virus serotype 8 efficiently delivers genes to muscle and heart. Nat. Biotechnol. *23*, 321–328.

Warf, M.B., and Berglund, J.A. (2010). Role of RNA structure in regulating pre-mRNA splicing. Trends Biochem. Sci. *35*, 169–178.

Wassarman, D., and Steitz, J. (1992). Interactions of small nuclear RNA's with precursor messenger RNA during in vitro splicing. Sci. (New York, NY) *257*, 1918–1925.

Weiler, T., Greenberg, C.R., Nylen, E., Halliday, W., Morgan, K., Eggertson, D., and Wrogemann, K. (1996). Limb-girdle muscular dystrophy and Miyoshi myopathy in an aboriginal Canadian kindred map to LGMD2B and segregate with the same haplotype. Am. J. Hum. Genet. *59*, 872–878.

Weiler, T., Bashir, R., Anderson, L.V.B., Davison, K., Moss, J.A., Britton, S., Nylen, E., Keers, S., Vafiadaki, E., Greenberg, C.R., et al. (1999). Identical Mutation in Patients with Limb Girdle Muscular Dystrophy Type 2B Or Miyoshi Myopathy Suggests a Role for Modifier Gene(s). Hum. Mol. Genet. *8*, 871–877.

Wein, N., Avril, A., Bartoli, M., Beley, C., Chaouch, S., Laforêt, P., Behin, A., Butler-Browne, G., Mouly, V., Krahn, M., et al. (2010). Efficient bypass of mutations in dysferlin deficient patient cells by antisense-induced exon skipping. Hum. Mutat. *31*, 136–142.

Weiss, R.A., Griffiths, D., Villesen, P., Aagaard, L., Wiuf, C., Pedersen, F., Hughes, J., Coffin, J., Barbulescu, M., Turner, G., et al. (2006). The discovery of endogenous retroviruses. Retrovirology *3*, 67.

Weller, M.L., Amornphimoltham, P., Schmidt, M., Wilson, P.A., Gutkind, J.S., and Chiorini, J.A. (2010). Epidermal growth factor receptor is a co-receptor for adeno-associated virus serotype 6. Nat. Med. *16*, 662–664.

Wenzel, K., Carl, M., Perrot, A., Zabojszcza, J., Assadi, M., Ebeling, M., Geier, C., Robinson, P.N., Kress, W., Osterziel, K.-J., et al. (2006). Novel sequence variants in dysferlin-deficient muscular dystrophy leading to mRNA decay and possible C2-domain misfolding. Hum. Mutat. *27*, 599–600.

Wright, W.E. (1985). Myoblast senescence in muscular dystrophy. Exp. Cell Res. *157*, 343–354.

Wu, Z., Miller, E., Agbandje-McKenna, M., and Samulski, R.J. (2006). 2,3 and 2,6 N-Linked Sialic Acids Facilitate Efficient Binding and Transduction by Adeno-Associated Virus Types 1 and 6. J. Virol. *80*, 9093–9103.

Wu, Z., Yang, H., and Colosi, P. (2010). Effect of Genome Size on AAV Vector Packaging. Mol. Ther. *18*, 80–86.

Xiao, X., Li, J., and Samulski, R.J. (1996). Efficient long-term gene transfer into muscle tissue of immunocompetent mice by adeno-associated virus vector. J. Virol. *70*, 8098–8108.

Xiao, X., Li, J., and Samulski, R.J. (1998). Production of high-titer recombinant adeno-associated virus vectors in the absence of helper adenovirus. J. Virol. *72*, 2224–2232.

Yakobson, B., Koch, T., and Winocour, E. (1987). Replication of adeno-associated virus in synchronized

cells without the addition of a helper virus. J. Virol. *61*, 972–981.

Yalklnoglu, A.Ö., Heilbronn, R., Bürkle, A., Schlehofer, J.R., and Hausen, H. Zur (1988). Dna amplification of adeno-associated virus as a response to cellular genotoxic stress. Cancer Res. *48*, 3123–3129.

Yan, X.B., Tang, C.H., Huang, Y., Fang, H., Yu, Z.Q., Wu, L.M., and Liu, R.Y. (2010). Alternative splicing in exon 9 of glucocorticoid receptor pre-mRNA is regulated by SRp40. Mol. Biol. Rep. *37*, 1427–1433.

Yang, J., Zhou, W., Zhang, Y., Zidon, T., Ritchie, T., and Engelhardt, J.F. (1999). Concatamerization of adeno-associated virus circular genomes occurs through intermolecular recombination. J. Virol. *73*, 9468–9477.

Yasunaga, S., Grati, M., Cohen-Salmon, M., El-Amraoui, A., Mustapha, M., Salem, N., El-Zir, E., Loiselet, J., and Petit, C. (1999). A mutation in OTOF, encoding otoferlin, a FER-1-like protein, causes DFNB9, a nonsyndromic form of deafness. Nat. Genet. *21*, 363–369.

Yasunaga, S., Grati, M., Chardenoux, S., Smith, T.N., Friedman, T.B., Lalwani, A.K., Wilcox, E.R., and Petit, C. (2000). OTOF encodes multiple long and short isoforms: genetic evidence that the long ones underlie recessive deafness DFNB9. Am. J. Hum. Genet. *67*, 591–600.

Yean, S.L., and Lin, R.J. (1991). U4 small nuclear RNA dissociates from a yeast spliceosome and does not participate in the subsequent splicing reaction. Mol. Cell. Biol. *11*, 5571–5577.

Yeo, G., and Burge, C.B. (2004). Maximum Entropy Modeling of Short Sequence Motifs with Applications to RNA Splicing Signals. J. Comput. Biol. *11*, 377–394.

Zennou, V., Petit, C., Guetard, D., Nerhbass, U., Montagnier, L., and Charneau, P. (2000). HIV-1 genome nuclear import is mediated by a central DNA flap. Cell *101*, 173–185.

Zhong, L., Zhou, X., Li, Y., Qing, K., Xiao, X., Samulski, R.J., and Srivastava, A. (2008). Single-polarity Recombinant Adeno-associated Virus 2 Vector-mediated Transgene Expression In Vitro and In Vivo: Mechanism of Transduction. Mol. Ther. *16*, 290–295.

Zhou, X., Zeng, X., Fan, Z., Li, C., McCown, T., Samulski, R.J., and Xiao, X. (2008). Adeno-associated Virus of a Single-polarity DNA Genome Is Capable of Transduction In Vivo. Mol. Ther. *16*, 494–499.

Zhu, J., Mayeda, A., and Krainer, A.R. (2001). Exon identity established through differential antagonism between exonic splicing silencer-bound hnRNP A1 and enhancer-bound SR proteins. Mol. Cell *8*, 1351–1361.

Zieve, G.W., and Feeney, R.J. (1990). Cytoplasmic Assembly and Nuclear Transport of the snRNP Particles. (Springer, Berlin, Heidelberg), pp. 51–85.

Zieve, G.W., and Sauterer, R.A. (1990). Cell biology of the snRNP particles. Crit. Rev. Biochem. Mol. Biol. *25*, 1–46.

Zincarelli, C., Soltys, S., Rengo, G., and Rabinowitz, J.E. (2008). Analysis of AAV serotypes 1-9 mediated gene expression and tropism in mice after systemic injection. Mol. Ther. *16*, 1073–1080.

Zufferey, R., Dull, T., Mandel, R.J., Bukovsky, A., Quiroz, D., Naldini, L., and Trono, D. (1998). Self-inactivating lentivirus vector for safe and efficient in vivo gene delivery. J. Virol. *72*, 9873–9880.

Zufferey, R., Donello, J.E., Trono, D., and Hope, T.J. (1999). Woodchuck hepatitis virus posttranscriptional regulatory element enhances expression of transgenes delivered by retroviral vectors. J. Virol. *73*, 2886–2892.

Zuker, M. (2003). Mfold web server for nucleic acid folding and hybridization prediction. Nucleic Acids Res. *31*, 3406–3415.